



Study on self-assembly molecules for innovative food structure design

A Ph.D. dissertation presented by
Fabio Valoppi

to the
University of Udine

for the degree of Ph.D. in the subject of
Food Science (Cycle XXVIII)
Department of Food Science

UNIVERSITY OF UDINE
Italy
March 2016

Supervisors: Maria Cristina Nicoli, Professor
Department of Food Science
University of Udine, Italy

Sonia Calligaris, PhD
Department of Food Science
University of Udine, Italy

Coordinator: Mara Lucia Stecchini, Professor
Department of Food Science
University of Udine, Italy

Reviewers: Alejandro G. Marangoni, Professor
Department of Food Science
University of Guelph, Canada

Perla Relkin, Professor
Department of Engineering and Science of Food and Bioproducts
AgroParisTech-Centre de Massy, France

I declare that my Ph.D. thesis has been amended to address all the Referee's comments.

Acknowledgments

I would like to thank prof. M. C. Nicoli and dr. S. Calligaris for their help and supervision during these three years; dr. L. Barba for her technical assistance and guidance during Synchrotron XRD analysis and for data analysis; prof. C. Lagazio for his help with statistical analysis; dr. M. Munari for her technical assistance in the lab; prof. A. G. Marangoni for his supervision during my stay in Canada; dr. F. Peyronel for her technical assistance in prof. Marangoni's lab, for performing USAXS analysis and for data analysis; prof. N. Poklar Ulrih and dr. N. Šegatin for their support and technical help with dielectric measurements during my stay in Slovenia; dr. S. Smith for her technical assistance and guidance with SEM analysis; dr. S. Zanadri for performing furan analysis; Miss C. Blach for performing the melting profile with p-NMR, and dr. G Muner for his support in MRI analysis.

Table of contents

List of abbreviations	7
Preface	9
Abstract	11
Chapter 1 ♦ Introduction	13
1.1 Food world demand and food scientists challenges.....	13
1.2 Food nanotechnology and food structure design	14
1.3 Self-assembly structuring molecules for food applications	15
1.3.1 Organogels	16
1.3.2 Emulsions	18
1.4 Aim and outline of this Ph.D. thesis	21
PART I ♦ Polar lipids.....	23
PART I A ♦ Polar lipids as structuring agents: basic studies.....	25
Chapter 2 ♦ Binary systems	27
2.1 Fatty alcohols	27
2.1.1 Aim of the study	27
2.1.2 Materials and methods.....	27
2.1.2.1 <i>Materials</i>	27
2.1.2.2 <i>Sample preparation</i>	27
2.1.2.3 <i>Minimum gelling concentration</i>	27
2.1.2.4 <i>Back extrusion</i>	27
2.1.2.5 <i>Accelerated oil release test (AORT)</i>	28
2.1.2.6 <i>Proton nuclear magnetic resonance (p-NMR)</i>	28
2.1.2.6.1 <i>Solid fat content (SFC)</i>	28
2.1.2.6.2 <i>T₂ spin-spin relaxation time</i>	28
2.1.2.7 <i>Polarized light (PL) microscopy</i>	28
2.1.2.8 <i>Cryogenic scanning electron microscopy (Cryo-SEM)</i>	29
2.1.2.9 <i>Differential scanning calorimetry (DSC)</i>	29
2.1.2.10 <i>Powder X-ray diffraction (XRD)</i>	30
2.1.2.11 <i>Ultra small angle X-ray scattering (USAXS)</i>	30
2.1.2.12 <i>Data analysis</i>	31
2.1.3 Results and discussion	31
2.1.3.1 <i>Thermal, nanostructural, and aggregating characterization</i>	31
2.1.3.2 <i>Micro, macro, and mechanical characterization</i>	38
2.1.4 Conclusions	47
2.2 Monoglyceride organogel.....	48
2.2.1 Aim of the study	48
2.2.2 Materials and methods.....	48
2.2.2.1 <i>Materials</i>	48
2.2.2.2 <i>Monoglyceride organogel preparation</i>	48

2.2.2.3	<i>Oil fatty acid composition</i>	48
2.2.2.4	<i>Oil viscosity</i>	48
2.2.2.5	<i>Dielectric Properties</i>	48
2.2.2.6	<i>Polarized light (PL) microscopy</i>	49
2.2.2.7	<i>Firmness</i>	49
2.2.2.8	<i>Differential scanning calorimetry (DSC) analysis</i>	49
2.2.2.9	<i>Data analysis</i>	50
2.2.3	Results and discussion	50
2.2.3.1	<i>Oil fatty acid composition, viscosity and dielectric properties</i>	50
2.2.3.2	<i>Organogel dielectric, thermal, microstructural, and mechanical properties</i>	52
2.2.4	Conclusions	57
Chapter 3	♦ Ternary systems based on monoglyceride	59
3.1	Effect of strong and weak bases on monoglyceride gelled emulsions	59
3.1.1	Aim of the study	59
3.1.2	Materials and methods	59
3.1.2.1	<i>Materials</i>	59
3.1.2.2	<i>Monoglyceride gelled emulsions preparation</i>	59
3.1.2.3	<i>pH</i>	60
3.1.2.4	<i>Visual appearance</i>	60
3.1.2.5	<i>Rheological analysis</i>	60
3.1.2.6	<i>PL microscopy</i>	60
3.1.2.7	<i>DSC analysis</i>	60
3.1.2.8	<i>Synchrotron X-ray diffraction (XRD) analysis</i>	60
3.1.2.9	<i>Data analysis</i>	61
3.1.3	Results and discussion	61
3.1.3.1	<i>pH and visual appearance</i>	61
3.1.3.2	<i>Viscoelastic behavior and microstructure</i>	62
3.1.3.3	<i>DSC and XRD analysis</i>	65
3.1.4	Conclusions	66
3.2	Milk and simulated milk ultrafiltrate (SMUF) as aqueous phase in monoglyceride gelled emulsions	68
3.2.1	Aim of the study	68
3.2.2	Materials and methods	68
3.2.2.1	<i>Materials</i>	68
3.2.2.2	<i>Sample preparation</i>	68
3.2.2.2.1	<i>Simulated milk ultrafiltrate (SMUF) solutions</i>	68
3.2.2.2.2	<i>UHT skim milk-oil-monoglyceride mixtures</i>	69
3.2.2.3	<i>Compositional state diagram</i>	69
3.2.2.4	<i>pH</i>	69
3.2.2.5	<i>Rheological analysis</i>	69
3.2.2.6	<i>PL microscopy</i>	69
3.2.2.7	<i>Synchrotron XRD analysis</i>	70
3.2.2.8	<i>Data analysis</i>	70
3.2.3	Results and discussion	70
3.2.3.1	<i>Characterization of UHT skim milk-based monoglyceride systems</i>	70
3.2.3.2	<i>Rheological and microstructural investigation of selected UHT skim milk-based gelled emulsions</i>	74

3.2.4 Conclusions	77
-------------------------	----

PART I B ♦ Polar lipids as fat mimetics: applicative studies 79

Chapter 4 ♦ Monoglyceride gelled emulsion and organogels as palm oil replacer and ω -3 delivery systems 81

4.1 Effect of palm oil replacement with monoglyceride organogel and gelled emulsion on sweet bread properties.....	81
4.1.1 Aim of the study	81
4.1.2 Materials and methods.....	81
4.1.2.1 <i>Materials</i>	81
4.1.2.2 <i>Sample preparation</i>	81
4.1.2.2.1 <i>Organogel</i>	81
4.1.2.2.2 <i>Gelled emulsions</i>	81
4.1.2.2.3 <i>Sweet bread</i>	82
4.1.2.2.4 <i>Sample cutting and storage</i>	82
4.1.2.3 <i>Specific volume</i>	82
4.1.2.4 <i>Moisture content</i>	82
4.1.2.5 <i>Water activity</i>	82
4.1.2.6 <i>Crumb grain</i>	82
4.1.2.6 <i>Firmness</i>	83
4.1.2.6.1 <i>OG and GE</i>	83
4.1.2.6.2 <i>Crumb bread</i>	83
4.1.2.7 <i>Magnetic resonance imaging (MRI)</i>	83
4.1.2.8 <i>Data analysis</i>	83
4.1.3 Results and discussion	84
4.1.4 Conclusions	89
4.2 Omega-3 enriched biscuits with low levels of heat-induced toxicants: effect of formulation and baking conditions.....	90
4.2.1 Aim of the study	90
4.2.2 Materials and methods.....	90
4.2.2.1 <i>Materials</i>	90
4.2.2.2 <i>Preparation of monoglyceride–flax-seed oil–water gelled emulsion</i>	90
4.2.2.3 <i>Short dough biscuits preparation</i>	90
4.2.2.4 <i>Temperature monitoring and thermal effect computation</i>	91
4.2.2.5 <i>Acrylamide analysis</i>	91
4.2.2.6 <i>Furan analysis</i>	92
4.2.2.7 <i>Color analysis</i>	92
4.2.2.8 <i>Total solid content determination</i>	92
4.2.2.9 <i>Lipid extraction</i>	92
4.2.2.10 <i>Peroxide value determination</i>	92
4.2.2.11 <i>Rheological analysis</i>	93
4.2.2.12 <i>Firmness</i>	93
4.2.2.13 <i>Polynomial equations and statistical analysis</i>	93
4.2.3 Results and discussion	94
4.2.3.1 <i>Gelled emulsion formulation and its incorporation in the dough</i>	94

4.2.3.2 Identification of baking conditions at reduced pressure of omega-3 PUFAs enriched biscuits	95
4.2.4 Conclusions	101

PART II ♦ Delivery systems for lipophilic bioactive compounds.....103

Chapter 5 ♦ Effect of lipid physical state on selected bioactive compound stability 105

5.1 Structure studies on curcumin and β -carotene added to solid fat matrices	105
5.1.1 Aim of the study	105
5.1.2 Materials and methods	105
5.1.2.1 Materials.....	105
5.1.2.2 β -carotene or curcumin containing lipid matrices preparation ...	105
5.1.2.3 DSC analysis.....	106
5.1.2.4 Synchrotron XRD analysis.....	106
5.1.2.5 PL microscopy	106
5.1.2.6 Data analysis.....	106
5.1.3 Results and discussion	106
5.1.4 Conclusions	113
5.2 Effect of solid fat content on curcumin and β -carotene degradation kinetics	114
5.2.1 Aim of the study	114
5.2.2 Materials and methods	114
5.2.2.1 Materials.....	114
5.2.2.2 β -carotene or curcumin containing lipid matrices	114
5.2.2.3 Color analysis.....	114
5.2.2.4 Data analysis	114
5.2.3 Results and discussion	115
5.2.4 Conclusions	120

Chapter 6 ♦ Effect of system composition on delivery systems production 121

6.1 Development of nano and microemulsions using the phase inversion temperature (PIT) method.....	121
6.1.1 Aim of the study	121
6.1.2 Materials and methods	121
6.1.2.1 Materials.....	121
6.1.2.2 Emulsified systems preparation by phase inversion temperature (PIT) method.....	121
6.1.2.3 Visual appearance	122
6.1.2.4 Phase inversion temperature (PIT) determination using viscosity measurement.....	122
6.1.2.5 Emulsion viscosity	122
6.1.2.6 Dynamic laser scattering	122
6.1.2.7 Image acquisition.....	122
6.1.2.8 Bright field microscopy.....	123
6.1.2.9 Synchrotron XRD analysis.....	123
6.1.2.10 Curcumin analysis	123
6.1.2.10.1 Extraction of curcumin from emulsified systems	123

6.1.2.10.2	<i>Extracted curcumin HPLC analysis</i>	123
6.1.2.11	<i>Data analysis</i>	123
6.1.3	Results and discussion	124
6.1.3.1	<i>Effect of aqueous phase and temperature on nano and microemulsions formation</i>	124
6.1.3.2	<i>Effect of lipid phase on nano and microemulsions formation</i>	126
6.1.3.2.1	<i>Lemon oil loading capacity maximization in nano and microemulsions</i>	128
6.1.3.3	<i>Selected microemulsions loaded with curcumin</i>	131
6.1.4	Conclusions	133

Insight ♦ Performance of selected transparent emulsion containing lemon oil in beverage prototype under different thermal treatments 135

General conclusions and future directions.....	141
References	143
List of publications relevant to this Ph.D. research activity	155
List of additional publications	155
List of submitted and in-progress manuscripts.....	155
Contributions to national and international conferences	156

List of abbreviations

ADI	Acceptable Daily Intake
ANOVA	Analysis of Variance
AORT	Accelerated Oil Release Test
CCF	Face Centered Central Composite Design
Cryo-SEM	Cryogenic Scanning Electron Microscopy
CO-MG	Monoglyceride added with co-surfactants
C ₁₂ OH	1-dodecanol
C ₁₄ OH	1-tetradecanol
C ₁₆ OH	1-hexadecanol
C ₁₈ OH	1-octadecanol
C ₂₀ OH	1-eicosanol
C ₂₂ OH	1-docosanol
DSC	Differential Scanning Calorimetry
EPI	Emulsion Point Inversion
EVO	Extra Virgin Olive
GC	Gas-Chromatography
GE	Gelled Emulsion
HLD	Hydrophilic Lipophilic Deviation
HPLC	High Performance Liquid Chromatography
HS-SPME	Head Space Solid Phase Micro Extraction
MCT	Medium Chain Triacylglyceriol
MG	Monoglyceride
MRI	Magnetic Resonance Imaging
MS	Mass Spectrometry
OG	Organogel
OR	Ostwal Ripening
O/W	Oil in Water
O/W/W	Oil in Water in Water
PIC	Phase Inversion Composition
PIT	Phase Inversion Temperature
PL	Polarized light
p-NMR	Proton Nuclear Magnetic Resonance
PPP	Tripalmitin
PUFA	Poly Unsaturated Fatty Acids
SAXS	Small Angle X-ray Scattering
SD	Standard Deviation
SE	Spontaneous Emulsification
SFC	Solid Fat Content
SMUF	Simulated Milk UltraFiltrate
SOR	Surfactant to Oil Ratio
SSS	Tristearin
TAG	Triacylglycerol
UHT	Ultra High Temperature
USAXS	Ultra-Small Angle X-ray Scattering
WAXS	Wide Angle X-ray Scattering
W/O	Water in Oil
W/O/W	Water in Oil in Water
XRD	X-Ray Diffraction

Preface

In the last decades, humans have been using their knowledge and fantasy to build up new tailored supramolecular structures thanks to the understanding of the deep connection between molecular geometry and surface curvature. The driving forces that are used to assemble the desired structures can be basically attributed to free energy minimization (thermodynamics) and velocity of structures assembly (kinetics). From this complex interplay among molecules, structures can be tailored depending on the final aim. The accurate selection of components followed by the understanding of interactions among them, in combination with the choice of processing conditions will affect the final structure. Building blocks, such as lipids, surfactants, proteins, and polysaccharides are used to create food-grade structures. The final goal of the resulting structures is to improve food quality as well as reduce outbreaks of food related diseases. The “Holy Grail” is, thus, develop nanostructured materials that can be considered a food able to satisfy the orosensory experience of consumers as well as help their lives to be improved.

In this context, this Ph.D. thesis aimed to investigate the ability of selected food-grade building blocks to self-assemble into different structures as a function of system, environmental, and processing conditions. The resulting materials were then characterized at different length scales (nano, micro and macro) in order to study their hierarchical organization. Finally, the feasible application of selected systems in target products was evaluated.

Abstract

In this Ph.D. thesis, the ability of selected self-assembly molecules to form structures as a function of system, environmental, and processing conditions was studied at different length scales (nano, micro, and macro). In particular, the attention was pointed on hydrophobic as well as a mixture of hydrophobic and hydrophilic media.

Different analytical techniques were used to investigate the levels of the matter of the resulting materials. Synchrotron X-ray diffraction, powder X-ray diffraction, differential scanning calorimetry, pulsed nuclear magnetic resonance, dielectric spectroscopy, and dynamic laser light scattering were used to investigate the nano and molecular structuration of the obtained systems. The microscopic level was investigated using polarized light microscopy, cryo-scanning electron microscopy, ultra-small angle X-ray scattering, and magnetic resonance imaging. Finally, the macroscopic level was investigated using large and small deformation analysis, visual appearance, accelerated oil release test, and colorimetric analysis. Besides this structural analysis, emphasis was also pointed on some chemical analysis in the attempt to determine the formation of toxicant molecules (furans, acrylamide, peroxides) or the degradation of bioactive molecules.

In this thesis, binary systems composed of fatty alcohols with different carbon chain length added to peanut oil, and monoglycerides added to different oils were studied. Fatty alcohols turned out to be promising building blocks in the attempt to structure an edible oil. Depending on cooling rate applied, fatty alcohol carbon chain length, and concentration, it is possible to obtain systems with different performances. On the other hand, monoglyceride structured systems showed that thermal, mechanical and microstructural characteristics were greatly affected by oil fatty acids composition and its dielectric properties.

Ternary systems composed by oil, aqueous phase and monoglycerides were then studied. Results highlighted that the aqueous phase as well as the ratio among ingredients are of crucial importance to obtain a gelled emulsified structure. In particular the composition of the aqueous phase allowed to tune the resulting material in all the length scales studied depending on anions, proteins and salts present added to the system.

The applicability of selected structured systems was studied in bakery products such as sweet bread and biscuits with the aim of reducing saturated fat and deliver high quantities of essential fatty acids. Thanks to monoglyceride gelled emulsions it was possible to obtain sweet bread samples with quality characteristics comparable to those of sweet bread control prepared using palm oil. Moreover, gelled emulsions containing PUFAs coupled with a vacuum baking process were able to obtain enriched biscuits allowing low levels of toxicants formation.

The study was then pointed on selected bioactive molecules. In particular β -carotene and curcumin were able to alter the crystal morphology of solid lipids used as carriers. This alteration was then translated into different bioactive molecules degradation rates. Finally, transparent emulsions delivering bioactive molecules as well as essential oils were developed. Processing conditions and ingredients ratio were the key elements to obtain stable transparent systems. These systems were then diluted into fancy drink prototypes and thermally stressed. The protective ability of the carrier was basically dependent on the treatment applied.

Introduction

1.1 Food world demand and food scientists challenges

The evolution from hunter-gatherers to farmers, with the discover of agriculture and primitive food storage, allowed humans to establish settlements that grew and expanded over time and space as people discovered new technological solutions to problems. This phenomenon led to an important diversification of human needs depending on geographical position, society structure, and available technology. Food is one of the primary needs and its demand can be defined, from a basic point of view, the amount of food, which is source of nutrients, needed by a person to survive on a day basis (Floros, Newsome, Fisher, Barbosa-Canovas, Chen, Dunne, German, Hall, Heldman, Karwe, Knabel, Labuza, Lund, Newell-McGloughlin, Robinson, Sebranek, Shewfelt, Tracy, Weaver, & Ziegler, 2010). However, quite recently, humans understood over time that food is not only a primary need but also a tool to prevent nutrition-related diseases and improve their physical and mental well-being (Siro, Kapolna, Kapolna, & Lugasi, 2008). Thus, nowadays food demand is a heterogeneous need that evolved, still evolving and will evolve over time and space with human being.

The complex world that is around us can be simply categorized, in terms of food needs, into 3 different categories based on industrialization progress (which one can consider the result of the factors that could have affected food demand in a specific country): (i) underdeveloped, (ii) developing, and (iii) developed countries. Each country has different needs that have to be matched in order to survive and develop. For example, underdeveloped countries require to improve food safety as well as the availability of fortified foods in order to overcome infections and malnutrition problems (Bain, Awah, Geraldine, Kindong, Sigal, Bernard, & Tanjeko, 2013; Sasson, 2012). On the contrary, developing countries ask for fortified foods to overcome micronutrients deficiency beside low calories foods to reduce the increasing incidence of overweight and diabetes (Azais-Braesco, Brighenti, Paoletti, Peracino, Scarborough, Visioli, & Vogele, 2009; Govindaraj, 2015). Finally, developed countries are looking for low calories foods as well, but there is a growing interest of consumers on new foods with specific functionalities and environmental sustainability (Cencic & Chingwaru, 2010). Moreover, besides these needs, future food world demand will deeply increase: the estimated population by 2050 will reach 9 billion people and food world production should increase by about 70% to satisfy world demand (Floros *et al.*, 2010).

The production of food that can meet the needs and requests of different countries is also constrained by the ability of a country to consume food (i.e. the actions needed to prepare and eat a determined food are limited by country technology) and by religious constrains as well as by the ability of a country to store food preventing its spoilage. Final mark to keep in mind is that food consumption is also determined by pleasure rather than be just a mere mechanical process driven by the need of calories (Lowe & Butryn, 2007; Mela, 2006).

Thus, the challenges for food scientists all over the world are various. Indeed, in order to match each country's needs and requests, food scientists diversified research into different sectors (i.e. food production, food safety, food packaging, conventional food processing, novel food processing, food waste management, food nanotechnology). These disciplines, however, are only partially able to help fulfilling present and future food world demand. More research is needed and more disciplines will born in the future to help and cooperate

with existing ones in order to assure to each country the possibility to go on based on a nutritional and dietary point of view.

1.2 Food nanotechnology and food structure design

Within this extremely complex scenario, food nanotechnology can be a powerful tool to be implemented and studied in order to help matching food world demand.

Nanotechnology is the fundamental multidisciplinary understanding and control of matter – which encompasses physics, chemistry, and biology – characterized by scales ranging from individual atoms or molecules to submicron dimensions (~ 1 – 100 nm range), as well as the integration of these materials into larger systems (Bhushan, 2010; Floros *et al.*, 2010; Klaessig, Marrapese, & Abe, 2011; Weiss, Takhistov, & McClements, 2006). Food nanotechnology is a branch of nanotechnology with a major interest on the comprehension and production of materials able to increase food safety, keep trace of any extrinsic and intrinsic food changes, and production of systems able to encapsulate and deliver functional ingredients (Weiss *et al.*, 2006). Some examples of food nanotechnology branches are nanoencapsulation, nanocomposites in food packaging, coatings containing nanoparticles, nanoemulsions, polymeric nanoparticles, and edible nanocoatings and nanomaterials (Sekhon, 2010). In order to obtain nanostructures, three main approaches are nowadays used: top-down (miniaturization or size-shrinking approach), bottom-up (production of nanoentities that are assembled into nanostructures or microstructures), and supramolecular self-organization (production of complex structures by controlling the assembly of molecules by hierarchical growth) (Lehn, 2002). In food nanotechnology, the bottom-up and the supramolecular self-organization approach are the most used. The driving force allowing these processes is free energy minimization. Indeed, molecules tend to reorganize over space and time to reach an equilibrium that has the lowest energetic state obtainable in a given system. Furthermore, the resulting nanostructures can interact by themselves giving rise to a supramolecular organization growing from nano to macroscopic scale. This is the hierarchical growth of structures which is present in foods, like meat, fruit, vegetables, etc. and all processed foods (Joardder, Kumar, & Karim, 2015). However, if the desired structure is at nanoscopic level and no further organization is wanted (non-equilibrium state of the matter), kinetic hindrance has to be introduced.

In order to design a defined structure, the molecular properties as well as the effect of the environment characteristics have to be known. Four main classes of food-grade building blocks can be used: lipids, surfactants and polar lipids, proteins, and polysaccharides. From a basic point of view, the driving forces which allow these interactions to take place are mainly categorized in: hydrophobic, electrostatic, hydrogen bonds, and entropy effects (Chandler, 2005; Hyde, Andersson, Larsson, Blum, Landh, Lidn, & Ninham, 1997; McClements, Decker, Park, & Weiss, 2009; Mendes, Baran, Reis, & Azevedo, 2013). These interactions are the results of the chemical structure of the building blocks as well as physicochemical properties of the solvent. A schematization of the cognitive steps for the understanding of these structural hierarchies is given in Figure A.

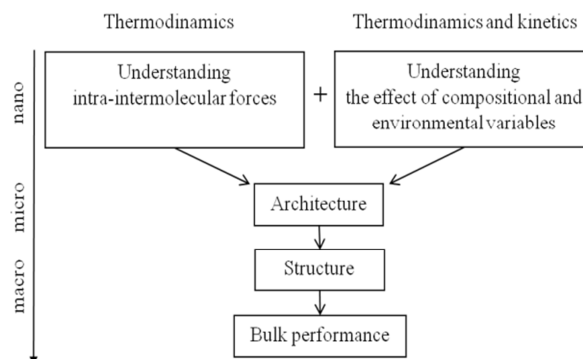


Figure A. Cognitive steps for the understanding of structural hierarchies.

Food structure design relies, thus, on the use of molecules that introduced in a given environment can, spontaneously or under the influence of extra factors, interact. The resulting systems can be due to phase separation, spontaneous self-assembly, directed self-assembly, or directed assembly processes (McClements *et al.*, 2009). These processes are the key elements for building new structures.

1.3 Self-assembly structuring molecules for food applications

The ability of molecules to spatially and temporally organize spontaneously in a given solvent is a process that is ubiquitous in nature (Mendes *et al.*, 2013; Rogers, 2016). This phenomenon known as self-assembly is driven by building blocks molecular geometry. Indeed, the aggregation of molecules in a given environment allows the production of a surface characterized by a determined curvature while forming geometrical supramolecular aggregates. The curvature is, thus, the alphabet of a more complex language that can be written using self-assembly (Hyde *et al.*, 1997).

The structuration of edible materials using the self-assembly approach in food structure design is considered one of the most promising approaches. Using the aforementioned building blocks (surfactants and polar lipids, lipids, proteins, polysaccharides, their derivatives, and combination thereof) it is possible to build up an architecture that has unique features responding to a determined need. However, besides the food-grade property of the structuring molecules, other characteristics have to be held by the structuring agents: they have to be cheap, efficient (low percentages to get the desired result), and versatile (easy to be tailored) (Co & Marangoni, 2012). The structuring efficiency of these molecules depends on different factors, such as concentration, environmental and processing conditions, ingredient ratio, molecular structure and, as previously mentioned, interactions among the structuring agents and other molecules (McClements *et al.*, 2009). Different structures, such as nanotubes, nanofibrilles, filaments, liposomes, coacervates, etc. can be formed and separated from the surrounding media in order to obtain protective micro and nanostructures (Augustin & Hemar, 2009; L. Y. Chen, Remondetto, & Subirade, 2006). On the other hand, it is possible to use the building blocks to structure the medium in which they are introduced. In the latter case, since a solid or semisolid structure is usually desired, the structuring molecule has to be neither soluble nor insoluble in the solvent. Indeed, a balance between these two aspects is needed to establish interactions with other structuring molecules (to obtain a network) and with the solvent (to entrap it within the forming network) (Co & Marangoni, 2012).

Usually, the solvents that are structured can be divided in aqueous (hydrophilic), non-aqueous (hydrophobic), and mixtures of both. In the first case it is possible to obtain the so

called hydrogels, in the second case the materials are called organogels, in the third case a dispersion of one solvent in the other one is formed (emulsion). Hereafter, the attention will be pointed on solvent structuration through self-assembly building blocks with a particular focus on organogels and emulsions.

1.3.1 Organogels

Organogels are defined as self-standing, thermoreversible, anhydrous, viscoelastic materials structured by a three-dimensional supramolecular network of self-assembled molecules (organogelators) with limited solubility in an organic liquid (Rogers, Wright, & Marangoni, 2009b).

The ability to structure non-aqueous systems such as oils by proteins and polysaccharide was partially explored and still under study. Up to date, the only known polysaccharide able to directly structure liquid oil is ethylcellulose (Laredo, Barbut, & Marangoni, 2011). Adding ethylcellulose in oil and increasing the system temperature above ethylcellulose T_g allows this polymer to be dispersed uniformly and during cooling it can rearrange and interact with oil allowing a gelled structure to be obtained (Davidovich-Pinhas, Barbut, & Marangoni, 2015). The amount of ethylcellulose, its esterification degree, type and quality of oil as well as processing conditions are exploited to tailor organogel properties (Gravelle, Barbut, & Marangoni, 2012; Gravelle, Barbut, Quinton, & Marangoni, 2014; Gravelle, Davidovich-Pinhas, Zetzl, Barbut, & Marangoni, 2016). However, some researchers proposed indirect methods to structure edible oils by means of proteins and polysaccharides. In particular, Romoscanu and Mezzenga (2006) described an emulsion-templated technique where a β -lactoglobulin-stabilized oil-in water emulsion was converted into a protein-in-oil gel upon interfacial protein cross-linking and water evaporation. The final material was constituted of up to 99.9% of oil entrapped into a protein matrix. Also in this case, the material could be tailored controlling the processing condition of emulsion fabrication as well as the enzymatic cross-linking process. As regards water-soluble polysaccharides, two indirect approaches were studied by Patel, Cludts, Bin Sintang, Lewille, Lesaffer, and Dewettinck (2014a), and Patel, Schatteman, Lesaffer, and Dewettinck (2013). The first one was an emulsion-templated approach similar to that previously described, where an oil-in-water emulsion stabilized using a combination of cellulose derivatives (hydroxy propyl methylcellulose and methylcellulose) and xanthan gum was prepared. These emulsions were then subjected to evaporation of the water phase. The resulting organogel was characterized by high gel strength, thermostability and thixotropic recovery (Patel *et al.*, 2014a). The second approach was a foam-templated approach, where a foam prepared using hydroxy propyl methylcellulose was freeze dried in order to obtain a cryogel. The latter one was then used to adsorb oil and after the application of shear gave an organogel characterized by thermostability and good oil retention over time (Patel *et al.*, 2013).

Lipids such as saturated triacylglycerols (TAGs), waxes, and a mixture of phytosterols and phytosterols esters were studied as structuring agents mainly in hydrophobic media due to their chemical structure. The conventional and oldest method to structure oils are saturated TAGs. They are used to give structure to a liquid oil thanks to their ability to form hierarchical structures where TAGs molecules organize themselves into lamellar superstructures. The latter builds up a crystalline nanoplatelet, that assembles in spherulites which eventually give rise to a colloidal crystal network (Marangoni, Acevedo, Maleky, Co, Peyronel, Mazzanti, Quinn, & Pink, 2012). From a nanoscopic point of view, it is known that TAGs organize over space and time into three main polymorphic forms: hexagonal α , orthorhombic β' , and triclinic β (Sato, Ueno, & Yano, 1999). TAGs can crystallize in a hydrophobic media with different polymorphic forms depending on external (cooling rate, tempering, pressure, additives, impurities, application of shear, solvent) and internal (molecular structure) factors (Sato, 2001; Sato, Bayes-Garcia, Calvet, Cuevas-Diarte, &

Ueno, 2013). In particular, fast cooling rates allow α form to be formed with small crystal dimensions, while slow cooling rates lead to β' or β forms with bigger crystals to be formed (Sato *et al.*, 2013). Also shear induces some changes at the nanoscopic level. In cocoa butter and milk fat the application of shear induces a preferential orientation of crystals along with the appearance of new subtypes of polymorphic forms (Maleky & Marangoni, 2008; Mazzanti, Guthrie, Sirota, Marangoni, & Idziak, 2004). Thus, carefully choosing the type of TAG as well as controlling process parameters can lead to the desired material. Unfortunately compared to other structuring strategies the minimum amount of TAGs to obtain a structured systems is 20% (Co & Marangoni, 2012).

Waxes from different plants (candelilla, sunflower, rice bran, carnauba, berries, and candleberry) as well as from insects (lac insect and bees) were studied to gel oils (Blake, Co, & Marangoni, 2014; Patel, Babaahmadi, Lesaffer, & Dewettinck, 2015; Patel & Dewettinck, 2015; Toro-Vazquez, Morales-Rueda, Dibildox-Alvarado, Charo-Alonso, Alonzo-Macias, & Gonzalez-Chavez, 2007; Yilmaz & Ogutcu, 2014). These molecules once dispersed in liquid oil and melted were able to form a supramolecular three-dimensional anhydrous network of interconnected structures able to entrap and retain oil during cooling (Rogers *et al.*, 2009b). A great advantage of organogels prepared using waxes relies on the easy way and relative low temperatures needed to prepare the gelled systems. Moreover, a relatively small amount (between 0.5 and 2% w/w) allowed liquid oil to be gelled where self-assembled wax nanoplatelets were formed. These systems can also be engineered using shear and cooling rate to tailor their physical properties (Blake & Marangoni, 2015a, 2015d). Finally, the ability to structure liquid oil was studied using a mixture of phytosterols and phytosterols esters (Bot & Agterof, 2006). In particular, β -sitosterol and γ -oryzanol mixture was able to self-assemble into tubules giving rise to an organogel. These tubules were characterized by a diameter in the 6.7 – 8.0 nm range with a wall thickness of 0.8 – 1.2 nm where the oil was present outside and inside the tubule (Bot, den Adel, Roijers, & Regkos, 2009). The resulting structured material had tunable characteristics depending on concentration, ratio between β -sitosterol and γ -oryzanol, and oil viscosity and polarity. The best ratio in terms of structuring efficiency was 2:3 (β -sitosterol: γ -oryzanol) (Bot & Agterof, 2006), whereas high oil viscosity and polarity slowed down the formation of the tubules due to kinetic hindrance leading to gels with lower melting points as well as lower strength (Calligaris, Mirolo, Da Pieve, Arrighetti, & Nicoli, 2014; Sawalha, Margry, den Adel, Venema, Bot, Flöter, & van der Linden, 2013). Unfortunately, a drawback of these systems is that tubules formation is a slow process at low structuring molecules concentration. Indeed, systems containing 5% (w/w) β -sitosterol + γ -oryzanol (ratio 2:3) in flax-seed oil and triolein needed 72 and 552 hours to completely gel, respectively (Calligaris *et al.*, 2014).

In the last decade much effort was directed towards surfactants and polar lipids organogelation. In particular, monoglycerides (Da Pieve, Calligaris, Co, Nicoli, & Marangoni, 2010; Yilmaz & Ogutcu, 2014), 12-hydroxystearic acid (Rogers, Wright, & Marangoni, 2008a), fatty acids, and fatty alcohols (Daniel & Rajasekharan, 2003), are some examples of the tested structuring agents. Authors were able to identify different types of microstructures, such as platelets, needle-like, rosette-like, fibrils, etc., depending on organogelator chemical structure and concentration as well as type of oil used. On this topic, Co and Marangoni (2012) stated that the impurities present in oil may be the cause of the observed differences rather than any intrinsic difference between oil triacylglycerol composition.

In particular, monoglyceride organogels caught the attention of different research groups since this surfactant is widely used in food industry. The ability to structure an edible oil as well as the characteristics of the resulting materials were greatly affected by monoglycerides purity where the higher the purity the lower the ability of the organogel to retain oil and the larger the crystals in the material (Lopez-Martinez, Morales-Rueda, Dibildox-Alvarado,

Charo-Alonso, Marangoni, & Toro-Vazquez, 2014). Since oil retention is an important characteristic that has to be tailored in order to get the organogel to be stable over time as well as to release oil when necessary, Da Pieve *et al.* (2010) studied the possibility to tailor the crystals using shear. It was found that shear allowed weaker gels to be formed with greater crystals domains and lower oil retention ability compared to samples statically crystallized. Another molecule that was studied is 12-hydroxystearic acid. In particular, the fibrillar nature of the crystals that allowed organogels to be structured was extensively studied in order to engineer its oil retention capacity playing with processing temperatures and 12-hydroxystearic acid concentration. This allowed to obtain different fibrils that formed a more or less stable organogel (Rogers *et al.*, 2008a; Rogers, Wright, & Marangoni, 2008b, 2009a).

Up to nowadays very little and fragmented information is present in literature about fatty alcohols and fatty acids organogels. Indeed, Daniel and Rajasekharan (2003) demonstrated that it is possible to gel sunflower and lavender oil using fatty acids and fatty alcohols with chain lengths comprised in the 16–31 range. Then Gandolfo, Bot, and Flöter (2004) demonstrated that using a mixture of stearic acid and stearyl alcohol, it was possible to obtain a synergistic effect in terms of gel strength when a 3:7 ratio (stearic acid:stearyl alcohol) was used.

Finally, mixtures of structuring agents were proposed. One interesting example is the network formed by lecithin and sorbitan tri-stearate in a 50:50 ratio. In this case, Perneti, van Malssen, Kalnin, and Flöter (2007) found that crystals were formed by sorbitan tri-stearate thanks to the presence of lecithin that was also responsible for the weak junctions among crystals. Further examples are ethylcellulose and monoglyceride mixtures. Lopez-Martinez, Charo-Alonso, Marangoni, and Toro-Vazquez (2015) found that the addition of ethylcellulose had a synergistic effect with monoglycerides in terms of mechanical properties as well as oil retention.

The application of different organogels in some food products as hydrogenated/saturated fat replacers, and oil migration inhibitors has been studied. In particular, ethylcellulose organogels were successfully used as saturated fat replacer in frankfurters (Zetzl, Marangoni, & Barbut, 2012) as well as in heat resistant chocolate (Stortz & Marangoni, 2013). Rice bran wax organogel was used in ice cream in order to increase the unsaturated level of lipids (Zulim Botega, Marangoni, Smith, & Goff, 2013), and sunflower wax and beeswax organogels were used in cookies preparation (Yilmaz & Ogutcu, 2015). In addition, Hughes, Marangoni, Wright, Rogers, and Rush (2009) studied the ability of 12-hydroxystearic acid organogel to inhibit oil-migrator in a cream-filled chocolate confection as well as the ability of this organogel to incorporate and release β -carotene during digestion. These authors found out that the presence of this structuring agent retarded the release of β -carotene compared to bulk oil.

1.3.2 Emulsions

Emulsions are defined as dispersions of at least two immiscible liquids (usually oil and water), where one of the liquids is the continuous phase while the other liquid is dispersed as spherical or spheroidal droplets (McClements, 2005; McClements *et al.*, 2009). Usually, these systems are stabilized using emulsifiers, that are molecules able to be adsorbed into droplet surfaces thanks to the presence of hydrophilic and lipophilic groups. Some examples of emulsifiers are proteins, polysaccharides, polar lipids, surfactants, etc. (McClements, 2005). Depending on spatial distribution of the two phases, emulsions can be classified as conventional emulsion, such as oil in water (O/W), and water in oil (W/O), or multiple emulsion, such as, oil in water in oil (O/W/O), and water in oil in water (W/O/W) (McClements *et al.*, 2009). Emulsions can be further categorized taking into account their mean particle diameter as well as their thermodynamic stability. In particular, taking as an

example O/W systems, emulsions or macroemulsions are defined as thermodynamically unstable dispersions of oil spherical droplets with mean radii in the 100 nm – 100 µm range dispersed in an aqueous phase (McClements & Rao, 2011). When the mean radii of emulsions are reduced in the 10 – 100 nm range, systems are defined as nanoemulsions (McClements, 2012; McClements & Rao, 2011). Finally, O/W microemulsions are, by definition, thermodynamically stable isotropic dispersions of oil spheroidal droplets with mean radii in the 2 – 100 nm range dispersed in an aqueous phase (Augustin & Hemar, 2009; McClements, 2012; McClements & Rao, 2011; Rao & McClements, 2011). Another interesting property of emulsified systems is their optical appearance. In particular, emulsions appear optically turbid or opaque due to the strong light scattering of their particles, on the contrary, nano and microemulsions appear optically transparent or opalescent (slightly turbid) due to the limited light scattering of their small particles (McClements & Rao, 2011). Emulsions are generally produced using the so called high-energy methods, where disruptive forces generated by mechanical devices (such as high pressure valve homogenizer, microfluidizer, and ultrasonic homogenizer) are used to obtain a dispersion of oil droplets in an aqueous phase (McClements, 2005). On the other hand, microemulsions are mainly obtained using low-energy methods allowing the spontaneous formation of oil droplets in systems containing two immiscible phases (oil and water) and a proper emulsifier (Anton & Vandamme, 2009; McClements & Rao, 2011). Different low-energy methods have been proposed in literature: spontaneous emulsification (SE) (Solans & Solè, 2012; Yang, Marshall-Breton, Leser, Sher, & McClements, 2012), emulsion point inversion (EPI) (Anton, Benoit, & Saulnier, 2008; Ostertag, Weiss, & McClements, 2012), phase inversion composition (PIC) (Solans & Solè, 2012; Yu, Li, Xu, Hao, & Sun, 2012), and phase inversion temperature (PIT) (Anton & Vandamme, 2009; McClements & Rao, 2011; Solans & Solè, 2012) methods. Finally, nanoemulsions can be obtained using both high- and low-energy methods, modulating the processing parameters and system composition (Kentish, Wooster, Ashokkumar, Balachandran, Mawson, & Simons, 2008; Sadeghpour Galooyak & Dabir, 2015; Solans & Solè, 2012; Wooster, Golding, & Sanguansri, 2008). The formation of macro, nano, or microemulsions, greatly depends on single components characteristics (aqueous phase, lipid phase, and emulsifiers), besides the applied preparation method. Indeed, viscosity, density, polarity, physical state of lipid phase are some examples of characteristics that have to be taken into account to drive the formation of emulsified systems. As an example, oils with high viscosity tend to form emulsions with higher mean droplets radii in a O/W emulsion (McClements & Rao, 2011). When saturated TAGs are used in emulsified systems, resulting emulsions are composed by solid lipid particles dispersed in a liquid aqueous phase (McClements, 2013; Weiss, Decker, McClements, Kristbergsson, Helgason, & Awad, 2008). Important characteristics of the aqueous phase that are often used to modulate the formation of emulsified systems are pH, ionic strength, polarity, viscosity, and density. Indeed, when proteins and polysaccharides are used as stabilizing agents, pH can be used to charge the stabilizer on droplet surface and increase the stability of the resulting droplet (Chanamai & McClements, 2002; Combrinck, Otto, & du Plessis, 2014). Finally, emulsifiers chemical structure, physical state, as well as concentration, number of lipophilic and hydrophilic groups and their dependence on temperature can lead to the formation of macro, nano, or microemulsions (McClements, 2005; McClements & Rao, 2011). Moreover, in some cases, when emulsifier concentration is enough to allow their interaction, a gelled emulsified system can be formed. One example that have been studied by different authors are gelled emulsions prepared using saturated monoglyceride (Batte, Wright, Rush, Idziak, & Marangoni, 2007a, 2007b; Calligaris, Da Pieve, Arrighetti, & Barba, 2010). Indeed, monoglyceride can form different lamellar bilayers around oil droplets entrapping high quantities of oil. At high water content the system appears as a liquid emulsion. Increasing MG content, the walls become continuous

from one droplet to the next leading to a continuous solid network. The material that can be obtained is a cream-like matrix with rheological features of spreadable fats and shortenings. The properties of the formed gel are affected by a number of compositional and processing factors, such as MG and co-surfactant type and concentration, temperature, application of shear, aqueous phase pH and ionic strength, and presence of an oil gelling material (such as waxes) (Batte *et al.*, 2007a, 2007b; Blake & Marangoni, 2015b; Goldstein, Marangoni, & Seetharaman, 2012). However, gelled emulsified systems can be also obtained gelling the continuous phase. On this topic, Chung, Degner, and McClements (2014) obtained a semi-solid O/W emulsion using starch as gelling material of the aqueous phase. Firoozmand and Rousseau (2013) explored the possibility to use the thermodynamic incompatibility of mixtures of starch and gelatin in water to obtain an oil in water multiple emulsion. The obtained material was characterized by a droplet-type or bicontinuous gel morphologies and rheological properties that were dependent on oil proportion, its addition to the initial phase and presence of a surfactant such as polysorbate 20. Patel, Rajarethinem, Gredowska, Turhan, Lesaffer, De Vos, Van de Walle, and Dewettinck (2014b) used waxes from lac insects to gel the oil phase (continuous phase) of a W/O emulsion.

Due to emulsified systems versatility and tunability, their application as food structuring systems, substitutes of certain ingredients such as hydrogenated/saturated fats, and protective and delivery systems for target molecules have been studied. Nano and microemulsions appear of particular interest from a technological point of view in the beverage sector since they could be diluted into appropriate concentration into water solutions to give clear and transparent beverages. In particular, physically stable nanoemulsions prepared with the SE method where fish oil as source of ω -3 fatty acids was used as lipid phase were studied by Walker, Decker, and McClements (2015). Saberi, Fang, and McClements (2013) studied the possible use of SE to prepare nanoemulsions as delivery systems for vitamin E. Finally Saberi, Fang, and McClements (2015) used the same method to prepare optically transparent thermally reversible nanoemulsions for lemon aroma delivery. On the other hand, Zhang, Hayes, Chen, and Zhong (2013) used the PIT method to obtain transparent or opalescent systems to delivery β -carotene dissolved in soybean oil or anhydrous milk fat. Moreover, Rao and McClements (2011) used the PIT method to delivery lemon oil. In both cases, the maximum amount of lipids incorporated in transparent systems was around 10% (w/w). Finally, Su and Zhong (2015) thanks to the PIT method incorporated 1.5% (w/v) lemon oil in transparent emulsions using a mixture of Tween 20 and sodium caseinate.

Regarding monoglyceride gelled emulsions, few applicative examples are available in literature. In particular, most of the studies are focused on bakery products, showing that these emulsions are good candidates for hydrogenated/saturated fats replacing (Goldstein & Seetharaman, 2011; Manzocco, Anese, Calligaris, Quarta, & Nicoli, 2012a; Manzocco, Calligaris, Da Pieve, Marzona, & Nicoli, 2012b).

1.4 Aim and outline of this Ph.D. thesis

This Ph.D. thesis aims to investigate the ability of selected self-assembly molecules to form structures with defined characteristics. To this aim, the attention was focused on fatty alcohols, monoglyceride, triacylglycerols, and Tween 80. All these molecules were tested in hydrophobic media (organogels) or in emulsions, as outlined in Table A. The resulting structures were characterized at three different length scales (nano, micro, and macro) in order to obtain detailed information about the hierarchical organization of the resulting materials.

Table A. Studied systems in this Ph.D. thesis.

Building blocks	Environment	Structure
Fatty alcohols	Hydrophobic	Organogel
Monoglyceride	Hydrophobic	Organogel
	Hydrophobic + hydrophilic	Gelled emulsion
Tristearin	Hydrophobic	Organogel
Tripalmitin	Hydrophobic	Organogel
Tween 80	Hydrophobic + hydrophilic	Transparent emulsion

In particular, this thesis was divided in:

- Part I, polar lipids as structuring agents;
 - Part I A was focused on the self-assembly properties of fatty alcohols and monoglyceride. The ability of fatty alcohols (paragraph 2.1) and monoglycerides (paragraph 2.2) to structure edible oils as well as the ability of monoglycerides to structure emulsions (paragraphs 3.1 and 3.2) were studied;
 - Part I B was focused on the application of selected materials as solid fat replacers as well as polyunsaturated fatty acids delivery and protective systems in sweet bread (paragraph 4.1) and biscuits (paragraph 4.2);
- Part II, delivery systems for lipophilic bioactive compounds. The second part was aimed to study the effect of lipid physical state on physical location (paragraph 5.1) and stability (paragraph 5.2) of β -carotene and curcumin. Finally, the development of nano and microemulsions using the PIT method based on non-ionic surfactant was studied (paragraph 6.1).

PART I

Polar lipids

Aim

The aim of this part is to investigate the self-assembly ability of selected polar lipids as structuring agents in different solvents. To this aim monoglycerides and fatty alcohol were considered. The ability of monoglycerides and fatty alcohols to structure edible oils as well as the ability of monoglycerides to structure emulsions were studied with a particular emphasis on nano, micro and macrostructure. Finally, the possible application of the resulting materials as solid fat replacers as well as polyunsaturated fatty acids delivery and protective systems were studied in sweet bread and biscuits.

PART I A
Polar lipids as structuring agents: basic studies

Binary systems

2.1 Fatty alcohols

2.1.1 Aim of the study

The capacity of fatty alcohols to structure oil has been scarcely studied in literature (Daniel & Rajasekharan, 2003; Gandolfo *et al.*, 2004). Thus, a systematic study on fatty alcohols organogels was carried out to understand the applicability of these molecules as oil gelators. In particular, phase transition behavior of 1-dodecanol, 1-tetradecanol, 1-hexadecanol, 1-octadecanol, 1-eicosanol, and 1-docosanol in peanut oil was studied. The effect of cooling rate, storage time, and carbon chain length on structural, thermal, and mechanical characteristics was studied. All the experimental work described in this paragraph was carried out at the University of Guelph (Canada), under the supervision of prof. Alejandro G. Marangoni.

2.1.2 Materials and methods

2.1.2.1 Materials

1-dodecanol (C₁₂OH, purity ≥ 98%), 1-tetradecanol (C₁₄OH, purity ≥ 97.0%), 1-eicosanol (C₂₀OH, purity ≥ 98.0%), 1-docosanol (C₂₂OH, purity ≥ 98.0%), and isobutanol (2-methyl-1-propanol, purity ≥ 99%) were purchased from Sigma-Aldrich (Oakville, Canada). 1-hexadecanol (C₁₆OH, purity ≥ 99.5%) and 1-octadecanol (C₁₈OH, purity ≥ 95.0%) were purchased from Fluka (Oakville, Canada) and Acros Organics (Ottawa, Canada), respectively. Peanut oil was purchased in a local market.

2.1.2.2 Sample preparation

Organogels were prepared mixing peanut oil with increasing percentage of fatty alcohols at 80 °C in an oven for at least 10 minutes until crystalline material was completely melted. Samples were then mixed using a hot plate magnetic stirrer at 80 °C. The molten system was then transferred into containers for further analysis and cooled quiescently at room temperature (around 22 °C) hereafter called slow cooling or cooled at 7 °C using a thermostatic cell or a circulating water bath (Isotemp 3006D, Fisher Scientific, Ottawa, Canada), hereafter called fast cooling. Samples were then equilibrated at 25 or 20 °C for different times before analysis (2 h, 1, 7, 14, 30, 54 days).

2.1.2.3 Minimum gelling concentration

The minimum gelling concentration was defined as the minimum concentration of fatty alcohol needed to obtain a self-standing sample that did not flow after turning the container up-side down. Samples were prepared pouring around 10 g of molten organogel into 20-mL scintillation vial, and fatty alcohol concentration was gradually increased by 0.5% (w/w) concentration. Each sample was prepared at least in triplicate and tested after 24 h of storage.

2.1.2.4 Back extrusion

Back extrusion analysis was performed using a TA.XT2 texture analyzer (Stable Micro Systems, Texture Technologies Corp., Scarsdale, USA). In particular, molten organogels containing 5% (w/w) fatty alcohols were poured into a 16 mm diameter and 125 mm height disposable culture tube (Fisher Scientific, Pittsburgh, USA) and slow and rapid cooled. The

cylindrical stainless steel probe (height: 89.00 mm, diameter: 9.20 mm) with a truncated spherical head (height: 6.75 mm, diameter: 10.20 mm) was mounted on a 5 kg (49 N) compression head, and samples were penetrated for 30 mm at 1.5 mm/s. Force-time curves were obtained and firmness reported was taken as the average of the final quarter of the test. Five tubes for three independent replicate were tested. All samples were tested after 24 h of storage at 20 °C.

2.1.2.5 Accelerated oil release test (AORT)

Around 1.2 – 1.3 mL of molten sample was placed into 1.5 mL microtubes (Diamed, Mississauga, Canada) and centrifuged at 14000 rpm (12800 x g) for 30 min using a microcentrifuge (Eppendorf mod. 5410, Hamburg, Germany). Prior analysis, the centrifuge was cooled at 7 °C in order to avoid overheating of the samples during centrifugation. The temperature after centrifugation of samples was around 17 – 18 °C. Immediately after centrifugation, microtubes were inverted and oil was drained for 5 min. Residual oil was then removed using absorbing paper. The released oil was computed as percentage ratio between the mass of expressed oil over the total mass of sample.

2.1.2.6 Proton nuclear magnetic resonance (p-NMR)

2.1.2.6.1 Solid fat content (SFC)

SFC measurements were performed using a 20 MHz (0.47 T) mq20 Series Bruker NMR Spectrometer (Bruker, Milton, Canada). Molten organogels containing 5% (w/w) fatty alcohols were poured into 10 mm diameter glass NMR tubes and crystallized isothermally at 20 °C. Resulting samples were then stored for 2 weeks at 20 °C prior analysis. The melting profile of organogels was obtained equilibrating the tubes in a circulating water bath (Isotemp3006D, Fisher Scientific, Ottawa, Canada). Temperature was increased stepwise by 5 °C from 10 to 60 °C and samples equilibrated at each temperature for 30 min before reading.

2.1.2.6.2 T_2 spin-spin relaxation time

Low resolution proton nuclear magnetic resonance was performed on a 20 MHz (0.47 T) mq20 Series Bruker NMR Spectrometer (Bruker, Milton, Canada) connected to a circulating water bath (Isotemp 3006D, Fisher Scientific, Ottawa, Canada) in order to keep the cell temperature at 20 °C. Molten organogels were poured into 10 mm diameter glass NMR tubes and cooled. Samples were subjected to a Carr-Purcell-Meiboom-Gill (CPMG) spin echo pulse sequence where the pulse lengths were obtained using the manufacturer calibration procedure, corresponding in 2.68 μ s for the 90° pulses and 5.24 μ s for the 180° pulse. All the other parameters were adjusted in order to obtain an optimal intensity of the signal, and the pulse delay (τ) was kept as short as possible to minimize effects of chemical exchange and diffusion on the decay curve. The T_2 spin-spin relaxation was calculated from the free induction decay (FID) profile using an inverse Laplace transformation through CONTIN application together with Minispec software v. 2.3 (Bruker, Milton, Canada). Finally, peaks maxima were determined using PeakFit v. 4.12 software (Systat Software, Inc., San Jose, USA) using the best fit tool based on residual errors minimization.

2.1.2.7 Polarized light (PL) microscopy

Samples were analyzed using a Leica DMRXA2 polarized light (PL) optical microscope (Leica Microsystems Canada Inc., Richmond Hill, Canada) connected to a Retiga 1300i CCD digital camera (Retiga, Burnaby, Canada). One drop of molten organogel was placed in the middle of a glass slide and a glass cover slip was centered above the drop, both preheated at 80 °C. Samples were then cooled at room temperature or at 7 °C and stored at 20 °C up to 30 days. Samples were analyzed at room temperature using a 100x and 400x magnification.

Images were acquired and processed using Volocity v. 6.2.1 software (PerkinElmer, Woodbridge, Canada) and saved in *tiff* format with a resolution of 1920 × 1440 pixels. The resulting images were further processed using Image-Pro® Plus v. 6.3 (Media Cybernetics, Inc., Bethesda, MD, USA) in order to obtain crystal sizes. A spatial calibration was first performed by using the 200 µm reference line. Images were converted in gray scale (8 bit) and equalized by best fit tool. Pixels with luminosity in the 70–255 range were associated with crystals. Crystals in each image were subdivided into five classes, depending on the maximum length of the longest line joining two points of the crystal's outline and passing through the centroid (average size): class 1 consisted of crystals with 0 – 5 µm size, class 2 consisted of crystals with 5 – 10 µm size, class 3 consisted of crystals with 10 – 50 µm size, class 4 consisted of crystals with 50 – 100 µm size, and class 5 consisted of crystals with more than 100 µm size. The percentage ratio between the number of crystals belonging to each class and the total number of crystals in the image was calculated.

2.1.2.8 Cryogenic scanning electron microscopy (Cryo-SEM)

The method proposed by Blake and Marangoni (2015c) for sample de-oiling and Cryo-SEM sample preparation was used with some modifications. In particular, a known amount (less than 100 mg) of organogel prepared as reported in minimum gelling concentration paragraph was gently transferred onto 25 mm diameter polycarbonate disks containing 0.4 µm pores (Poretics, AMD Manufacturing Inc., Mississauga, Canada). This disk was laid on a piece of Whatman 1 filter paper and samples were de-oiled by adding isobutanol dropwise on organogel surface. The binary system:oil ratios were 1:0.5, 1:10, 1:20, and 1:25 for samples containing 5% (w/w) C₁₆OH, C₁₈OH, C₂₀OH, and C₂₂OH, respectively. After de-oiling, samples were dried for 48 h before imaging. The polycarbonate paper, loaded with de-oiled sample, was then cut in squares of 1 cm x 1 cm and glued on a copper holder using Tissue-Tek O.C.T. Compound (Canemco Supplies, St. Laurent, Canada). The copper holder was then plunged into nitrogen slush (-207 °C) and subsequently transferred to a sample preparation chamber (less than -160 °C, under vacuum) (Emitech K1250x, Ashford, UK) for platinum sputter coating. The final thickness of platinum coat was around 20-30 nm. The copper holder was finally transferred to the SEM unit (Hitachi S-570, Tokyo, Japan), which was at -155 °C under vacuum. Samples were imaged using an acceleration voltage of 10 kV and Quartz PCI v. 8 (Quartz Imaging Corp, Vancouver, Canada) application software was used to capture images of the samples. Images were saved in *tiff* format resulting in 1696 x 2048 pixels.

2.1.2.9 Differential scanning calorimetry (DSC)

DSC analysis was carried out using a Mettler Thermal Analysis DSC 1 (Mettler-Toledo, Inc., Mississauga, Canada). Heat flow and temperature calibration were achieved using indium (heat of fusion 28.45 J/g, m.p. 156.6 °C). Pure fatty alcohols and binary systems with different concentration of fatty alcohols were prepared according to the sample preparation section (paragraph 2.1.2.2, pag. 23) and 6 – 8 mg of sample were carefully weighted in 40 µL aluminum DSC pans, closed with hermetic sealing. Samples were heated at 80 °C for 10 min, cooled from 80 to 5 °C at 5 °C/min, equilibrated for 10 min, and heated from 5 to 80 °C at 5 °C/min under nitrogen flow (20 mL/min). An empty pan was used as a reference in the DSC cell. The peak melting temperature (T_m) was taken as the minimum value of heat flow during transition. Total peak enthalpy was obtained by integration of the melting curve. The machine equipment program STARe ver. 12.10a (Mettler-Toledo, Inc., Mississauga, Canada) was used to plot and analyze the thermal data. Finally, Hildebrand equation (eq. 2.1) was used to model thermal data.

$$\ln x = \frac{\Delta H_f}{R} \left(\frac{1}{T_f} - \frac{1}{T_m} \right) \quad (\text{eq. 2.1})$$

where x , ΔH_f , and T_f are the molar fraction or the weight fraction, melting enthalpy (J/mol), and the melting temperature (K) of the crystalline compound, respectively. R is the universal gas constant (8.314 J/mol K), and T_m is the melting temperature of the binary mixture.

2.1.2.10 Powder X-ray diffraction (XRD)

Molten binary systems were poured in a glass sample holder with an area of 20×20 mm and depth of 1 mm. After cooling, sample excess was scraped from the glass sample holder using the edge of a spatula. Organogels containing 5% (w/w) fatty alcohols were stored at 25 °C and analyzed at different times using a Rigaku Multiflex X-ray Diffractometer (RigakuMSC Inc., The Woodlands, USA), while samples containing 100, 70, and 30% (w/w) fatty alcohols were analyzed after 1 h of equilibration at 20 °C. X-rays were generated setting the copper source at 44 kV and 40 mA resulting in 1.54 Å X-ray wavelength. The setting for the divergence slit, scattering slit, and receiving slit, were 0.5°, 0.5°, and 0.3 mm, respectively. Temperature of samples during data collection were controlled using a water bath (Isotemp mod. 6200, Fisher-Scientific, Inc., Pittsburgh, USA) connected to a flat surface heat exchanger placed under the glass sample holder and a thermocouple placed underneath the glass sample holder was used to monitor the temperature during the entire experiment. Samples were scanned from 1.1 to 35.0° at a scanning speed of 1° per min. Resulting diffraction patterns were processed and analyzed using MDI Jade v. 9.0.1 (Materials Data Inc., Livermore, CA, USA). In particular, a spline cubic baseline was mounted on diffraction pattern as background line and peaks were determined using a profile shape function (i. e. Pearson-VII, pseudo-Voigt, Gaussian, and Lorentzian) that allowed residual error of fit to be minimized.

2.1.2.11 Ultra small angle X-ray scattering (USAXS)

Molten binary systems were poured in a sample holder composed by a glass cover slip attached to a 1 mm thick press-to-seal silicon isolator with holes 8-9 mm in diameter (Grace Bio-Labs, Bend, USA). After the sample was crystallized at room temperature, another glass cover slip was attached to the silicon isolator to avoid sample structural damaging.

1D-collimated USAXS measurements were carried out at beam-line 9 ID at the Advanced Photon Source (APS) (Argonne National Laboratory, Illinois, USA). A Bonse-Hart instrument was used to collimate the X-rays and to collect the data (Ilavsky, Zhang, Allen, Levine, Jemian, & Long, 2013; Long, Jemian, Weertman, Black, Burdette, & Spal, 1991). The basic set up for edible fat samples was described by Peyronel, Pink, and Marangoni (2014b), which can be summarized as a pair of collimating crystals, followed by a ion chamber, the isolator-sample holder mounted on a plate, a pair of analyzer crystals, and a photodiode detector. During experiments at the APS data were acquired using the Spec software for diffraction experiments.

Data reduction and analysis were performed using the Irena IgorPro-based software (Ilavsky & Jemian, 2009) following the procedure proposed by Peyronel *et al.* (2014b). In particular, the Unified Fit model (Beaucage, 1995, 1996) was used, which employs a non-linear regression analysis. The analysis consists of the identification of different regions (levels) in the q -space, which are characterized by two parameters: (i) a parameter P related to the slope of the curve which gives information about the internal structure of the scatterer via a fractal dimension, D , (Pink, Quinn, Peyronel, & Marangoni, 2013) and (ii) a parameter R_g , which identifies the average radius of gyration of the scatterers giving rise to the structure with the fractal dimension D . Edible fat systems had shown a maximum of 3 slopes and two radii of

gyration for level 1 and level 2 when Unified Fit was used (Peyronel, Quinn, Marangoni, & Pink, 2014c).

Through models, computer simulations (Pink *et al.*, 2013; Quinn, Peyronel, Gordon, Marangoni, Hanna, & Pink, 2014) and experiments (Peyronel, Ilavsky, Mazzanti, Marangoni, & Pink, 2013; Peyronel, Ilavsky, Pink, & Marangoni, 2014a), the D value has been shown to be a reliable parameter. On the other hand, the R_g is the exponent in the formula (Beaucage & Schaefer, 1994) and it should be considered only as an indicator of sizes, rather than a precise value. Having this in mind, R_g was used to calculate the average radius (R) of the scatterers as spheres (eq. 2.2) (Peyronel *et al.*, 2013).

$$R = \sqrt{\frac{5}{3}} R_g \quad (\text{eq. 2.2})$$

2.1.2.12 Data analysis

All determinations were expressed as the mean \pm standard error of at least two measurements from three experiment replications ($n \geq 6$), if not otherwise specified. Data were processed using GraphPad Prism v. 5.03 (GraphPad Software, Inc., La Jolla, USA). Statistical analysis was performed using R v. 3.0.2 (The R foundation for Statistical Computing). Bartlett's test was used to check the homogeneity of variance, one way ANOVA was carried out and Tukey-test was used as post-hoc test to determine statistical significant differences among means ($p < 0.05$). Linear regression analysis by least squares regression was performed and the goodness of fit was evaluated on the basis of statistical parameters of fitting (R^2 , p , standard error) and the residual analysis.

2.1.3 Results and discussion

2.1.3.1 Thermal, nanostructural, and aggregating characterization

Figure 2.1A shows the crystallization curves of binary systems containing peanut oil and different percentages of $C_{20}OH$, chosen as an example among fatty alcohols considered in this study.

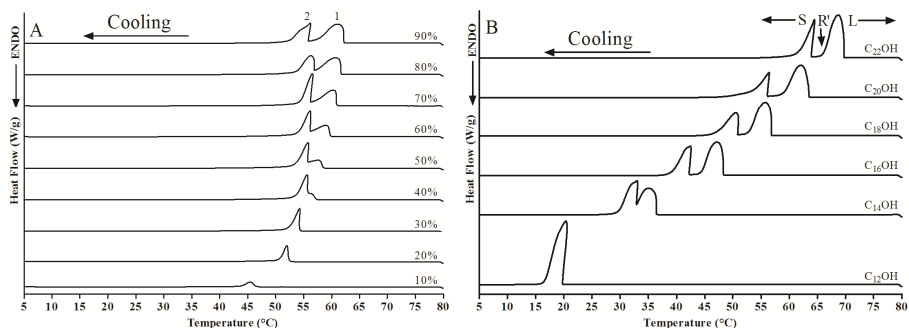


Figure 2.1. Crystallization curves of binary systems containing peanut oil and different percentages of $C_{20}OH$ (A) and different pure fatty alcohols (B) obtained at 5 °C/min.

Two exothermic peaks were recorded during cooling of the pure $C_{20}OH$ fatty alcohol (Figure 2.1B) as well as mixtures containing from 90 to 40% (w/w) fatty alcohol concentration (Figure 2.1A). It can be noted that peak 1 shifted to low temperature as the concentration of fatty alcohol decreased; while no changes in peak temperature was noted for peak 2. Below 40% (w/w) $C_{20}OH$, the peak 1 disappeared or appeared as shoulder of peak 2. This behavior was observed for all other considered fatty alcohols ($C_{22}OH$, $C_{18}OH$, $C_{16}OH$, and $C_{14}OH$).

The only difference recorded was the change of the critical percentage at which two separated peaks were detectable for $C_{14}OH$ samples. In this case, below 60% (w/w) content of the fatty alcohol only peak 2 was recorded (data not shown).

As shown in Figure 2.1B, the crystallization temperature of peak 1 and 2 progressively decreased as fatty alcohol chain length decreased. As reported in literature, fatty alcohols with both odd and even carbon chain length show similar crystallization process to *n*-alkanes and the following transitions during cooling have been reported: liquid (L) \rightarrow rotator phase (R') \rightarrow solid (S) (Metivaud, Lefevre, Ventolà, Negrier, Moreno, Calvet, Mondieig, & Cuevas-Diarte, 2005; Ventolà, Calvet, Cuevas-Diarte, Oonk, & Mondieig, 2004; Ventolà, Ramírez, Calvet, Solans, Cuevas-Diarte, Negrier, Mondieig, van Miltenburg, & Oonk, 2002; Yamamoto, Nozaki, & Hara, 1990). To confirm the presence of the rotator phase, pure fatty alcohols were analyzed using XRD. Figure 2.2 shows the XRD patterns recorded for pure $C_{22}OH$, $C_{20}OH$, $C_{18}OH$, $C_{16}OH$, and $C_{14}OH$, at temperature in between peak 1 and 2 (65.8, 58.2, 52.0, 44.1, and 33.3 °C, respectively). It was found that pure $C_{14}OH$ and $C_{16}OH$ showed a single peak in the WAXS region ($15^\circ \leq 2\theta \leq 25^\circ$) at 4.18 Å that could be ascribed to a pseudo-hexagonal phase. This rotator phase corresponds to R'_{II} as reported by Metivaud *et al.* (2005). On the other hand, pure $C_{18}OH$, $C_{20}OH$, and $C_{22}OH$ showed three peaks in the WAXS region that were associated to a pseudo-monoclinic rotator phase namely called R'_{IV} as reported by Ventolà, Calvet, Cuevas-Diarte, Ramirez, Oonk, Mondieig, and Negrier (2004).

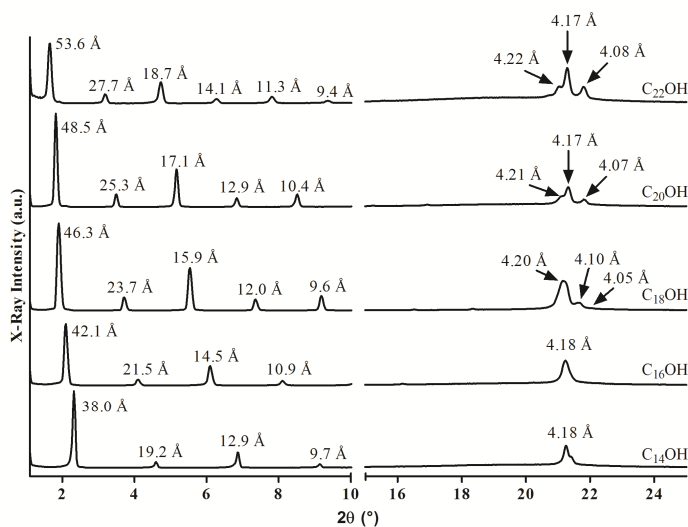


Figure 2.2. XRD patterns recorded for neat $C_{22}OH$, $C_{20}OH$, $C_{18}OH$, $C_{16}OH$, and $C_{14}OH$ at 65.8, 58.2, 52.0, 44.1, and 33.3 °C, respectively.

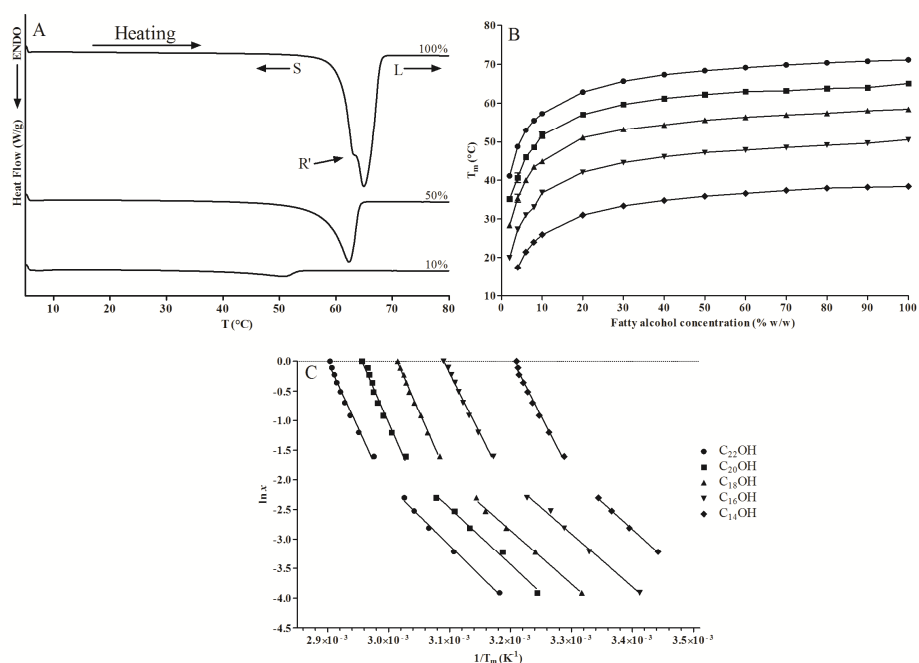


Figure 2.3. Melting curves of systems containing 100, 50, and 10% (w/w) C₂₀OH in peanut oil (A) obtained at 5 °C/min, peak melting temperature as a function of concentration of fatty alcohols in peanut oil for all binary systems considered (B), and Hildebrand plot for binary systems with regression lines (C).

The melting behaviors of pure fatty alcohols as well as fatty alcohols binary systems were then studied. Figure 2.3A shows the melting curves of selected systems containing 100, 50, and 10% (w/w) C₂₀OH. One main melting peak was recorded in all cases. Other fatty alcohols showed similar behavior (data not shown).

In Figure 2.3B the temperature of the melting peak of all the samples considered was reported as a function of fatty alcohol concentration in peanut oil. It should be noted that peak temperature decreased as fatty alcohol concentration also decreased. In particular, it was found that all systems showed a decrease of *circa* 10 °C from 100 to 20% (w/w) fatty alcohol concentration, whereas about 15 °C decrease of the peak melting temperature was observed in the region 10 to 2% (w/w) fatty alcohol concentration. Finally, it can be noted that the peak melting temperature increased with the length of the fatty alcohol carbon chain. This is in agreement with other authors considering binary systems composed of crystalline compounds, such as triacylglycerols (TAGs), waxes, and saturated fatty acids, diluted in liquid oil (Ahmadi, Wright, & Marangoni, 2008; Blake *et al.*, 2014; T. Inoue, Hisatsugu, Yamamoto, & Suzuki, 2004).

The solubilization process of a crystalline compound in liquid oil can be modelled using the Hildebrand equation (eq. 2.1), as described by Ahmadi *et al.* (2008). When a straight line in a ln x vs 1/T_m plot is observed, it can be hypothesized that the solubility of the crystalline compound in oil can be described as ideal (Ahmadi *et al.*, 2008). Figure 2.3C shows the Hildebrand plot for the binary systems considered. It can be noted that the Hildebrand equation cannot be used to describe the melting temperature dependence of the fatty alcohol concentration, since deviations were observed below 10% (w/w) fatty alcohol concentration.

Thus, the solubilization of fatty alcohol in peanut oil did not follow an ideal behavior probably due to the interactions with the solvent.

For this reason, to describe the observed data, two different domains were considered: one from 0 to $-1.61 \ln x$ (corresponding to 100 and 20% w/w fatty alcohol concentration) and from -2.30 to $-3.91 \ln x$ (corresponding to 10 and 2% w/w fatty alcohol concentration). In the two regions, two different Hildebrand equations (eq. 2.1) describing the dissolution process were obtained ($R^2 \geq 0.97$; $p < 0.05$). The regression coefficients obtained (Table 2.1) can be used to calculate the melting temperature of a mixture corresponding to a defined fatty alcohol content in the binary systems. For instance, considering butter as target fat that has a melting temperature of about 34 °C, the calculated concentrations of C₁₄OH, C₁₆OH, C₁₈OH, C₂₀OH, and C₂₂OH needed to mimic butter was 38.4, 8.2, 3.5, around 2, and less than 2% (w/w), respectively.

Table 2.1. Hildebrand equation regression coefficients (slopes and intercepts) for binary systems containing the studied fatty alcohols in the selected domains.

Fatty alcohol	First domain (0 to -1.61)		Second domain (-2.30 to -3.91)	
	Slope (K)	Intercept (-)	Slope (K)	Intercept (-)
C ₂₂ OH	-22585 ± 1099	65.5 ± 3.2	-10157 ± 411	28.4 ± 1.3
C ₂₀ OH	-23777 ± 1353	70.3 ± 4.0	-9582 ± 517	27.2 ± 1.6
C ₁₈ OH	-23568 ± 490	71.0 ± 1.5	-9054 ± 271	26.1 ± 0.9
C ₁₆ OH	-20582 ± 660	63.6 ± 2.1	-8976 ± 427	26.7 ± 1.4
C ₁₄ OH	-20179 ± 881	64.7 ± 2.8	-9335 ± 272	28.9 ± 0.9

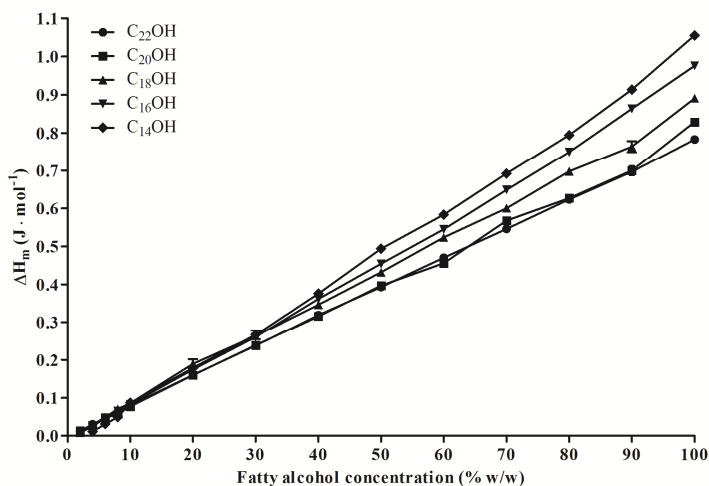


Figure 2.4. Melting enthalpy (ΔH_m) as a function of fatty alcohols concentration in peanut oil.

Finally, the melting enthalpy data were calculated. In Figure 2.4 melting enthalpy as a function of fatty alcohol concentration is reported. As expected, the melting enthalpy increased linearly as the amount of crystalline compound in the binary system increased ($R^2 > 0.99$ and $p < 0.05$). The melting enthalpy of shorter chain fatty alcohols was higher than that of longer fatty alcohols at fatty alcohol content $> 50\%$ (w/w) in the system. Moving to lower concentrations ($< 50\%$ w/w) this trend disappeared and no differences in melting enthalpy were observed as a function of fatty alcohol chain length. These results can be explained considering the different packing of the carbon chains. In particular, a more dense

crystalline structure is expected to require more energy to destroy the structure. Thus, it can be hypothesized that C₁₄OH packed in a more dense phase at high concentrations compared to other fatty alcohols.

The further part of experiments was addressed to understand the effect of fatty alcohols concentration on their crystalline structure. Figure 2.5A shows the WAXS and SAXS patterns of binary systems containing C₂₀OH at different concentrations after fast cooling at 7 °C. The WAXS region ($2\theta \geq 15^\circ$) of pure C₂₀OH as well as mixtures containing more than 30% (w/w) fatty alcohols showed peaks at 4.28, 4.10, 3.97, and 3.63 Å characteristics of the monoclinic γ -form, as discussed by Ventolà *et al.* (2002) and Metivaud *et al.* (2005). As regards the SAXS region ($2\theta < 8^\circ$), one main peak at 45.6 Å corresponding to the d_{001} , followed by its higher order reflection peaks, was observed. The results in the SAXS region was previously found in monoglyceride binary systems and waxes binary systems by Da Pieve *et al.* (2010) and Blake *et al.* (2014), respectively. These authors suggested that the crystalline compounds organize themselves in lamellar structures with a thickness equal to the d_{001} reflection (45.6 Å in the present study). It can be noted that the lamellar thickness remained constant moving from 100 to 30% (w/w) C₂₀OH concentration (Figure 2.5A).

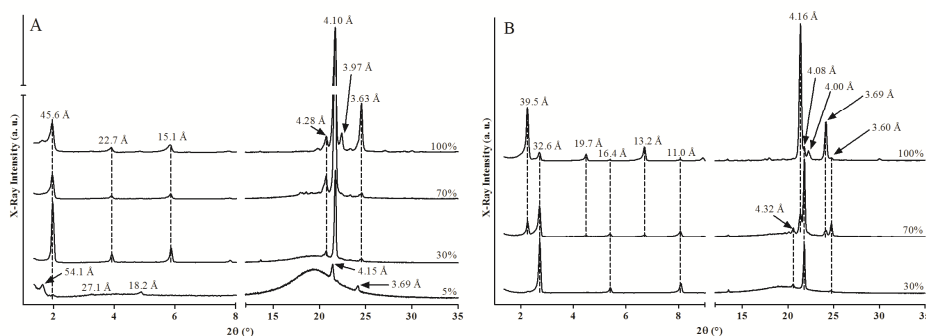


Figure 2.5. XRD patterns for binary systems containing C₂₀OH (A) and C₁₄OH (B) in peanut oil at different concentrations fast cooled.

Different was the behavior of the 5% (w/w) C₂₀OH containing system that presented in WAXS region two peaks at 4.15 and 3.69 Å that can be related to the presence of orthorhombic β' -form. On the other hand, two peaks at 45.6 Å and 54.1 Å were observed in the SAXS region. These peaks suggested that during cooling two crystal families were formed. Similar results were found also for binary systems containing C₂₂OH, C₁₈OH, and C₁₆OH (data not shown). The lamellar thickness of systems containing 5% (w/w) C₂₂OH, C₂₀OH, C₁₈OH, and C₁₆OH are reported in Table 2.2. It can be observed that, as expected, the lamellar thickness decreased as the length of the carbon chain of the fatty alcohols decreased. The trend was linear ($R^2 > 0.99$, $p < 0.05$). It is interesting to note that by changing the cooling methodology (fast or slow) to obtain samples, no differences in XRD results were found (data not shown).

The only exception to the described behaviors were the samples containing C₁₄OH at different concentrations (Figure 2.5B). First of all, the 5% (w/w) C₁₄OH system did not form a semi-solid material and thus was not analyzed. Systems containing 100, 70 and 30% (w/w) C₁₄OH showed the contemporary presence of both γ - and β' -form with two different lamellar thickness.

Table 2.2. *d* values for the two crystal families found in the SAXS region in binary systems containing 5% (w/w) $C_{22}OH$, $C_{20}OH$, $C_{18}OH$, and $C_{16}OH$.

Fatty alcohol	Crystal family 1 (Å)	Crystal family 2 (Å)
$C_{22}OH$	59.5	49.8
$C_{20}OH$	54.1	45.6
$C_{18}OH$	48.5	41.2
$C_{16}OH$	43.6	36.8

Samples containing 5% (w/w) of fatty alcohols were then stored at 25 °C for up to 54 days to highlight possible polymorphic changes. During storage, no changes in crystal structure were detected. However, significant modifications of the peaks intensity was recorded: the intensity of crystal family 1 progressively decreased in concomitance with an increase of the intensity of crystal family 2 (Figure 2.6).

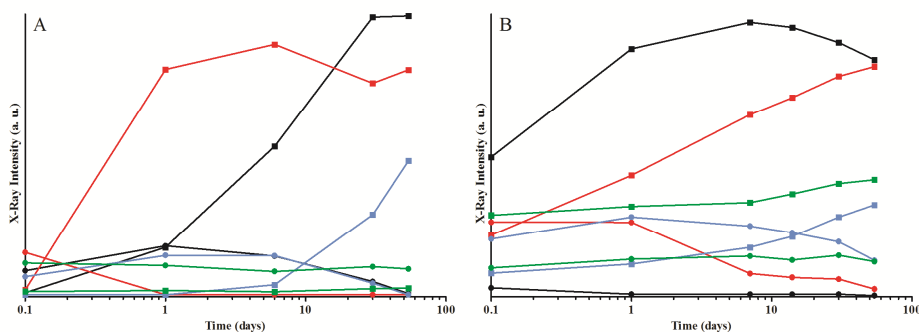


Figure 2.6. Evolution of crystal family 1 (○) and 2 (□) for binary systems containing 5% (w/w) $C_{22}OH$ (green), $C_{20}OH$ (blue), $C_{18}OH$ (red), and $C_{16}OH$ (black) in peanut oil fast (A) and slow (B) cooled.

These events could be due to the progressive interpenetration of the fatty alcohol acyl chains during storage. Moreover, it could not be underestimated that possible release of oil from lamellas. A schematic representation of these events is reported in Figure 2.7.

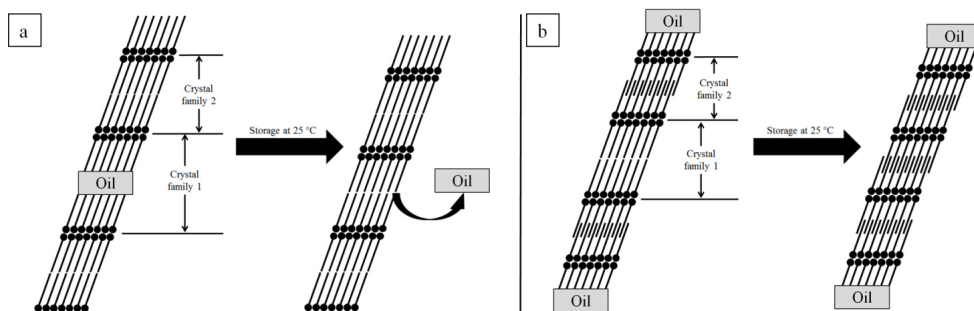


Figure 2.7. Schematization of possible fatty alcohol binary system crystals modifications during storage.

To determine if the cooling rate and/or the fatty alcohol carbon chain length affected the rate of conversion from crystal family 1 to crystal family 2, the time at which the intensity of

family 1 peak matched family 2 peak intensity ($t_{1:1}$) was calculated. Table 2.3 shows the $t_{1:1}$ for binary systems containing 5% (w/w) different fatty alcohols cooled at 7 °C (fast cooling) or ambient temperature (slow cooling). It can be noted that both cooling methodologies and fatty alcohol chain length affected the $t_{1:1}$. The higher the carbon chain length the longer the $t_{1:1}$ for fast cooled samples. The only exception was that of the binary system containing C₁₈OH and can be attributed to the lower purity of C₁₈OH compared to the other fatty alcohols considered.

Comparing slow and fast cooled samples, $t_{1:1}$ of binary systems containing C₁₈OH and C₂₀OH was not affected by cooling methodology. On the other hand, systems containing C₁₆OH and C₂₂OH highlighted the influence of the cooling method. The slow cooling allowed these systems to form crystals in the more stable form (lower lamellar thickness).

Table 2.3. Time at which the intensity of family 1 peak matched family 2 peak intensity ($t_{1:1}$) of binary systems containing 5% (w/w) of different fatty alcohols in peanut oil cooled at 7 °C (fast cooling) and ambient temperature (slow cooling).

Fatty alcohol	$t_{1:1}$ (days)	
	Fast cooling	Slow cooling
C ₂₂ OH	> 54	< 0.1
C ₂₀ OH	10	10.5
C ₁₈ OH	0.14	0.16
C ₁₆ OH	1	< 0.1

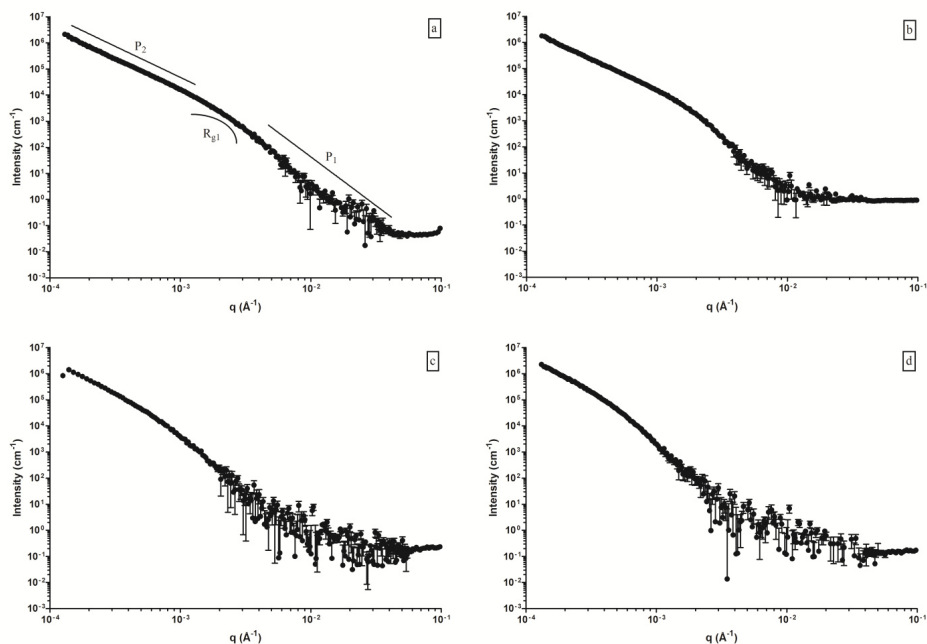


Figure 2.8. USAXS data for binary systems containing 5% of C₂₂OH (a), C₂₀OH (b), C₁₈OH (c), and C₁₆OH (d) in peanut oil slowly cooled.

Finally, ultra-small X-ray scattering (USAXS) was applied to characterize the supramolecular structures formed by fatty alcohols in binary systems. USAXS is a new and powerful non-destructive analytical technique able to investigate crystalline structures from

nanoscopic to microscopic level (Peyronel *et al.*, 2014a). With USAXS it is possible to investigate a diffraction region which is not accessible using conventional X-ray diffraction experimental setup. Crystalline aggregates from 10 nm to more than 5 μm can be characterized (Peyronel *et al.*, 2014a). The application of USAXS on edible fats was introduced by Pink *et al.* (2013), Peyronel *et al.* (2013), and Peyronel *et al.* (2014b). These authors used computer simulations to predict and validate experimental USAXS patterns on tristearin or tripalmitin in triolein at different concentrations. Figure 2.8 shows the USAXS data for binary systems containing 5% (w/w) C₂₂OH (a), C₂₀OH (b), C₁₈OH (c), and C₁₆OH (d) cooled at room temperature. Data were interpreted applying the Unified Fit model. This model describes the scattering of systems containing different structures idealized approximately as spherical objects combining the Guinier's law and the Porod power law. The first law is reflected as a knee in a log intensity - log q plot, whereas the second law is reflected as a straight line (Figure 2.8). The spherical objects are characterized by an average radius of gyration (R_g), which can be calculated using the Guinier's law, while information on the internal structure of these objects is given by the exponent P of the Porod power law. Different structural levels can be found in systems containing edible fats as described by Peyronel *et al.* (2014a). The structural level can be described by its R_g and P parameters. In the present study, two structural levels characterized by P_1 , R_{g1} , and P_2 parameters were detected (Figure 2.8 and Table 2.4). As regards the first structural level, all the systems under study showed a $|P_1|$ value greater than 4. This means that the surfaces of the aggregating particles are diffuse and the edge between solid and liquid phase is not well defined. R_{g1} was then used to calculate the radii of the spherical objects (R). It can be noted that binary systems containing C₂₂OH and C₂₀OH showed similar radii. These spheres were smaller than those formed by C₁₈OH and C₁₆OH (Table 2.4). Finally, in the second structural level it was found that the $|P_2|$ values were between 2 and 3. According to Peyronel *et al.* (2014b), when $1 \leq |P| < 3$, the P value indicates the mass fractal dimension of the aggregates. In this case, these spherical objects aggregate (probably *via* reaction limited cluster-cluster aggregation, RLCA) to form a disordered distribution of mass embedded in a 3D space.

Table 2.4. Unified Fit model parameters obtained for binary systems containing 5% (w/w) fatty alcohol slowly cooled.

Fatty alcohol	$ P_1 $ (-)	R_{g1} (\AA)	R (\AA)	$ P_2 $ (-)
C ₂₂ OH	4.35	1477	1907	2.35
C ₂₀ OH	4.30	966	1247	2.26
C ₁₈ OH	4.19	5498	7098	2.60
C ₁₆ OH	4.66	5925	7649	2.70

2.1.3.2 Micro, macro, and mechanical characterization

Figure 2.9 shows the minimum gelling concentration of fatty alcohols with different carbon chain length in peanut oil as affected by cooling rate. Above each curve, systems formed self-standing materials that did not flow after the container was turned up-side down. It can be noted that as the fatty alcohol chain length increased, the minimum gelling concentration decreased for both cooling rates. Organogels slowly cooled showed a lower minimum gelling concentration compared to fast cooled samples. The difference in terms of concentration between curves for each fatty alcohol can be considered as the sensitivity of the material to cooling rates. This sensitivity was higher for organogels containing C₁₄OH, C₁₆OH, and C₁₈OH compared to organogels containing C₂₀OH, and C₂₂OH.

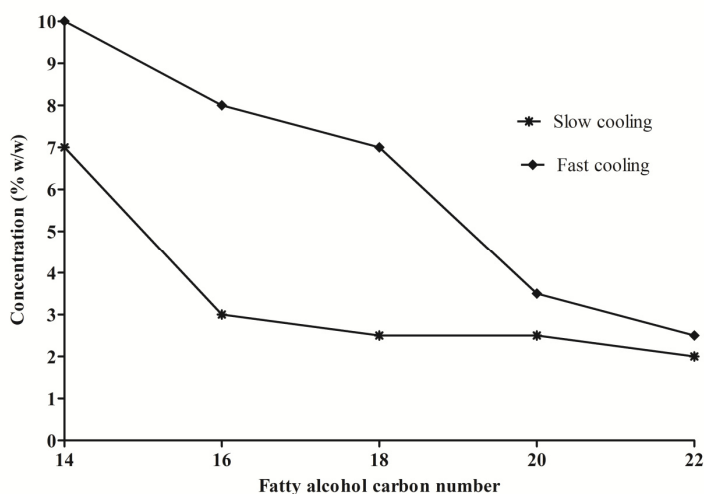


Figure 2.9. Minimum gelling concentration for organogels containing fatty alcohols with different carbon chain length and peanut oil obtained using fast and slow cooling rates.

These differences can be related to the carbon chain length as well as to solubility of the crystalline compound in oil after crystallization. As pointed out by Co and Marangoni (2012), a good gelator has to be partially insoluble in oil to be able to crystallize and form a gel network, and partially soluble to interact with the surrounding solvent entrapping it in the crystalline network. In the light of applying these systems in food products as hydrogenated/saturated fat replacers, a convenient fatty alcohol percentage to be used is 5% (w/w). C₁₄OH containing organogel did not crystallize below 5% (w/w) using both cooling rates, thus it was not further considered.

In the present study selected organogels containing 5% (w/w) fatty alcohols were analyzed using p-NMR in order to determine the solid fat content (SFC) as a function of temperature.

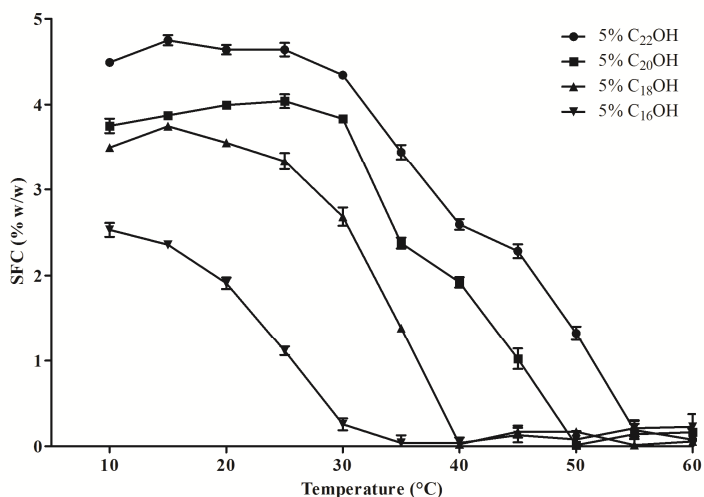


Figure 2.10. Solid fat content (SFC) as a function of temperature for organogels containing 5% (w/w) C₂₂OH (●), C₂₀OH (■), C₁₈OH (▲), and C₁₆OH (▼) in peanut oil during melting.

Figure 2.10 shows the evolution of SFC as a function of temperature during melting of organogels containing 5% (w/w) C₂₂OH, C₂₀OH, C₁₈OH, and C₁₆OH. It can be noted that all considered organogels did not show the theoretical SFC value (5% w/w) even at low temperatures, indicating that part of the fatty alcohol was solubilized in the oil. The figure shows also that the higher the fatty alcohol chain length the higher the SFC at the same temperature. This trend was observed in the entire melting profile. As the temperature increased, samples decreased their SFC until complete melting in the following order: C₁₆OH – C₁₈OH – C₂₀OH – C₂₂OH. Finally, it can be noted that the melting process for these organogels is quite slow. For instance, the decrease of SFC for C₂₂OH containing organogel started at 30 – 35 °C and the sample completely melted at 55 – 60 °C.

Organogels used as fat replacer have also to have firmness similar to that of the replaced fat and the ability to retain oil over time (Co & Marangoni, 2012; Rogers *et al.*, 2009b).

Table 2.5. Back extrusion results for samples containing 5% (w/w) C₂₂OH, C₂₀OH, C₁₈OH and C₁₆OH in peanut oil slow and fast cooled after 1 days of storage at 20 °C.

Fatty alcohol	Force (N)	
	Slow cooling	Fast cooling
	C ₂₂ OH	0.654 ± 0.027
C ₂₀ OH	0.824 ± 0.033	0.514 ± 0.027
C ₁₈ OH	0.800 ± 0.100	n.m.
C ₁₆ OH	0.319 ± 0.024	n.m.

n.m. = not measured (systems were below critical gelling concentration)

Table 2.5 shows the results of back extrusion analysis for samples containing 5% (w/w) C₂₂OH, C₂₀OH, C₁₈OH and C₁₆OH slow and fast cooled after 1 days of storage at 20 °C. It can be noted that for slow cooling, the highest force needed to penetrate the samples was reached by systems containing C₂₀OH and C₁₈OH, followed by C₂₂OH and C₁₆OH. As regards fast cooling rate, it has to be remembered that systems containing 5% (w/w) C₁₆OH and C₁₈OH did not form a plastic material since they were below the minimum gelling concentration (Figure 2.9), thus they were not analyzed. C₂₀OH containing organogel showed a reduction of force between cooling rates. On the contrary, systems containing C₂₂OH gained force moving from slow to fast cooling.

To better understand fatty alcohol behavior in peanut oil, the effect of fatty alcohol chain length, cooling rate, and storage time on oil release was thus investigated.

Table 2.6. Released oil at different storage times for organogels containing 5% (w/w) C₂₂OH, C₂₀OH, C₁₈OH and C₁₆OH in peanut oil slow and fast cooled. Samples stored at 20 °C.

Time (days)	Released oil (% w/w)							
	Slow cooling				Fast cooling			
	C ₂₂ OH	C ₂₀ OH	C ₁₈ OH	C ₁₆ OH	C ₂₂ OH	C ₂₀ OH	C ₁₈ OH	C ₁₆ OH
1	0.015 ± 0.002	0.003 ± 0.003	0.226 ± 0.046	3.225 ± 0.549	0.317 ± 0.211	14.386 ± 2.312	58.041 ± 7.110	79.997 ± 0.091
	0.003 ± 0.015	0.019 ± 0.012	0.386 ± 0.023	5.427 ± 0.275	1.800 ± 0.323	26.490 ± 1.809	74.574 ± 0.347	80.790 ± 0.237
14	0.052 ± 0.010	0.118 ± 0.008	3.120 ± 1.021	10.484 ± 0.332	3.143 ± 0.597	34.927 ± 2.340	74.805 ± 0.430	81.667 ± 0.184
	0.097 ± 0.073	0.053 ± 0.010	2.085 ± 0.793	9.607 ± 1.045	4.278 ± 0.311	42.661 ± 0.613	74.093 ± 1.223	81.749 ± 0.172

Table 2.6 shows the evolution over time of oil release after centrifugation for organogels containing 5% (w/w) C₂₂OH, C₂₀OH, C₁₈OH, and C₁₆OH for slow and fast cooling rates. As regards slow cooling, after one day of storage at 20 °C organogel containing C₁₆OH released more oil than all other organogels. During storage the oil release increased reaching a constant value after 14 day for samples containing C₁₆OH and C₁₈OH. On the other hand, samples containing C₂₀OH and C₂₂OH released a negligible (< 0.12% w/w) amount of oil during 30 days of storage. As regards fast cooled samples, 5% (w/w) C₁₆OH and C₁₈OH containing samples were below the minimum gelling concentration (Figure 2.9) and were composed of a dispersion of crystals in oil. The high values of oil release are due to the separation of the crystals from the bulk oil.

Fast cooled samples containing 5% (w/w) C₂₂OH and C₂₀OH showed higher oil release values after one day of storage compared to those slowly cooled. Also in this case the oil release increased over time during 30 days of storage, reaching the maximum value of 42.7 and 4.3% (w/w) for samples containing C₂₀OH and C₂₂OH, respectively. It seems that the organogel composed by C₂₂OH was less sensible to the cooling rates compared to the organogel containing C₂₀OH in accordance with Figure 2.9. Changes in oil release observed during storage can be attributed to nano and microstructural changes. Indeed, the ability of a material to retain oil can be due to nano and micro spaces, cavities, and capillaries formed between crystalline aggregates, in other words material porosity is related to aggregation at different length scales. On the other side ability of the crystalline aggregate to bind oil onto its surface, and more in general to be covered by oil, is more related to the molecular scale. (Blake *et al.*, 2014; Peyronel *et al.*, 2013; Peyronel, Quinn, Marangoni, & Pink, 2015; Razul, MacDougall, Hanna, Marangoni, Peyronel, Papp-Szabo, & Pink, 2014). Nano and microstructural changes over time can be due to changes in polymorphism, crystals aggregation, porosity, etc. that eventually can lead to a better or worse oil retention.

In order to identify the major cause of oil release, p-NMR (spin-spin T₂ relaxation time) and PL microscopy were carried out, in the attempt to elucidate which component has a higher influence on oil retention.

Table 2.7. T₂ relaxation times for organogels containing 5% (w/w) C₂₂OH, C₂₀OH, C₁₈OH, and C₁₆OH in peanut oil slow and fast cooled after 1 day of storage at 20 °C.

Fatty alcohol	T ₂ relaxation time	
	(ms)	
	Slow cooling	Fast cooling
C ₂₂ OH	70.2 ± 0.7	68.2 ± 1.2
C ₂₀ OH	70.8 ± 1.3	67.1 ± 0.1
C ₁₈ OH	68.5 ± 0.4	67.7 ± 0.6
C ₁₆ OH	146.3 ± 0.8	149.2 ± 4.1

Table 2.7 shows the T₂ relaxation time for organogels containing 5% (w/w) C₂₂OH, C₂₀OH, C₁₈OH, and C₁₆OH slow and fast cooled after 1 day of storage at 20 °C. These values came from the relaxation spectra and were calculated on the basis of the free induction decay profile. It has to be remembered that higher T₂ relaxation times indicate a higher mobility of oil in the matrix since it relaxes later compared to a crystalline material (Rogers *et al.*, 2009a). It can be noted that keeping constant the cooling rate, C₁₆OH showed in both cases a higher relaxation time compared to all the other organogels considered. This value was close to that of peanut oil (data not shown) indicating a higher mobility of oil in this organogel. On the other hand, keeping constant the fatty alcohol chain length it was found that the relaxation time was not influenced by the applied cooling rate. Finally, samples slowly cooled were stored for 30 days at 20 °C and measured again. No differences were found between slowly cooled samples after 1 and 30 days of storage (data not shown).

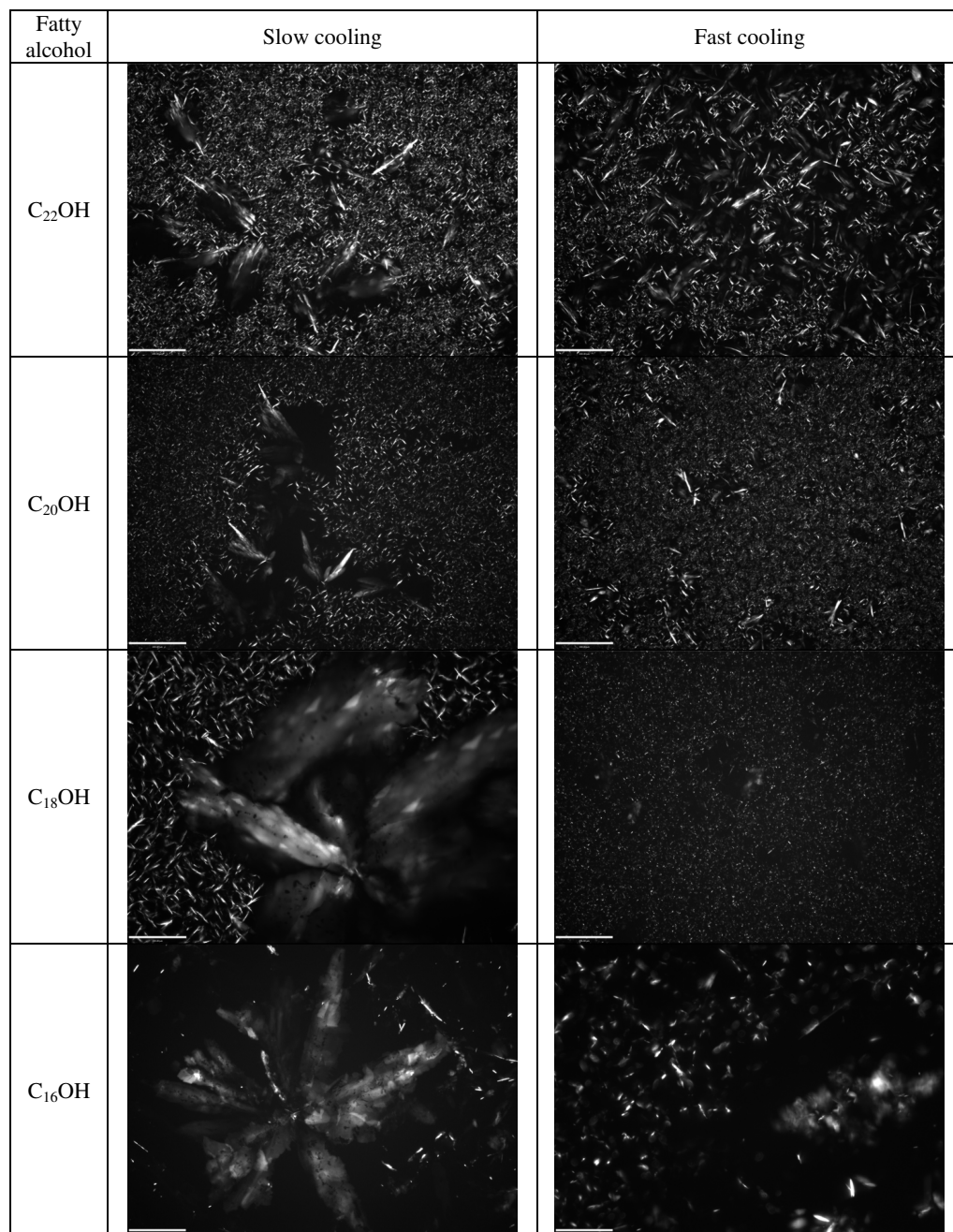
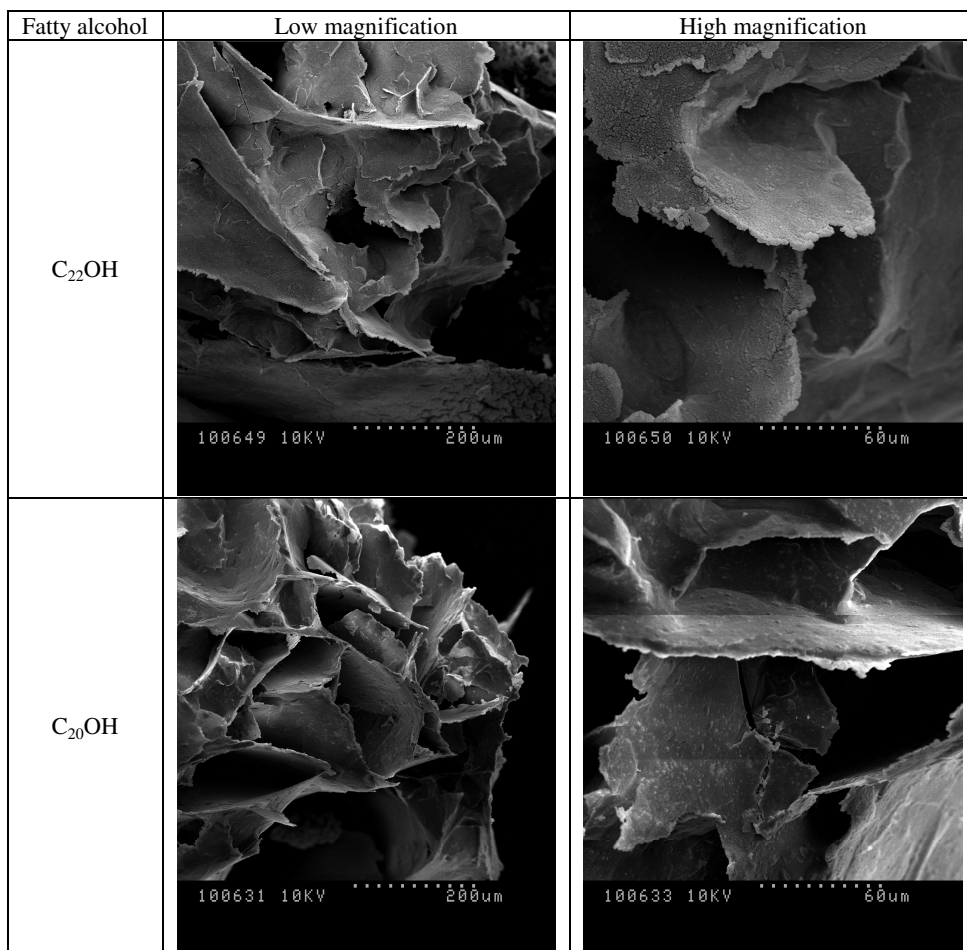


Figure 2.11. Polarized light micrographs of organogels containing 5% (w/w) C₂₂OH, C₂₀OH, C₁₈OH, and C₁₆OH in peanut oil slow and fast cooled after 1 day of storage at 20 °C. Scale bar 200 μm.

In the attempt to investigate the physical component of oil release, micrographs of organogels containing 5% (w/w) C₂₂OH, C₂₀OH, C₁₈OH, and C₁₆OH slow and fast cooled after 1 day of storage at 20 °C were taken (Figure 2.11). It has to be remembered that using polarized light all crystalline compounds are represented by bright areas whereas isotropic

liquids such as oil are represented by dark zones. It can be noted that all samples showed in Figure 2.11 exhibited an inhomogeneous structure that was maintained up to 30 days of storage at 20 °C. These structures can be described as needle-like and rosette-like aggregates (Blake *et al.*, 2014; Yilmaz & Ogutcu, 2014). However, it can be noted a trend: the higher the fatty alcohol chain length the smaller the crystal sizes. Moreover, the effect of cooling rate seemed greater for C₁₆OH and C₁₈OH containing sample rather than C₂₂OH and C₂₀OH containing samples. Indeed, the first two systems did not form a gelled structure (Figure 2.9) but rather a dispersion of crystals in oil when fast cooled.

The morphology of these aggregates was confirmed by scanning electron microscopy.



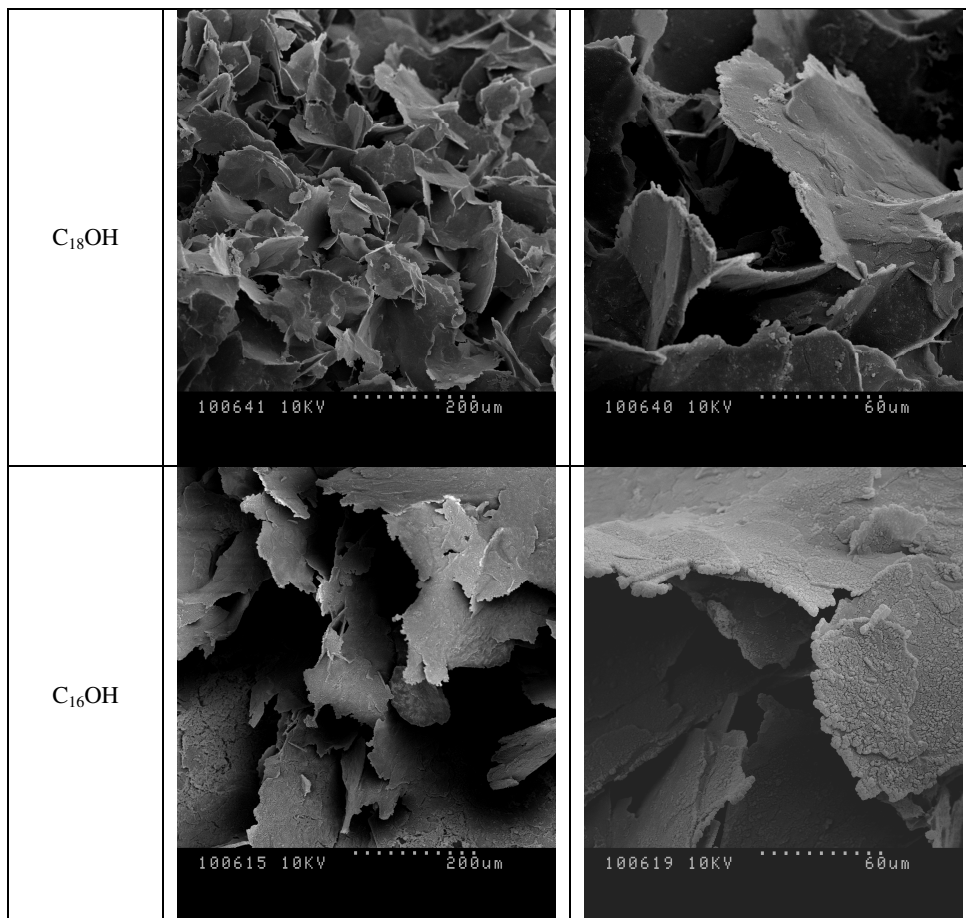
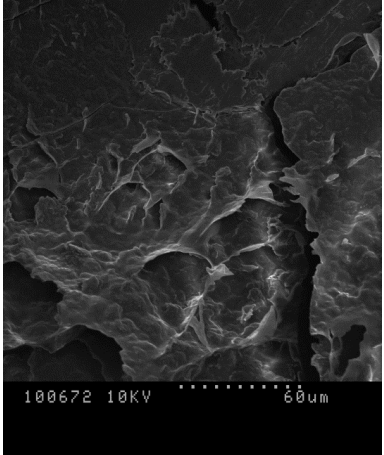
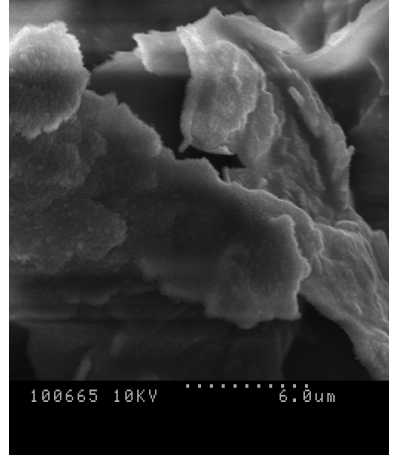
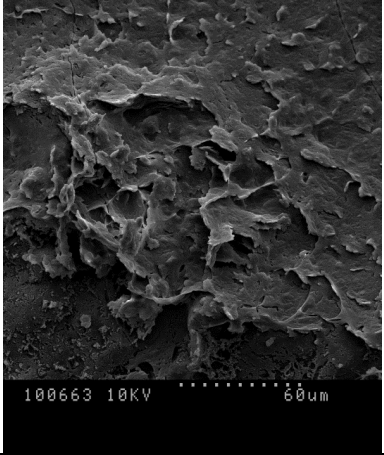
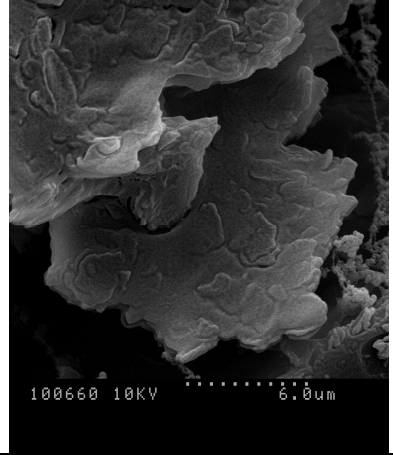
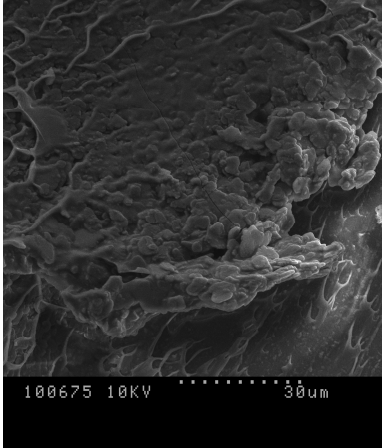
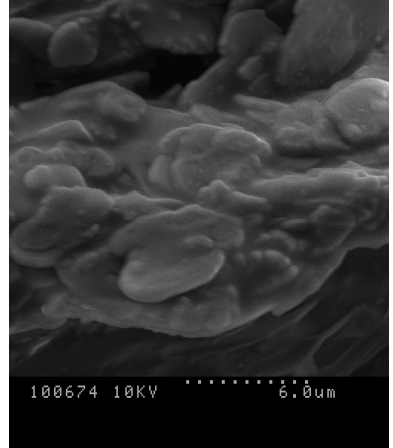


Figure 2.12a. Scanning electron micrographs of organogels containing 5% (w/w) $C_{22}OH$, $C_{20}OH$, $C_{18}OH$, and $C_{16}OH$ in peanut oil slow cooled imaged at two different magnifications.

Fatty alcohol	Low magnification	High magnification
C ₂₂ OH		
C ₂₀ OH		
C ₁₈ OH		

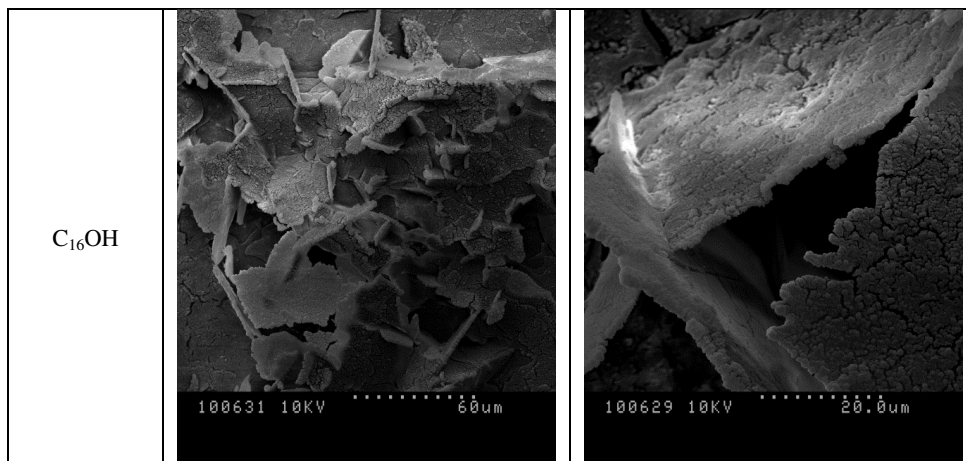


Figure 2.12b. Scanning electron micrographs of organogels containing 5% (w/w) $C_{22}OH$, $C_{20}OH$, $C_{18}OH$, and $C_{16}OH$ in peanut oil fast cooled imaged at two different magnifications. Please note that high and low magnification among samples are different.

Figure 2.12a and b show the scanning electron micrographs of organogels containing 5% (w/w) $C_{22}OH$, $C_{20}OH$, $C_{18}OH$, and $C_{16}OH$ slow and fast cooled. It can be noted that observed structures showed a platelet-like morphology. Fast cooling induced the formation of platelets 10 times smaller than slow cooling. The aggregates observed in Figure 2.11 can be due to the same structure observed in Figure 2.12a and b, only oriented in a different way: perpendicular or parallel to the glass cover slip. Fatty alcohols can have partially crystallized starting from the glass cover slip and other in the oil between the glass cover slip and the glass slide exhibiting a needle-like and rosette-like morphology, respectively. This behavior was also found and described by Blake and Marangoni (2015c). However, authors suggested that since the edge of the platelet is attached to the glass cover slip it can be used for a rough calculation of the crystal size.

PL micrographs showing a more homogeneous distribution of crystals were then used to compute crystal numbers and sizes. Tables 2.8a and b show the computed crystal size corresponding to the maximum mean diameter of the object and crystal percentage. Total objects were also reported. Data support the previous observations, the crystal sizes for slow cooled samples were greater as the fatty alcohol chain length decreased. Indeed, as shown in Table 2.8a, the amount of total objects decreased and crystals belonging to class 4 (from 50 to 100 μm) and 5 (from 100 to 1000 μm) increased. Fast cooled systems showed a similar trend. On the other hand, comparing systems containing the same fatty alcohol but slow and fast cooled, it can be noted that the effect of cooling rate was greater as the fatty alcohol chain length decreased.

Table 2.8a. Computed crystal size corresponding to the maximum mean diameter of the object, its percentage and total objects for 5% (w/w) $C_{22}OH$, $C_{20}OH$, $C_{18}OH$, and $C_{16}OH$ in peanut oil organogels slow cooled.

Fatty alcohol	Class										Total objects
	1		2		3		4		5		
	Crystal (%)	Mean diameter (μm)	Crystal (%)	Mean diameter (μm)	Crystal (%)	Mean diameter (μm)	Crystal (%)	Mean diameter (μm)	Crystal (%)	Mean diameter (μm)	
$C_{22}OH$	57.6	2.2	27.6	6.9	14.6	16.2	0.2	60.9	0.0	-	11478
$C_{20}OH$	65.5	2.2	26.0	6.8	8.4	14.5	0.0	-	0.0	-	9179
$C_{18}OH$	45.9	1.8	18.6	7.0	30.7	22.7	4.4	65.0	0.4	123.6	1568
$C_{16}OH$	65.4	1.5	11.8	6.9	17.5	24.3	4.5	71.0	0.8	132.1	508

Table 2.8b. Computed crystal size corresponding to the maximum mean diameter of the object, its percentage and total objects for 5% (w/w) C₂₂OH, C₂₀OH, C₁₈OH, and C₁₆OH in peanut oil organogels fast cooled.

Fatty alcohol	Class										Total objects
	1		2		3		4		5		
	Crystal (%)	Mean diameter (μm)	Crystal (%)	Mean diameter (μm)	Crystal (%)	Mean diameter (μm)	Crystal (%)	Mean diameter (μm)	Crystal (%)	Mean diameter (μm)	
C ₂₂ OH	63.1	2.2	25.2	6.8	11.6	16.6	0.1	69.1	0.0	-	11517
C ₂₀ OH	74.0	2.1	19.8	6.7	6.2	14.7	0.0	-	0.0	-	13516
C ₁₈ OH	77.3	2.3	19.4	6.6	3.3	13.6	0.0	-	0.0	-	11632
C ₁₆ OH	46.3	2.8	37.3	6.9	16.5	15.0	0.0	-	0.0	-	1935

The microstructure of these organogels thus can partially explain the observed releasing of oil over time.

Since all organogels under study had the same percentage of fatty alcohols and since image analysis pointed out that the number of crystals in the matrix increased with fatty alcohol chain length, the presence of possible microchannels as well as pores able to entrap and retain oil, increased with fatty alcohol chain length. However, microstructure is not the only responsible for oil retention. Indeed, nanostructure could have had a major effect. As previously described in paragraph 2.1.2.1, fatty alcohols organogels were characterized by two crystal families with orthorhombic β' polymorphism. The crystal family of bigger dimensions (higher d_{001}) decreased over time while the crystal family with smaller dimensions increased. This nanostructural change could have led to an enlargement of the nanocavities. Thus, the combined effect of microstructure as well as nanostructural changes could have resulted in a macroscopic release of oil, in terms of differences over storage time, fatty alcohols chain length, and cooling rate.

2.1.4 Conclusions

The effect of cooling rate, storage time, fatty alcohols concentration and chain length on physical properties as well as nano, micro, and macrostructural characteristics of organogel were studied.

Thermal behavior as well as nanostructure were greatly affected by fatty alcohol concentration in organogels. It was found that nanostructure changed during storage: the polymorphic form of 5% (w/w) fatty alcohols organogels did not change up to 54 days while a contraction of the crystalline structure was clearly observed. Moreover, the amount of fatty alcohol needed to gel peanut oil was higher for short fatty alcohol chain length as well as for fast cooling rate. Firmness and oil release for samples containing 5% (w/w) fatty alcohols were affected by both cooling rate and fatty alcohols chain length. Indeed, samples that were fast cooled released more oil than those slowly cooled while variations in firmness values were ascribed to both factors considered. Finally, aged samples showed an increase in oil release, that was attributed to the crystalline structure contraction observed during storage. Organogels that were slowly cooled with 20 and 22 carbon atoms in fatty alcohol acyl chain showed the best performing results in terms of stability over time and physical properties.

2.2 Monoglyceride organogel

2.2.1 Aim of the study

In this paragraph, the study of monoglyceride organogels is described. Different authors highlighted the ability of these self-assembling molecules to gel oils (Da Pieve *et al.*, 2010; Da Pieve, Calligaris, Panozzo, Arrighetti, & Nicoli, 2011; Lopez-Martinez *et al.*, 2014). The aim of this research was to investigate if the measurement of the dielectric properties of oils could give insights on the structure and physical properties of the resulting monoglyceride organogels. The measure of oil dielectric properties is today proposed as an easy and non-destructive tool to determine the deterioration degree during frying as well as possible oil adulterations (Kumar, Singh, & Tarsikka, 2013) and thus can be a powerful technique to predict organogel properties based on oils characteristics. Dielectric properties measurements were carried out at the University of Ljubljana (Slovenia), under the supervision of prof. Nataša Poklar Ulrih.

2.2.2 Materials and methods

2.2.2.1 Materials

Castor, cod liver, corn, extra virgin olive (EVO), flax-seed, peanut, and sunflower oil were purchased in a local market. MyverolTM saturated monoglycerides (MG) (fatty acid composition: 1.4% C14:0, 59.8% C16:0, 38.8% C18:0; melting point 68.05 ± 0.5 °C) was kindly offered by Kerry Ingredients and Flavour (Bristol, United Kingdom). Miglyol 812 N (medium chain triacylglycerols, MCT) was kindly provided by Cremer Oleo GmbH & Co. KG (Hamburg, Germany). Cyclohexane was purchased from Sigma-Aldrich (Saint Louis, USA).

2.2.2.2 Monoglyceride organogel preparation

Before organogel preparation, all oils were kept at 1.2 kPa for at least 30 min using a Rotavapor (Büchi Labortechnik AG, Flawil, Switzerland) to degas and remove moisture. Castor oil was kept at least 60 min at reduced pressure because of its high viscosity. Aliquots of 30 g of a mixture composed by different oils added with 10% (w/w) of MG were weighted in a 100 mL beaker. The mixture was heated at 70 °C under magnetic stirring in a temperature controlled water bath. After MG melting, samples were maintained at least 10 min at the same temperature under magnetic stirring. Finally, samples were crystallized in a water bath until reaching 20 °C. Organogels (OGs) were stored in a desiccator at room temperature for at least 12 h before analysis.

2.2.2.3 Oil fatty acid composition

The fatty acid composition of samples was determined by capillary GC analysis after alkaline treatment in accordance to the European Official Methods of Analysis (1991).

2.2.2.4 Oil viscosity

Oil viscosities were measured by small amplitude dynamic measurements using the rheometer Stresstech Rheometer (Reologia Instruments AB, Lund, Sweden) with application software Stresstech v.4. The experiments were performed using concentric cylinder geometry and measurements were carried out at 20 °C. The temperature control was obtained using a circulating coolant connected to a thermostat. The shear rate was increased step-wise from 0.3 to 120 s⁻¹. All the oils considered showed a Newtonian behavior.

2.2.2.5 Dielectric Properties

The dielectric properties were measured following the capacitive method proposed by Prevc, Cigic, Vidrih, Poklar Ulrih, and Segatin (2013). In particular, a E4980A precision LCR

meter and a 16452 A liquid test fixture (Agilent Technologies, Santa Clara, USA) were used. Depending on the matrix analyzed, different test fixture filling methods were used. In particular, OGs were placed in the open test fixture and then gently pressed until the test fixture was closed; oils were directly injected in the closed test fixture. After a short compensation of the liquid dielectric test fixture, the parallel capacitance and resistance were measured without and with the samples, at 50 uniformly distributed frequencies in the range from 100 Hz to 2 MHz. All of the measurements were carried out at 20 °C. The temperature control was performed using a 7320 high-precision water bath (Fluke, Everett, USA) and a 5627A/1502A external thermometer system (Fluke, Everett, USA). The dielectric parameters were calculated from the measures of the capacitance and the equivalent resistance of the lipids (eq. 2.3).

$$\varepsilon' = \frac{C_p}{K_c} \quad (\text{eq. 2.3})$$

where ε' is the dielectric constant, as the real part of the relative permittivity, C_p is the capacitance of the model lipid corrected for “stray” capacitance, and K_c is the mean cell constant. Following Midmore, Hunter, and O'Brien (1987), the cell constant and stray capacitance was determined from measurements made with air and cyclohexane at 20 °C. The mean cell constant and stray capacitance was computed by averaging the results determined in the optimal frequency range from 10 to 500 kHz. The dielectric loss factor, ε'' , as the imaginary part of the relative permittivity, is shown in eq. 2.4.

$$\varepsilon'' = \frac{1}{\omega R_p K_c} \quad (\text{eq. 2.4})$$

where R_p is the resistance of the lipid sample, ω is the angular frequency ($\omega = 2\pi f$), and f is the frequency.

2.2.2.6 Polarized light (PL) microscopy

Organogels were analyzed using a PL optical microscope (Leica DM 2000, Leica Microsystems, Heerburg, Switzerland) connected with a Leica EC3 digital camera (Leica Microsystems, Heerburg, Switzerland). One drop of the sample was placed in the middle of a glass slide and a glass cover slip was centered above the drop. Samples were analyzed at room temperature using a 200x magnification. Images were acquired and processed using the application software Leica Suite LAS EZ (Leica Microsystems Heerburg, Switzerland). Images were saved in *jpeg* format resulting in 2048 × 1536 pixels.

2.2.2.7 Firmness

Firmness of each OG was measured by a puncture test at 20 ± 2 °C using an Instron 4301 Universal Testing machine (Instron International Ltd, High Wycombe, UK). 30 g of OG crystallized in a 100 mL becker was penetrated using a cylindrical probe of 12.7 mm diameter mounted on a 100 N compression head. Crosshead speed was set at 25 mm/min and gels were penetrated for 5 mm. Force–distance curves were obtained from the puncture tests and firmness was taken as the maximum force (N) required to puncture the sample.

2.2.2.8 Differential scanning calorimetry (DSC) analysis

DSC analysis was carried out using a TA4000 differential scanning calorimeter (Mettler-Toledo, Greifensee, Switzerland) connected to a GraphWare software TAT72.2/5 (Mettler-Toledo, Greifensee, Switzerland). Heat flow calibration was achieved using indium (heat of fusion 28.45 J/g). Temperature calibration was carried out using hexane (m.p. −93.5 °C), water (m.p. 0.0 °C) and indium (m.p. 156.6 °C). Samples were prepared by carefully

weighing 15–20 mg in 160 μL aluminum DSC pans, closed without hermetic sealing. Samples were heated from 20 to 80 $^{\circ}\text{C}$ at 5 $^{\circ}\text{C}/\text{min}$ under nitrogen flow (20 mL/min) during analysis. An empty pan was used as a reference in the DSC cell. The start of melting transition was taken as on-set (T_{on}) that is the point at which the extrapolated baseline intersects the extrapolated tangent of the calorimetric peak in the transition state. Temperature corresponding to the transition peak was also computed (T_{peak}). The machine equipment program STARe ver. 8.10 (Mettler-Toledo, Greifensee, Switzerland) was used to plot and analyze the thermal data.

2.2.2.9 Data analysis

All determinations were expressed as the mean \pm standard error of at least two measurements from two experiment replicates ($n \geq 4$). Statistical analysis was performed by using R v. 3.0.2 (The R foundation for Statistical Computing). Bartlett's test was used to check the homogeneity of variance, one way ANOVA was carried out and Tukey-test was used as post-hoc test to determine statistical significant differences among means ($p < 0.05$). Linear regression analysis by least squares minimization was performed using GraphPad Prism v.5.03 (GraphPad Software, San Diego, USA). The goodness of fit was evaluated on the basis of statistical parameters of fitting (R^2 , p , standard error) and the residual analysis.

2.2.3 Results and discussion

2.2.3.1 Oil fatty acid composition, viscosity and dielectric properties

Table 2.9 shows the fatty acid composition and viscosity of oils considered in the study. As expected, the typical fatty acids composition of the selected oils was obtained and different viscosity values were recorded. In particular, castor oil had the highest viscosity value followed by EVO, sunflower, peanut, corn, and flax-seed oil. Finally, cod liver oil and MCT showed the lowest viscosity values.

Table 2.9. Fatty acid composition (% w/w) of castor, cod liver, corn, extra virgin olive (EVO), flax-seed, medium chain triacylglycerols (MCT), peanut, and sunflower oil.

Fatty acid	Castor	Cod liver	Corn	EVO	Flax-seed	MCT	Peanut	Sunflower
C8:0	nd	nd	nd	nd	nd	56.93	nd	nd
C10:0	nd	nd	nd	nd	0.1	42.86	0.2	nd
C12:0	nd	nd	nd	nd	0.1	0.12	nd	nd
C14:0	nd	6.0	nd	nd	nd	nd	nd	0.1
C15:0	nd	0.5	nd	nd	nd	nd	nd	nd
C16:0	1.4	16.0	13.2	11.3	6.1	nd	8.5	6.4
C16:1	nd	9.1	nd	1.0	0.1	nd	0.2	0.1
C17:0	nd	1.1	nd	0.2	0.1	nd	0.1	nd
C17:1	nd	1.2	nd	0.1	0.1	nd	0.1	nd
C18:0	1.6	2.6	1.6	3.0	4.5	nd	2.4	2.9
C18:1	4.2	24.3	32.2	77.8	20.3	nd	66.7	25.7
C18:2	5.4	3.2	51.8	5.5	13.0	nd	14.3	63.7
C18:3	0.5	1.9	0.8	0.6	54.9	nd	0.1	0.1
C20:0	0.1	nd	0.4	0.3	0.2	nd	1.2	0.2
C20:1	0.3	9.9	nd	0.2	0.1	nd	1.8	0.1
C20:4	nd	8.2	nd	nd	nd	nd	nd	nd
C20:5	nd	11.8	nd	nd	nd	nd	nd	nd
C21:0	nd	2.7	nd	nd	nd	nd	nd	nd
C22:0	nd	0.5	nd	nd	0.2	nd	2.8	0.6
C24:0	nd	1.0	nd	nd	0.1	nd	1.6	0.2
Ricinoleic acid	86.5	nd	nd	nd	nd	nd	nd	nd
Viscosity (Pa·s)	1.023	0.045	0.059	0.078	0.054	0.033	0.057	0.061

Standard Deviation (SD) fatty acid < 0.2 (w/w); nd: not detectable or < 0.1% (w/w); Standard Deviation (SD) viscosity < 0.015 Pa·s

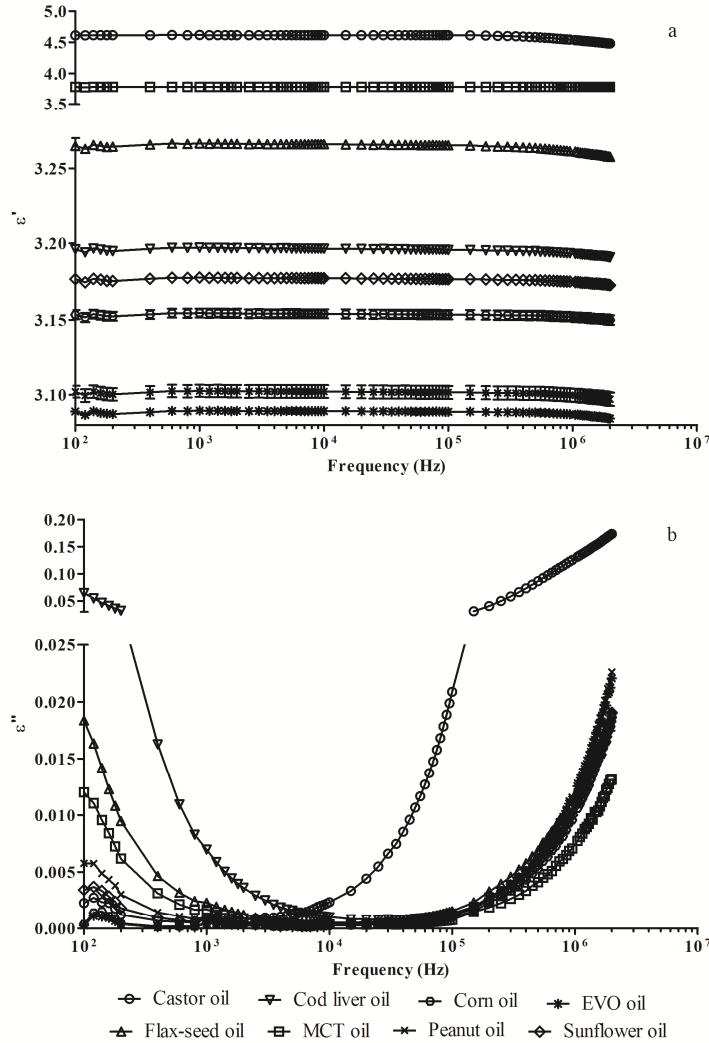


Figure 2.13. Dielectric constant (a) and dielectric loss (b) as a function of frequency for different oils. Error bars represent standard error.

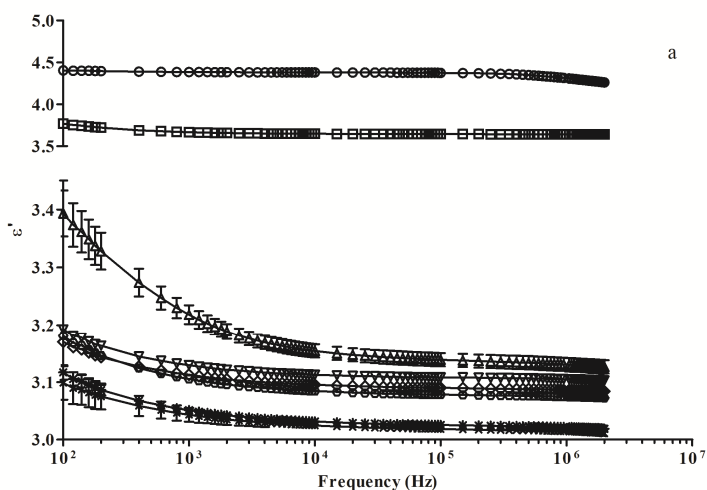
Figure 2.13 shows dielectric constant (a) and dielectric loss (b) of selected oils as a function of frequency. The oil dielectric constant resulted not dependent on the frequency in range 100 Hz to 500 kHz. On the contrary, oil dielectric constants slightly decreased as the frequency increased in the range from 500 kHz to 2 MHz. This decrease is a typical characteristic of the dielectric spectrum due to the beginning of the dielectric dispersion (Lizhi, Toyoda, & Ihara, 2008; Prevc *et al.*, 2013). It can be noted that castor oil showed the highest dielectric constant (Figure 2.13a) probably due to its high polarity as a consequence of the high content of ricinoleic acid rich in hydroxylic groups (around 86% w/w - Table 2.9). The dielectric constant spectrum of MCT was just below that of castor oil. MCT was characterized by the presence of the medium chain fatty acids C8 and C10 (Table 2.9) and this probably led to a dielectric constant higher than that of other considered oils rich in long chain fatty acids. Finally, the dielectric properties of other oils followed the order: flax-seed

> cod liver > sunflower > corn > peanut > EVO oil. As described by Lizhi *et al.* (2008), oils rich in linoleic acid have higher dielectric constants than those of oils rich in oleic acid. In agreement with this observation, flax-seed oil, containing the highest linolenic acid amount (Table 2.9), showed the highest dielectric constant values in comparison to other vegetable oils. The dielectric constant value sequence perfectly fitted with oil linoleic acid content: sunflower > corn > peanut > EVO oil. As regards cod liver oil, the heterogeneity of the fatty acid profile (Table 2.9) give reason of the difficultly predictable dielectric properties on the basis of fatty acid content.

In agreement with findings of other authors (C. Inoue, Hagura, Ishikawa, & Suzuki, 2002; Lizhi *et al.*, 2008; Prevc *et al.*, 2013), the dielectric loss (Figure 2.13b) showed a clear frequency dependence. In particular, a reverse bell shape trend was observed in all oils. Typically, the dielectric loss at high frequencies increases as a consequence of dipolar rotation. Dipoles rotating and colliding with the neighbor molecules dissipate energy as heat, increasing the dielectric loss (Prevc *et al.*, 2013).

2.2.3.2 Organogel dielectric, thermal, microstructural, and mechanical properties

The addition of MG under defined conditions to the selected oils led to the formation of plastic materials that did not flow by turning up side down the container of the sample.



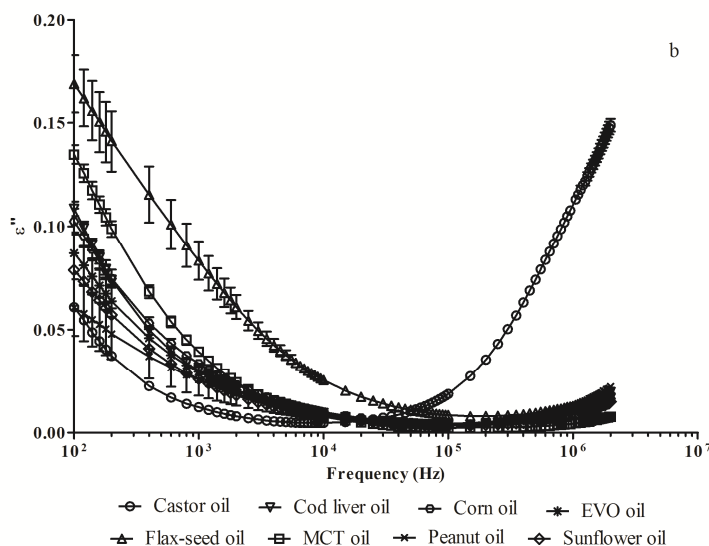
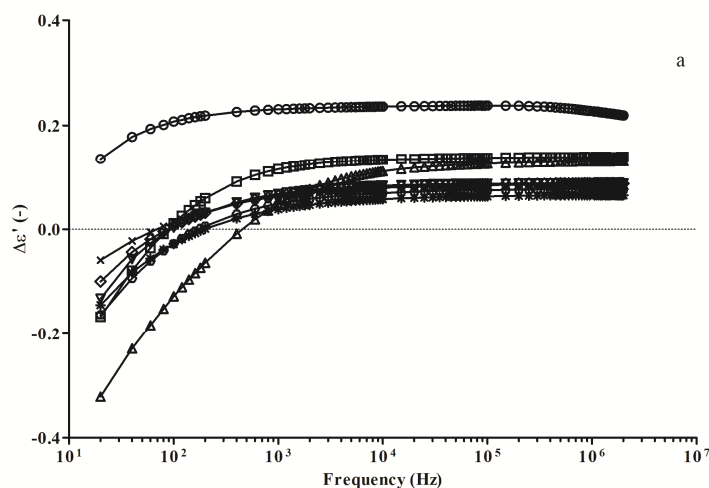


Figure 2.14. Dielectric constant (a) and dielectric loss (b) as a function of frequency for organogels containing 10% (w/w) MG in different oils. Error bars represent standard error.

Figure 2.14 shows both organogel dielectric constant (a) and dielectric loss (b) as a function of frequency. In our knowledge, there is no data of dielectric properties of organogels in literature. The dielectric constant showed a high dependency on frequency at low frequency values, with the only exception of castor oil containing sample. Moving to higher frequencies, the dependence on the frequency progressively decreased. This behavior was different from that observed in bulk oils, for which no frequency dependence of the dielectric constant was recorded (Figure 2.13a). As regards the dielectric loss (Figure 2.14b), a reverse bell-shaped trend, similar to that described in Figure 2.13b, was measured. It can be noted that the increase of the dielectric loss spectra for OG samples was shifted at higher frequencies in comparison to bulk oils.



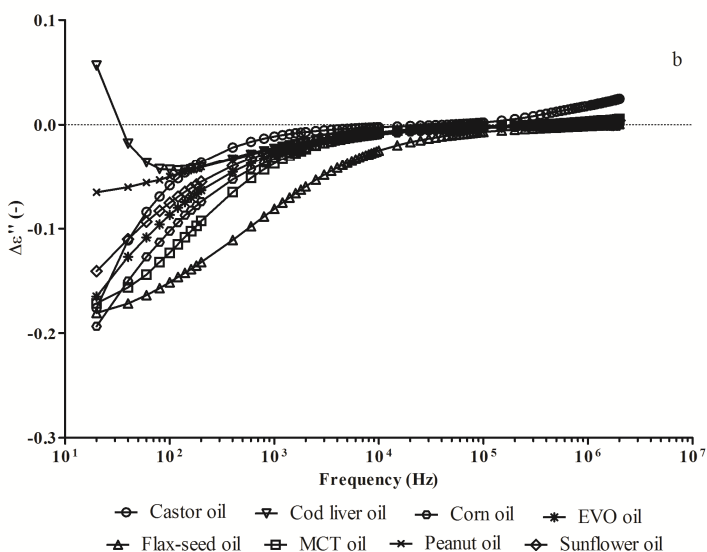


Figure 2.15. $\Delta\epsilon'$ (a) and $\Delta\epsilon''$ (b) calculated as differences between ϵ' or ϵ'' of oil and organogels containing 10% (w/w) MG in different oils, respectively.

To compare OG results with those of bulk oils, the difference between the dielectric constant or dielectric loss of oil and OG ($\Delta\epsilon'$ and $\Delta\epsilon''$) was computed (Figure 2.15a and b, respectively). At low frequencies, being $\Delta\epsilon' < 0$, OG dielectric constants were higher than that of oils, with the only exclusion of castor oil. This can be attributed to the dielectric relaxation process (RP) which seems occur for MG network in OG samples. Moving to frequencies higher than 10^3 Hz, $\Delta\epsilon'$ became > 0 for all the considered systems and thus ϵ' of the oils were higher than that of OGs. This phenomenon could be ascribed to the reduced ability of triacylglycerol molecules entrapped in MG network to orientate inside the electric field. On the contrary, $\Delta\epsilon''$ was in general lower than 0, highlighting that this parameter was higher for OGs than for oils. Moreover, a broadening of ϵ'' signal (Kremer, Huwe, Schönhals, & Rozanski, 2003), attributed to MG, probably due to entrapped oil inside MG network, was found in Figure 2.14b at low frequencies, which is more explicit for flax-seed oil and MCT containing samples and less for peanut oil containing sample.

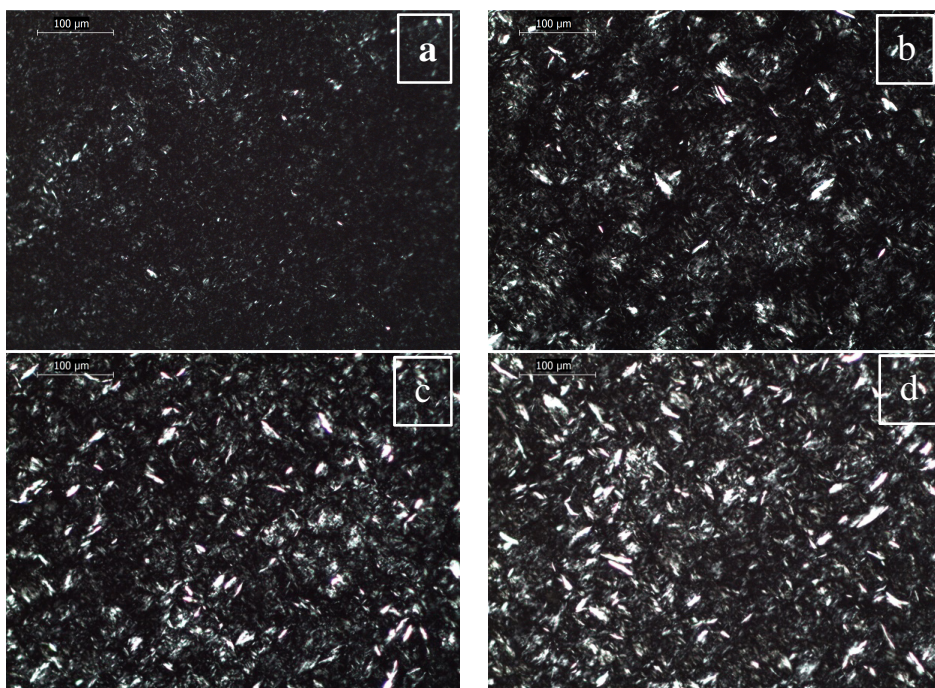
To better study the OG network characteristics as a function of oil type, thermal analysis was performed. In accordance with literature, samples showed a broad melting event with a long tail towards lower temperatures indicating that the dissolution process of the structuring agent starts at low temperatures (data not shown).

Table 2.10. T_{on} , T_{peak} from calorimetric curves of OGs prepared with 10% (w/w) MG in castor, cod liver, corn, EVO, flax-seed, MCT, peanut, and sunflower oil.

Oil	T_{on} (°C)	T_{peak} (°C)
Castor	44.84 ± 0.43 ^e	54.21 ± 0.14 ^c
Cod liver	56.62 ± 0.23 ^a	64.55 ± 0.46 ^a
Corn	55.52 ± 0.12 ^{ab}	64.39 ± 0.44 ^a
EVO	57.41 ± 0.47 ^a	64.27 ± 0.06 ^a
Flax-seed	54.27 ± 0.50 ^{bc}	64.16 ± 0.13 ^a
MCT	48.79 ± 0.62 ^d	57.35 ± 0.38 ^b
Peanut	56.03 ± 0.05 ^{ab}	64.76 ± 0.19 ^a
Sunflower	52.99 ± 0.22 ^c	62.81 ± 0.66 ^a

a,b,c,d,e: means with different letters in the same column are significantly different ($p < 0.05$).

Table 2.10 reports the T_{on} and T_{peak} obtained from the calorimetric melting curves of OGs prepared with castor, cod liver, corn, EVO, flax-seed, MCT, peanut, and sunflower oil. It can be noted that castor oil and MCT containing samples showed the lowest T_{on} and T_{peak} values. On the contrary, T_{on} and T_{peak} of other systems resulted comparable. Results seem to indicate the formation of weaker gels in castor oil and MCT containing samples as compared with those of other organogels.



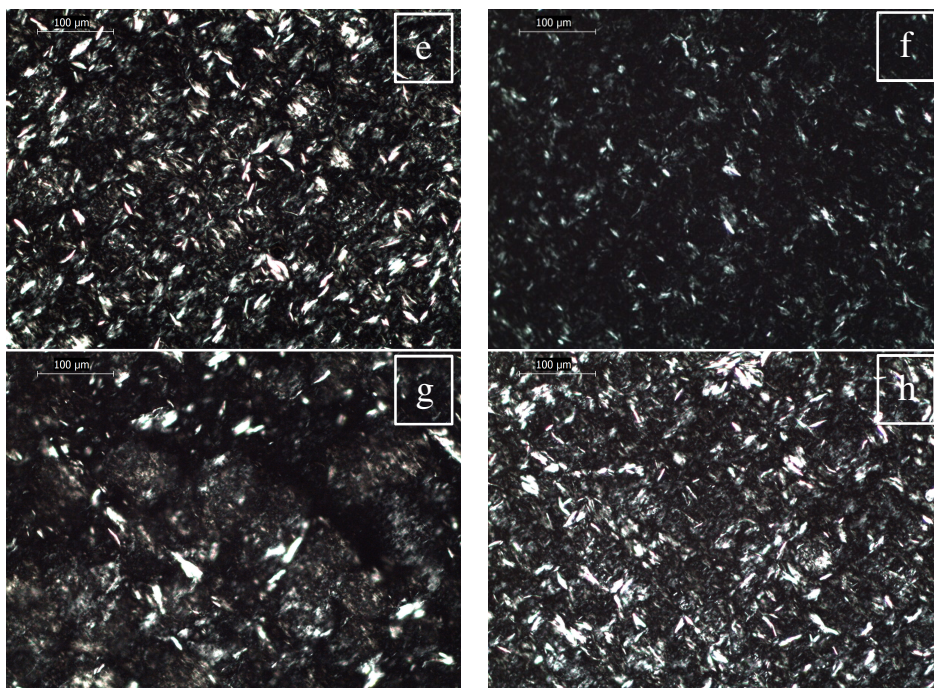


Figure 2.16. Micrographs of organogels containing 10% (w/w) MG in castor (a), cod liver (b), corn (c), EVO (d), flax-seed (e), MCT (f), peanut (g), sunflower (h) oil.

These results were confirmed by data obtained with polarized light microscopy (Figure 2.16). It should be remembered that bright areas refer to crystalline monoglyceride platelets, while dark areas represent liquid oil. Observing the morphology of the crystals, it can be noted that vegetable oils and cod liver oil showed a huge number of aggregates with a dimension of about 30-40 μm . On the contrary, smaller aggregates were observed in the images of MCT and castor oil containing sample. This result seems to confirm thermal and dielectric data.

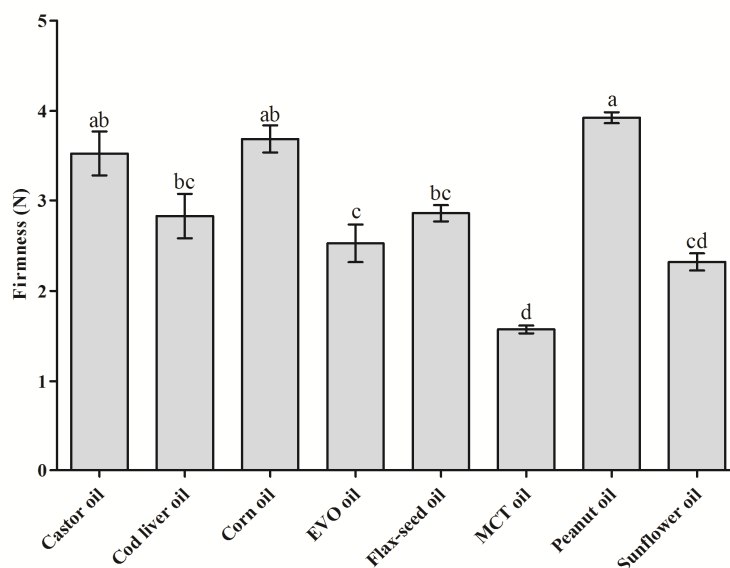


Figure 2.17. Firmness of organogels containing 10% (w/w) MG in different oils. Bars with different letters are statistically different ($p < 0.05$). Error bars represents standard errors.

Finally, the firmness of organogels, expressed as maximum force to penetrate the sample, was determined to study the macroscopic behavior of gels (Figure 2.17). The differences among samples appeared not so high and without a specific trend, with the exclusion of MCT containing sample. It should be remembered that MCT was the oil with the lowest viscosity and the second highest dielectric constant. Both factors could affect the gel firmness leading to a weak gel network in a less viscous medium. Considering castor oil organogel, it should be expected a low firmness due to the weak gel network present in the samples as evidenced by previous results. On the contrary, firmness resulted higher than that of MCT gel. This is probably due to the high viscosity of castor oil (Table 2.9). Thus, firmness results can be interpreted considering that this parameter is the resultant of the effect of gel network strength and oil viscosity.

Based on previous acquired results, linear regression analysis was performed between oil dielectric properties and organogel thermal properties and firmness. Among different parameters, the oil dielectric constant ϵ' resulted well correlated with the organogel melting temperature (T_{on}) and peak at melting (T_{peak}) with R^2 equal to 0.93 and 0.90, respectively ($p < 0.05$). The regression equations ($\epsilon' = -7.2767T_{peak} + 86.968$ and $\epsilon' = -7.7917 T_{on} + 79.975$ considering T_{peak} and T_{on} , respectively) can be used to estimate the organogel thermal properties based on oil dielectric constant. On this regard, it should be noted that considering only oils composed of long chain fatty acids (vegetables oils as well as cod liver oil) the differences in dielectric properties did not allow to predict the organogel properties. It could be inferred that the differences in fatty acid composition and thus in dielectric properties were not so important to affect the MG network in organogels.

2.2.4 Conclusions

In this paragraph it was studied the possible relationship between oil dielectric properties and monoglyceride-based organogel structure and physical properties. Results acquired highlighted that the dielectric properties of bulk oil can be used to predict the thermal properties of the gel. In particular, the oils with the highest dielectric constant values (castor

oil and MCT) resulted in the less structured organogels with the lowest melting temperatures. It can be hypothesized that the higher ability to make dipole-dipole rotation of these oils could partially hinder the monoglycerides capacity to form networks among crystal clusters. This led to the formation of smaller aggregates that can be easily destroyed during heating. However, it should be noted that the effect of the dielectric properties of oil can be well evidenced only considering oils characterized by a peculiar fatty acid composition. On the contrary, oils containing mainly long chain fatty acids showed similar behavior in MG network formation.

Ternary systems based on monoglyceride

3.1 Effect of strong and weak bases on monoglyceride gelled emulsions

3.1.1 Aim of the study

When binary monoglyceride-water systems are heated above the Krafft temperature, the hydrocarbon chains convert to a disordered state and water penetrates among the ordered polar groups (Larsson, 2009). The resulting structure composed by a liquid crystal lamellar phase made of double layers of monoglycerides separated by water layers converts into the so called α -gel phase when temperature is reduced to below the Krafft temperature. The α -gel phase can also transform to the coagel phase, made of a network of plate-like β -crystals dispersed in the water phase (Heertje, Roijers, & Hendrickx, 1998). The addition of oil in such systems can lead to the formation of an emulsion or a gelled emulsion (Batte *et al.*, 2007b). The latter system is a cream-like matrix with rheological feature of spreadable fats and shortenings. However, few studies are available in literature on the effect of processing parameters and composition of the system on gelled emulsion (Batte *et al.*, 2007a, 2007b; Blake & Marangoni, 2015b; Goldstein *et al.*, 2012). In this paragraph, the attention was focused on the effect of anionic salt aqueous phase on the ability of monoglyceride to stabilize gelled emulsions. In particular, anions chosen were derived from weak bases, commonly used in bakery product formulations as leavening agents. To this aim, aqueous solutions containing different concentrations of potassium bicarbonate (KHCO_3), sodium bicarbonate (NaHCO_3), ammonium bicarbonate (NH_4HCO_3) and sodium acetate (CH_3COONa) were considered as water phase in the preparation of gelled emulsions. Sodium hydroxide (NaOH) and potassium hydroxide (KOH) aqueous solutions were used as control solutions.

3.1.2 Materials and methods

3.1.2.1 Materials

MyverolTM saturated monoglyceride (MG) was kindly offered by Kerry Ingredients and Flavour (Bristol, United Kingdom). Sunflower oil was purchased in a local market. Sodium hydroxide (NaOH), potassium hydroxide (KOH), ammonium bicarbonate (NH_4HCO_3), sodium bicarbonate (NaHCO_3), sodium acetate (CH_3COONa), palmitic acid, and stearic acid were purchased from Sigma Aldrich (Milan, Italy). Potassium bicarbonate (KHCO_3) was purchased from J.T.Baker (Deventer, The Netherlands). All solutions were prepared using milli-Q water.

3.1.2.2 Monoglyceride gelled emulsions preparation

Monoglyceride gelled emulsions were prepared using a constant ratio among ingredients:

- lipid phase: 36.4% (w/w) sunflower oil;
- water phase: 56.4% (w/w) of aqueous solutions containing 1, 10, 100 and 1000 mM of NaOH , KOH , KHCO_3 , NaHCO_3 , NH_4HCO_3 , or CH_3COONa ;
- monoglyceride-co-surfactant (CO–MG) mixture: 7.2% (w/w) of MG–co-surfactant mixture made of MG mixed with palmitic and stearic acid in a ratio of 10:1:1 (w/w).

The water phase and oil–CO–MG mixtures were heated separately to 70 °C in a water bath. After complete melting of CO–MG, oil and water phases were mixed and then homogenized using a high speed homogenizator DI 25 (Ika-Werke, Staufen, Germany) at 59,000 x g for 1

min while maintaining the temperature at 70 °C. Subsequently, the mixture was cooled in an ice bath and then stored at 4 °C for 24 h before analysis.

3.1.2.3 pH

pH was measured using a Basic 20 pH meter (Crison Instruments, S.A., Barcelona, Spain) mounted with an electrode for solids (52–32, Crison Instruments, S.A., Barcelona, Spain). Standard calibration was done using three different buffers at pH 4, 7 and 9. All measurements were made at 25 °C.

3.1.2.4 Visual appearance

The visual appearance of the samples was recorded 24 h after preparation. The sample was turned up-side down and considered as a gel when it did not flow or flowed only slightly and as a liquid emulsion when it easily flowed. Finally, phase separation indicated when the sample was made of two distinct phases.

3.1.2.5 Rheological analysis

A Stresstech Rheometer (Reologia Instruments AB, Lund, Sweden) with application software Stresstech v.4 was used to determine the storage (G'), the loss modulus (G''), the complex dynamic module (G^*), and the tangent of the phase angle ($\tan \delta$). The measurements were performed in a 40 mm parallel-plate geometry system. The temperature control was obtained by means of a circulating coolant connected to a thermostat. Aliquots of about 4–5 g of gelled sample were placed on the temperature-controlled measuring plate and the measuring gap was set at 2 mm. To determine the linear viscoelastic region for the samples, dynamic stress sweep measurements at a frequency of 1 Hz from 0.1 Pa to 100 Pa were conducted at 20 °C. G' , G'' and G^* moduli were obtained for a frequency scan from 0.1 to 10 Hz using a fixed stress value included in the linear viscoelastic region. Finally, G^* modulus as a function of frequency (ω) was used to calculate the number of rheological units (z) and their strength (A) as reported by Gabriele, de Cindio, and D'Antona (2001) (eq. 3.1).

$$G^* = A\omega^{1/z} \quad (\text{eq. 3.1})$$

3.1.2.6 PL microscopy

Samples were analyzed following the same procedure and using the same equipment reported in paragraph 2.2.2.6 (pag. 45).

3.1.2.7 DSC analysis

Samples were analyzed following the same procedure and using the same equipment reported in paragraph 2.2.2.8 (pag. 45). The heating ramp was set from 20 to 80 °C at 10 °C/min. Total peak enthalpy was obtained by integration of the melting curve.

3.1.2.8 Synchrotron X-ray diffraction (XRD) analysis

X-ray diffraction patterns were recorded at the X-ray diffraction beam-line 5.2 at the Synchrotron Radiation Facility Elettra located in Trieste (Italy). The X-ray beam emitted by the wiggler source on the Elettra 2 GeV electron storage ring was monochromatized by a Si(111) double crystal monochromator, focused on the sample and collimated by a double set of slits giving a spot size of 0.2 × 0.2 mm. A drop of sample was lodged into a nylon pre mounted 20 μm cryoloop for crystallographic experiments (0.7–1.0 mm) (Hampton Research HR4-965, Aliso Viejo, CA, USA). Sample temperature was controlled by means of a 700 series cryocooler (Oxford Cryosystems, Oxford, UK) with an accuracy of ~1 °C. Analysis were performed at 20 °C. Data were collected at a photon energy of 12.398 keV ($\lambda = 1.0 \text{ \AA}$), using a 2M Pilatus silicon pixel X-ray detector (DECTRIS Ltd., Baden, Switzerland).

Bidimensional patterns collected with Pilatus were calibrated by means of a LaB6 standard and integrated using the software FIT2D (Hammersley, Svensson, Hanfland, Fitch, & Hausermann, 1996). Peak position search and indexing of the XRD patterns obtained by the crystalline phases was performed using the program Winplotr (Roissnel & Rodríguez-Carvajal, 2000) and Checkcell (Laugier & Bochu, 2000).

3.1.2.9 Data analysis

All determinations were expressed as the mean \pm standard error of at least two measurements from two experiment replicates ($n \geq 4$). Statistical analysis was performed by using R v. 3.0.2 (The R foundation for Statistical Computing). Bartlett's test was used to check the homogeneity of variance, one way ANOVA was carried out and Tukey-test was used as post-hoc test to determine statistical significant differences among means ($p < 0.05$). Non-linear regression analysis of rheological data was performed on TableCurve 2D software (Jandel Scientific, ver. 5.01). Levenberg–Marquardt algorithm was used to perform least squares function minimization and the goodness of fit was evaluated on the basis of statistical parameters of fitting (R^2 , p , standard error) and the residual analysis.

3.1.3 Results and discussion

3.1.3.1 pH and visual appearance

Table 3.1 shows the concentration and relevant pH of the aqueous solutions containing different bases used to prepare the ternary systems. The visual appearance, as well as the pH of the resultant monoglyceride–oil–aqueous systems, was also reported. Depending on the base used and its concentration, different outcomes were obtained.

Considering firstly NaOH that is generally used in literature to prepare monoglyceride-structured emulsions, gels were obtained at 1 and 10 mM NaOH aqueous solution concentration. On the contrary, a liquid system resulted when using 100 mM solution concentration, whereas a waxy partially separated system was achieved at 1000 mM NaOH concentration.

For an indication of the role of the cation in the system, NaOH was substituted with KOH. Results obtained were not different from the NaOH systems, indicating that the type of cation did not affect the system structure (data not shown). It is likely that Na^+ and K^+ were dispersed in the system at the same concentration, exhibiting the same effect on the swelling capacity of the monoglyceride.

Moving to other bases considered (KHCO_3 , NaHCO_3 , NH_4HCO_3 , and CH_3COONa), all bicarbonate containing systems gelled, independently on the cation (Table 3.1). A case in point was that of sodium acetate that did not allow the formation of a stable emulsion indicating that acetate ions hindered proper swelling of the system. It can be hypothesized that the presence of acetate ions can disturb monoglycerides self-organization around oil droplets leading to the system phase separation. From these results, samples in the gel form were considered in further experiments.

Table 3.1. Concentration and relevant pH of aqueous solutions containing NaOH, KOH, KHCO₃, NaHCO₃, NH₄HCO₃, and CH₃COONa, as well as the visual appearance and pH of the resulted ternary systems.

Component	Concentration (mM)	Solution pH	Visual appearance	System pH
NaOH	1	11.10 ± 0.08	Gel	5.32 ± 0.02
	10	12.05 ± 0.05	Gel	6.82 ± 0.03
	100	12.87 ± 0.02	Liquid	10.09 ± 0.07
	1000	13.82 ± 0.01	Phase separation	-
KOH	1	11.56 ± 0.04	Gel	5.51 ± 0.15
	10	12.20 ± 0.02	Gel	6.54 ± 0.04
	100	13.10 ± 0.03	Liquid	10.36 ± 0.05
	1000	13.98 ± 0.05	Phase separation	-
KHCO ₃	1	8.64 ± 0.04	Gel	5.32 ± 0.03
	10	8.54 ± 0.03	Gel	6.53 ± 0.02
	100	8.43 ± 0.01	Gel	7.83 ± 0.05
	1000	8.33 ± 0.01	Gel	8.79 ± 0.01
NaHCO ₃	1	8.66 ± 0.04	Gel	5.35 ± 0.05
	10	8.55 ± 0.05	Gel	6.59 ± 0.04
	100	8.46 ± 0.02	Gel	8.02 ± 0.02
	1000	8.05 ± 0.03	Gel	8.59 ± 0.01
NH ₄ HCO ₃	1	8.12 ± 0.01	Gel	5.31 ± 0.02
	10	8.07 ± 0.02	Gel	6.56 ± 0.02
	100	8.05 ± 0.03	Gel	8.28 ± 0.07
	1000	7.87 ± 0.07	Gel	8.94 ± 0.04
CH ₃ COONa	1	6.54 ± 0.04	Phase separation	-
	10	7.25 ± 0.02	Phase separation	-
	100	7.75 ± 0.01	Phase separation	-
	1000	8.11 ± 0.01	Phase separation	-

3.1.3.2 Viscoelastic behavior and microstructure

Table 3.2 reports storage (G') and loss (G'') moduli as well as the $\tan \delta$ (G''/G') values of the gelled samples. As expected, all systems behaved like weak gels as confirmed by mechanical spectra, in which G' and G'' were parallel in the frequency domain, with G' higher than G'' . Both rheological parameters progressively decreased as the salt concentration increased in a concentration range from 1 to 100 mM. This reduction followed an exponential equation in the case of bicarbonate ion containing samples ($R^2 > 0.99$, $p < 0.05$). On the other hand, at 1000 mM concentration an increase in rheological parameters was observed. $\tan \delta$ values, as expected, confirm the elastic dominant behavior of the samples. In all cases, independent on salt type, 1 and 1000 mM samples, and 10 and 100 mM highlighted comparable $\tan \delta$ values. The described behavior of rheological parameter was commonly independent of the cation present, confirming that the alkaline anion concentration rather than that of the cation governed the ternary system structure.

Table 3.2. Elastic modulus (G'), loss modulus (G''), and $\tan \delta$ of monoglyceride gelled emulsions containing sunflower oil, CO-MG, and NaOH, KOH, KHCO_3 , NaHCO_3 , and NH_4HCO_3 at different concentration recorded at 1 Hz.

Compound	Concentration (mM)	G' (Pa)	G'' (Pa)	$\tan \delta$ (-)
NaOH	1	20056 ± 431 ^a	7332 ± 349 ^a	0.365 ± 0.010 ^a
	10	4625 ± 115 ^b	952 ± 14 ^b	0.206 ± 0.002 ^b
KOH	1	25748 ± 3131 ^a	10158 ± 807 ^a	0.397 ± 0.017 ^a
	10	4794 ± 90 ^b	1012 ± 49 ^b	0.211 ± 0.006 ^b
KHCO_3	1	20008 ± 1571 ^a	7675 ± 254 ^a	0.385 ± 0.012 ^a
	10	5234 ± 171 ^c	1105 ± 27 ^c	0.211 ± 0.003 ^b
	100	946 ± 75 ^d	195 ± 12 ^d	0.207 ± 0.012 ^b
	1000	7574 ± 167 ^b	2711 ± 28 ^b	0.358 ± 0.001 ^a
NaHCO_3	1	19273 ± 412 ^a	7361 ± 55 ^a	0.382 ± 0.014 ^a
	10	4131 ± 457 ^c	807 ± 74 ^c	0.196 ± 0.003 ^b
	100	823 ± 87 ^d	172 ± 14 ^d	0.210 ± 0.003 ^b
	1000	10894 ± 815 ^b	4110 ± 139 ^b	0.377 ± 0.001 ^a
NH_4HCO_3	1	22058 ± 98 ^a	7966 ± 6 ^a	0.361 ± 0.019 ^a
	10	5533 ± 316 ^c	1144 ± 51 ^c	0.207 ± 0.002 ^b
	100	1308 ± 65 ^d	291 ± 11 ^d	0.222 ± 0.005 ^b
	1000	6857 ± 480 ^b	2412 ± 81 ^b	0.352 ± 0.001 ^a

a,b,c,d : means with different letters in the same column keeping constant compound type are significantly different ($p < 0.05$).

The weak gel model proposed by Gabriele *et al.* (2001) was applied to better understand rheological data. Oscillatory data was then fitted with eq. 3.1. In the model, z represents the number of flow unit interacting with one another to give the observed flow response; A represents the strength of the interactions among these units (Gabriele *et al.*, 2001).

Table 3.3. Weak gel model estimated parameters A and z of monoglyceride gelled emulsions containing sunflower oil, CO-MG, and NaOH, KOH, KHCO_3 , NaHCO_3 , and NH_4HCO_3 at different concentrations. Error represent standard error of model fitting.

Compound	Concentration (mM)	A ($\text{Pa} \cdot \text{s}^{1/z}$)	z (-)
NaOH	1	20974 ± 234	5.10 ± 0.18
	10	4620 ± 24	8.26 ± 0.20
KOH	1	25770 ± 323	5.08 ± 0.21
	10	4787 ± 24	8.26 ± 0.20
KHCO_3	1	20629 ± 239	5.10 ± 0.18
	10	5431 ± 25	8.40 ± 0.21
	100	695 ± 7	8.70 ± 0.53
	1000	7817 ± 73	5.03 ± 0.15
NaHCO_3	1	19656 ± 228	5.03 ± 0.18
	10	4121 ± 17	8.77 ± 0.23
	100	813 ± 7	7.87 ± 0.37
	1000	11098 ± 137	4.65 ± 0.17
NH_4HCO_3	1	22245 ± 250	5.10 ± 0.18
	10	5493 ± 30	8.20 ± 0.27
	100	1299 ± 10	8.06 ± 0.33
	1000	7173 ± 39	4.85 ± 0.07

Table 3.3 shows the z and A values obtained. Regression analysis showed a good determination parameter (> 0.93) and statistically significant model parameters ($p < 0.05$). Systems containing solutions at 1 mM concentration showed a low number of rheological

units (z parameter) with strong interactions among them (A parameter). Moving to samples containing 10 and 100 mM solutions, they showed comparable z value even if the gel strength was lower in 100 mM containing samples. Finally, systems obtained with 1000 mM solutions showed z values comparable to those of 1 mM systems with a concomitant increase of A parameter values, indicating that the strength of the gel was higher than that of systems containing 10 and 100 mM solutions but lower than that of those prepared with 1 mM solutions. These results can be related to the microstructure of the samples.

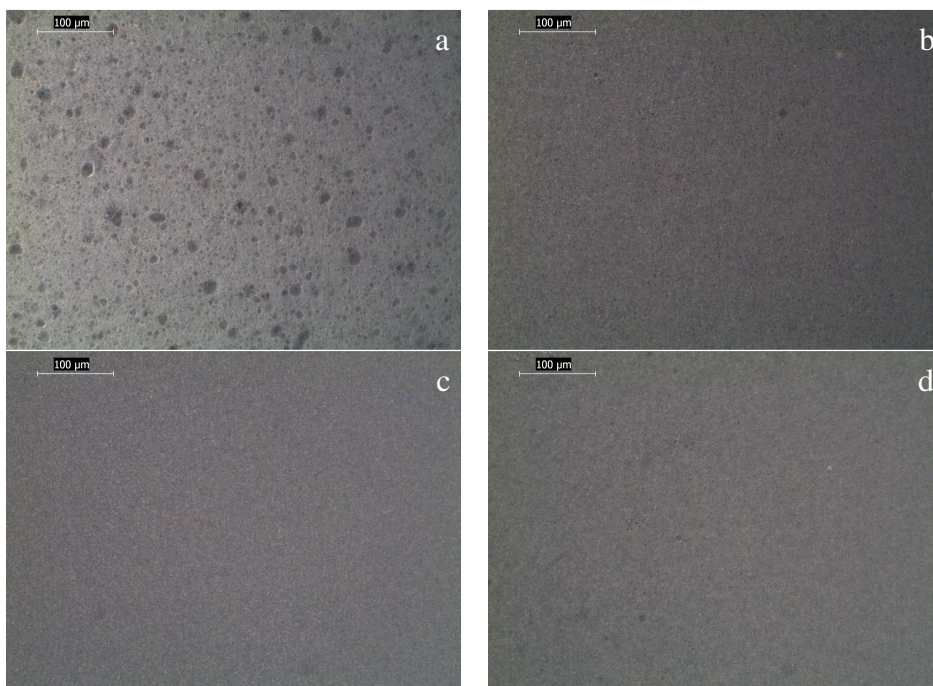


Figure 3.1. Polarized light micrographs of monoglyceride gelled emulsions containing sunflower oil, CO-MG, and 1 (a), 10 (b), 100 (c) and 1000 (d) mM KHCO_3 .

Figure 3.1 shows the polarized light micrographs of monoglyceride gelled emulsions containing KHCO_3 , taken as an example among different salts. It can be noted that the system prepared with 1 mM aqueous solution (Figure 3.1a) was made of dispersed oil droplets (dark zones) surrounded by crystalline monoglyceride shells (bright areas). These MG shells allow the entrapping of oil in the matrix and, when enough inter-connections among MG shells are present, a semi-solid gel was obtained (Batte *et al.*, 2007a, 2007b; Calligaris *et al.*, 2010). Moving to samples made with higher KHCO_3 concentration, oil droplets progressively decreased in size (Figure 3.1 b–c–d). Similar microstructures were observed in samples containing the other type of bases (data not shown).

Based on these results, it can be inferred that in the lowest concentrated sample (1 mM) each oil droplet had a higher number of monoglyceride bilayers than in higher concentrated samples. This can be justified taking into account the surface/volume ratio and remembering that all samples have the same amount of monoglyceride: the higher the oil droplet diameter the lower the surface/volume ratio. Thus, less surfactant per volume unit was required to cover the interface increasing the amount of monoglyceride that can form double layers around each droplet. This led to an increase of the network links that eventually increased the gel strength.

3.1.3.3 DSC and XRD analysis

The structure modifications as a function of base concentration were also confirmed by differential scanning calorimetry (DSC) analysis.

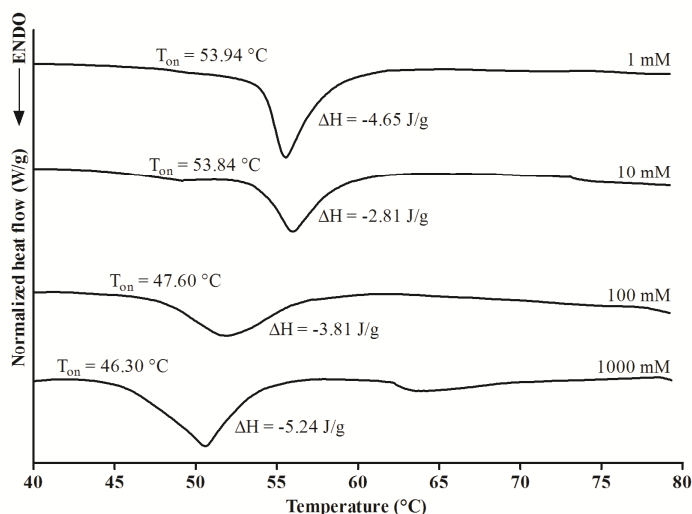


Figure 3.2. Melting calorimetric curves of ternary systems containing sunflower oil, CO-MG, and KHCO_3 at different concentration. Onset melting temperature and melting enthalpy are also reported.

All systems showed one endothermic peak corresponding to the disruption of the network among MG lamellar bilayers, followed by the melting of the crystalline MG. In Figure 3.2 the melting curves of KHCO_3 containing samples are shown. The melting temperatures of systems containing 1 and 10 mM solutions were comparable, whereas the mixture prepared with 100 mM and 1000 mM solution presented a significant shift at lower temperature of the thermal event. This confirms the weaker interactions among MG shells in these samples. Other different salts tested showed the same behavior (data not shown).

Finally, synchrotron XRD diffraction patterns were acquired to obtain information on crystal packing on monoglycerides in the systems.

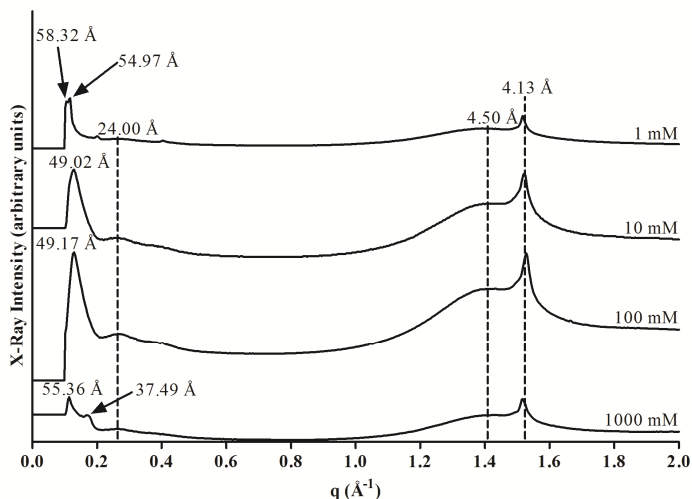


Figure 3.3. XRD diffraction patterns of ternary systems containing sunflower oil, CO-MG, and KHCO_3 at different concentration. Peaks positions expressed in Å are also reported.

Also in this case, data of KHCO_3 was taken as example (Figure 3.3). In agreement with literature, two bumps associated with the amorphous organization of triacylglycerol molecules in the sunflower oil were detected (around 4.50 and 24.00 Å) (Calligaris, Arrighetti, Barba, & Nicoli, 2008; Ollivon, Keller, Bourgaux, Kalnin, Villeneuve, & Lesieur, 2006). Besides these bumps, one evident peak at 4.13 Å was detected in the wide angle area ($q > 1 \text{ \AA}^{-1}$). This peak is typical of the 2D planar hexagonal packing of glycerol head groups, as has been well described by C. H. Chen and Terentjev (2009). In the small angle area ($q < 1 \text{ \AA}^{-1}$), the diffraction patterns highlighted an intense peak at 54.97, 49.02, 49.17, and 55.36 Å, respectively for mixtures containing 1, 10, 100 and 1000 mM salt concentration. Besides these peaks, samples containing 1 and 1000 mM KHCO_3 solutions showed an additional signal at 58.32, and 37.49 Å, respectively. Results showed that there was a reduction of the lamellar thickness as the salt concentration increased. Thus, the increase of the concentration of negative charges in the system seems to generate a compression of monoglyceride lamellar bilayer. However, the further increase of concentration at 1000 mM caused changes of lamellar thickness leading to the formation of two crystal families, one with lamellar thickness comparable to that of the sample containing 1 mM KHCO_3 solution, and one with the lowest thickness value (37.49 Å). It is interesting to note, that the decrease of the interplanar distance of the peak at $q < 1 \text{ \AA}^{-1}$ was recorded not only for samples containing weak bases, but also for NaOH containing samples. In fact, a shift from 57.11 to 49.21 Å was noted in 1 and 10 mM containing samples, respectively (data not shown).

3.1.4 Conclusions

The acquired results highlighted that the macro, micro and nanostructure of MG-gels can be obtained not only using strong bases in the aqueous phase, as widely reported in literature, but also by considering the weak base bicarbonate. The structure and viscoelastic properties of these gels can be tailored not only by selecting the base that best fits with the intended application, but also by using different base concentrations in the aqueous phase. In this context, the characteristics of the cation considered in combination with HCO_3^- or with OH^- anion did not affect the final results. The structure changes as a function of base concentration were schematized as shown in Figure 3.4.

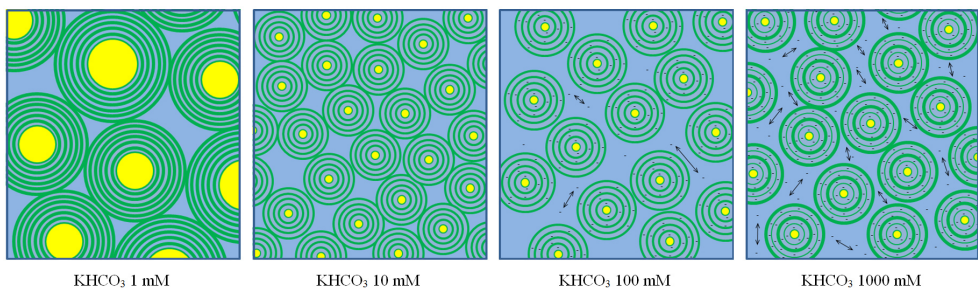


Figure 3.4. Schematic representation of oil droplets (yellow) surrounded by monoglycerides bilayer shells (green). Arrows represent electrostatic repulsion induced by negative (-) charges.

In samples containing 1mM solution of bicarbonates, a strong gel structure was formed. At this concentration, the bilayer thickness was higher than in other samples obtained. It should be noted that the gel pH value was around 5.30 units allowing the acid co-surfactants (palmitic and stearic acid) to be partially ionized. Increasing the concentration to 10 mM, the pH of gels rose to 6.60 units and almost all co-surfactants were neutralized increasing the negative charges on the double layers. This led to weaker gels and smaller oil droplets as well as with lower lamellar thickness. With the further increase of solution concentration to 100 mM, the gel pH reached 8.00 and all co-surfactants were neutralized. Under these conditions, HCO_3^- anions were in the aqueous phase increasing the repulsions among monoglyceride bilayers, thus leading to weaker gels even if the lamellar thickness was similar to that of samples containing 10 mM HCO_3^- solutions. Finally, monoglyceride gels obtained with 1000 mM bicarbonate solutions reached a pH equal to 8.80. These systems had all ionized co-surfactants and a higher number of HCO_3^- anions in comparison to 100 mM solution were present. This increased the repulsions among monoglyceride bilayers and among oil droplets. When a high number of anions were in the aqueous phase, the repulsive forces they generated with anionic co-surfactants and among themselves led to a strengthening of the system. The lamellar thickness was comparable to that of gel containing 1 mM bicarbonate solution. In addition, a family of crystals with lower thickness also appeared.

3.2 Milk and simulated milk ultrafiltrate (SMUF) as aqueous phase in monoglyceride gelled emulsions

3.2.1 Aim of the study

In paragraph 3.1, the importance of negative charges on monoglyceride gelled emulsions was highlighted. Since the swelling of monoglyceride double layers is governed by the positive and negative charges present in the medium, also major and minor components of complex aqueous phases, such as milk, could greatly affect the possibility to obtain stable gelled emulsions by combining milk, oil and monoglyceride. In this paragraph, the effect of UHT skim milk used as aqueous phase on physical and structural characteristics of monoglyceride gelled emulsions was studied. Moreover, simulated milk ultrafiltrate solutions (SMUF) added or not with whey proteins and/or caseins were considered as water phase in systems to better understand the influence of milk constituents on monoglyceride structuring behavior.

3.2.2 Materials and methods

3.2.2.1 Materials

MyverolTM saturated distilled monoglyceride (MG) (fatty acid composition: 1.4% C14:0, 9.8% C16:0, 38.8% C18:0; melting point 68.05 ± 0.5 °C) was kindly offered by Kerry Ingredients and Flavour (Bristol, United Kingdom). Sunflower oil and UHT skim milk (pH= 6.70 at 25 °C) were purchased in a local market. Other chemicals used were lactose monohydrate ($C_{12}H_{22}O_{11} \cdot H_2O$), sodium citrate dihydrate ($Na_3C_6H_5O_7 \cdot 2H_2O$), potassium sulfate (K_2SO_4), sodium hydroxide (NaOH), potassium chloride (KCl). They were purchased from Carlo Erba Reagenti (Milan, Italy). Potassium citrate monohydrate ($K_3C_6H_5O_7 \cdot H_2O$), potassium phosphate dibasic (K_2HPO_4), calcium chloride bihydrate ($CaCl_2 \cdot 2H_2O$), potassium phosphate monobasic (KH_2PO_4), and co-surfactant mixture of palmitic and stearic acids 1:1 (w/w) were purchased from Sigma Aldrich (Milan, Italy). Magnesium chloride hexahydrate ($MgCl_2 \cdot 6H_2O$) was purchased from J.T.Baker (Deventer, Holland), potassium carbonate (K_2CO_3) was purchased from Panreac Quimica Sau (Barcelona, Spain) and sodium phosphate bibasic (Na_2HPO_4) was purchased from E. Merck (Darmstadt, Germany). All solutions were prepared using milli-Q water. Commercial whey protein concentrate (WPC – minimum protein content 80%, maximum fat content 7%) and sodium caseinate (SC – minimum 80%) powders were provided by Borculo Domo Ingredients (Zwolle, The Netherlands).

3.2.2.2 Sample preparation

3.2.2.2.1 Simulated milk ultrafiltrate (SMUF) solutions

SMUF solutions having different pH values were prepared according to Rosmaninho and Melo (2006), with some modifications. Table 3.4 shows SMUF solution composition used in this work. SMUF solution was prepared by adding the components reported in Table 3.4 in milli-Q water and by stirring the mixture for 30 min at ambient temperature. The resulting solution had a pH value of 8.62. The pH of the solution was then modified using concentrated HCl or KOH both 1 M in order to avoid dilution effects.

Table 3.4. SMUF solution composition

Component	Concentration (mM)
K ₂ HPO ₄	11.48
Na ₃ C ₆ H ₅ O ₇ · 2H ₂ O	6.09
K ₃ C ₆ H ₅ O ₇ · H ₂ O	3.70
K ₂ SO ₄	1.03
K ₂ CO ₃	2.17
KCl	8.05
CaCl ₂ · 2H ₂ O	8.98
MgCl ₂ · 6H ₂ O	3.20
C ₁₂ H ₂₂ O ₁₁ · H ₂ O	138.77

3.2.2.2.2 UHT skim milk-oil-monoglyceride mixtures

Ternary mixture composition was the following:

- Lipid phase: sunflower oil;
- Water phase: UHT skim milk, SMUF solution at different pH values, or SMUF solution at pH 6.70 added with sodium caseinate 2.6 g/L or/and 0.7 g/L whey protein concentrate;
- CO-MG: MG was added with a co-surfactant mixture of palmitic and stearic acid 1:1 (w/w) in a ratio of 5:1 (w/w).

The water phase as well as oil-CO-MG mixtures were separately heated at 70 °C in a water bath. After complete melting of CO-MG, oil and water phases were mixed and then homogenized by using a high speed homogenisator DI 25 (Ika-Werke, Staufen, Germany) at 59,000 x g for 1 min maintaining the temperature of 70 °C. Finally, the mixture was cooled in an ice bath and then stored at 4 °C for 24 h before analysis. A total of 62 samples was prepared considering different ingredients ratio.

3.2.2.3 Compositional state diagram

The visual appearance of the samples was recorded after 1 and 15 days of storage at 4 °C. In particular, the sample was considered as a gel when it did not flow by tuning up side down the container; as liquid emulsion when it flowed; as broken systems when the sample was made of fragments of white gel dispersed in a continuous oil phase.

3.2.2.4 pH

Samples were analyzed following the same procedure and using the same equipment reported in paragraph 3.1.2.3 (pag. 56)

3.2.2.5 Rheological analysis

Samples were analyzed following the same procedure and using the same equipment reported in paragraph 3.1.2.5 (pag. 56)

3.2.2.6 PL microscopy

Samples were analyzed following the same procedure and using the same equipment reported in paragraph 2.2.2.6 (pag. 45). Selected images were analyzed with Image-Pro® Plus v. 6.3 (Media Cybernetics, Inc., Bethesda, MD, USA). A spatial calibration was firstly performed by using the 100 µm reference line. Then, by using the best fit circle tool, a circle over each drop was manually drawn and the radius was automatically calculated. The mean radius (± SD) was calculated.

3.2.2.7 Synchrotron XRD analysis

Samples were analyzed following the same procedure and using the same equipment reported in paragraph 3.1.2.8 (pag. 56), with some modifications. Data were collected at a photon energy of 8.266 keV ($\lambda = 1.5 \text{ \AA}$), moreover, the signal falls observed in the diffraction patterns are due to the data acquisition modality of the detector.

3.2.2.8 Data analysis

All determinations were expressed as the mean \pm standard error of at least two measurements from two experiment replications. Statistical analysis was performed by using R v. 3.0.2 (The R foundation for Statistical Computing). Bartlett's test was used to check the homogeneity of variance, one way ANOVA was carried out and Tukey-test was used as post-hoc test to determine statistical significant differences among means ($p < 0.05$). Linear regression analysis by least squares regression was performed and the goodness of fit evaluated on the basis of statistical parameters of fitting (R^2 , p , standard error) and the residual analysis.

3.2.3 Results and discussion

3.2.3.1 Characterization of UHT skim milk-based monoglyceride systems

Figure 3.5 shows the compositional state diagram of mixtures containing different ratios among co-surfactant monoglyceride mixture (CO-MG), sunflower oil and UHT skim milk.

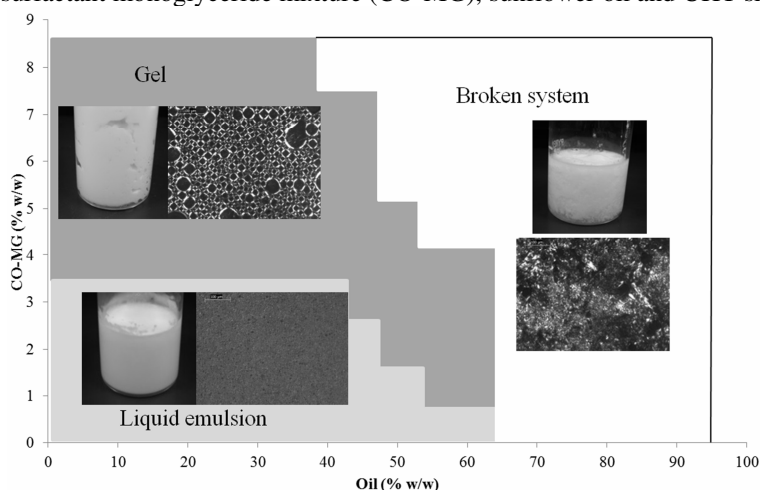


Figure 3.5. Compositional state diagram based on visual appearance of UHT skim milk-sunflower oil-CO-MG systems. Examples of visual appearance and micrographs of samples belonging to different diagram regions were reported. Micrographs magnification 200x.

Examples of macroscopic and microscopic features of the samples belonging to different diagram region were also reported. A white semi-solid material that did not flow after turning up-side down was observed below 65% (w/w) oil and more than 1% (w/w) CO-MG content (Gel region). These gel systems showed a pH ranging from 5.7 to 6.7. Decreasing the oil content, higher quantities of CO-MG were required to form the gel. Observing microscopic image, oil droplets (dark zones) surrounded by crystalline monoglyceride shells (bright areas) can be noted. The inter-connection among shells formed the network that stabilized the system, as previously described by Batte *et al.* (2007b). The gels remained stable after 15 days of storage at 4 °C. The only exceptions were samples containing more than 8% (w/w) CO-MG that showed syneresis. This result can be probably due to the

polymorphic transformation of the less thermodynamically stable α form to the more stable β form (C. H. Chen & Terentjev, 2010; Heertje *et al.*, 1998). The liquid systems were formed when the CO-MG and oil content were below 3.5 and 45.0% (w/w), respectively. They appeared as liquid white emulsions containing small droplets of oil dispersed in a continuous water phase and stabilized by monoglycerides. In these cases, the quantity of CO-MG was not enough to form a continuous network among droplets (C. H. Chen & Terentjev, 2010). Also these samples were stable after 15 days of storage at 4 °C, excluding systems containing less than 1.5% (w/w) CO-MG. Finally, when the oil content was higher than 65.0% (w/w) and CO-MG was below 4.0% (w/w), a curdled material was obtained (broken system region). Similar results were acquired increasing CO-MG content and reducing oil up to 8.5 and 40.0% (w/w), respectively.

To study the nanostructure of the samples, synchrotron XRD analysis was performed on three representative samples belonging to gel, liquid emulsion and broken system regions (Figure 3.6).

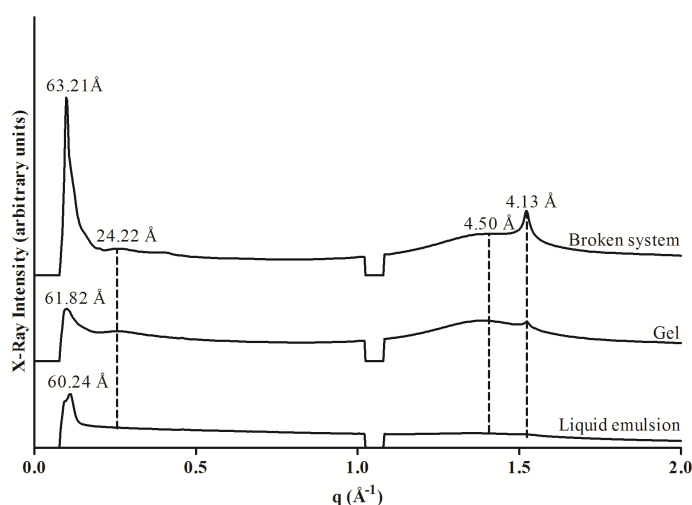
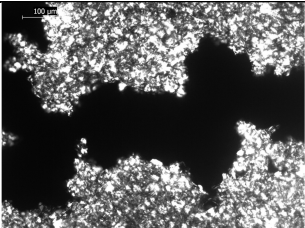
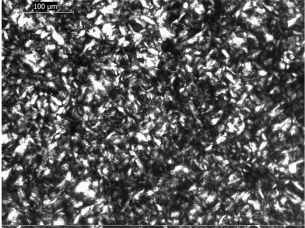
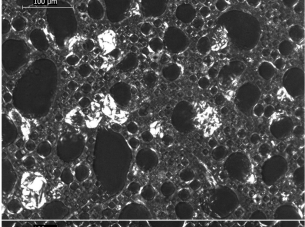
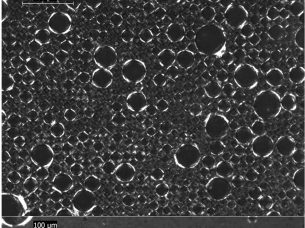
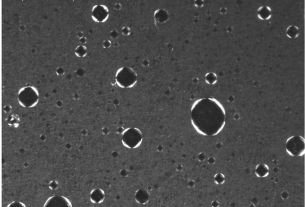


Figure 3.6. Synchrotron XRD patterns of samples belonging to different regions of the compositional state diagram. Broken system: 8.4%(w/w) CO-MG and 42.3% (w/w) oil; gel: 3.2% (w/w) CO-MG and 48.0% (w/w) oil; liquid emulsion: 2.0% (w/w) CO-MG and 15.0% (w/w) oil.

Two bumps at 4.50 and 24.22 Å were observed in all considered XRD patterns. These bumps can be associated with the short-range organization of triacylglycerol molecules in the liquid phase, as previously evidenced by different authors for different food lipids (Calligaris *et al.*, 2008; Lopez, Lavigne, Lesieur, Keller, & Ollivon, 2001; Ollivon *et al.*, 2006). In the wide angle area ($q > 1 \text{ \AA}^{-1}$) one additional peak was recorded at 4.13 Å in all samples. As reported by C. H. Chen and Terentjev (2010), this signal can be associated to the 2D planar hexagonal packing of glycerol heads. As expected, the intensity of this peak progressively increased as CO-MG content increased. In the small angle area ($q < 1 \text{ \AA}^{-1}$) the most intense peak was recorded at 63.21, 61.82, and 60.24 Å for broken system, gel and liquid emulsion, respectively. These peaks were followed by corresponding reflections. The interplanar distances of the peaks at the lowest q value corresponded to the thickness of lamellar bilayer (C. H. Chen & Terentjev, 2010) and were in good agreement with literature data on systems made of oil, saturated MG and NaOH aqueous solution (Calligaris *et al.*, 2010; Heertje *et al.*, 1998). These results suggested that saturated monoglycerides organized forming similar

lamellar structure in all systems considered. However, the networking capacity at mesoscale level changed resulting in different macroscopic structures.

On the basis of results acquired, UHT skim milk can be used to obtain MG-gels delivering high quantities of oil. To better understand the effect of milk constituents, a mixture containing 7.2% CO-MG and 36.4% oil was prepared using a SMUF solution having the milk pH (6.70 at 25 °C).

Aqueous phase	Visual appearance	Micrographs
SMUF at pH 6.70	Phase separation	
SMUF at pH 9.00	Phase separation	
SMUF at pH 10.50	Syneresis	
SMUF at pH 11.00	Gel	
SMUF at pH 6.70 + SC	Gel with evident syneresis	

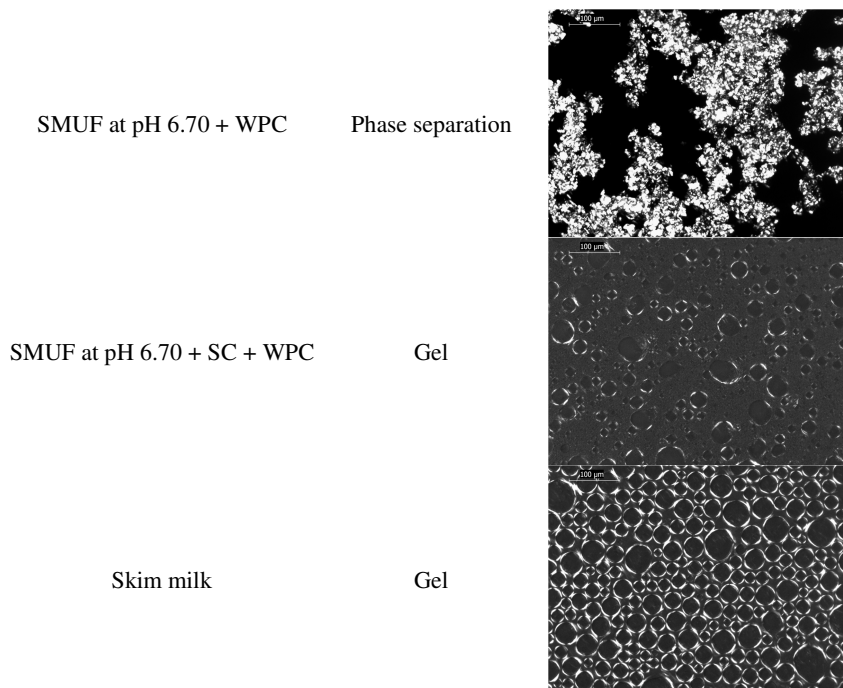


Figure 3.7. Visual appearance and micrographs of systems containing 7.2% (w/w) CO-MG, 36.4% (w/w) oil and 56.4% (w/w) SMUF solutions at different pH values, SMUF solution added with 2.6 g/L sodium caseinate (SC) and/or 0.7 g/L whey proteins concentrate (WPC), and UHT skim milk. Magnification 200x.

The system did not form a gel but a clear phase separation was noted. A progressive increase of structuring capacity was observed by increasing the pH value in SMUF solution. The typical gel structure was formed only at pH 11.00 (Figure 3.7). Thus, only increasing the availability of co-surfactants negative charges it was possible to obtain a stable milk-gel. At lower pH values, co-surfactant dissociation was moderate and the presence of cations could shield the electrostatic charges from the dissociated co-surfactant, inhibiting the swelling. The dissociation of co-surfactants was favored as the pH increased allowing the gel formation.

Since gels cannot be obtained at the native UHT skim milk pH using the SMUF solutions, interactions among MG, salts and milk proteins can be hypothesized to explain above described results. Both caseins and whey proteins have well known amphiphilic properties. This could create a competition between MG and proteins at the interface. Such competition could induce the binding and/or adsorption of proteins at the water/oil interface within MG bilayers and/or the displacement of protein from the emulsion droplets (Boots, Chupin, Killian, Demel, & de Kruijff, 1999; Euston, Singh, Munro, & Dalgleish, 1995; Leenhouts, Demel, deKruijff, & Boots, 1997; Pelan, Watts, Campbell, & Lips, 1997).

In order to understand the effect of milk proteins in studied systems, SMUF solutions at UHT skim milk pH value were added with sodium caseinate and/or whey protein concentrate using the typical concentration found in milk. In this context it should be remembered that the SMUF model systems used in this experiment cannot be completely assimilated to the UHT skim milk for different reasons, such as sodium caseinate dispersion state and presence in WPC of free glycomacropptide. Both casein and whey proteins individually solubilized in SMUF solutions did not allow the formation of a stable gel, even though a certain degree of structuration can be observed in sodium caseinate containing system (Figure 3.7). Only by

mixing these two components, gels can be obtained as evidenced in Figure 3.7 by a certain degree of interconnection among oil droplets surrounded by crystallized MG. It is interesting to remember that the gel made of UHT skim milk showed a well ordered MG network (Figure 3.5). Results seem to indicate that both casein and whey protein contributed to the gel formation. It can be hypothesized that casein and whey protein could change the emulsion stabilization interacting with MGs or they could favor gel formation by shielding the electrical charges in the medium due to the presence of different salts.

3.2.3.2 Rheological and microstructural investigation of selected UHT skim milk-based gelled emulsions

In the second part of the research, the effect of the system composition on rheological and microstructural properties of UHT skim milk-based gel was investigated. To this purpose, different samples belonging to the gel region in the compositional state diagram (Figure 3.5) were selected. Although each sample appeared as a white gel at macroscopic level, differences in microstructure and rheological properties were observed.

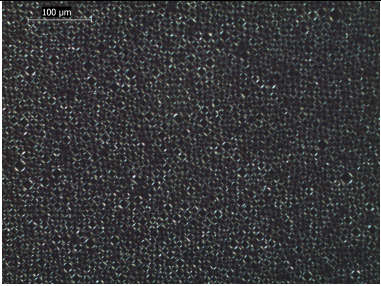
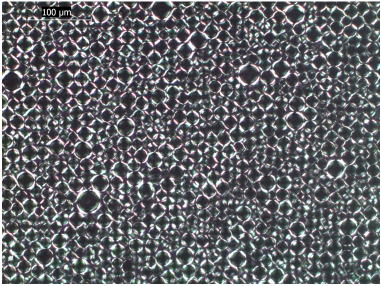
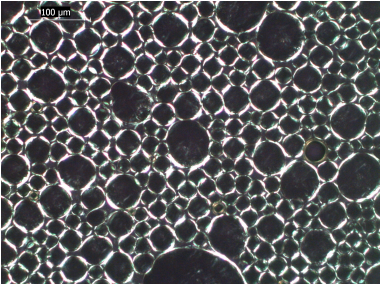
Oil content (% w/w)	Micrographs	Mean radius (μm)
23.6		4.62 ± 0.91
30.0		6.38 ± 1.16
45.0		13.32 ± 7.10

Figure 3.8. Micrographs and mean droplets radius of UHT skim milk-based gels containing 7.2% (w/w) CO-MG and increasing percentages of oil (23.6, 30.0, and 45.0% w/w). Magnification 200x.

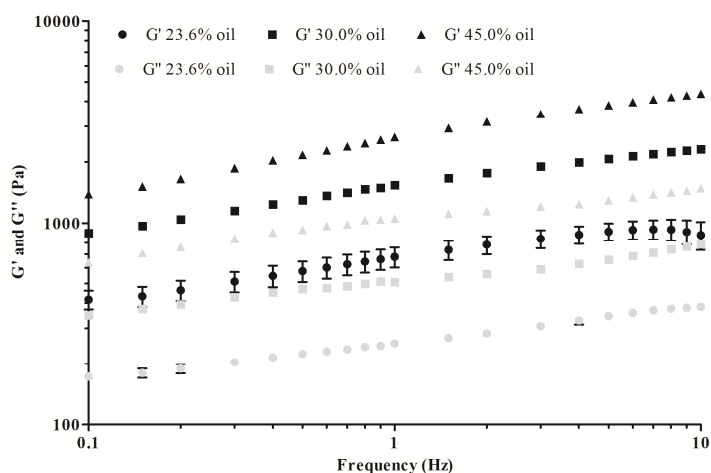


Figure 3.9. Storage (G') and loss (G'') moduli of UHT skim milk-based gels containing 7.2% (w/w) CO-MG and increasing percentages of oil (23.6, 30.0, and 45.0% w/w). Error bars represent standard error.

Figure 3.8 shows the micrographs and relative mean radius of oil droplets of samples containing 7.2% (w/w) CO-MG and increasing oil content (23.6, 30.0, and 45.0%). As the oil content increased, the radius of droplets progressively increased leading to a decrease of surface/volume ratio where MGs were engaged. The increase of droplet size was accompanied by an increase of the rheological parameters G' and G'' (Figure 3.9), indicating that stronger gel networks were formed. The changes of rheological parameters as a function of oil content followed a linear trend ($R^2 > 0.96$, $p < 0.05$).

Moving to another compositional diagram area, samples containing 50.0 and 60.0% (w/w) of oil and increasing CO-MG content (2.0, 3.0 and 4.0% w/w) were imaged as shown in Figure 3.10.

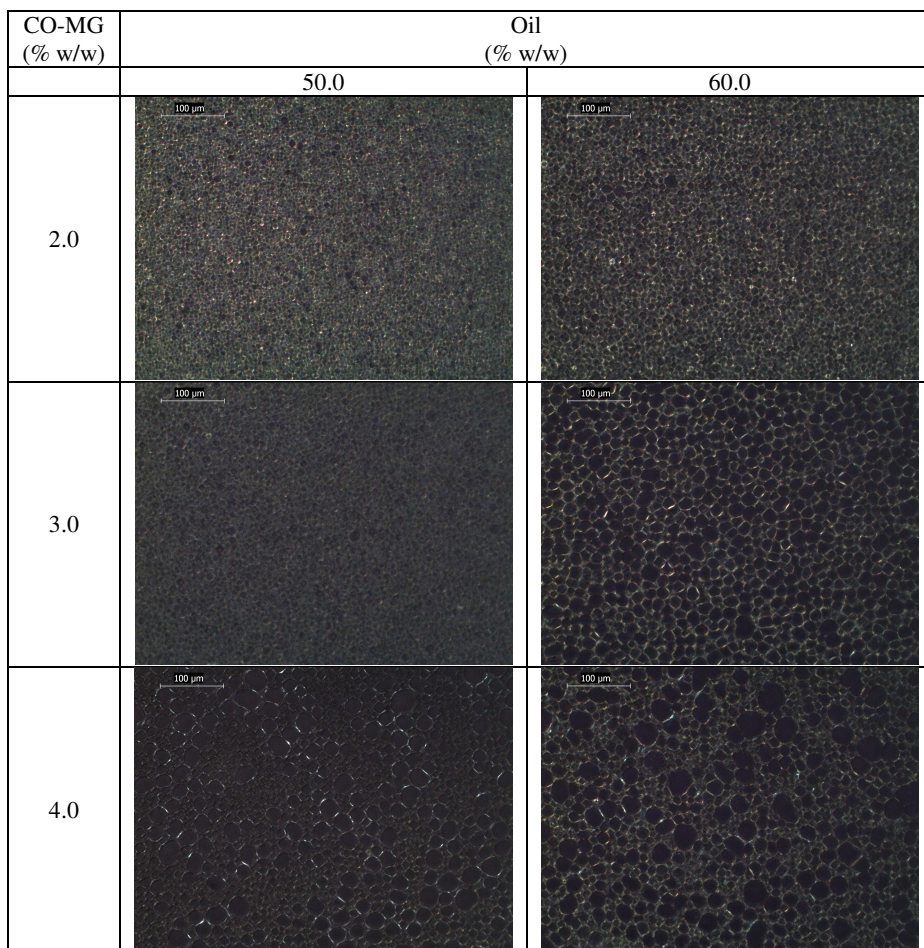


Figure 3.10. Micrographs of UHT skim milk-based gels containing increasing quantity of oil and CO-MG. Magnification 200x.

In this case, the images acquired did not allow the calculation of droplet mean radius, especially at low MG content. However, the increase of droplets size in concomitance with oil content appeared evident by visual observation, confirming previously reported data. Similar increase can be noted also increasing CO-MG and keeping constant oil content. This result seems to indicate that the additional MG in the medium was preferably engaged in the network stabilization rather than in the formation of new oil droplets.

Table 3.5. G' and G'' recorded at 1 Hz of milk-based gels containing increasing quantity of oil and CO-MG.

CO-MG (% w/w)	Oil (% w/w)	G' (Pa)	G'' (Pa)
2.0	50.0	376±1 ^d	92±5 ^c
	60.0	1048±41 ^c	351±21 ^d
3.0	50.0	1307±68 ^{bc}	420±5 ^d
	60.0	1509±93 ^b	543±22 ^c
4.0	50.0	2159±73 ^a	740±32 ^b
	60.0	2390±18 ^a	852±6 ^a

^{a,b,c,d,e}: means with different letters are significantly different ($p < 0.05$).

The modification of the droplets diameter was followed by changes of rheological parameters (Figure 3.10 and Table 3.5). By increasing CO-MG and keeping constant the oil content, a linear increase of rheological parameters was observed confirming the formation of a stronger gel network as MG concentration increase ($R^2 > 0.96$, $p < 0.05$).

3.2.4 Conclusions

Results obtained in this study highlighted the possibility to use UHT skim milk as water phase in the preparation of gels encapsulating high quantities of liquid oil. The systems were structured by lamellar phases formed by saturated monoglycerides surrounding oil. On the other hand, the water phase was absorbed among head polar groups of lamellae. The capacity to incorporate water was highly affected by the water phase composition and availability of negative charges allowing the swelling of bilayers. In UHT skim milk-based systems the complex interplay among proteins and salts dispersed in the medium allowed the formation of stable liquid emulsion when the CO-MG and oil contents were below 3.5 and 45.0% (w/w), respectively. Gels were obtained below 65.0% (w/w) of oil with CO-MG content higher than 1.0% (w/w). The relative ratio among ingredients determined the rheological properties of the systems. In general, as the oil and/or CO-MG content increased, the gel strength also increased, in concomitance with mean droplet diameters. Thus, the structure of the gels can be tailored depending on the application expected.

PART I B
Polar lipids as fat mimetics: applicative studies

Monoglyceride gelled emulsion and organogels as palm oil replacer and ω -3 delivery systems

4.1 Effect of palm oil replacement with monoglyceride organogel and gelled emulsion on sweet bread properties

4.1.1 Aim of the study

Monoglyceride gelled emulsions, as previously described, are white cream-like matrices with rheological features of spreadable fats and shortenings. Different authors used these systems as saturated fat replacers in white bread, short dough pastry, croissants, danishes, and cookies (Blake & Marangoni, 2015b; Goldstein & Seetharaman, 2011; Manzocco *et al.*, 2012a; Manzocco *et al.*, 2012b). However, no comparative studies are present in literature on saturated fat replacement using monoglyceride gelled emulsions and organogels. To this aim this paragraph describes palm oil substitution using monoglyceride organogel and gelled emulsion in sweet bread. Quality characteristics, staling over time, as well as lipid distribution inside sweet bread were determined.

4.1.2 Materials and methods

4.1.2.1 Materials

MyverolTM saturated monoglyceride (MG) (fatty acid composition: 1.4% C14:0, 59.8% C16:0, 38.8% C18:0; melting point 68.05 ± 0.5 °C) was kindly offered by Kerry Ingredients and Flavour (Bristol, United Kingdom). Palm oil (saturated fatty acid percentage 51.14% w/w) and sunflower oil (saturated fatty acid percentage 9.67% w/w) were kindly provided by Unigrà (Conselice, Italy). co-surfactant mixture of palmitic and stearic acids 1:1 (w/w) was purchased from Sigma Aldrich (Milan, Italy). Type 0 wheat flour, sugar, egg powder, yeast, and table salt were purchased in a local market.

4.1.2.2 Sample preparation

4.1.2.2.1 Organogel

Sunflower oil and palm oil organogels (OG) were prepared as described by Da Pieve *et al.* (2010). Monoglycerides were added to the lipid matrix at a concentration of 5% (w/w). The mixtures were stirred with a magnetic rod at 70 °C in a water bath. The samples were then cooled at 20 °C under static conditions. The organogels were examined and used after 24 h of storage at 20 °C.

4.1.2.2.2 Gelled emulsions

Sunflower oil and palm oil gelled emulsions (GE) were prepared according to Calligaris *et al.* (2010). Briefly, MG was mixed with a co-surfactant mixture of palmitic and stearic acid 1:1 (w/w) in a ratio of 5:1 (w/w). The water phase was composed of 1 mM NaOH in deionized milli-p water to promote the partial neutralization of the co-surfactant mixture and obtain a properly swollen phase. The samples were prepared by mixing the water solution and the MG/co-surfactant/oil phase previously heated at 70 °C in a water bath and homogenizing using a high speed homogenizer DI 25 (Ika-Werke, Staufen, Germany) at 59,000 x g for 1 min. Finally, the mixture was cooled at 20 °C in a water bath and then stored at 4 °C for 24 h before usage. The concentration by weight of each constituent in the GE was

as follows: monoglyceride/co-surfactant 2.7% (w/w), palm or sunflower oil 42.1% (w/w), water 55.2% (w/w).

4.1.2.2.3 Sweet bread

The basic formulation of sweet bread loaves consisted of 45.4% (w/w) flour, 23.1% (w/w) water, 18.7% (w/w) palm or sunflower oil, 7.1% (w/w) sugar, 3.9% (w/w) egg powder, 1% (w/w) yeast and 0.8% (w/w) salt. Loaves of approximately 500 g were obtained using a domestic bread making machine (OW200030, Moulinex, China), where mixing, leavening and baking were performed *in situ*. The ingredients were poured in the bread making machine basket having parallelepiped shape (length of 18.5 cm; width of 13.0 cm; height of 10.0 cm) in the following order: water, fat, premixed dry ingredients. The selected program included: 5 min kneading, 5 min resting, 20 min kneading, 65 min leavening, 1 min kneading, 52 min leavening, 45 min baking. At the end of baking, loaves were cooled at room temperature for 1 h before use. The basic formulations were modified substituting (w/w) palm oil and sunflower oil with their respective OG or GE. The substitution was made maintaining constant the ratio among ingredients of the basic formulation. In the case of GE containing formulations, water was added directly within the gel. In other words, the quantity of gel added instead of palm oil allowed to include in the bread formulation the same quantity of water of the basic formulation. Additional samples were prepared by adding the unstructured ingredients used in OG containing samples to the basic formulation instead of the lipid matrix. Samples were prepared in triplicate.

4.1.2.2.4 Sample cutting and storage

Six slices of 20 mm thickness were cut from the central portion of each loaf, packed in high barrier film pouches and stored at 20 °C for up to 14 days.

4.1.2.3 Specific volume

Bread loaf specific volume (cm³/g) was obtained by rapeseed displacement according to Approved Method 10-05 (AACC, 2000).

4.1.2.4 Moisture content

Moisture content was measured using a gravimetric method (AOAC, 2000). Around 2 g of crumb sample was dried in a vacuum oven (1.32 kPa) at 75 °C until constant weight (*circa* 12 h).

4.1.2.5 Water activity

Crumb water activity was determined using a dew-point measurement system (Aqualab 4TEV, Decagon Devices, Inc., Pullman, USA) at 25 ± 1 °C.

4.1.2.6 Crumb grain

Bread slice images were acquired using an image acquisition cabinet (Immagini & Computer, Bareggio, Italy) equipped with a digital camera (EOS 550D, Canon, Milan, Italy). In particular, the digital camera was placed on an adjustable stand positioned 60 cm above a black cardboard base where the bread slice was placed. Light was provided by 4 100 W frosted photographic floodlights, in a position allowing minimum shadow and glare. Other camera settings were: shutter time 1/125 s, F-Number F/6.0, focal length 60 mm. Images were saved in *jpeg* format resulting in 3456 × 2304 pixels. Image-Pro® Plus v. 6.3 (Media Cybernetics, Inc., Bethesda, USA) was used to analyze crumb grain. Crumb area (10⁶ pixels) was converted in gray scale (8 bit) and equalized by best fit tool. Pixels with luminosity in the 215–255 range were associated with crumb bubbles. Bubbles in each image were subdivided into three classes, depending on their average size: the first class (small bubbles)

consisted of bubbles with 10–100 pixels; the second class (medium bubbles) included bubbles with 100–2500 pixels; the third class (large bubbles) consisted of bubbles with more than 2500 pixels. The percentage ratio between the number of bubbles belonging to each class and the total number of bubbles in the image was calculated.

4.1.2.6 Firmness

Samples were analyzed using the same equipment reported in paragraph 2.2.2.7 (pag. 45). Where firmness was taken as the maximum force (N) required to puncture the sample.

4.1.2.6.1 OG and GE

Firmness of OG and GE was measured by a puncture test at 20 ± 2 °C. OG and GE were poured in 20 mm diameter cups and tested by using a 6.2 mm diameter cylinder mounted on a 100 N compression head. Crosshead speed was set at 25 mm/min and gels were penetrated for 5 mm.

4.1.2.6.2 Crumb bread

Firmness of bread crumb was measured by a uniaxial compression test at 20 ± 2 °C. The sweet bread slices were tested by using a 12.7 mm diameter cylinder mounted on a 100 N compression head. Crosshead speed was set at 50 mm/min and the sweet bread slices were penetrated for 5 mm.

4.1.2.7 Magnetic resonance imaging (MRI)

MRI analysis was used to study the proton mobility/density in the samples. MR images were acquired using the MR scanner Echelon™ (Hitachi Medical Systems, Tokyo, Japan) mounted with a 1.5 T permanent magnet and 33 mT/m gradient field strength. The 16 channel RAPID brain coil and the ORIGIN™ MR operating software (Hitachi Medical Systems, Tokyo, Japan) interface were used. Images of transverse sections were obtained with multislice Spin-Echo sequence of T1 according to the following parameters: 180×180 mm for field-of-view (FOV), 22 ms for echo time (TE), 400 ms for repetition time (TR), 2.0 mm section thickness. Images of transverse sections were obtained with multislice Spin-Echo sequence of STIR (T2 with fat signal suppression) according to the following parameters: 180 × 180 mm for field-of-view (FOV), 10 ms for echo time (TE), 2500 ms for repetition time (TR), 110 ms for inversion time (TI), 1.2 mm section thickness. Images were saved in *jpeg* file format resulting in 100 × 280 pixels.

Digital MR images were analyzed using Image-Pro® Plus v. 6.3 (Media Cybernetics, Inc., Bethesda, USA). In particular, images were converted to gray scale (8 bit) and processed with the Fast Fourier Transform Tool. The frequency of luminosity of the image pixels was obtained. The percentage of gray and white pixels was calculated as percentage ratio between the sum of pixels with luminosity in the 170–255 range and the overall sum of pixels in the bread image ignoring the black background.

4.1.2.8 Data analysis

All determinations were expressed as the mean \pm standard error of at least three measurements from three experiment replications ($n \geq 9$). Statistical analysis was performed by using R v. 3.0.2 (The R foundation for Statistical Computing). Bartlett's test was used to check the homogeneity of variance, one way ANOVA was carried out and Tukey-test was used as post-hoc test to determine statistically significant differences among means ($p < 0.05$).

4.1.3 Results and discussion

Table 4.1 shows the firmness of organogel (OG) and gelled emulsion (GE) samples containing palm or sunflower oil.

Table 4.1. Firmness of organogel (OG) and gelled emulsion (GE) containing palm or sunflower oil.

Oil type	Sample	Firmness (N)
Palm oil	OG	1.362±0.004 ^a
	GE	0.082±0.003 ^b
Sunflower oil	OG	0.068±0.004 ^c
	GE	0.029±0.002 ^d

^{a,b,c,d}: means with different letters are significantly different ($p < 0.05$).

All systems are structured thanks to the self-assembly properties of saturated monoglycerides (MG) forming a gel network in hydrophobic or hydrophilic domain, respectively. However, it should be observed that the gel network structure in OG and GE is different, as extensively reported in literature (Batte *et al.*, 2007b; Da Pieve *et al.*, 2010). For this reason, the firmness of the OG and GE samples containing the same lipid fraction resulted different. As expected, the gels containing palm oil showed higher firmness due to the concomitant presence of both MG and palm oil triacylglycerol crystals. The OG and GE samples were used to obtain sweet breads. Control samples were prepared by using palm oil or sunflower oil alone (control) as well as in combination with unstructured MG (MG-control). Samples containing sunflower oil allowed a saturated fat reduction of about 81% (w/w). No statistically significant differences ($p > 0.05$) of crumb water activity (0.94 ± 0.02) and water content ($27.2 \pm 0.9\%$ w/w) were detected among the different samples. The appearance of the samples is shown in Figure 4.1.

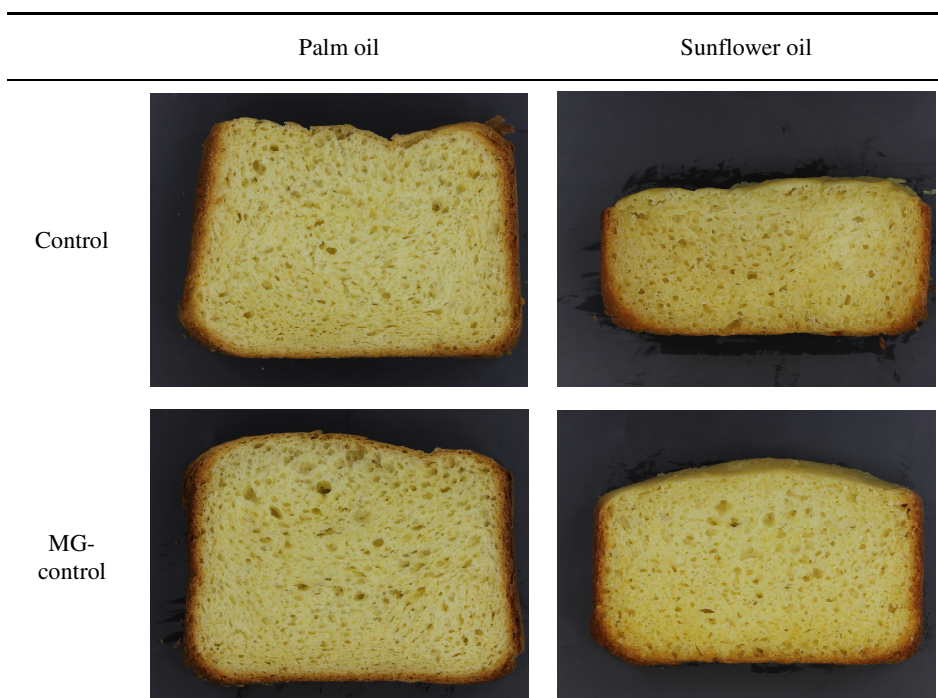




Figure 4.1. Images of sweet bread prepared using organogels (OG) or gelled emulsions (GE) containing palm or sunflower oil. Control: sweet bread prepared using palm or sunflower oil. MG-control: sweet bread prepared using palm or sunflower oil in combination with unstructured MG.

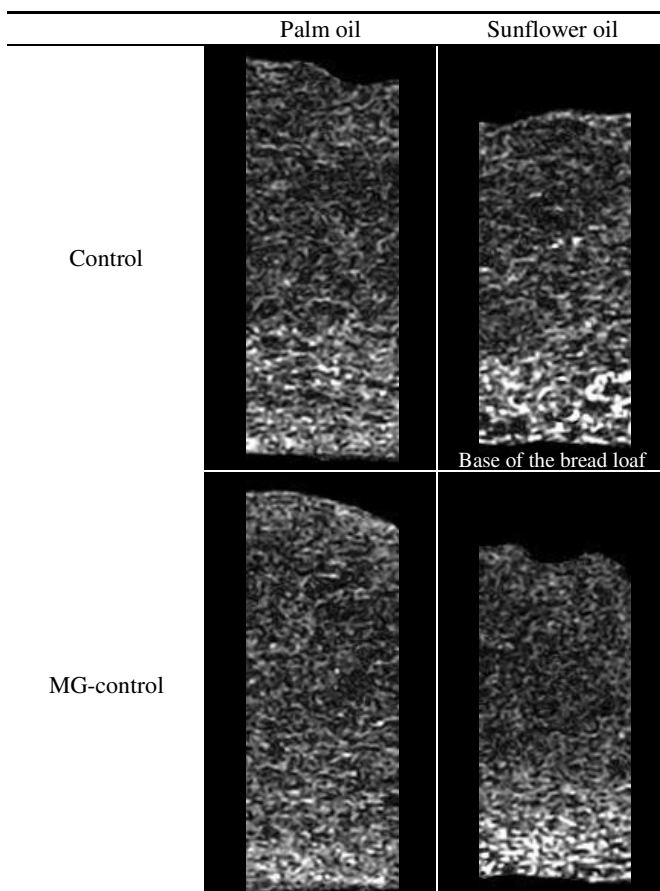
Observing the images, all sweet breads prepared with palm oil showed similar appearance with a well leavened structure. On the other hand, the incorporation of sunflower oil in the formulations resulted in lower leavening. This result can be attributed to the fact that liquid oil did not homogeneously spread over flour hindering the development of a well aerated structure (Brooker, 1996; Chin, Rahman, Hashim, & Kowng, 2010; Manohar & Rao, 1999). By contrast, sweet bread containing sunflower oil GE presented a reasonable aerated structure. These visual observations were consistent with data relevant to bread specific volume and crumb grain (Table 4.2).

Table 4.2. Specific volume, number of small (10 – 100 pixels), medium (100 – 2500 pixels) and large (> 2500 pixels) bubbles of sweet breads prepared using organogels (OG) or gelled emulsions (GE) containing palm or sunflower oil. Control: sweet bread prepared using palm or sunflower oil. MG-control: sweet bread prepared using palm or sunflower oil in combination with unstructured MG.

Oil type	Sample	Specific volume (cm ³ /g)	Number of bubbles		
			Small	Medium	Large
Palm oil	Control	3.09±0.02 ^{ac}	1118±36 ^a	400±14 ^{ab}	24±1 ^a
	MG-control	3.32±0.15 ^a	1162±6 ^{ab}	360±15 ^{bc}	22±1 ^a
	OG	3.29±0.01 ^a	1086±32 ^a	340±19 ^{bc}	22±2 ^a
	GE	3.32±0.08 ^a	1120±81 ^a	395±8 ^{ab}	22±1 ^a
Sunflower oil	Control	2.41±0.12 ^b	1609±97 ^c	428±7 ^a	8±1 ^b
	MG-control	2.77±0.06 ^{bc}	1238±102 ^{ac}	330±7 ^c	20±1 ^{ac}
	OG	2.38±0.11 ^b	1539±56 ^{bc}	312±8 ^c	14±2 ^{bc}
	GE	3.17±0.03 ^{ac}	1018±73 ^a	320±11 ^c	22±1 ^a

^{a,b,c}: means with different letters in the same column are significantly different ($p < 0.05$).

The specific volume of sunflower oil GE bread was actually not significantly different from that of all bread samples containing palm oil. Other samples prepared with sunflower oil (OG and MG control) were characterized by a significantly lower specific volume. Similar considerations can be drawn for the crumb grain, expressed as number of bubbles with different size. Also in this case, the bread prepared with sunflower oil GE showed a number of small and large bubbles in the same magnitude range of those characterizing palm oil samples. These results indicate that the structuration of sunflower oil as GE greatly affected its bakery performances. In particular, its inclusion into OG did not give additional advantages in comparison to sunflower oil alone. Only when both water phase and sunflower oil were introduced in the recipe as GE, the quality characteristics of sweet bread were improved obtaining samples with macro-structure and leavening performance comparable to those containing palm oil, but with a significant lower content of saturated fat. Data on GE effects are in agreement with those reported by Manzocco *et al.* (2012a) on white bread. As previously hypothesized by these authors, the incorporation of sunflower oil within GE in bread could favor its uniform distribution in the dough. The GE network could thus replace the functionality of the triacylglycerol crystal network present in plastic fats (i.e. palm oil). To support these hypotheses, MRI analysis were performed. MRI observations are represented by transverse section images of sweet breads (Figure 4.2).



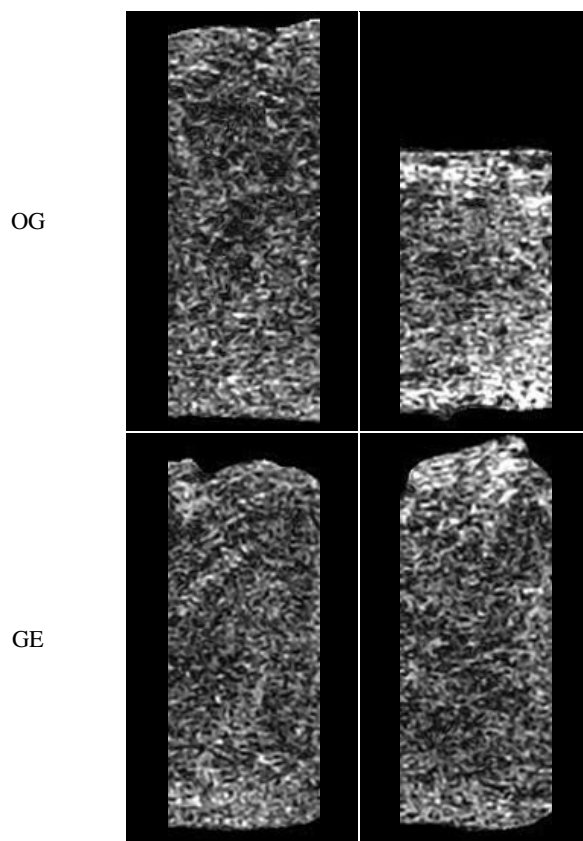


Figure 4.2. T1 Spin-Echo MR images (100 × 280 pixels) of breads prepared using organogels (OG) or gelled emulsions (GE) containing palm or sunflower oil. Control: sweet bread prepared using palm or sunflower oil. MG-control: sweet bread prepared using palm or sunflower oil in combination with unstructured MG.

Original images were characterized by areas with different gray levels, well described by luminosity intensity. Brighter areas, which present greater resonance signal, show locations where proton density/mobility is high; on the contrary darker zones correspond to portions with lower proton density/mobility. The intensity of the signal is determined by the thermal interactions between the resonating protons and other magnetic nuclei in the environment. When protons are held by other molecules present in the magnetic environment, their motion slows considerably and a lower signal can be detected, giving reason for darker areas in the images. It should be noted that the protons of both water and lipids can contribute to the resonance signal. In other words, bright areas observed in the MR images could account for inhomogeneous distribution of moisture and/or lipids in bread.

Intense bright areas were detected at the base of the bread loaves (Figure 4.2). It is noteworthy that ingredients were mixed in the bread making machine after their pouring in the order: water, fat, dry ingredients. These preparation conditions could be associated to a non-uniform distribution of the lipid fraction in the dough, giving reason for the presence of high luminosity areas at the base of the loaves. Moreover, additional bright areas were observed in other parts of the bread images, as well evidenced in samples containing sunflower oil OG and GE (Figure 4.2).

To confirm that brighter areas were associated to fat, MR images were acquired in the STIR mode. This is a peculiar Spin-Echo sequence allowing the suppression of the signal

associated with the lipid phase. Upon lipid signal suppression, the bright areas observed in T1 acquisition mode (Figure 4.2) completely disappeared (data not shown). This result clearly confirms the association of the bright areas observed in the images reported in Figure 4.2 with lipids having high proton mobility. To quantify the mobility of lipid protons in the breads, the amount of bright areas in the loaf images was computed using image analysis. Bright areas were characterized by pixels having luminosity between 170 and 255. The percentage of pixels with this luminosity range (bright pixels) in the MR images of breads prepared according to the different formulations was thus calculated (Table 4.3).

Table 4.3. Percentage of pixels with luminosity between 170 and 255 in the MR images (Spin-Echo sequence of T1) of breads prepared using organogels (OG) or gelled emulsions (GE) containing palm or sunflower oil. Control: sweet bread prepared using palm or sunflower oil. MG-control: sweet bread prepared using palm or sunflower oil in combination with unstructured MG.

Oil type	Sample	Pixels with 170-255 luminosity (%)
Palm oil	Control	3.66
	MG-control	2.77
	OG	3.63
	GE	3.91
Sunflower oil	Control	11.95
	MG-control	7.21
	OG	18.50
	GE	6.41

All breads containing palm oil showed a similar percentage of bright pixels, accounting for comparable density/mobility of lipid protons. In the case of the samples containing sunflower oil, the percentage of bright areas was generally higher. This result could be attributed to the higher proton mobility in the liquid sunflower oil than in the partially crystallized palm oil. Moreover, the percentage of bright pixels was in the order: OG > Control > MG-control > GE. These results clearly confirm the critical role of lipid structuring in controlling proton mobility and favoring a uniform distribution of the lipid fraction in the dough.

Finally, since monoglycerides have well known softening and anti-staling properties (Gomez, del Real, Rosell, Ronda, Blanco, & Caballero, 2004; Purhagen, Sjöo, & Eliasson, 2011; Sawa, Inoue, Lysenko, Edwards, & Preston, 2009), the effect of fat replacement on sweet bread firmness and staling was studied (Table 4.4).

Table 4.4. Firmness after preparation (0 days) and after 14 days of storage at 20 °C of breads prepared using organogels (OG) or gelled emulsions (GE) containing palm or sunflower oil. Control: sweet bread prepared using palm or sunflower oil. MG-control: sweet bread prepared using palm or sunflower oil in combination with unstructured MG.

Oil type	Sample	Firmness (N)	
		0 days	14 days
Palm oil	Control	1.56±0.07 ^a	5.22±0.15 ^a
	MG-control	0.87±0.05 ^c	3.63±0.09 ^b
	OG	1.05±0.06 ^{bc}	3.42±0.06 ^b
	GE	0.78±0.05 ^c	2.82±0.10 ^c
Sunflower oil	Control	1.44±0.01 ^a	5.56±0.06 ^a
	MG-control	0.99±0.06 ^{bc}	3.31±0.15 ^b
	OG	1.28±0.08 ^{ab}	3.36±0.07 ^b
	GE	0.78±0.03 ^c	2.82±0.06 ^c

^{a,b,c}: means with different letters in the same column are significantly different ($p < 0.05$).

Control breads prepared with palm or sunflower oil alone presented higher initial firmness than samples containing MG ($p < 0.05$), confirming the softening capacity of monoglycerides. However, the structure in which they were engaged affected their performances. MG-control breads and breads containing GE showed the lowest firmness. On the contrary, initial higher firmness was detected in the case of bread containing OG. This could be the result of MG involvement in oil networking, making them less available to interact with other ingredients in promoting bread softening. The way by which MG interacts with other ingredients could also account for the different staling of breads stored for up to two week at 20 °C (Table 4.4). After 14 days of storage, control samples were firmer than all samples containing MG. However, breads containing GE appeared more resistant to staling than samples with OG. These results can be associated with the different capacity of MG to form complexes with starch components, depending on the structuring strategy applied. The understanding of these complex interactions needs more in depth research and appears of particular interest in the attempt to clarify the behavior of these molecules in multi component systems.

4.1.4 Conclusions

The substitution of palm oil with sunflower oil structured by monoglyceride self-assembly networks could represent a feasible strategy to design low saturated fat bakery products. In the case of sweet bread, the results acquired demonstrate that the structuring strategy greatly affects the final characteristics of the product. Palm oil substitution with gelled emulsion containing sunflower oil resulted in sweet bread with quality characteristics comparable to that of a control palm oil sample, but with a saturated fat reduction of about 81% (w/w). The presence of MG crystallized lamellas could probably favor the distribution of oil over flour, replacing the typical functionality of triacylglycerol crystal networks. On the contrary, when oil was embedded in an organogel, bread showed an inhomogeneous lipid distribution with a less leavened and firmer structure. This behavior was attributed to the MG engagement in oil networking, making them less available to interact with other ingredients.

Results reported in this study highlight that complex interactions among food components could be expected, especially among monoglycerides, starch and lipids. More in-depth research is needed to elucidate this complex interplay in the attempt to effectively apply novel structural approaches to obtain low saturated fat foods, designed to have similar sensory attributes and shelf-lives as conventional products.

4.2 Omega-3 enriched biscuits with low levels of heat-induced toxicants: effect of formulation and baking conditions

4.2.1 Aim of the study

In this paragraph, the ability of monoglyceride gelled emulsions to deliver ω -3 fatty acids using flax-seed oil in biscuits was studied. In order to avoid lipid oxidation, unconventional baking conditions were exploited using a reduced pressure oven. Quality characteristics as well as toxicants levels were determined in order to define the best performing temperature-pressure-time conditions.

4.2.2 Materials and methods

4.2.2.1 Materials

MyverolTM saturated monoglyceride (MG) (fatty acid composition: 1.4% C14:0, 59.8% C16:0, 38.8% C18:0; melting point 68.05 ± 0.5 °C) was kindly donated by Kerry Ingredients and Flavour (Bristol, United Kingdom). Isooctane, 1-butanol and sodium bicarbonate were from Carlo Erba Reagents (Milan, Italy); methanol, ethyl ether stabilized with 2% of ethanol, 2,3,3-[²H₃] acrylamide (d₃-acrylamide), C₄D₄O (d₄-furan), anhydrous sodium sulphate, co-surfactant mixture of palmitic and stearic acids 1:1 (w/w) were from Sigma Aldrich (Milan, Italy); barium chloride and ferrous sulphate were from Panreac (Barcelona, Spain); ammonium thiocyanate was from Emsure (Damstadt, Germany). Type 0 wheat flour, sucrose, eggs, skimmed milk powder, table salt, sodium bicarbonate (NaHCO₃), baking powder, palm oil were purchased in a local market. Flax-seed oil was from Solimè (Cavriago, Italy). According to producer indications, total omega-3 fatty acids in flax-seed oil were 53.4%. All solutions were prepared using milli-Q water.

4.2.2.2 Preparation of monoglyceride–flax-seed oil–water gelled emulsion

The monoglyceride–flax-seed oil–water gel, hereafter called gelled emulsion (GE) was prepared according to the slightly modified method of Calligaris *et al.* (2010). MG was mixed with a co-surfactant mixture of palmitic and stearic acids 1:1 (w/w) in a ratio of 5:1 (w/w). The water phase consisted of 1 mM NaHCO₃ in deionized milli-Q water to promote the partial neutralization of the co-surfactant mixture and obtain a properly swollen phase. The gelled emulsion was obtained by mixing the flax-seed oil, previously heated at 70 °C, with the MG/co-surfactant mixture up to complete dissolution, followed by the addition of the heated (70 °C) water solution. The two phases were then homogenized by using a high speed homogenizer (DI 25, Ika-Werke, Staufen, Germany) at 59,000 x g for 90 s. Afterwards, the mixture was cooled at 4 °C in an ice bath and then stored at 4 °C for 24 h before use. The concentration of each constituent in the gelled emulsion was as follows: MG/co-surfactant, 4.8% (w/w), flax-seed oil, 47.6% (w/w), water solution, 47.6% (w/w).

4.2.2.3 Short dough biscuits preparation

The non-water ingredients consisted of type 0 wheat flour, sucrose, eggs, skimmed milk powder, table salt, baking powder, palm oil or GE were added to the recipe at 54, 15, 0.7, 0.3, 0.2, 1.1, and 29% on total weight, respectively. The fat concentration of the gelled emulsion added to the formulation corresponded to 15% (w/w). All the ingredients except the palm oil or gelled emulsion and the wheat flour were first mixed for 15 min by using a kneader (Hobart, N50CE, Ohio, USA). Afterwards, the palm oil or GE was incorporated and mixed for 5 min, followed by the addition of the wheat flour and kneaded for further 15 min. After mixing, the dough was sheeted to 8 mm thickness and cut to a diameter of 50 mm. The samples were baked in an oven (5Pascal, VS-25 SC, Trezzano S/N, Milan, Italy) connected to a rotary vacuum pump (BOC Edwards, E2M40, Crawley, West Sussex, UK) able to achieve a pressure of 1.33 Pa in a few seconds when the oven was empty. Once the desired

temperature was reached, two dough biscuits, previously weighed (approximately 5 g each), were introduced in the central rear part of the oven on a plate and the vacuum pump was immediately switched on. The time needed to achieve the desired vacuum was less than 10 s. Computation of treatment duration started once the set pressure value was achieved. Baking was carried out at different pressures, temperatures and times according to a central composite design. To study the GE performance in the formulation, extra trials were carried out at 180 °C and atmospheric pressure for 20 min. After the treatments, samples were immediately removed from the oven and cooled to room temperature. Afterwards, they were transferred into high barrier film pouches, sealed, and stored at -18 °C until analysis were performed.

4.2.2.4 Temperature monitoring and thermal effect computation

Temperature changes during baking were measured by a copper-constantan thermocouple probe (Ellab, Denmark), whose tip (2.0 mm) was placed on the sample surface. The thermal effect F (min) was computed using the following equation (Ball, 1923):

$$F = \int_0^t 10^{\left(\frac{T - T_{ref}}{z}\right)} dt \quad (\text{eq. 4.1})$$

where T_{ref} is the reference temperature, which was chosen equal to 200 °C, a baking process being generally carried out at temperatures around 200 °C, T is the actual temperature of the treatment (°C), t is the time (min) of the treatment, and z represents the increase in temperature that causes a 10-fold increase in the reaction rate, which was reported to be equal to 56 °C for the browning reaction (Sacchetti, Di Mattia, Pittia, & Mastrocola, 2009).

4.2.2.5 Acrylamide analysis

Acrylamide determination was carried out according to the method of Anese, Bortolomeazzi, Manzocco, Manzano, Giusto, and Nicoli (2009). Briefly, 1000 µL of an aqueous solution of 2,3,3-[²H₃] acrylamide (d₃-acrylamide) (0.20 µg/mL) as internal standard and 15 mL of milli-Q water were added to 1 g of finely ground biscuit weighed into a 100 mL centrifuge tube. After extraction at 60 °C for 30 min under magnetic stirring, the mixture was centrifuged at 12000 x g for 15 min at 4 °C (Beckman, Avanti Centrifuge J-25, Palo Alto, USA). Aliquots of 10 mL of the clarified aqueous extract were cleaned-up by solid phase extraction (SPE) on an Isolute Env+, 1 g (Biotage, Sweden) conditioned with 5 mL of methanol and 5 mL of water. 10 mL of the extract were loaded onto the SPE column followed by 10 mL of water to elute interference compounds. Acrylamide was then eluted with 5 mL of a mixture of methanol (60% v/v) in water. The volume of the eluted fraction was reduced under vacuum, to about 1.5 – 2 mL by using a rotary evaporator (Laborata 4001, Heidolph, Schwabach, Germany) at a temperature of 80 °C and filtered through a 0.45 µm membrane filter before further analysis. LC-ESI-MS-MS in positive ion mode analysis was performed by a Finnigan LXQ linear trap mass spectrometer (Thermo Electron Corporation, San Josè, USA) coupled to a Finnigan Surveyor LC Pump Plus equipped with a thermostated autosampler and a thermostated column oven. The analytical column was a Waters Spherisorb ODS2 (250 x 2.0 mm, 5 µm). Elution was carried out at a flow-rate of 0.1 mL/min, in isocratic conditions at 30 °C using as mobile phase a mixture of 98.9% water, 1% methanol and 0.1% formic acid (v/v/v). Full scan MS/MS was carried out by selecting the ions at m/z 72 and m/z 75 as precursor ions for acrylamide and d₃-acrylamide, respectively. The area of the chromatographic peaks of the extracted ion at m/z 55, due to the transition 72 > 55, and at m/z 58, due to the transition 75 > 58 were used for the quantitative analysis. The quantitative analysis was carried out with the method of the internal standard. The relative response factor of acrylamide with respect to d₃-acrylamide was calculated daily by analyzing a

standard solution. For each run, analysis were made at least in duplicate. Acrylamide concentration was expressed as ng/g of dry matter.

4.2.2.6 Furan analysis

Furan determination was carried out by combining solid phase micro-extraction (SPME) and GC-MS analysis according to the slightly modified method of Bianchi, Careri, Mangia, and Musci (2006). Briefly, aliquots of 2 g sample were added with 2 mL NaCl 20 g/100 g water solution of d₄-furan (30 µg/kg; internal standard). SPME experiments were performed with a 85 µm carboxen polydimethylsiloxane fiber (Supelco, Bellfonte, PA, USA). Incubation time and temperature of the fiber were 5 min and 40 °C, respectively; extraction time and temperature were 20 min and 40 °C, respectively. Desorption was carried out at 270 °C for 2 min. GC oven temperature program was: 40 °C for 5 min, 15 °C/min to 300 °C. Mass spectrometer was operated in selected ion monitoring mode and the current of the following ions was recorded: m/z 68 and 39 for furan and m/z 72 and 42 for d₄-furan. Ion ratios were used to confirm the identification of the analyte; standard addition calibration method was applied for the correspondent quantification. The relative response factor of furan with respect to d₄-furan was calculated daily by analyzing a standard solution. For each run, analysis were made in duplicate. Furan concentration was expressed as ng/g of dry matter.

4.2.2.7 Color analysis

Color analysis was carried out on five different points of sample surface using a tristimulus colorimeter (Chromameter-2 Reflectance, Minolta, Osaka, Japan) equipped with a CR-400 measuring head. The instrument was standardized against a white tile before measurements. Color was expressed in lightness (L*), red to green (a*) and yellow to blue (b*) scale parameters and a* and b* were used to compute the hue angle ($\tan^{-1} b^*/a^*$) (Clydesdale, 1978)

4.2.2.8 Total solid content determination

Samples were analyzed following the same procedure reported in paragraph 4.1.2.4 (pag. 78).

4.2.2.9 Lipid extraction

Lipids were extracted following the methodology described by Kristensen, Orlien, Mortensen, Brockhoff, and Skibsted (2000). Before extraction, ethyl ether was purified from peroxides using a saturated aqueous solution of FeSO₄ and then separated and dried using anhydrous sodium sulphate. In brief, about 10 g sample was added with 30 mL of isooctane and homogenized using a high speed homogenizer (DI 25, Ika-Werke, Staufen, Germany) at 9,000 rpm for 2 min. The blend was added with 30 mL of isooctane, 30 mL of methanol and 60 mL of ethyl ether and stirred at room temperature at 700 rpm for 20 min and then let statically settle. The liquid part was added with anhydrous sodium sulphate and the supernatant filtered through Whatman n. 1 filter paper and evaporated using a rotary evaporator (Laborata 4001, Heidolph, Schwabach, Germany) at 120 rpm and 50 °C, decreasing the pressure from 900 mbar to 15 mbar in 30 min. The lipid fraction was finally transferred to a 10 mL vial, saturated with nitrogen, sealed and stored at -30 °C until analysis were performed.

4.2.2.10 Peroxide value determination

Peroxide value was determined following the method of Shantha and Decker (1994). Lipid samples (0.016 g) were added with 2.8 mL of methanol/butanol solution (2:1 v/v) followed, after vortexing, by the addition of 0.015 mL of ferrous ion solution (prepared through the mixture of 0.033 M BaCl₂ and 0.036 M FeSO₄) and 0.015 mL of 3.94 M ammonium

thiocyanate. After 20 min of incubation at room temperature, absorbance was measured at 510 nm with a UV-2501 PC spectrophotometer (Shimadzu, Kyoto, Japan). The peroxide value (PV) expressed as milliequivalents of oxygen per kilogram of fat was calculated using the following equation:

$$PV = \frac{(A_s - A_b) \cdot m}{55.84 \cdot m_0 \cdot 2} \quad (\text{eq. 4.2})$$

where A_s is the absorbance of the sample, A_b is the absorbance of the blank prepared by mixing all the reagents except for the extracted lipids, m is the slope of the calibration curve of Fe^{3+} concentration vs absorbance, m_0 is the mass in grams of the sample, and 55.84 is the atomic weight of iron.

4.2.2.11 Rheological analysis

Samples were analyzed following the same procedure and using the same equipment reported in paragraph 3.1.2.5 (pag. 56).

4.2.2.12 Firmness

Samples were analyzed using the same equipment reported in paragraph 2.2.2.7 (pag. 45). The instrument was equipped with a 5 kN load cell. Biscuits were positioned on two bars and broken by applying a cross-head speed of 5 mm/s to the blade edge. Firmness was defined as the maximum force required to break the biscuit. From each baking experiment, six biscuits were analyzed.

4.2.2.13 Polynomial equations and statistical analysis

Modelling was aimed at describing the variation of water content, color, peroxide value, acrylamide, and furan concentrations as a function of the variables of the central composite design. In particular, a 3 factors face centered central composite design was used, here after called CCF. The three considered factors were baking temperature, time and pressure. The ranges of variables were chosen on the basis of information from the preliminary trials, showing that the application of values outside the considered intervals led to under processed or over-processed samples. For each factor, extreme lower and upper values were combined to form the factorial part of the design (8 factorial points). To complete the CCF, 6 axial points (combinations of the extreme value of one factor and the intermediate level for the others) and 1 central point (combination of the intermediate values of the three factors) were defined.

All the factorial and axial points were replicated once while the central point was replicated 6 times. The full set of sampling points is reported in Table 4.5. As pressure values of different magnitude were considered, they were expressed in logarithmic scale for data modelling. A software package (Statistica for Windows v. 10, StatSoft, Inc., Tulsa, USA) was used to fit the second order response surface to the observed data according to the following equation:

$$y = B_0 + \sum_{i=1}^k B_i x_i + \sum_{i=1}^k B_{ii} x_i^2 + \sum_{j>i \geq 1}^k B_{ij} x_i x_j \quad (\text{eq. 4.3})$$

where B_0 is a constant, and B_i , B_{ii} , B_{ij} are regression coefficients of the model, x_i and x_j are the independent variables in coded values, and k is the number of factors.

Shapiro-Wilk test was used to evaluate normality of the data, while the possible presence of outliers and the homogeneity of variance were evaluated by residual analysis. Goodness of fit was measured with the adjusted determination coefficient (R_{adj}^2). p -values for the coefficients of the response surface were defined using standard t -test.

Three-dimensional surface plots were drawn to illustrate the effects of the considered factors on the responses. To this purpose, the values of the response were plotted on the z-axis against the two most relevant factors, keeping the third one fixed to a constant value (the central one).

4.2.3 Results and discussion

4.2.3.1 Gelled emulsion formulation and its incorporation in the dough

To incorporate flax-seed oil in the dough, a monoglyceride flax-seed oil–water gel, hereafter called gelled emulsion, was developed. A maximum amount of 47.6% (w/w) of flax-seed oil was incorporated into the gel. As expected, the flax-seed oil-based gelled emulsion presented gel-like properties, the G' modulus being higher than the G'' modulus (8.88 ± 0.11 kPa and 2.46 ± 0.14 kPa, respectively), in agreement with the literature for monoglyceride-oil–water systems (Batte *et al.*, 2007b; Calligaris *et al.*, 2010). As well documented in the literature, the gelled emulsion elasticity is attributable to the monoglycerides that, while self-assembling, may form a network of crystallized vesicles containing oil (Batte *et al.*, 2007b). The gelled emulsion was added to the dough formulation at 29% on total weight and its performance visually evaluated and compared with a control biscuit containing palm oil. After baking at 180 °C for 20 min at atmospheric pressure, a gelled emulsion containing biscuit regular in shape and color ($L^* = 65 \pm 2$ and hue angle = 74 ± 1 , and $L^* = 69 \pm 1$ and hue angle = 78 ± 1 , for the gelled emulsion and palm oil containing biscuits, respectively) was obtained. The firmness of the gelled emulsion containing biscuit was slightly lower than that of the palm oil containing control sample (38 ± 8 N and 52 ± 10 N, respectively), although they did not differ significantly in water content ($< 3\%$ w/w). These results indicate that the use of the gelled emulsion allowed biscuits with desired quality to be obtained, in agreement with previous findings (Anese, Quarta, Peloux, & Calligaris, 2011; Goldstein & Seetharaman, 2011; Manzocco *et al.*, 2012b). Therefore, the gelled emulsion was used to further prepare omega-3 PUFAs enriched samples to be subjected to baking according to a 3 factors face centered central composite design (CCF).

4.2.3.2 Identification of baking conditions at reduced pressure of omega-3 PUFAs enriched biscuits

Table 4.5 shows the water content, hue angle, peroxide value as well as acrylamide and furan concentrations of biscuits containing the gelled emulsion subjected to baking under different conditions according to the CCF.

Table 4.5. Combinations of temperature, pressure, and time of different runs and experimental results \pm standard deviation of a three factors face centered central composite design.

Run	Temperature (°C)	Pressure (Log Pa)	Time (min)	Water content (% w/w)	Hue angle ($\tan^{-1} b^*/a^*$)	Peroxide value (mEq O ₂ /kg _{fat})	Acrylamide (ng/g)	Furan (ng/g)
1	150	5.00	45	6.03 \pm 0.16	79.2 \pm 0.3	3.07 \pm 0.03	125.7 \pm 4.4	10 \pm 2
2	150	5.00	35	9.06 \pm 0.13	81.3 \pm 0.5	2.40 \pm 0.01	51.3 \pm 1.9	11 \pm 2
3	197	5.00	35	2.49 \pm 0.01	71.8 \pm 0.5	20.12 \pm 0.71	419.2 \pm 18.8	27 \pm 4
4	197	5.00	45	0.48 \pm 0.06	67.7 \pm 2.3	10.92 \pm 3.60	709.3 \pm 31.5	174 \pm 24
5	150	2.17	45	5.14 \pm 0.01	90.9 \pm 0.4	3.07 \pm 0.02	10.0 \pm 1.1	20 \pm 3
6	150	2.17	35	5.09 \pm 0.02	90.8 \pm 0.5	2.40 \pm 0.01	9.0 \pm 0.7	9 \pm 1
7	197	2.17	45	0.40 \pm 0.02	67.8 \pm 2.7	2.30 \pm 0.08	225.7 \pm 6.4	9 \pm 2
8	197	2.17	35	0.54 \pm 0.07	73.8 \pm 2.6	2.62 \pm 0.02	199.6 \pm 4.5	12 \pm 2
9	174	2.17	40	1.59 \pm 0.12	90.8 \pm 0.6	2.60 \pm 0.01	19.2 \pm 1.6	9 \pm 2
10	174	5.00	40	5.25 \pm 0.09	75.1 \pm 0.6	5.15 \pm 0.21	220.5 \pm 6.9	9 \pm 2
11	174	3.60	45	0.82 \pm 0.25	85.7 \pm 2.3	1.75 \pm 0.02	75.1 \pm 2.4	9 \pm 1
12	174	3.60	35	1.31 \pm 0.10	90.1 \pm 2.0	4.72 \pm 0.59	42.7 \pm 0.6	9 \pm 1
13	197	3.60	40	0.38 \pm 0.04	69.3 \pm 3.2	6.00 \pm 0.41	255.5 \pm 3.5	11 \pm 2
14	150	3.60	40	2.42 \pm 0.08	92.0 \pm 0.2	2.57 \pm 0.01	7.8 \pm 1.2	9 \pm 2
15	174	3.60	40	0.87 \pm 0.16	88.1 \pm 1.9	4.05 \pm 0.05	51.5 \pm 2.5	10 \pm 1
16	174	3.60	40	1.47 \pm 0.02	91.6 \pm 1.2	1.92 \pm 0.02	86.0 \pm 3.0	9 \pm 1
17	174	3.60	40	0.71 \pm 0.05	90.0 \pm 1.5	1.62 \pm 0.02	31.9 \pm 1.0	10 \pm 2
18	174	3.60	40	0.53 \pm 0.01	88.1 \pm 4.4	2.02 \pm 0.07	77.6 \pm 0.8	9 \pm 2
19	174	3.60	40	0.83 \pm 0.03	87.9 \pm 3.6	2.72 \pm 0.05	94.6 \pm 3.5	31 \pm 5
20	174	3.60	40	1.23 \pm 0.19	90.4 \pm 1.6	2.55 \pm 0.00	42.8 \pm 2.0	13 \pm 3

The regression coefficients and their relative analysis of variance of the polynomial models for the dependent variables are presented in Table 4.6.

Table 4.6. Regression coefficients of the models for water content, hue angle, peroxide value and acrylamide.

Variable	Water content	Hue angle	Peroxide value	Acrylamide
Intercept	40.204	-219.914	70.835	7538.511
Temp	-0.305 ^{***}	4.108 ^{***}	-0.766 ^{***}	-61.552 ^{***}
Temp ²	0.0006	-0.012 ^{**}	0.003	0.146 ^{**}
LogP	-2.371 ^{**}	0.551 ^{**}	-13.007 ^{***}	-766.073 ^{***}
LogP ²	1.174 ^{***}	-2.199 [*]	0.605	38.846 [*]
Time	0.053	-0.301	0.592 [*]	-83.160 ^{**}
Time ²	-0.0001	0.022	0.022	0.324
Temp x LogP	0.010	0.062	0.097 ^{***}	2.039 ^{***}
Temp x Time	0.0009	-0.011	-0.012 [*]	0.256 [*]
LogP x Time	-0.087	0.038	-0.156	5.930 ^{**}
R ² adj	0.882	0.884	0.871	0.953

^{*}: $p < 0.05$; ^{**}: $p < 0.01$; ^{***}: $p < 0.001$

The R²_{adj} values for the responses were higher than 0.871. As it can be observed in Table 4.5, all factor combinations, except that including the highest factors values (run 4), allowed furan accumulation to be prevented. In fact, in contrast with the biscuit baked at atmospheric pressure and 197 °C for 45 min that presented a furan concentration of 174 ng/g, furan levels were always lower than 32 ng/g and in most cases below the quantification limit (10 ng/g) for this molecule. As a consequence, it was not possible to find an appropriate model to

describe these data. The results showed that temperature as well as the linear and quadratic terms of log pressure had a significant effect on moisture content, showing p -values lower than 0.001, 0.01, and 0.001, respectively. To evaluate the effects of the independent variables on the dependent ones and to predict the optimum values of each variable for maximum/minimum yield, three-dimensional response surface plots were generated.

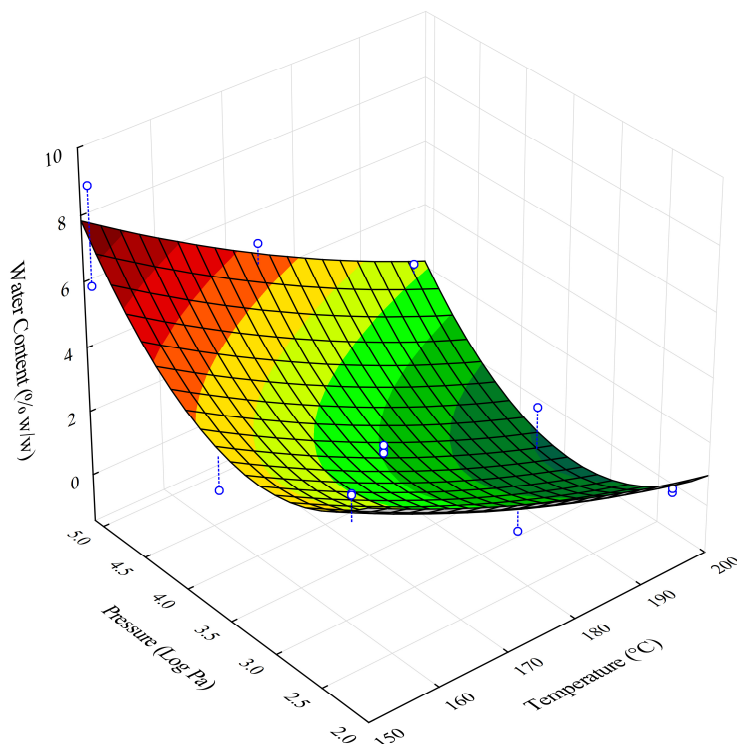


Figure 4.3. Response surface plot showing the effect of baking temperature and pressure on water content of short dough biscuits. A constant value (central point) was imposed to the third independent variable (time) of the CCF.

Figure 4.3 shows the response surface plot relevant to the effect of temperature and pressure on water content changes occurring in the biscuits during baking. As expected, the lowest moisture contents were achieved at the highest temperature and pressure conditions. Results also show that baking at reduced pressure slightly favored moisture removal. This can be attributable to a stripping effect towards water, that was promoted by the low pressure inside the oven. Moreover, Figure 4.3 shows that, in these experimental conditions, the minimum water content was obtained at pressure values of 0.15 kPa (corresponding to 3.6 Log Pa). It is noteworthy that a 3% (w/w) moisture, that is the highest water content acceptable for biscuits, was also achieved by 40 min baking at the lowest temperature (150 °C) and pressure (0.15 kPa). It is well-known that color is an important quality parameter for biscuits. Color development is the result of the formation of brown polymers (i.e. melanoidins) in the advanced stages of non-enzymatic browning reactions. As color development has been associated to acrylamide formation, light brown is considered an acceptable color for biscuits (Food Drink Europe, 2013) . Biscuits color changes were assessed by means of color measurements and expressed as hue angle. A decrease in hue angle is an index of browning development. According to the results shown in Table 4.6, temperature and pressure as both

linear and quadratic terms, significantly affected the hue angle of the biscuits, although the influence of pressure quadratic term was lower than that of the other factors.

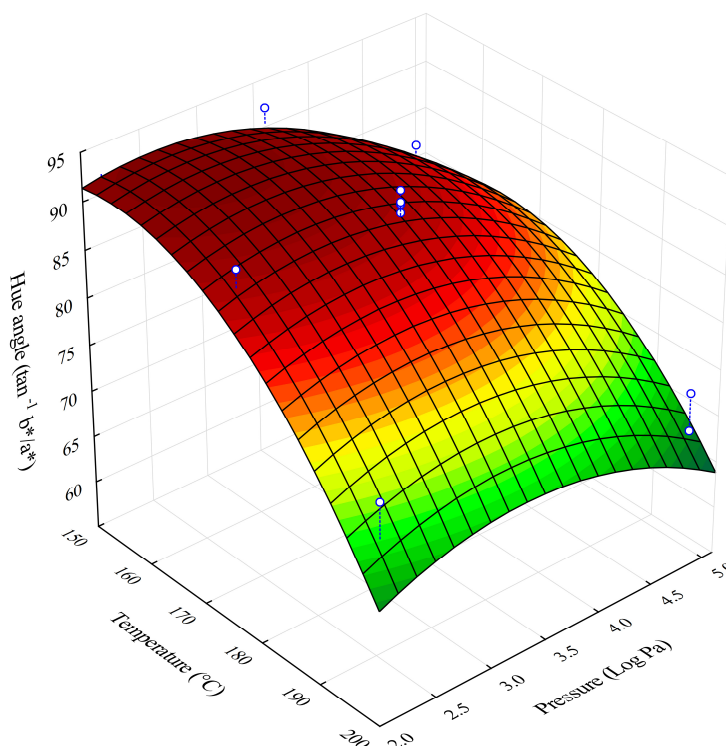


Figure 4.4. Response surface plot showing the effect of baking temperature and pressure on hue angle of short dough biscuits. A constant value (central point) was imposed to the third independent variable (time) of the CCF.

Figure 4.4 shows the response surface plot relevant to the effect of temperature and pressure on the hue angle of the biscuits subjected to baking. Baking at the lowest temperature and pressure conditions led to the least colored biscuits, while lower hue angle values (i.e. the higher color development) were achieved at temperatures higher than 190 °C at both high and low pressure values. It is noteworthy that baking at ambient pressure allowed color development to occur at lower temperature as compared to the vacuum process. These results suggest that moisture and color values acceptable for biscuit production can be actually achieved at reduced pressure conditions. As already pointed out, due to its chemical feature, omega-3 PUFAs are very susceptible to oxidative reactions, that may be favored by the high baking temperature. To study the influence of the independent variables on the oxidation of omega-3 fatty acids, the peroxide value of the biscuit lipid fraction was measured (Table 4.5). Temperature and pressure as linear and interactive terms were the major factors influencing this parameter ($p < 0.001$), while time and the interaction between time and temperature had a lower effect ($p < 0.05$) (Table 4.6).

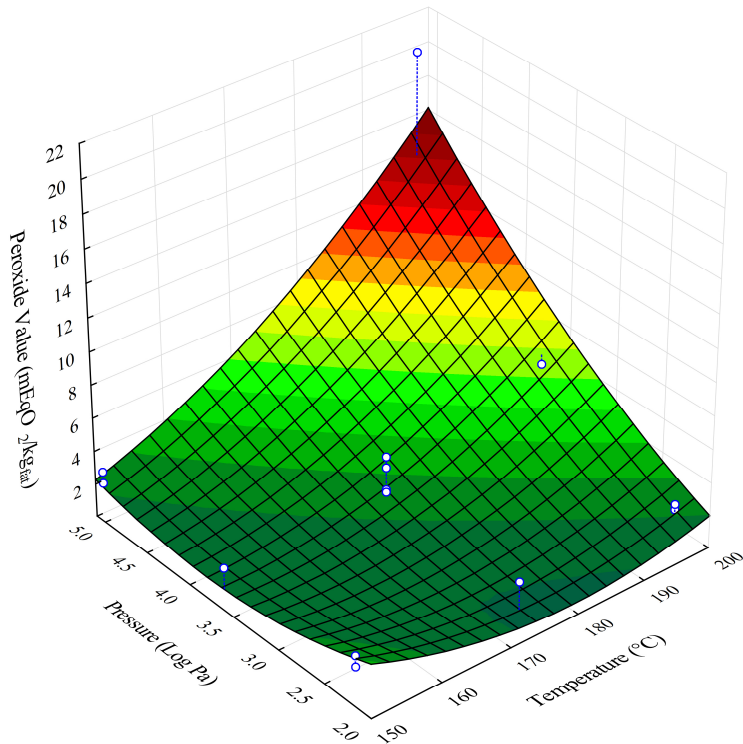


Figure 4.5. Response surface plot showing the effect of baking temperature and pressure on peroxide value of the lipid fraction of short dough biscuits. A constant value (central point) was imposed to the third independent variable (time) of the CCF.

The maximum peroxide value was achieved at the highest temperature and pressure values, whereas no peroxide formation was detected in biscuits subjected to baking at any temperature when the pressure was kept at intermediate or low values (Figure 4.5). It can be suggested that when baking was performed at reduced pressure conditions, the low oxygen concentration present inside the oven would prevent oxidative reactions to occur. The effect of the process variables on acrylamide formation in the biscuits was also evaluated. As already stated, considerably high amounts of this heat-induced toxic molecule can form upon baking of cereal products (Claus, Carle, & Schieber, 2008). In particular, acrylamide formation proceeds faster in the final steps of baking in correspondence of low moisture contents (Brathen & Knutsen, 2005) along with brown development (Gokmen & Senyuva, 2006). The ANOVA showed that all the process variables, except the quadratic term of time, affected the formation of the toxic molecule, although with different significance (Table 4.6). Temperature and pressure as linear and interactive terms were the process variables most affecting the acrylamide yields, as indicated by their smaller p -values.

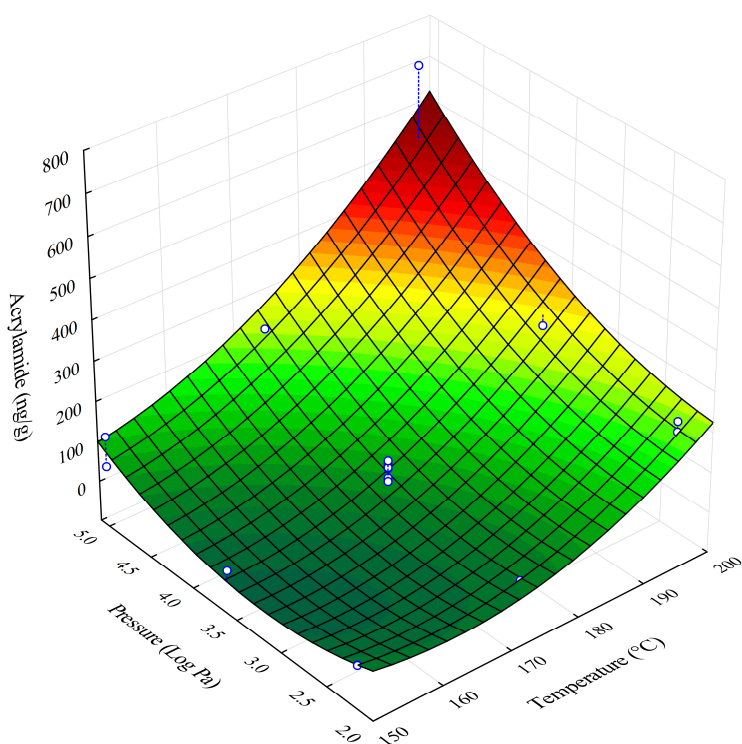


Figure 4.6. Response surface plot showing the effect of baking temperature and pressure on acrylamide concentration of short dough biscuits. A constant value (central point) was imposed to the third independent variable (time) of the CCF.

The effects of the interactions between pressure and temperature on acrylamide formation are shown in Figure 4.6. A maximum acrylamide level was attained at the highest pressure and temperature values. Acrylamide levels lower than 500 ng/g, that is the maximum recommended concentration in biscuits (EFSA, 2013), were formed at any temperature when pressure was reduced from atmospheric to intermediate or low values. Overall, these results suggest that, within the limits of the present study, baking at high temperature and reduced pressure allowed biscuits with acceptable water content and color to be obtained, while minimizing omega-3 PUFAs degradation by oxidative reaction as well as acrylamide and furan formation. In particular, the combination 174 °C - 3.99 kPa - 45 min allowed biscuits responding to these characteristics to be obtained. In order to compare the impact of pressure on non-enzymatic browning reaction independently of the combination of temperature and time experienced by the sample during baking, data relevant to hue angle and acrylamide (Table 4.5) were further elaborated. In particular, they were plotted against the thermal effect F , that is the time-temperature combination received by the dough at each baking time (Figure 4.7a and b).

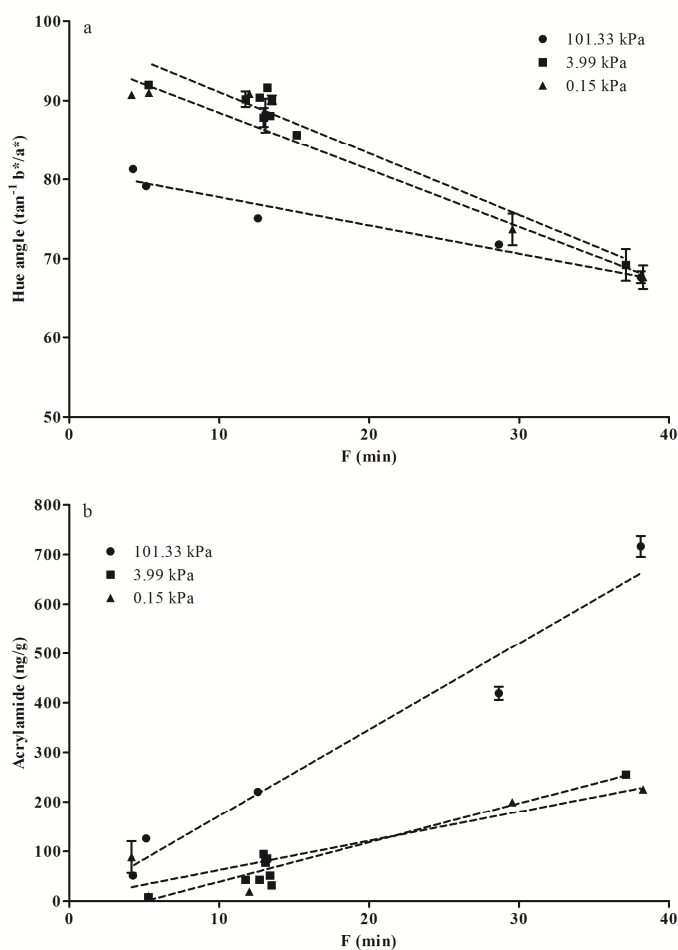


Figure 4.7. Hue angle (a) and acrylamide concentration (b) of short dough biscuits subjected to baking under reduced pressure conditions as a function of the thermal effect F .

Table 4.7. Rate constants \pm 95% confidence interval errors computed from the slopes of the linear regression of hue angle and acrylamide concentration of short dough biscuits subjected to baking under different pressure conditions vs the thermal effect.

Parameter	Pressure (kPa)	Rate constant ($\tan^{-1}b^*/a^* \text{ min}^{-1}$; ng/g min^{-1})	R^2_{adj}
Hue angle	101.3	-0.36 ± 0.15^a	0.936
	3.99	-0.77 ± 0.17^b	0.927
	0.15	-0.72 ± 0.27^b	0.947
Acrylamide	101.3	17.29 ± 6.17^a	0.952
	3.99	7.91 ± 1.97^b	0.904
	0.15	5.88 ± 5.32^b	0.740

^{a,b}. For each parameter considered, significant difference is indicated by different letters ($p < 0.05$).

Table 4.7 shows the rate constants computed from the slopes of the linear regression of hue angle and acrylamide concentration of short dough biscuits subjected to baking under different pressure conditions vs F . The computed rate constants showed statistical differences

from 0 ($p < 0.05$). The pseudo zero order rate constant of hue angle in the biscuits baked at atmospheric pressure was higher (i.e. indicating a slower browning development) than those found for the biscuits obtained at lower pressures. In particular, discrepancies in hue angle among the biscuits were higher at low F values and decreased with the increasing of F , becoming similar at approximately 38 min (i.e. the highest F value received by the samples). Moreover, no significant differences between the rate constant computed for the baking processes carried out at 3.99 and 0.15 kPa were found ($p > 0.05$). This lower value of hue angle rate constant (i.e. higher rate of color development) at low pressure can be attributed to faster water removal due to the low pressure inside the oven (Table 4.5). In addition, as exemplified in Table 4.7, the rate of acrylamide formation for increasing F values was greater for the biscuits baked at ambient pressure than for samples cooked at reduced pressure. Similar results have been previously found for coffee subjected to roasting under low pressure conditions (Anese, Nicoli, Verardo, Munari, Mirolo, & Bortolomeazzi, 2014). These data seem to suggest that (a) lower acrylamide is formed at reduced pressure conditions or (b) as soon as the toxic molecule is generated, the low pressure generated inside the oven would promote acrylamide removal, thus preventing its accumulation. Moreover, in the latter case, as acrylamide is a water soluble molecule, it is likely that its removal occurs along with that of water. Similar mechanisms can be suggested for furan. In this case, all the baking conditions at reduced pressure were effective in keeping furan levels below the quantification limit (Table 4.5). According to the removal mechanism, it can be suggested that as soon as furan is formed, it is almost quantitatively removed due to its higher volatility as compared with acrylamide.

4.2.4 Conclusions

The results of this study indicate that baking at high temperature and reduced pressure allowed to obtain biscuits with acceptable water content and color, while minimizing omega-3 PUFAs degradation by oxidative reaction as well as acrylamide and furan levels. In particular, results of the experimental plan showed that the combination 174 °C - 3.99 kPa - 45 min resulted effective in producing biscuits with acrylamide concentration and peroxide value below 100 ng/g and 2 mEqO₂/kg_{fat} respectively, as well as furan at negligible levels. As compared with the conventionally baked sample (200 °C - 101.3 kPa - 35 min), these baking conditions led to an acceptable reduction in brown development. It is noteworthy that this is in line with the indications given by the Food Drink Europe (2013) association stating that producing lighter colored biscuits, without increasing the moisture content, could represent a strategy to reduce acrylamide content. Moreover, as the application of baking at low pressure conditions may be responsible for the removal of desired flavor compounds, sensory analysis has to be performed.

Although further research should be conducted at pilot and industrial scale to find optimum process conditions, these results suggest that baking under reduced pressure could have a great economic impact, due to the large diffusion of this food category; not only the conventional bakery products but also the functional ones are becoming very popular.

PART II

Delivery systems for lipophilic bioactive compounds

Aim

The aim of this part is to investigate the effect of lipid physical state on bioactive molecule stability in bulk and emulsified systems. To this aim β -carotene and curcumin were chosen as target compounds.

Transparent emulsified systems delivering bioactive molecule by low-energy emulsification methods were then developed. To this purpose the self-assembly properties of the non-ionic surfactant Tween 80 were exploited.

Effect of lipid physical state on selected bioactive compound stability

5.1 Structure studies on curcumin and β -carotene added to solid fat matrices

5.1.1 Aim of the study

Contradictory results on the effect of lipid carriers physical structure on bioactive molecule stability can be found in literature. Indeed, according to some studies, the inclusion of lipophilic compounds into a solid core improves their chemical stability (Nik, Langmaid, & Wright, 2012; Relkin, Jung, & Ollivon, 2009). On the contrary, other authors found a greater degradation rate of biomolecules in solid lipid carriers than in liquid lipid ones (Cornacchia & Roos, 2011; Helgason, Awad, Kristbergsson, Decker, McClements, & Weiss, 2009a; Qian, Decker, Xiao, & McClements, 2013). Blends of solid and liquid lipids have been also proposed to improve loading capacity for the active compounds (Gutiérrez, Albillos, Casas-Sanz, Cruz, García-Estrada, García-Guerra, García-Reverter, García-Suárez, Gatón, González-Ferrero, Olabarrieta, Olasagasti, Rainieri, Rivera-Patiño, Rojo, Romo-Hualde, Sáiz-Abajo, & Mussons, 2013). These contradictory observations can be ascribed to the complexity of parameters affecting lipids crystallization.

The aim of this paragraph is to understand the complex interplay between bioactive molecule and fat crystallization. To this aim, β -carotene and curcumin were chosen as lipophilic bioactive molecules. They were included in saturated monoglycerides, tripalmitin, and tristearin crystal matrices.

5.1.2 Materials and methods

5.1.2.1 Materials

Myverol™ saturated monoglyceride (MG) (fatty acid composition: 1.4% C14:0, 59.8% C16:0, 38.8% C18:0; melting point 68.05 ± 0.5 °C) was kindly donated by Kerry Ingredients and Flavour (Bristol, United Kingdom). Tripalmitin (PPP; purity $\geq 85\%$), tristearin (SSS; purity $\geq 85\%$), and crystalline β -carotene (purity $\geq 93\%$) were purchased from Sigma Aldrich (Milan, Italy). Curcumin [1,7-bis(4-idrossi-3-metossifenil)1,6-epta3,5-dione] (purity $\geq 80\%$) was purchased from Extrasynthese (Genay, Francia).

5.1.2.2 β -carotene or curcumin containing lipid matrices preparation

Aliquots of approximately 20 mg of crystalline MG, PPP or SSS were added with 5% (w/w) of crystalline β -carotene or curcumin in DSC pans (160 μ L, Mettler Toledo, Greifensee, Switzerland). Samples were heated in a TA4000 differential scanning calorimeter (Mettler-Toledo, Greifensee, Switzerland) from 20 to 200 °C at 2 °C/min to allow melting of fats, β -carotene and curcumin. Samples were then cooled from 200 to 20 °C at 2 °C/min. This procedure allowed β -carotene and curcumin to be finely dispersed in the lipid matrix. Sample aliquots were finally collected from the DSC pans and analyzed. Bulk lipids subjected to the same heating/cooling stages were taken as controls.

5.1.2.3 DSC analysis

Samples were analyzed using the same equipment reported in paragraph 2.2.2.8 (pag. 45) and using the heating/cooling profiles described in paragraph 5.1.2.2 (pag. 101). Total peak enthalpy was obtained by integration of the melting curve.

5.1.2.4 Synchrotron XRD analysis

Samples were analyzed following the same procedure and using the same equipment reported in paragraph 3.1.2.8 (pag. 56), with some modifications. Data were collected at a photon energy of 8.266 keV ($\lambda = 1.5 \text{ \AA}$).

5.1.2.5 PL microscopy

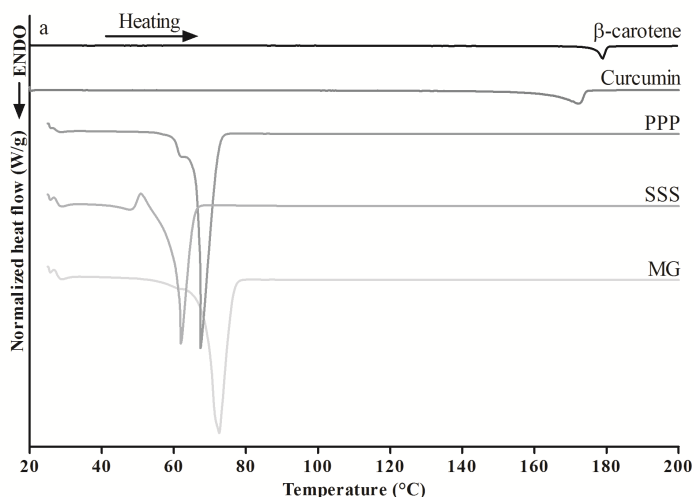
Samples subjected to DSC heating/cooling cycle were transferred in the middle of a glass slide and covered with a glass cover slip. The glass slides were transferred into the microscope allocation previously heated at 80 °C. Samples were then cooled (Linkam CSS450, Linkam Scientific Instruments, Surrey, UK) to 20 °C at 2 °C/min before being imaged at 200x using the same equipment and procedure described in paragraph 2.2.2.6 (pag. 45).

5.1.2.6 Data analysis

All determinations are expressed as the mean \pm standard error of at least two measurements from two experiment replications. Statistical analysis was performed by using R v. 3.0.2 (The R foundation for Statistical Computing). Bartlett's test was used to check the homogeneity of variance, one way ANOVA was carried out and Tukey-test was used as post-hoc test to determine significant differences among means ($p < 0.05$).

5.1.3 Results and discussion

Figure 5.1 shows the melting (a) and crystallization (b) profiles, recorded at 2 °C/min, of β -carotene, curcumin and bulk PPP, SSS, and MG.



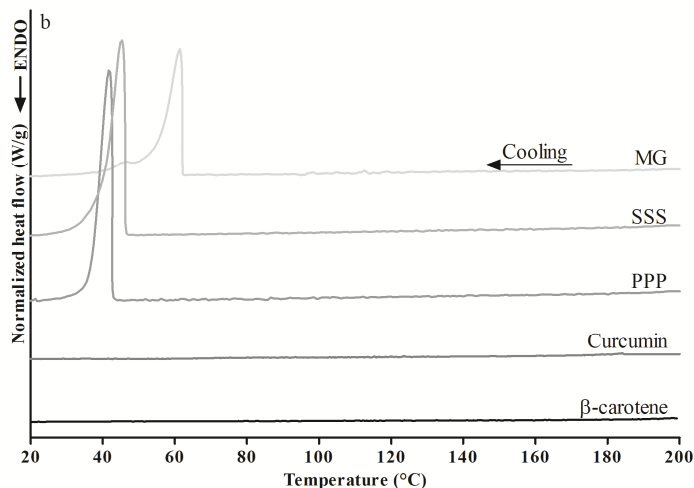


Figure 5.1. Melting (a) and crystallization (b) profiles of β -carotene, curcumin, PPP, SSS, and MG recorded during heating and cooling at 2 °C/min.

During heating, one main endothermic peak at 177 °C, 161.5 °C, 68.5 °C and 66.7 °C emerged respectively in β -carotene, curcumin, MG and PPP curves (Figure 5.1a). On the contrary, SSS showed two melting events (at $T_{on} = 43.4$ and 60.2 °C) with in between a crystallization phenomenon ($T_{on} = 49.2$ °C). This behavior is typical of polymorphic transformation of triacylglycerols: as the sample is heated, some of the less thermostable polymorphs melt, rearrange and recrystallize into more stable polymorphs (Himawan, MacNaughtan, Farhat, & Stapley, 2007). As expected, subsequent sample cooling caused fat recrystallization, which is well evidenced by the exothermic signals in the thermograms (Figure 5.1b). The two exceptions were β -carotene and curcumin which did not show any crystallization event, neither after three consecutive thermic cycles (from 20 to 200 °C and *vice versa*) at 2 °C/min nor after one thermal cycle at a lower cooling rate, i.e. 0.5 °C/min (data not shown).

The heating/cooling cycle from 20 to 200 °C and *vice versa* at 2 °C/min was also used to study the phase transition of MG, SSS, and PPP containing 5% (w/w) β -carotene (Figure 5.2) or curcumin (Figure 5.3).

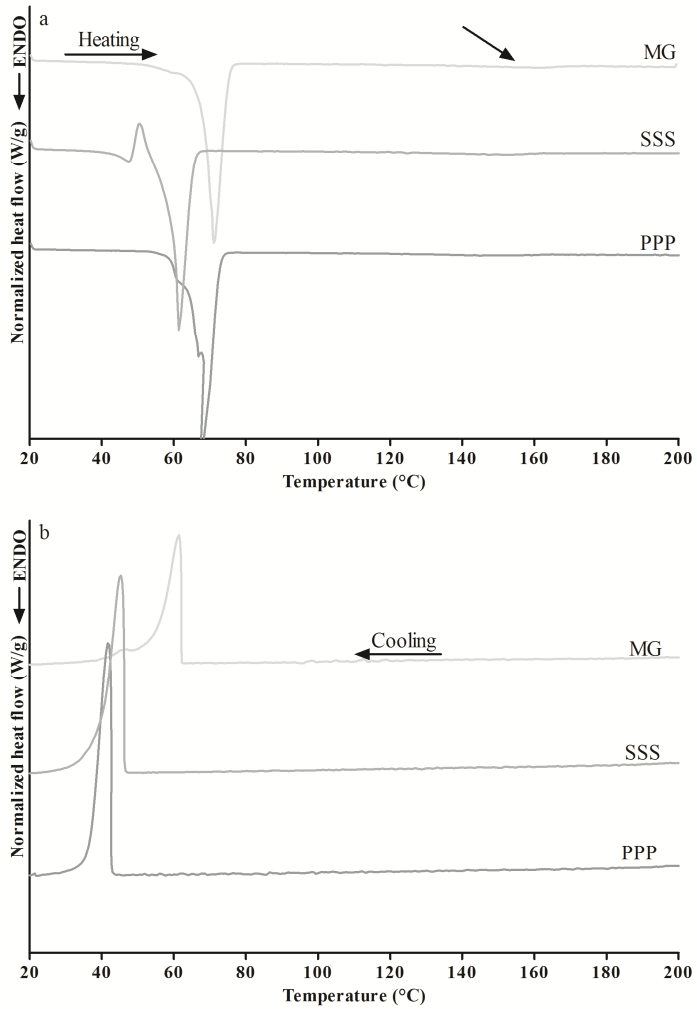


Figure 5.2. Melting (a) and crystallization (b) of MG, PPP, and SSS, added with 5% (w/w) of β -carotene recorded during heating and cooling at 2 $^{\circ}\text{C}/\text{min}$.

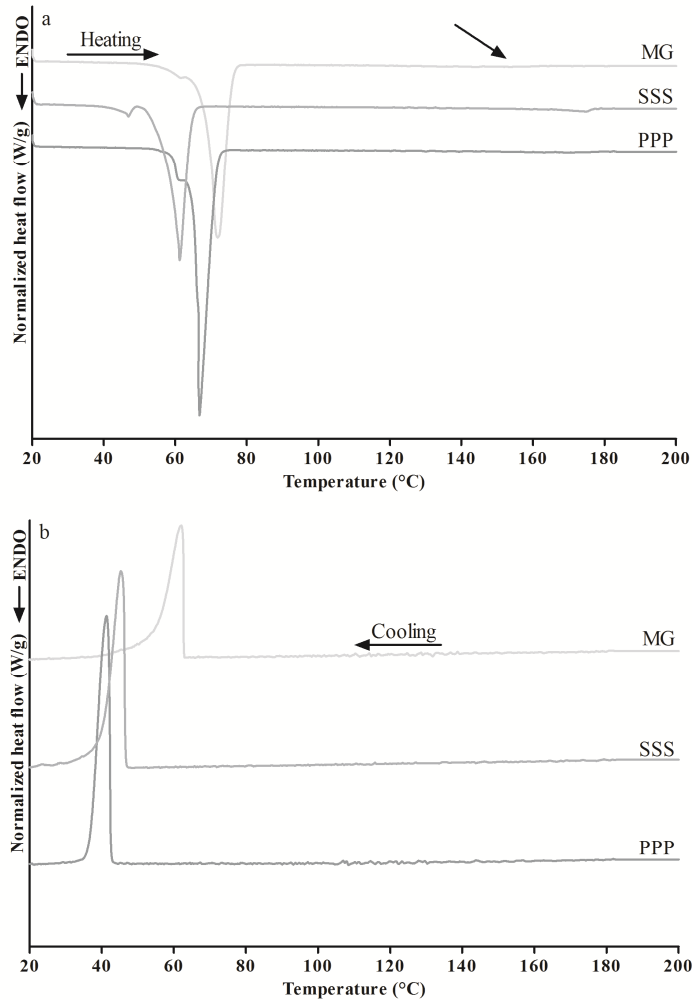


Figure 5.3. Melting (a) and crystallization (b) of MG, PPP, and SSS, added with 5% (w/w) of curcumin recorded during heating and cooling at 2 °C/min.

The melting profiles up to 200 °C of the mixed lipid matrices (Figures 5.2a and 5.3a) did not differ from those of the bulk lipids (Figure 5.1a). Approaching 140 °C, a slight endothermic signal attributable to β -carotene or curcumin melting was detected in all samples. The subsequent cooling phase induced lipid recrystallization. Although the thermograms were comparable to those relevant to the bulk counterparts (Figure 5.1b), a slight, but significant, decrease of crystallization temperature (T_{on}) of the β -carotene and curcumin containing samples was measured (Table 5.1).

Table 5.1. Crystallization temperatures of MG, PPP and SSS added or not with 5% (w/w) β -carotene and 5% (w/w) curcumin recorded during cooling at 2 °C/min.

Sample	Crystallization temperature (°C)		
	With β -carotene	With curcumin	Pure
MG	61.8 \pm 0.1 ^b	62.3 \pm 0.2 ^b	65.4 \pm 0.1 ^a
PPP	42.7 \pm 0.1 ^b	42.5 \pm 0.1 ^b	44.0 \pm 0.2 ^a
SSS	46.3 \pm 0.1 ^b	46.6 \pm 0.1 ^b	47.2 \pm 0.2 ^a

^{a,b}: means with common letters in the same row are not significantly different ($p > 0.05$).

These results would indicate a role of β -carotene and curcumin in retarding fats transition from the melt to crystal phase. Also in this case, additional cooling/heating cycles did not show any crystallization phenomena ascribable to β -carotene or curcumin phase transition (data not shown).

To better understand the influence of β -carotene and curcumin on fat crystallization, sample microstructure was determined by polarized light microscopy (Figure 5.4).

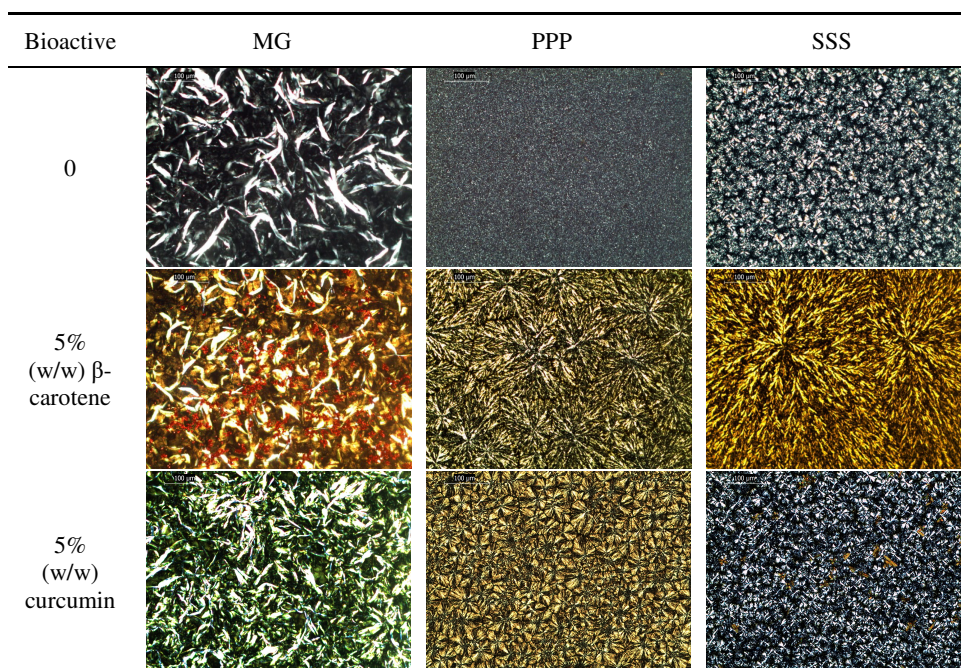


Figure 5.4. Images of bulk, 5% (w/w) β -carotene, and 5% (w/w) curcumin containing MG, PPP and SSS matrices.

Crystal platelets of about 100 μ m can be observed in the MG bulk sample as well as in 5% (w/w) β -carotene and curcumin containing MG. However, β -carotene aggregates (red dots) can be easily noted when the pigment was in the sample. On the contrary, the microstructure of the PPP and SSS matrices dramatically changed as a consequence of β -carotene addition. A dense packing of very small crystals was detected in bulk PPP matrix, while no-spherulitic clumps with a branched feature can be observed in presence of β -carotene. No red-colored spots of β -carotene aggregates are visible by naked eye. Similarly, the SSS samples presented spherulitic crystals that turned into branched structures when β -carotene was added.

On the contrary, curcumin did not affect the microstructure of SSS and curcumin aggregates (orange dots) are easily detectable in the sample. PPP sample showed a different structure which can be described as a mixture of the structures observed in bulk and 5% (w/w) β -carotene containing sample even if some aggregates were detectable in the sample.

It can be inferred that β -carotene and curcumin location inside the fat crystal network may change as a consequence of their molecular characteristics as well as those of the lipid matrix. Since MG are more polar than triacylglycerols, it can be postulated that β -carotene molecules segregate from MG forming aggregates. On the contrary, β -carotene could be incorporated into the solid phase of triacylglycerols, thereby altering crystal morphology. On the other hand, curcumin showed an opposite trend. As reported by Smith, Bhaggan, Talbot, and van Malssen (2011), the greater the molecular similarity between the guest molecule and bulk fat, the stronger the effect on crystal structure. In these experimental conditions, the similarity between β -carotene and PPP or SSS could favor carotenoid integration into the crystal matrix or its adhesion onto the crystal growth sites. Contrarily, MG and β -carotene molecular features being more dissimilar, the carotenoid might not participate to MG crystallization events, but might form clusters inside the solid matrix. As regards curcumin, the different chemical composition and structure allowed its integration in MG crystal matrix. On the other hand, curcumin formed clusters inside the solid matrix of PPP and SSS, affecting or not the final crystal morphology, respectively.

To understand whether β -carotene and curcumin affected also fat crystal polymorphic structure, synchrotron XRD analysis on bulk lipid matrices and samples containing 5% (w/w) of β -carotene or curcumin were performed.

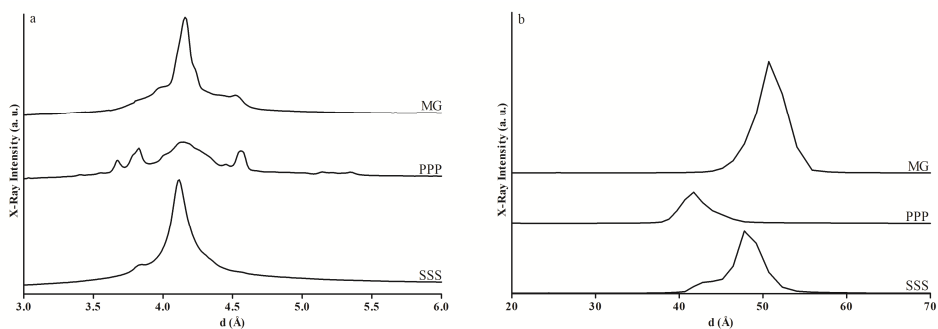


Figure 5.5. WAXS (a) and SAXS (b) patterns of bulk MG, PPP, and SSS.

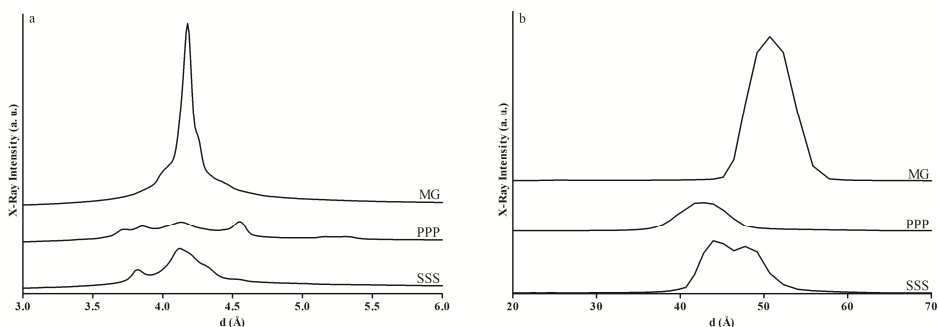


Figure 5.6. WAXS (a) and SAXS (b) patterns of MG, PPP, and SSS containing 5% (w/w) β -carotene.

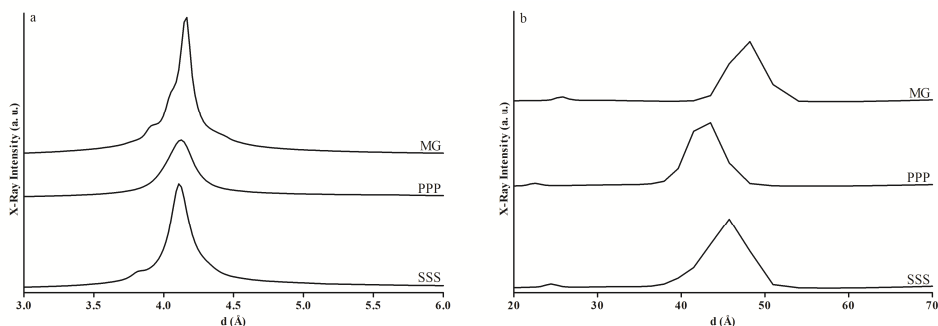


Figure 5.7. WAXS (a) and SAXS (b) patterns of MG, PPP, and SSS containing 5% (w/w) curcumin.

Figures 5.5, 5.6, and 5.7 show the wide angle X-ray diffraction (WAXS) (a) and small angle X-ray diffraction (SAXS) (b) patterns of the bulk, β -carotene and curcumin containing MG, PPP and SSS samples, respectively.

MG diffraction results showed that both β -carotene and curcumin did not affect the fat polymorphic structure: a single hexagonal α structure (4.17 Å) was observed in all samples analyzed. This phase was characterized by a c parameter of 51.16 Å in MG with or without β -carotene, and 47.72 Å in curcumin containing MG. In the case of the SSS matrix, no discrepancies were found in the WAXS region between samples with or without β -carotene and curcumin. In fact, hexagonal α and orthorhombic β' polymorphs were detected independently on β -carotene and curcumin addition to SSS. On the other hand, PPP matrix showed a similar pattern in the case of bulk and β -carotene containing sample while curcumin containing sample showed a completely different pattern. Hexagonal α and triclinic β polymorphs were detected in bulk PPP and β -carotene containing sample while only hexagonal α form was detected in curcumin containing PPP. In SAXS region, the relative intensity of the single peaks for PPP and SSS changed as a consequence of β -carotene addition. In particular, an increase of peak intensity at lower d values was noted, probably due to an increase of the β and β' amounts to the detriment of α crystals. On the other hand, the addition of curcumin in SSS and PPP had a minor effect on crystals c parameter.

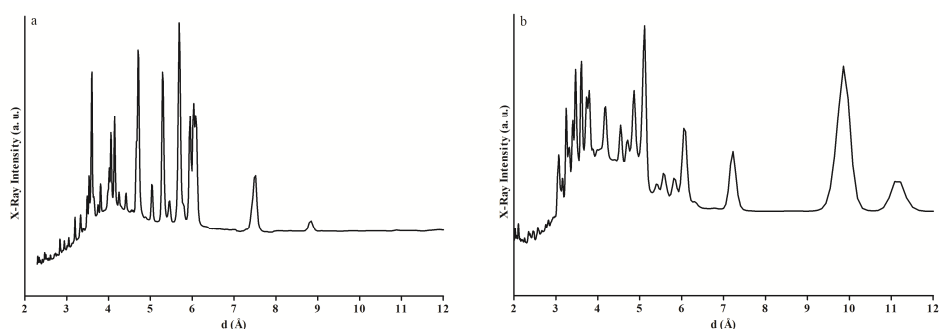


Figure 5.8. WAXS pattern of crystalline β -carotene (a) and curcumin (b).

The XRD pattern of crystalline β -carotene and curcumin were also determined (Figure 5.8). Regarding β -carotene, data are in good agreement with those reported by Sterling (1964), showing a monoclinic $P2_1/c$ crystal structure with β angle of 105.3° and a , b , and c cell parameters equal to 7.55, 9.51 and 24.80 Å, respectively. On the other hand, curcumin crystalline structure was a mixture of different polymorphs. In particular, data are in good

agreement with Sanphui, Goud, Khandavilli, Bhanoth, and Nangia (2011), showing a monoclinic $P2_1/n$ crystal structure with β angle of 95.0° and a , b , and c cell parameters equal to 12.57, 7.04 and 19.96 Å, respectively, and an orthorhombic $Pbca$ crystal structure with a , b and c cell parameters equal to 12.54, 7.99, and 34.46 Å, respectively. It is noteworthy that none of the peaks detected for MG, PPP, and SSS matrices (Figures 5.5, 5.6, and 5.7) can be associated with those observed in the β -carotene and curcumin crystal pattern (Figure 5.8), suggesting that the melted bioactive compounds did not reform the initial crystal structure upon subsequent cooling.

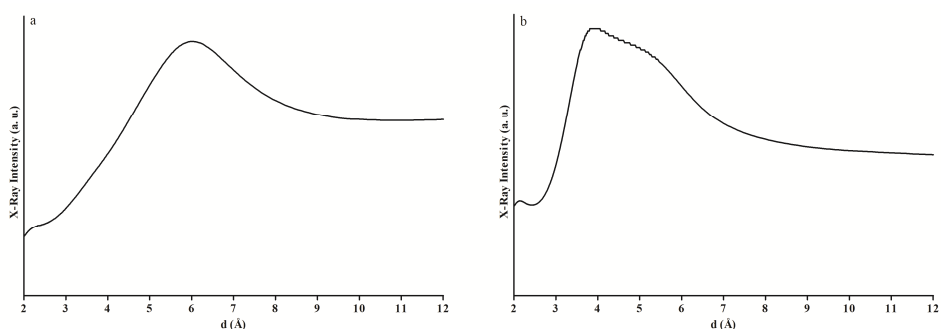


Figure 5.9. WAXS pattern of β -carotene (a) and curcumin (b) after DSC melting and cooling at $2^\circ\text{C}/\text{min}$.

In order to confirm this hypothesis, XRD patterns of β -carotene and curcumin after DSC melting and cooling were performed (Figure 5.9). It can be noted that one bump at 5.84 \AA (Figure 5.9a), and two bumps at 3.66 and 4.94 \AA (Figure 5.9b) were detected after DSC heating and cooling for β -carotene and curcumin samples, respectively. These data are in agreement with the already discussed DSC results, showing no recrystallization thermal event associable with β -carotene and curcumin phase transition. Therefore, it can be inferred that β -carotene and curcumin aggregates observed in Figure 5.4 are amorphous clusters.

5.1.4 Conclusions

Structural information acquired at different length scales highlighted that the presence of β -carotene or curcumin in fats greatly affects crystal morphology, crystal network structure and thermal properties of the lipid matrices. Depending on fats molecular characteristics, β -carotene participated (PPP and SSS) or withdraw (MG) to the fat crystallization. Triacylglycerol crystal morphology was altered by the presence of β -carotene probably through its incorporation into the solid phase. Contrarily, when added to MG, β -carotene formed clusters inside the solid matrix. On the other hand, curcumin showed an opposite trend in participating (MG) or withdrawing (SSS and PPP) to fat crystallization, changing only the polymorphic form of PPP, even though amorphous clusters were detectable inside PPP and SSS solid matrices.

5.2 Effect of solid fat content on curcumin and β -carotene degradation kinetics

5.2.1 Aim of the study

The aim of this paragraph was to study bioactive molecule stability in different fat matrices. To this aim, β -carotene and curcumin were included in blends of medium chain triacylglycerols (MCT) and saturated monoglycerides, tripalmitin, or tristearin. Degradation kinetics were evaluated during storage.

5.2.2 Materials and methods

5.2.2.1 Materials

The same materials described in paragraph 5.1.2.1 (pag. 101) were used. In addition, Miglyol 812 N (MCT) was kindly provided by Cremer Oleo GmbH & Co. KG (Hamburg, Germany).

5.2.2.2 β -carotene or curcumin containing lipid matrices

Mixtures containing solid fats (SSS, PPP or MG) and liquid triacylglycerols (MCT) at different solid fat content (100, 70, 50, 30, 10, and 0% w/w) were fully melted (in a water bath at 80 °C) and added with 0.06% (w/w) of crystalline β -carotene or curcumin. The mixtures were stirred with a magnetic rod in the dark under nitrogen until completely transparent solutions were obtained (i.e. visibly free of dispersed materials). Approximately 5.5 g of samples were placed in 6 cm diameter Petri dishes and covered with plastic caps. Petri dishes were then cooled and stored for up to 140 days in a temperature controlled incubator at 20 °C.

5.2.2.3 Color analysis

Changes in color were assessed by a tristimulus colorimeter (Chomameter-2 Reflectance, Minolta, Osaka, Japan) equipped with a CR-200 measuring head. The instrument was standardized against a white tile. Color was expressed by color Hunter coordinates L^* (lightness), a^* (redness) and b^* (yellowness) and a^* and b^* were used to compute the Hue angle (eq. 5.1) and Chroma (C^* , eq. 5.2) parameters (Clydesdale, 1978).

$$\text{Hue angle} = \begin{cases} \tan^{-1} \frac{b^*}{a^*} & \text{if } a > 0 \\ 90 & \text{if } a = 0 \\ \tan^{-1} \frac{b^*}{a^*} + 180 & \text{if } a < 0 \end{cases} \quad (\text{eq. 5.1})$$

$$C^* = \sqrt{(a^*)^2 + (b^*)^2} \quad (\text{eq. 5.2})$$

5.2.2.4 Data analysis

All determinations are expressed as the mean \pm standard error of at least five measurements from two experiment replications ($n \geq 10$). A software package (Statistica for Windows v. 10, StatSoft, Inc., Tulsa, USA) was used to fit distance weighted least squares surface to the observed data. Linear regression analysis by least squares regression was performed using R v. 3.0.2 (The R foundation for Statistical Computing), and the goodness of fit was evaluated on the basis of statistical parameters of fitting (R^2 , p , standard error) and the residual analysis.

5.2.3 Results and discussion

From a practical point of view and in the attempt to delivery β -carotene and curcumin in foods, trials were carried out to understand whether β -carotene and curcumin location, and structure in the lipid crystal network previously studied might affect its oxidative stability. To this aim, 0.06% (w/w) β -carotene and curcumin were added to mixtures of 100, 70, 50, 30, 10, and 0% (w/w) MG, PPP, or SSS mixed with saturated medium chain triacylglycerol (MCT). Samples were then stored at 20 °C for up to 140 days. At this concentration, β -carotene was completely solubilized in triacylglycerols, being its solubility in oils approximately 0.12% (w/w) (Borel, Grolier, Armand, Partier, Lafont, Lairon, & Azais-Braesco, 1996). Also curcumin was below its solubility limit that was found to be $0.20 \pm 0.10\%$ (w/w) for oils (Ahmed, Li, McClements, & Xiao, 2012).


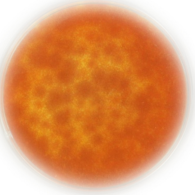



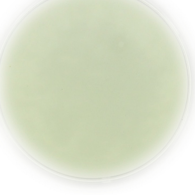
Sample	0 days		60 days	
	Appearance	Color parameters	Appearance	Color parameters
MG		$L^* = 42.8 \pm 0.2$ $a^* = 17.3 \pm 0.2$ $b^* = 16.3 \pm 0.2$		$L^* = 57.4 \pm 0.9$ $a^* = 20.2 \pm 0.8$ $b^* = 27.4 \pm 1.2$
PPP		$L^* = 63.4 \pm 0.9$ $a^* = 17.8 \pm 1.0$ $b^* = 50.7 \pm 1.4$		$L^* = 77.6 \pm 0.5$ $a^* = -1.6 \pm 0.4$ $b^* = 5.6 \pm 1.1$
SSS		$L^* = 61.1 \pm 0.1$ $a^* = 18.0 \pm 0.2$ $b^* = 31.3 \pm 0.1$		$L^* = 73.0 \pm 0.7$ $a^* = -3.1 \pm 1.1$ $b^* = 7.3 \pm 3.9$

Figure 5.10a. Appearance and color parameters of 0.06% (w/w) β -carotene containing 100% (w/w) MG, PPP, and SSS samples after 0 and 60 days of storage at 20 °C.


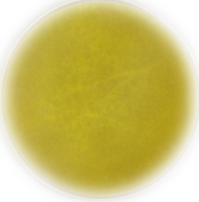



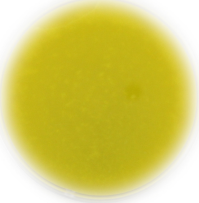
Sample	0 days		60 days	
	Appearance	Color parameters	Appearance	Color parameters
MG		L* = 50.7 ± 0.1 a* = -5.5 ± 0.2 b* = 41.2 ± 0.3		L* = 64.3 ± 0.3 a* = -3.0 ± 0.3 b* = 38.9 ± 0.3
PPP		L* = 78.8 ± 0.3 a* = -18.1 ± 0.2 b* = 53.7 ± 1.0		L* = 78.5 ± 0.3 a* = -16.7 ± 1.4 b* = 56.4 ± 1.0
SSS		L* = 72.1 ± 0.3 a* = -13.2 ± 0.2 b* = 46.9 ± 0.4		L* = 68.7 ± 0.1 a* = -3.6 ± 0.6 b* = 49.1 ± 0.2

Figure 5.10b. Appearance and color parameters of 0.06% (w/w) curcumin containing 100% (w/w) MG, PPP, and SSS samples after 0 and 60 days of storage at 20 °C.

Figure 5.10a shows the visual appearance of β -carotene containing 100% (w/w) MG, PPP, and SSS samples just after preparation and after 60 days of storage at 20 °C as well as the correspondent color values. The color differences among samples were clearly observable by naked eyes. The MG sample showed the most intense red/orange color and L* (lightness) and b* (yellowness) significantly lower than those of SSS and PPP. On the other hand, color dissimilarity between PPP and SSS can be mainly attributed to the b* values. As reported by Laughlin, Bunke, Eads, Laidig, and Shelley (2002), the color of pure β -carotene is strictly associated to its crystallinity: the carotenoid intense black/red color decreases moving from the crystalline state to a metastable phase within which the molecules are poorly aligned. Thus, the color diversity observed among samples could be related to the molecular organization of β -carotene inside the lipid crystal network. After 60 days of storage at 20 °C, PPP and SSS samples lost the orange color and were characterized by a yellowish-white color while MG samples showed a less marked changes in color parameters.

Figure 5.10b shows the visual appearance of curcumin containing 100% (w/w) MG, PPP, and SSS samples just after preparation and after 60 days of storage at 20 °C as well as the correspondent color values. The color differences among samples were less clear than those of β -carotene containing samples even if color parameter were different for each sample. During storage, however, no big changes were detected for PPP containing sample, while MG and SSS containing samples showed changes in all color parameters.

Thus, β -carotene and curcumin chemical degradation can be followed by monitoring the color change during storage.

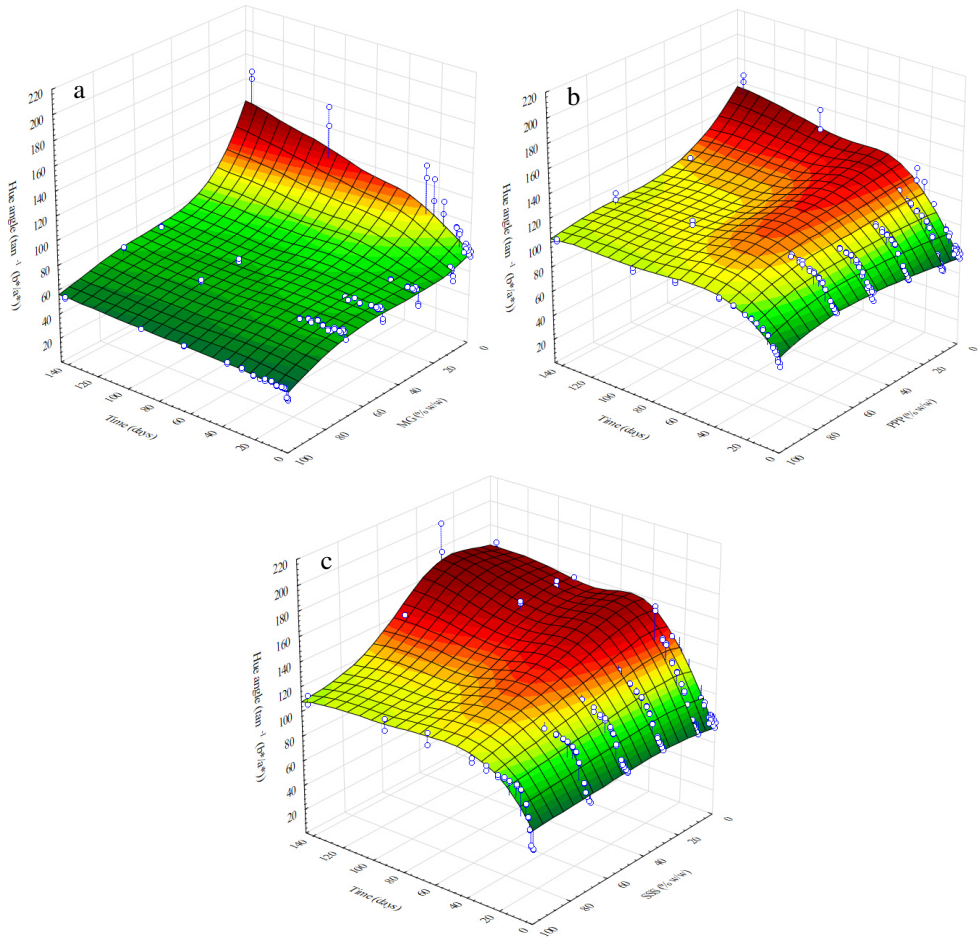


Figure 5.11. Hue angle values of 0.06% (w/w) β -carotene containing MG (a), PPP (b), and SSS (c) samples at different solid fat content (100, 70, 50, 30, 10, and 0% w/w) during storage at 20 °C.

Figure 5.11 shows the changes in hue angle of the 0.06% (w/w) β -carotene containing MG (a), PPP (b), and SSS (c) at different solid fat content (100, 70, 50, 30, 10, and 0% w/w) during storage at 20 °C. As known, an increase in this color parameter is an index of carotenoid bleaching. The color fading of MG samples was negligible. On the contrary, in the case of the PPP and SSS samples, a great increase of hue angle occurred within the first 10 days of storage, while prolonging the time color changed slightly.

The pseudo-zero order rate constants of hue angle data as a function of storage time for each concentration were calculated by linear regression analysis. MG containing samples showed at any concentration a rate constant which was not statistically different from 0 ($p > 0.05$). While PPP and SSS containing samples showed statistically significant rate constants ($R^2 \geq 0.93$ and $p < 0.05$).

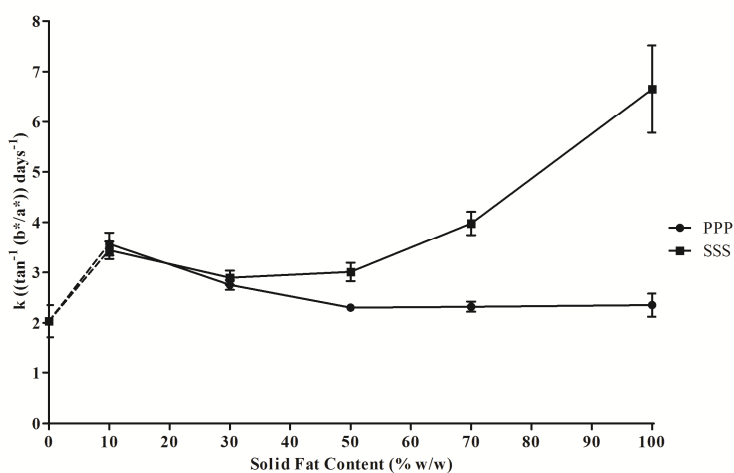


Figure 5.12. Pseudo-zero order rate constants as a function of solid fat content for 0.06% (w/w) β -carotene containing PPP, and SSS samples. Error bars represent standard error of fitting.

Figure 5.12 shows the pseudo-zero order rate constants as a function of solid fat content for 0.06% (w/w) β -carotene containing PPP, and SSS samples. When no solid fat is present in the matrix (0% w/w), a rate constant of about $2.0 \tan^{-1}(b^*/a^*) \text{ days}^{-1}$ characterizes β -carotene degradation. The addition of PPP or SSS increased β -carotene degradation at any concentration tested (Figure 5.12). In particular, considering PPP containing samples, the rate constant showed the lowest values after 50% (w/w) concentration, while SSS containing samples showed the lowest value at 30% (w/w) concentration. However, these rate constants were higher than that calculated for 0% (w/w) solid fat content. Thus, differences in structure organization between SSS and PPP systems could affect the rate of the color fading (see 100% w/w containing PPP and SSS). On this topic, Nik *et al.* (2012) reported that β -carotene was more stable when incorporated in solid lipid nanoparticles containing β -crystal than in presence of both β' and β -crystal. This observation is consistent with the highest oxidation rate detected in SSS (mainly in β' form) than in PPP (mainly in β).

Overall these results suggest that β -carotene is more stable to oxidation when it is not incorporated in the solid lipid phase, i.e. the MG systems. It is likely that the β -carotene amorphous aggregates that have been previously observed in the 100% (w/w) MG sample reduced the carotenoid surface exposed to oxidation (Figure 5.4). These results would partially explain some contradictory results of the literature on biomolecules stability in solid lipid carriers (Cornacchia & Roos, 2011; Helgason *et al.*, 2009a; Qian *et al.*, 2013; Relkin *et al.*, 2009). In fact, the chemical stability of lipophilic molecules incorporated into solid lipid cores could increase or decrease depending on biomolecule location inside the matrix and lipid structure organization.

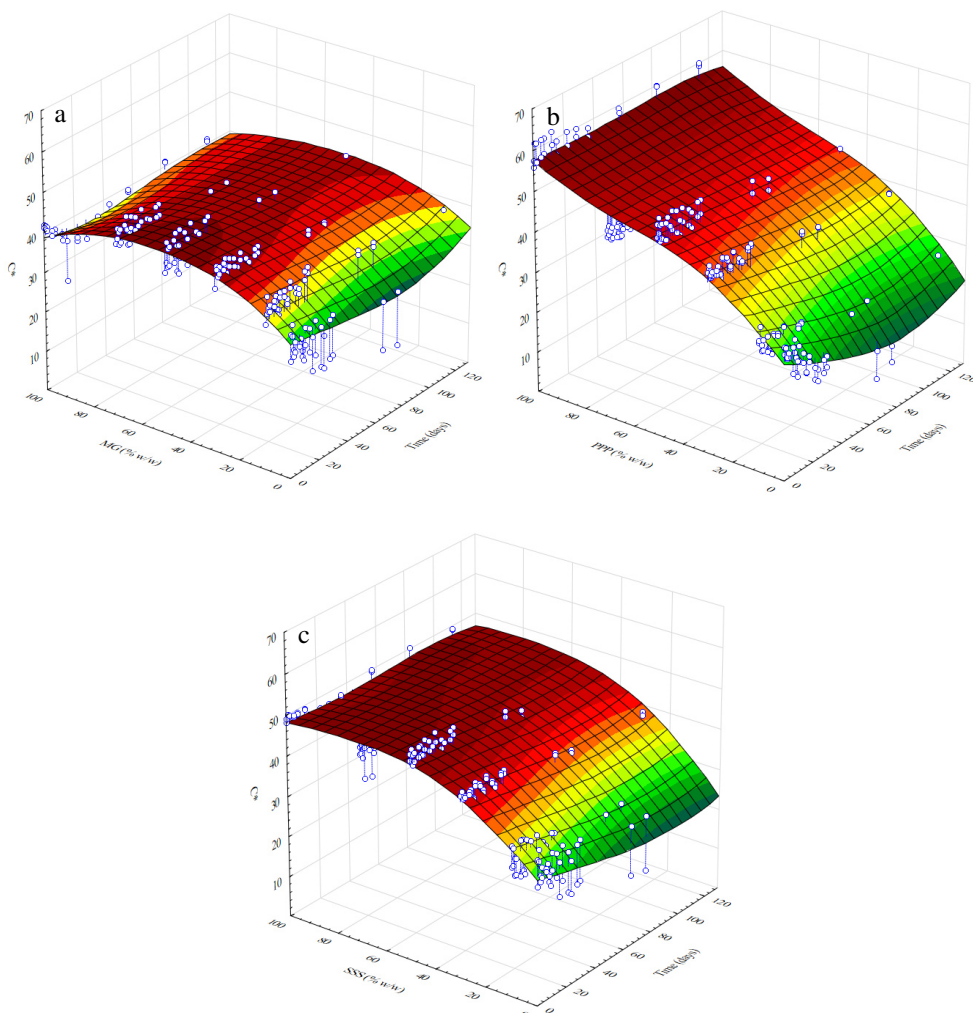


Figure 5.13. Chroma values (C^*) of 0.06% (w/w) curcumin containing MG (a), PPP (b), and SSS (c) samples at different solid fat content (100, 70, 50, 30, 10, and 0% w/w) during storage at 20 °C.

As regards curcumin degradation, chroma (C^*) was chosen as color parameter index since hue angle did not permit samples to be properly characterized. Figure 5.13 shows the changes in chroma (C^*) of the 0.06% (w/w) curcumin containing MG (a), PPP (b), and SSS (c) at different solid fat content (100, 70, 50, 30, 10, and 0% w/w) during storage at 20 °C. Chroma changes were mainly due to solid fat content rather than storage time as pointed out by Figure 5.13. A decrease in this color parameter can be considered an index of curcumin bleaching. The pseudo-zero order rate constants of chroma as a function of storage time for each concentration calculated by linear regression analysis on the first 10 days of storage was not statistically different from 0 ($p > 0.05$) for all systems and concentrations tested ($p > 0.05$), except for 100% (w/w) MG sample and 0% (w/w) solid fat content that showed a rate constant of $-0.41 \pm 0.03 \text{ C}^* \text{ days}^{-1}$ ($R^2 = 0.97$ and $p < 0.05$) and $-0.45 \pm 0.17 \text{ C}^* \text{ days}^{-1}$ ($R^2 = 0.42$ and $p < 0.05$), respectively.

5.2.4 Conclusions

The impact of β -carotene on fat crystallization described in chapter 5.1 translated in a different susceptibility of the pigment to degradation. The acquired results suggest that β -carotene is less prone to oxidation in the MG crystal network than in the PPP and SSS ones. On the other hand, curcumin did not undergo to color changes when PPP and SSS were present in the system while MG containing sample showed curcumin degradation only in 100% (w/w) MG system. Thus, the impact of curcumin on fat crystallization described in chapter 5.1 can be a partial explanation of the observed results.

Although further research efforts are needed to fully elucidate the mechanism of β -carotene-lipid and curcumin-lipid interactions, these results clearly showed that the choice of the lipid carrier may greatly affect bioactive compound stability. These conclusions seem to be crucial in the attempt to design efficient delivery systems, such as micro and nanoemulsions, where the presence of each component (i.e. surfactant, water phase composition) may have additional effects on β -carotene and curcumin oxidative stability.

Effect of system composition on delivery systems production

6.1 Development of nano and microemulsions using the phase inversion temperature (PIT) method

6.1.1 Aim of the study

Among different delivery systems based on self-assembly molecules the focus of this chapter was pointed on micro and nanoemulsions prepared using the phase inversion temperature method (PIT) and stabilized by non-ionic surfactant Tween 80. This method, introduced by Shinoda and Saito (1968) did not receive much attention in the food area. The process to obtain nano and microemulsions by using the PIT method consists in the heating of the coarse emulsion above the PIT. During heating the surfactant head groups are subjected to a progressive desolvation inducing molecular geometry changes (Klucker, Dalencon, Probeck, & Haensler, 2012). Once passed the PIT, the surfactant becomes more soluble in oil than in water leading to the phase inversion and the formation of a W/O emulsion. The further rapid cooling induces the surfactant to gain its original properties with a recovery of its original molecular geometry. This transition reduces surface tension point promoting the formation of finely dispersed oil droplets (Fernandez, Andre, Rieger, & Kuhnle, 2004). The extent of surfactant conformational changes is the result of temperatures applied during processing, but also system characteristics, such as physical and chemical properties of lipid phase, composition of aqueous phase (ionic salts, pH, alcohols), type of surfactant, presence and type of co-surfactant and co-solvent, and ratio among ingredients greatly affect the formation of micro and nanoemulsions (McClements & Rao, 2011). The effect of aqueous phase composition (NaCl and Tween 80 concentration) was first studied. A major emphasis was then given in the second part of the study to the lipid core where type, physical state, and concentration of lipids on nano and microemulsions formation were studied. Finally, selected systems were added with curcumin and the stability of the bioactive molecule was monitored over time.

6.1.2 Materials and methods

6.1.2.1 Materials

Extra virgin olive (EVO), castor, soybean, sunflower, and peanut oil and were purchased in a local market. Lemon oil was kindly provided by Enrico Giotti S.p.A. (Scandicci, Italy). Myverol™ saturated monoglyceride (MG) (fatty acid composition: 1.4% C14:0, 59.8% C16:0, 38.8% C18:0; melting point 68.05 ± 0.5 °C) was kindly offered by Kerry Ingredients and Flavour (Bristol, United Kingdom). Tripalmitin (PPP) (melting point: 66.5 ± 0.5 °C, purity $\geq 85\%$ w/w), tristearin (SSS) (melting 72.0 ± 0.5 , purity $\geq 85\%$ w/w), Tween 80, methanol (HPLC grade), and acetonitrile (HPLC grade) were purchased from Sigma-Aldrich (Milan, Italy). Curcumin (purity 80% and 99%) was purchased from Extrasynthese (Genay, France). NaCl was purchased from Carlo Erba (Milan, Italy). All solutions were prepared using milli-Q water.

6.1.2.2 Emulsified systems preparation by phase inversion temperature (PIT) method

Emulsions were prepared following the methodology proposed by Zhang *et al.* (2013) with some modifications. Tween 80 at different concentrations (10, 15, 20, 30 and 40% w/w) was mixed with aqueous solutions of NaCl (0.0, 0.4, 0.8, and 1.2 M) at 300 rpm overnight in

order to dissolve all the surfactant. Coarse emulsions were prepared slowly pouring the aqueous phase into different lipid matrices at different concentrations under magnetic stirring at 600 rpm for 10 minutes. When a solid lipid matrix was used (i.e. PPP, SSS, and MG) the aqueous phase and the lipid matrices were heated at 70 °C, and mixed at the same conditions above reported maintaining the temperature. In some cases, lipid phase was added with 0.06% (w/w) curcumin before coarse emulsion preparation. Lipid phase added with curcumin was stirred with a magnetic rod in the dark under nitrogen until completely transparent solutions were obtained (i.e. visibly free of dispersed materials). Aliquots of 8 g of the coarse emulsion was transferred into 10 mL vials, sealed and heated for 30 minutes at 90 °C in a water bath. Samples were then hand shook until a homogeneous system was obtained and finally cooled in an ice bath until reaching 20 °C.

6.1.2.3 Visual appearance

Emulsions were considered transparent when an object placed behind a 10 mL vial (22 mm pathway) filled with the obtained sample was clearly seen. Opaque samples were those that did not permit to observe any object, and opalescent samples were those that permit to observe an object behind the sample but not clearly.

6.1.2.4 Phase inversion temperature (PIT) determination using viscosity measurement

The PIT was determined following the procedure proposed by Zhang *et al.* (2013) with some modifications. The PIT was determined by considering the mixture containing 1% (w/w) lemon, EVO, and peanut oil and an aqueous phase composed of 15% (w/w) Tween 80 in NaCl solutions having different molar concentrations. The Stresstech Rheometer (Reologia Instruments AB, Lund, Sweden) with application software Stresstech v.4 was used to determine the viscosity of emulsions. The experiment was performed in a 25 mm bob cup geometry where coarse emulsions were loaded and thermally equilibrated at 95 °C for 2 minutes. Temperature was decreased at 0.5 °C/min from 95 to 25 °C using a circulating coolant connected to a thermostat (RTE-140, Neslab Instruments, inc., Newington, USA) and applying a shear rate of 100 s⁻¹. In order to reduce the water evaporation, a thin layer of sunflower oil was applied on the top of the sample. The phase inversion temperature was calculated using the tangents method.

6.1.2.5 Emulsion viscosity

Emulsions viscosity was recorded using a Stresstech Rheometer (Reologia Instruments AB, Lund, Sweden) with application software Stresstech v.4. In particular, 10 mL of sample was introduced in a 25 mm bob cup geometry and viscosity changes were recorded in a shear rate interval from 10 to 200 s⁻¹. All measurements were carried out at 25 °C.

6.1.2.6 Dynamic laser scattering

Particle size was determined using a Particle Sizer 380 ZLS analyzer (PSS NICOMP Particle Sizing system, Goleta, USA). Before analysis, emulsions were diluted with deionized water in order to avoid multiple scattering effects. Mean particle diameter was expressed as volume weighted mean diameter ± standard deviation (SD).

6.1.2.7 Image acquisition

Sample images were acquired using an image acquisition cabinet (Immagini & Computer, Bareggio, Italy) equipped with a digital camera (EOS 550D, Canon, Milan, Italy). In particular, the digital camera was placed on an adjustable stand positioned 60 cm in front of a white cardboard base where the vials were placed. Light was provided by 4 100 W frosted photographic floodlights, in a position allowing minimum shadow and glare. Images were saved in *jpeg* format.

6.1.2.8 Bright field microscopy

Emulsions were analyzed using the same equipment reported in paragraph 2.2.2.6 (pag. 45) without light polarization. One drop of coarse emulsion was placed in the middle of a glass slide and a glass cover slip was centered above the drop. Samples were heated from 20 to 90 °C at 5 °C/min using a thermostatic cell (Linkam CSS450, Linkam Scientific Instruments, Surrey, UK). Samples were analyzed using a 200x magnification.

6.1.2.9 Synchrotron XRD analysis

Samples were analyzed following the same procedure and using the same equipment reported in paragraph 3.1.2.8 (pag. 56). Data were collected at a photon energy of 8.266 keV ($\lambda = 1.5 \text{ \AA}$).

6.1.2.10 Curcumin analysis

6.1.2.10.1 Extraction of curcumin from emulsified systems

Curcumin was extracted from emulsions using methanol as solvent. In particular, 0.5 g of emulsion was added with 1 mL of solvent, shook at 35 Hz for 2 min using a vortex and then centrifuged at 3000 rpm for 10 min. The supernatant was transferred into a 2 mL vial for further analysis.

6.1.2.10.2 Extracted curcumin HPLC analysis

Curcumin analysis was carried out injecting 10 μL of the previously extracted bioactive from emulsions in a HPLC Shimadzu Nexera (Shimadzu, Kyoto, Japan) coupled to two LC-30AD pumps equipped with a SIL-30AC autosampler and a CTO-30 thermostated column oven. The analytical column was a Poroshell 120 EC-C18 4.6 x 150 mm, 2.7 μm column (Agilent, DTO Servizi, Spinea, Italy). Calibration curve was obtained using standard curcumin solutions in methanol at different concentration. The separation conditions are reported in Table 6.1.

Table 6.1. Separation conditions for extracted curcumin samples. A = water added with 1% (w/w) acetic acid; B = acetonitrile added with 1% (w/w) acetic acid.

Time (min)	A (%)	B (%)
0	55	45
12	55	45
32	0	100
40	0	100
45	55	45
48	55	45

The concentration of the compounds were determined using a diode array detector (SPD-M20A, Shimadzu, Kyoto, Japan) set at 420 nm and the response factor obtained by the calibration curve.

6.1.2.11 Data analysis

All determinations were expressed as the mean \pm standard error of at least two measurements from two experiment replicates ($n \geq 4$).

6.1.3 Results and discussion

6.1.3.1 Effect of aqueous phase and temperature on nano and microemulsions formation

Figure 6.1 shows visual aspect, and mean droplet diameter with its relative abundance for samples composed of 5% (w/w) EVO oil and 95% (w/w) of a aqueous phase composed by 30% (w/w) Tween 80 in NaCl solutions at 0.0, 0.4, 0.8, 1.2 M after thermal treatment at 90 °C for 30 min.



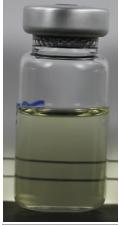

NaCl concentration (M)	Visual aspect	Mean droplet diameter \pm SD (nm)	Relative abundance (%)
0.0		16.9 \pm 2.9	52.2
		428.3 \pm 4.6	17.3
		789 \pm 83.5	30.5
0.4		16.7 \pm 3.0	100
0.8		16.6 \pm 3.0	100
1.2		16.7 \pm 3.1	100

Figure 6.1. Visual aspect, mean droplet diameter with its relative abundance for samples composed of 5% (w/w) EVO oil and a aqueous phase composed by 30% (w/w) Tween 80 in NaCl solutions at 0.0, 0.4, 0.8, 1.2 M after thermal treatment at 90 °C for 30 min.

It can be noted that all systems containing NaCl appeared transparent after thermal treatment showing a unimodal droplet diameter distribution with mean droplet diameter lower than 20 nm. On the other hand the absence of NaCl (0.0 M) did not allow transparent system to be formed, even if more than 50% of the droplets showed a diameter smaller than 20 nm (Figure 6.1). As described by different authors (McClements & Rao, 2011; Zhang *et al.*, 2013) the temperature where the phase inversion happens depends on different parameters such as physical and physicochemical properties of oil, ethylene oxide number of the surfactant head

group, concentration of alcohol, and concentration of salt. Samples composed by 1% (w/w) EVO, peanut, and lemon oil and a aqueous phase composed by 15% (w/w) Tween 80 in NaCl solutions at 0.0, 0.4, 0.8, 1.2 M were subjected to viscosity measurements in order to calculate the phase inversion temperature (PIT) of the systems during cooling from 95 to 25 °C. As an example, Figure 6.2 shows the viscosity changes as a function of temperature for systems containing lemon oil (1% w/w) and NaCl aqueous solution (0-1.2 M) and 15% (w/w) Tween 80. The curves showed a bell-shaped trend of viscosity as a function of temperature. As reported by Zhang *et al.* (2013), the point at which the viscosity shows a sharp increase during cooling corresponds to the PIT. The PIT decreased as NaCl concentration increased (Figure 6.2 - inset). This is a consequence of the known effect of NaCl on HLD value (Zhang *et al.*, 2013). It should be noted that similar experiments were performed also with peanut and EVO oil. No significant different results were recorded by using other liquid oils (data not shown).

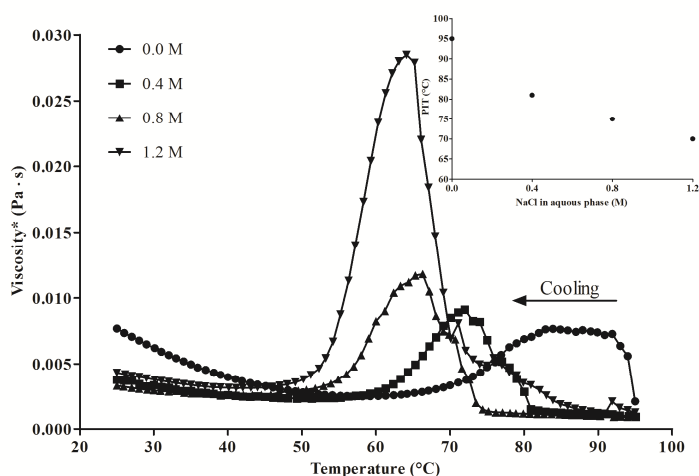


Figure 6.2. Viscosity as a function of temperature of systems containing lemon oil (1% w/w) and NaCl aqueous solution (0-1.2 M) and 15% (w/w) Tween 80. Figure inset: calculated PIT as a function of NaCl concentration.

Since temperatures of about 15 °C above the PIT are needed to obtain microemulsions with the PIT method (McClements & Rao, 2011) and to reduce the preparation temperature below 100 °C, next experiments have been carried out using solutions with 0.8 M NaCl concentration and 90 °C as heating temperature during emulsion preparation. In order to better understand the evolution of systems during heating and cooling, optical microscopy was used to follow the changes of coarse emulsion lipid droplet size.

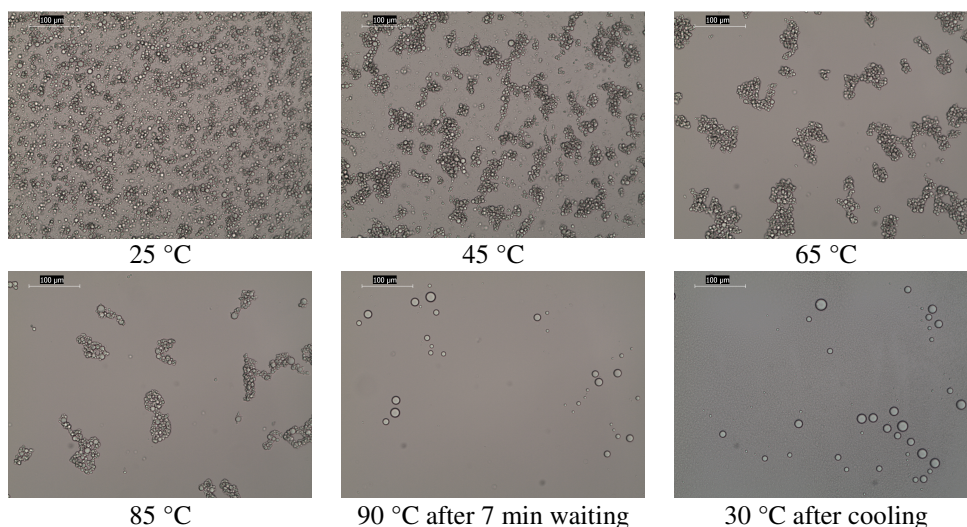


Figure 6.3. Bright field optical microscopy images of coarse emulsion (7.5% w/w EVO oil, aqueous phase composed of 30% (w/w) Tween 80 in 0.8 M NaCl solution) recorded during heating at 5 °C/min and after cooling at 20 °C/min. Magnification 200x.

Figure 6.3 shows the evolution of lipid droplets in coarse emulsion composed by 7.5% (w/w) EVO oil, and a aqueous phase composed by 30% (w/w) Tween 80 in 0.8 M NaCl solution. Images were taken during heating from 25 to 90 °C at 5 °C/min and after cooling to 30 °C at 20 °C/min. It can be noted that as the temperature increased, droplets aggregated decreasing their number. Finally at 90 °C no oil droplets were detected, and this can be attributed to the changes in surfactant molecular geometry (Rao & McClements, 2010) that did not allow lipid droplets to be stabilized and the system phase separated. Finally, after a rapid cooling of the system (20 °C/min) no oil droplets were detected, even if a modification of the background was visible indicating the formation of a different structure. It can be hypothesized that the rapid cooling induced the formation of small droplets ($d < 20$ nm) that were not visible using optical microscopy.

6.1.3.2 Effect of lipid phase on nano and microemulsions formation

The effect of different lipid matrices on nano and microemulsion formation was then investigated. A water phase composed by 30% (w/w) Tween 80 in 0.8 M NaCl was used. Six different oils (EVO, sunflower, soy, castor, peanut, and lemon oil), two saturated triacylglycerols (PPP and SSS) and a mixture of EVO oil and monoglyceride (MG) at different concentrations were used as lipid phases. Regarding oils, Figure 6.4 shows the mean particle diameter for emulsions obtained after thermal treatment using as lipid phases EVO, sunflower, soy, castor, peanut, and lemon oil as a function of oil percentage. It was found that EVO, sunflower, soy and peanut oil allowed transparent or slightly opalescent emulsions to be obtained up to 7.5% (w/w) oil (corresponding to a surfactant to oil ratio of 3.7) with a mean particle diameter smaller than 25 ± 10 nm. These systems thus can be classified as microemulsions due to their high SOR (surfactant to oil ratio > 1) and small diameter (≤ 30 nm) (Rao & McClements, 2011). On the other hand castor oil did not allow transparent emulsions to be obtained at any concentration from 1.0 to 9.0% (w/w), showing a diameter greater than 100 nm (Figure 6.4). Thus, castor oil allowed only nanoemulsions and emulsions to be obtained at concentrations equal to 1% and $\geq 3\%$ (w/w), respectively. It can be hypothesized that the hydroxyl group present in ricinoleic acid could disturb the formation of small oil droplets interacting with the surfactant and preventing optimal curvature to be

reached by the surfactant at oil/water interface during cooling. Finally, transparent emulsions characterized by particle diameter lower than 30 nm were obtained at concentrations equal or lower than 1.3% (w/w) (SOR = 22.7) for systems containing lemon oil. These systems can be classified as microemulsions. Opaque systems with particle diameters higher than 120 nm were obtained at higher oil concentrations. The difference in oil performances can be linked to oil chemical composition. Lemon oil, rich in terpenes such as limonene, is characterized by appreciable solubility in water differently from peanut oil rich in long-chain fatty acids. It can be hypothesized that presence of polar molecules could hinder the formation of stable micelles during phase inversion. As described by McClements *et al.* (2009), these molecules could be incorporated between surfactant tails changing the Tween 80 organization at the interface. In this situation, the Ostwald ripening (OR) phenomenon could be accelerated (during phase inversion and during storage) leading to a progressive increase of the mean particle diameter up to the emulsion physical separation (Li, Le Maux, Xiao, & McClements, 2009; McClements & Rao, 2011; Wooster *et al.*, 2008). The previously found critical SORs were confirmed varying both surfactant and oil concentrations (data not shown).

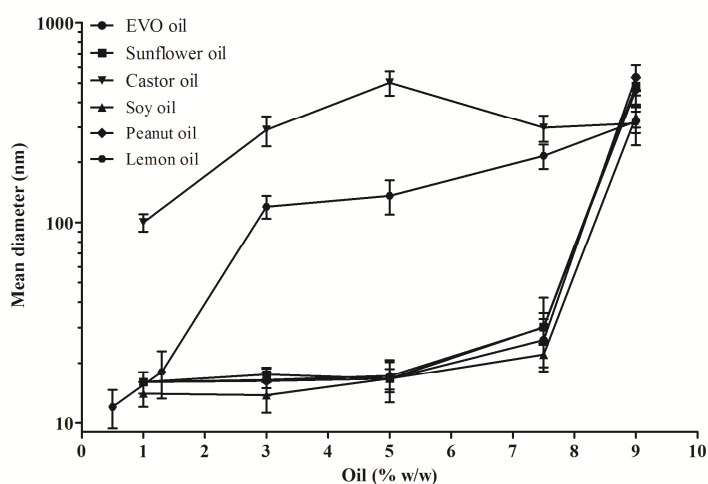


Figure 6.4. Mean particle diameter as a function of oil percentage for EVO, sunflower, castor, soy, peanut, and lemon oil used as lipid phase in emulsions obtained after thermal treatment. The aqueous phase was composed of 30% (w/w) Tween 80 in 0.8 M NaCl.

The addition of monoglyceride to liquid oils was previously described as one of the strategy used to gel oils and obtain the so called organogels (Co & Marangoni, 2012). In the attempt to obtain transparent emulsions with gelled lipid droplets, a system composed by MG to EVO oil ratio of 5:95 with a total lipid content of 5.0% (w/w) was investigated. Also in this case an aqueous phase composed of 30% (w/w) Tween 80 in 0.8 M NaCl was used. MG containing system allowed transparent emulsions with a mean particle diameter of 20 ± 5 nm to be obtained. Another strategy to obtain delivery systems is the preparation of solid lipid nanoparticles (SLN) that are emulsions with the lipid core in the crystalline state at room temperature (Helgason, Awad, Kristbergsson, McClements, & Weiss, 2009b). In this study, PPP and SSS were used as lipid core. These saturated triacylglycerols allowed transparent systems to be obtained up to 5.0% (w/w) (corresponding to a SOR of 5.70) with a mean particle diameter of about 20 ± 2 nm. In order to understand the effect of microemulsion preparation on polymorphism of PPP and SSS, and on MG crystallization inside lipid droplets, X-ray diffraction patterns with Synchrotron light were collected on samples containing 5.0% (w/w) of PPP and SSS, and systems containing EVO oil added with MG

(Figure 6.5). Sample containing PPP showed a mixture of hexagonal α and triclinic β polymorphs (Figure 6.5) with a c parameter of the crystal cell equal to 40.55 Å. SSS containing sample showed a mixture of hexagonal α and orthorhombic β' polymorphs (Figure 6.5). Similarly for PPP containing samples, 5.0% (w/w) SSS containing samples showed a peak at 43.98 Å. Finally, system containing MG showed only a bump in the wide angle region at 4.45 Å (Figure 6.5) related to the short-range organization of triacylglycerols in the liquid oil (Calligaris *et al.*, 2008). No peaks were detectable in this area, indicating that probably MG did not crystallize inside oil droplets. Due to amphiphilic properties of MG, these molecules could act as emulsifiers placing at the oil/water interface together with Tween 80 molecules. On the other hand, it could also be possible that the space inside oil droplets was not enough for MG to crystallize in presence of EVO oil. Even if no peaks were detectable in the wide angle area, Figure 6.5 shows two peaks in the small angle region.

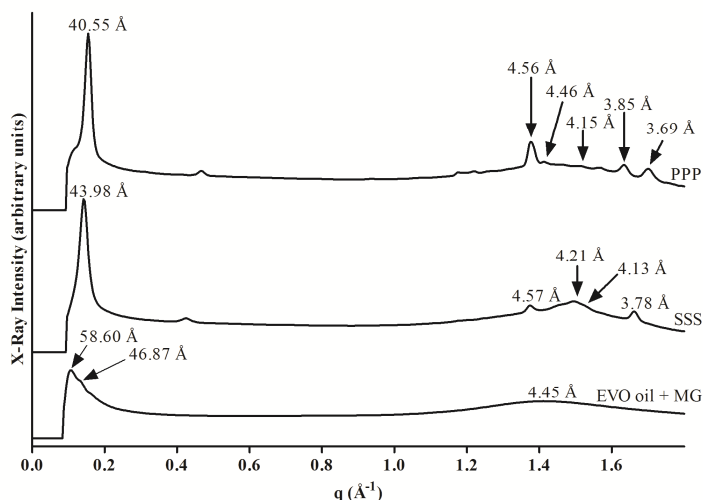


Figure 6.5. XRD patterns of microemulsions containing 5.0% (w/w) PPP, SSS, and a mixture of EVO oil and MG (95:5 ratio). The aqueous phase was composed of 30% (w/w) Tween 80 in 0.8 M NaCl.

6.1.3.2.1 Lemon oil loading capacity maximization in nano and microemulsions

Since transparent nano and microemulsions were able to load a relative low amount of lemon oil, and since the delivery of this essential oil is of great interest in the food industry, a formulation strategy was studied in order to increase the ability of these delivery systems to incorporate lemon oil keeping their transparency.

It was previously found that lemon oil molecules could have disturbed Tween 80 organization at the interface inducing OR also during the phase inversion. Since non-polar molecules that are soluble in the oil phase, but insoluble in the water phase, such as long chain triacylglycerol, could be used as ripening inhibitors (Sagalowicz & Leser, 2010), lipid phases containing both peanut oil and lemon oil were considered to retard emulsion destabilization and increase lemon oil delivery. Figure 6.6 shows the mean particle diameter of systems as a function of peanut oil in the lipid phase. In any case the total lipid content was 7.5% (w/w). It can be noted that the addition of peanut oil at any concentration above 25% (w/w) in the lipid phase allowed the mean particle diameter to be reduced from about 200 to 21 nm, leading to the formation of transparent emulsions.

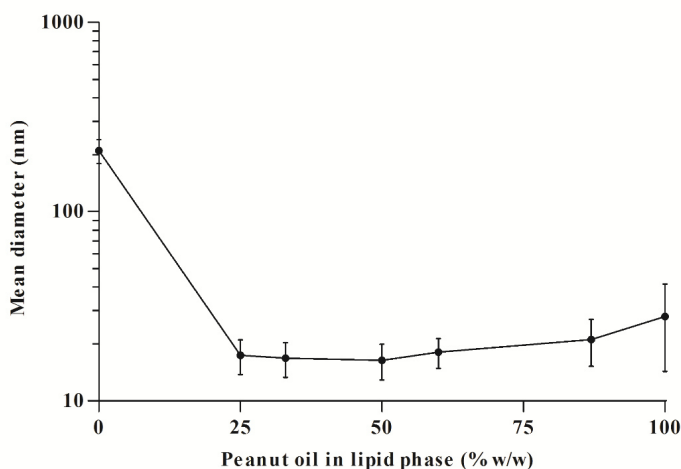


Figure 6.6. Mean particle diameter as a function of peanut oil content in the lipid phase. Total lipid content: 7.5% (w/w). Water phase: 30% (w/w) Tween 80 in 0.8 M NaCl solution.

In the attempt to understand the effect lipid phase composition on emulsion characteristics, mixtures of lemon oil and peanut oil at 1:1 (50% w/w of peanut oil) and 3:1 ratio (25% w/w of peanut oil) were used to form emulsions. The total lipid content as well as the Tween 80 content in the aqueous phase were progressively increased. Figure 6.7a and 6.7b shows the visual appearance of the resulting systems. Samples with mean particle diameter in the range 20 – 35 nm were optically transparent; 40 – 60 nm range opalescent; higher than 150 nm opaque. These latter systems were highly unstable and underwent phase separation. Observing the figure, it can be noted that transparent or opalescent systems can be obtained up to 20% (w/w) Tween 80 in the aqueous phase. On the other hand, the increase of oil content led to a progressive increase of mean particle diameter. Thus, the oil droplet size increased as the surfactant per oil volume unit decreased.

Keeping constant the percentage of surfactant, samples prepared with 25% (w/w) peanut oil in the lipid phase permitted to obtain emulsions with smaller droplet size in comparison to samples containing 50% (w/w) peanut oil in the lipid phase. In particular, the highest lemon oil quantity that could be delivered in transparent emulsion was 15% (w/w) in the sample containing 30% (w/w) Tween 80 in 0.8M NaCl solution and 20% (w/w) of total lipid phase composed of 25% (w/w) peanut oil (75% w/w lemon oil). It is interesting to note that opalescent but stable emulsions were obtained also by including up to 35% (w/w) of oil phase corresponding to 26% (w/w) of lemon oil.

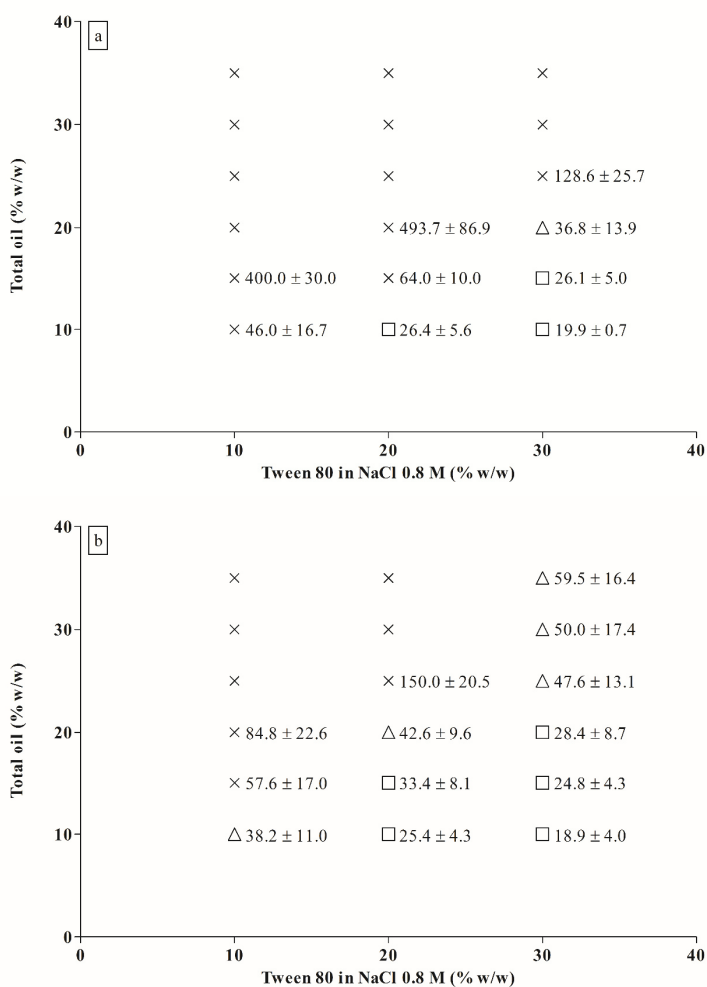


Figure 6.7. Visual appearance (opaque = x; opalescent = Δ; transparent = □) of systems containing increasing Tween 80 and lipid phase content. (a) peanut oil-lemon oil 50-50% (w/w) and (b) peanut oil-lemon oil 25-75% (w/w). The mean diameters ± SD (nm) of selected samples were also reported.

To better characterize emulsions, the viscosity of microemulsions containing 30% (w/w) Tween 80 in 0.8 M NaCl aqueous solution and increasing concentration of oil from 0 to 20% (w/w) (lemon oil-peanut oil 75-25% w/w) was measured. All considered samples exhibited a Newtonian behavior. It can be noted observing Figure 6.8 that the emulsion viscosity increased as oil content also increased. This result can be attributed to the increase of particle number and size from 18.9 to 28.4 nm, as shown in Figure 6.7b. It is likely that increasing the oil content while maintaining the surfactant concentration lead to the formation of a more crowded system.

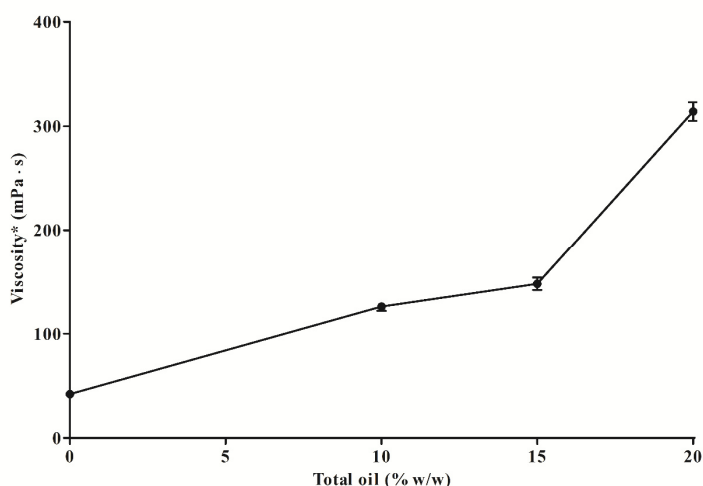


Figure 6.8. Microemulsions viscosity as a function of total oil content for lemon oil-peanut oil 75-25% (w/w). Water phase: 30% (w/w) Tween 80 in 0.8 M NaCl solution.

The acquired results indicate that the presence of peanut oil, containing long chain fatty acids, in the lipid phase beside lemon oil could increase the emulsion micellar stability. It can be hypothesized that the presence of long chain fatty acids favored the formation of small droplets by positioning near or within the oleic tails of Tween 80 allowing the optimum curvature to be reached. Moreover, the presence of peanut oil could reduce the interactions between lemon oil terpenes and Tween 80 oleic tails decreasing the development of the OR during the phase inversion as well as during storage. In other words it can be hypothesized the formation of a peanut oil layer between Tween 80 and lemon oil as schematized in Figure 6.9. Thus, the simultaneous presence of both oils seems to have a synergistic effect on transparent emulsions formation.

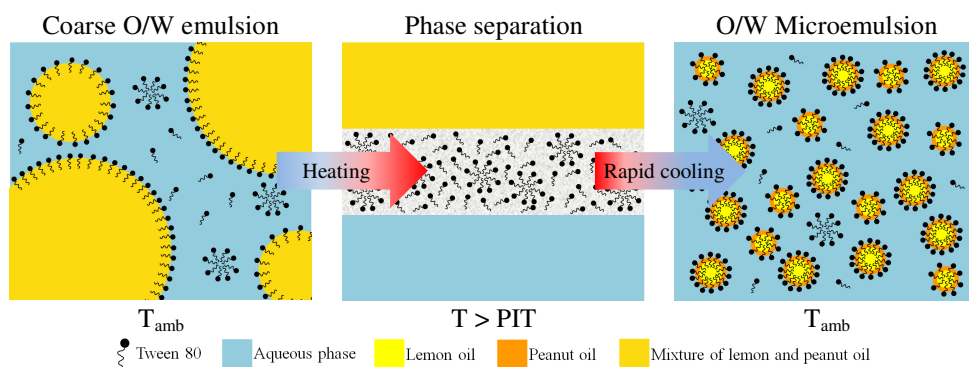


Figure 6.9. Schematic representation of microemulsion formation using PIT method.

6.1.3.3 Selected microemulsions loaded with curcumin

Selected microemulsions obtained in the first part of this work were loaded with curcumin. In particular, 30% (w/w) of Tween 80 in 0.8 M NaCl was used as water phase, and three different lipid phases fortified with 0.06% (w/w) curcumin were used: (i) 5.0% (w/w) EVO oil, (ii) 5.0% (w/w) of a mixture of EVO oil added with MG in a ratio of 95:5, and (iii) 5.0% (w/w) SSS. Figure 6.10 shows the visual appearance as well as the mean particle diameter of

obtained emulsions. All microemulsions appeared transparent with a yellowish color and no differences were detected between samples with and without curcumin in terms of mean particle diameter.




Lipid phase	Visual aspect	Mean particle diameter (nm)
5.0% (w/w) EVO oil		16.8 ± 2.21
5.0% (w/w) EVO oil + MG (95:5)		17.1 ± 2.63
5.0% (w/w) SSS		18.4 ± 2.52

Figure 6.10. Visual appearance and mean particle diameters of selected transparent microemulsions having the lipid phase loaded with 0.06% (w/w) curcumin.

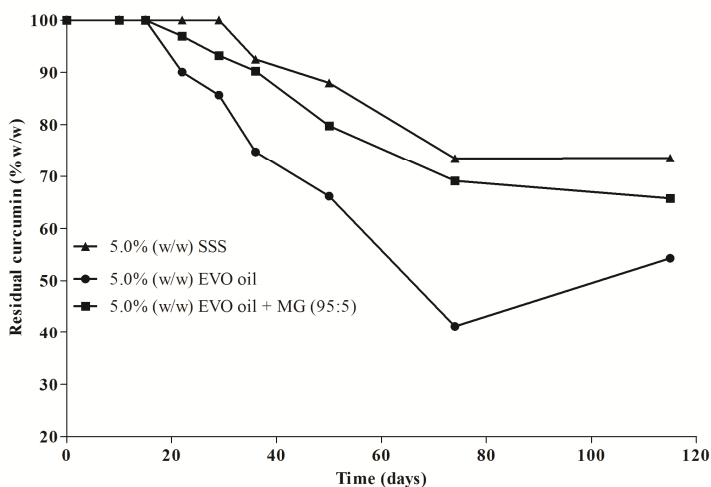


Figure 6.11. Evolution of residual curcumin (% w/w) in transparent microemulsions containing 5.0% (w/w) SSS, EVO oil, and EVO oil + MG (ratio 95:5) and water phase composed of 30% (w/w) Tween 80 in 0.8 M NaCl solution stored up to 115 day at 20 °C in dark.

Since the addition of curcumin did not affect the physical properties of microemulsions, bioactive molecule degradation was evaluated. Figure 6.11 shows the evolution of residual curcumin (% w/w) in transparent microemulsions containing 5.0% (w/w) SSS, EVO oil, and EVO oil + MG (ratio 95:5) and water phase composed of 30% (w/w) Tween 80 in 0.8 M NaCl solution stored up to 115 day at 20 °C in the dark. All samples showed an initial lag phase where no reduction of curcumin was observed. This lag phase had a duration which was different for each sample in the order: SSS, EVO oil + MG, and EVO oil containing samples. Over time, however, all samples showed a decrease of curcumin concentration. In particular, SSS containing sample showed the highest curcumin residual concentration up to 115 days of storage in the dark at 20 °C, followed by EVO oil + MG and EVO oil containing samples. In the case of SSS containing sample, curcumin could have been withdrawn from SSS network, forming clusters as shown in Figure 5.4 (pag. 106). This phenomenon could have protected curcumin against degradation. EVO oil containing sample showed the lowest curcumin residual concentration during storage in the dark at 20 °C, while the addition of a structuring agent such as MG allowed curcumin to be protected against degradation to some extent.

6.1.4 Conclusions

In this chapter it was studied the ability of Tween 80 as self-assembly molecule for the production of transparent emulsified systems. NaCl concentration in the aqueous phase greatly affected the phase inversion temperature. Indeed, PIT decreased as NaCl concentration increased. It was found also that the chemical as well as physical state of lipid phase affected transparency and stability of emulsified systems. Indeed, using an aqueous phase of 30% (w/w) Tween 80 in 0.8 M NaCl solution, the highest amount of lipid phase that was possible to incorporate in transparent systems was: 1.3% (w/w) lemon oil, 5.0% (w/w) PPP and SSS, and finally 7.5% (w/w) EVO, peanut, sunflower, and soybean oil. On the other hand castor oil did not allow transparent emulsions to be obtained at any tested concentration. It was also found that an extremely high amount of lemon oil (15% w/w) can be incorporated in transparent emulsions only if mixed with peanut oil in a 3:1 ratio (lemon:peanut oil) before the phase inversion (total oil delivered was 20% w/w). Finally, selected emulsions were loaded with curcumin and the evolution of the bioactive molecule was followed up to 115 days. It was found that curcumin stability was greatly affected by the physical state of the lipid core. In particular, SSS containing emulsions allowed curcumin degradation to be retarded comparing to EVO oil containing sample.

Performance of selected transparent emulsion containing lemon oil in beverage prototype under different thermal treatments

Aim of the study

The aim of this study was to investigate the effect of dilution and thermal treatments on selected transparent emulsion containing lemon oil (described in paragraph 6.1.3.2.1) in beverages prototypes.

Materials and methods

Materials

Peanut oil and sucrose were purchased in a local market. Lemon oil was kindly provided by Enrico Giotti S.p.A. (Scandicci, Italy). Tween 80, and citric acid monohydrate were purchased from Sigma-Aldrich (Milan, Italy). Curcumin (purity 80%) was purchased from Extrasynthese (Genay, France). NaCl, NaOH, and sodium benzoate were purchased from Carlo Erba (Milan, Italy). All solutions were prepared using milli-Q water.

Transparent emulsion prepared by phase inversion temperature (PIT) method

Transparent emulsion composed of 20% (w/w) oil with 3:1 ratio (lemon:peanut oil) added or not with 0.06% (w/w) curcumin, and an aqueous phase of 30% (w/w) Tween 80 in 0.8 M NaCl was prepared with the procedure described in paragraph 6.1.2.

Beverages preparation

Prototype of ethanol-free beverage

An aqueous solution containing 8.4 g/L of citric acid and having a pH value of 2.1, was added with 100 g/L of sucrose and 0.8 g/L of sodium benzoate. Finally, 5 g/L of transparent emulsion was added to the beverage prototype. Some beverages were then carbonated by using a Soda Stream Source carbonator (San Vendemiano, Italy). Beverages were stored at 20 °C up to 60 days.

Prototype of low-ethanol beverage

An aqueous solution containing 8.4 g/L of citric acid adjusted at pH value of 3.0 with NaOH, was added with 100 g/L of sucrose, 0.8 g/L of sodium benzoate, and 41.8 g/L of ethanol (corresponding to 5% v/v). Finally, 10 g/L of transparent emulsion was added to the beverage prototype. Beverages were stored at 20 °C up to 60 days.

Prototype of high-ethanol beverage

An aqueous solution containing 8.4 g/L of citric acid adjusted at pH value of 4.6 with NaOH, was added with 200 g/L of sucrose, 0.8 g/L of sodium benzoate, and 165.7 g/L of ethanol (corresponding to 20% v/v). Finally, 40 g/L of transparent emulsion was added to the beverage prototype. Beverages were stored at 20 °C up to 60 days.

Thermal treatments applied to beverages

Selected beverages were poured in a 1 L container and subjected to different thermal treatments. In particular, beverages were heated using a water bath at a temperature below emulsion PIT reaching 72 °C in around 30 min and keeping that temperature for 15 s.

A second thermal treatment was done above the emulsion PIT at 121 °C for 15 min by using an autoclave Orion PBI (Milan, Italy). All samples were rapidly cooled in an ice bath after thermal treatment.

Turbidity measurements

Aliquots of 2 mL of beverage prototypes were introduced in glass cuvette and turbidity was measured using a UV-2501 PC UV-VIS (Shimadzu, Kyoto, Japan) spectrophotometer recording the absorbance at 600 nm.

Image acquisition

Sample images were acquired using the same equipment described in paragraph 6.1.2.7 (pag. 118). In particular, bottles containing the samples were placed in front of a black cardboard before imaging.

Head Space-Solid Phase Micro Extraction (HS-SPME) procedure

2 mL of lemon oil or beverage prototypes added with transparent emulsion were poured into 10 mL vial sealed with airtight butyl stopper and metal ring. Samples were then equilibrated at 20 °C for 24 h. Before extraction, a Supelco fused silica fiber coated with a stationary phase consisting of three phases DVB/CAR/PDMS (50/30 µm) (Bellefonte, PA, USA) was conditioned for 10 min at 250 °C and then exposed to the headspace of the sample for 10 min. After the extraction process, the fiber was inserted immediately into the injection port of the gas chromatographer or gas chromatographer coupled with mass spectrometer for thermal desorption for 3 min.

Gas Chromatography (GC) analysis

The profile of volatile compounds for beverages was obtained using a gas chromatographer (FISONS 8540 Mega Series 2, Fisons Instrumentation, Milan, Italy), equipped with a capillary column (EC-VAX, 30 m x 0.25 mm i.d. x 0.25 µm film thickness, Alltech, Sedriano, Italy). A flame ionizing detector (FID HWD Control, Fison, Milan, Italy) was used to analyze the compounds. Oven temperature was programmed as follows: 50 °C hold 10 min, ramp at 10 °C min⁻¹ to 230 °C. Thermal desorption of compounds from the SPME fiber took place in the GC injector at 250 °C. Sample injection was conducted in split mode with a 1:3 split ratio. The carrier gas flow (helium) was adjusted to a rate of 1 mL min⁻¹. The data processing was performed using the program ChromCard version 1.18 (CE Instruments, Milan, Italy).

GC-mass spectrometry (MS) analysis

In order to identify the GC peaks, lemon oil was analyzed using a Saturn mass spectrometer (Varian, Palo Alto, USA) mounted with a ion trap detector (ITD), coupled with a GC mod. 3400 (Varian, Palo alto, USA) equipped with a capillary column (DB-VAX, 30 m x 0.25 mm i.d. x 0.25 µm film thickness, Alltech, Sedriano, Italy). The carrier gas flow (helium) was adjusted to a rate of 1 mL min⁻¹ and sample injection was conducted in split mode with a 1:40 split ratio. The gas chromatographic separation was conducted using the same oven program reported in the previous section.

Curcumin determination

Curcumin in diluted systems was determined using a UV-2501 PC UV-VIS (Shimadzu, Kyoto, Japan) spectrophotometer. In particular, 2 mL of sample were introduced in a cuvette and the absorbance was recorded at 425 nm. Measurements were carried out before and after thermal treatments.

Data analysis

All determinations were expressed as the mean \pm standard error of at least two measurements from two experiment replicates ($n \geq 4$). Statistical analysis was performed by using R v. 3.0.2 (The R foundation for Statistical Computing). ($p < 0.05$). Bartlett's test was used to check the homogeneity of variance, one way ANOVA was carried out and Tukey-test was used as post-hoc test to determine significant differences among means

Results and discussion

During this study, transparent emulsion that carried the highest amount of lemon oil (20% w/w oil with 3:1 ratio and an aqueous phase of 30% w/w Tween 80 in 0.8 M NaCl) was chosen. In order to evaluate transparent emulsion stability under different stresses over time, three beverage prototypes with different ethanol amount (ethanol-free: 0% v/v, low-ethanol content: 5% v/v, and high-ethanol content: 20% v/v) as well as different pH values (2.1, 3.0, 4.6) were added with different amounts of transparent emulsion and stored at 20 °C up to 60 days.

In particular, the amount of microemulsion added to each beverage prototype (see Beverage preparation in Material and methods section, pag. 130) was chosen considering the Acceptable Daily Intake (ADI) for Tween 80 as reported by FDA (McClements, 2005). The surfactant has a maximum ADI of 25 mg/kg bw die and calculations were made considering an average man of 70 kg consuming a maximum amount of 1 L ethanol-free beverage, 500 mL low-ethanol content beverage, and 200 mL high-ethanol content beverage.

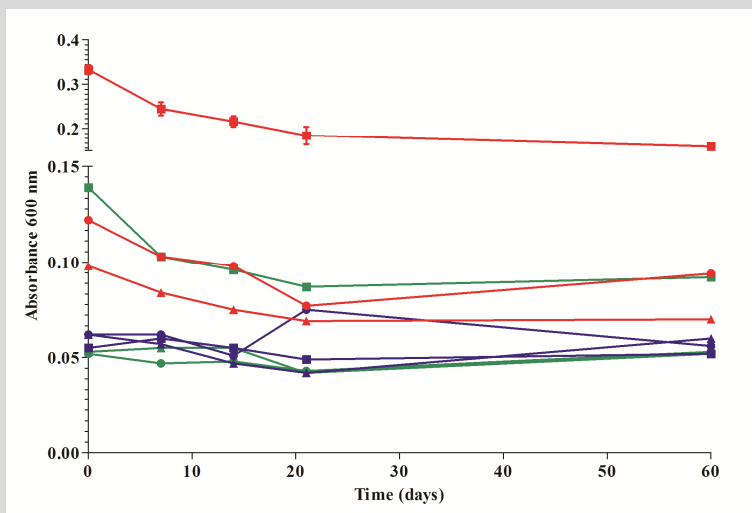


Figure I. Absorbance at 600 nm as a function of time for microemulsion added to ethanol-free (green), low-ethanol (blue), and high-ethanol (red) content beverages at 2.1 (circle), 3.0 (square), and 4.6 (triangle) beverage pH values.

Figure I shows the evolution of absorbance at 600 nm for ethanol-free, low-ethanol, and high-ethanol content beverages at different pH values (2.1, 3.0, and 4.6). It can be noted that, in general, most of the systems showed a decrease of absorbance values over time. High-ethanol content beverage showed higher absorbance values compared to other beverage prototypes with the same pH value. This can be due to both a higher ethanol concentration that could have destabilized the oil droplets and a higher microemulsion

concentration that could have undergone to coalescence or OR in the beverage prototype. Low-ethanol content beverages showed low absorbance values independently on the pH value up to 60 days. Finally, ethanol-free beverages showed slightly higher absorbance values for sample having pH value of 3.0. It has to be noted that the only sample that appeared slightly opalescent was the one showing the highest absorbance value in Figure I (high-ethanol content beverage at pH value of 3.0). Thus, oil droplets seem to remain stable even after dilution in different aqueous environments. In order to evaluate thermal stability of microemulsions diluted in beverages prototypes, ethanol-free beverage at pH value of 2.1 and low-ethanol beverage at pH value of 3.0 were subjected to two different thermal treatments: (i) below transparent emulsion PIT (72 °C x 15 s) and (ii) above PIT (121 °C x 15 min). Figure II shows the visual appearance of systems before and after the thermal treatments.

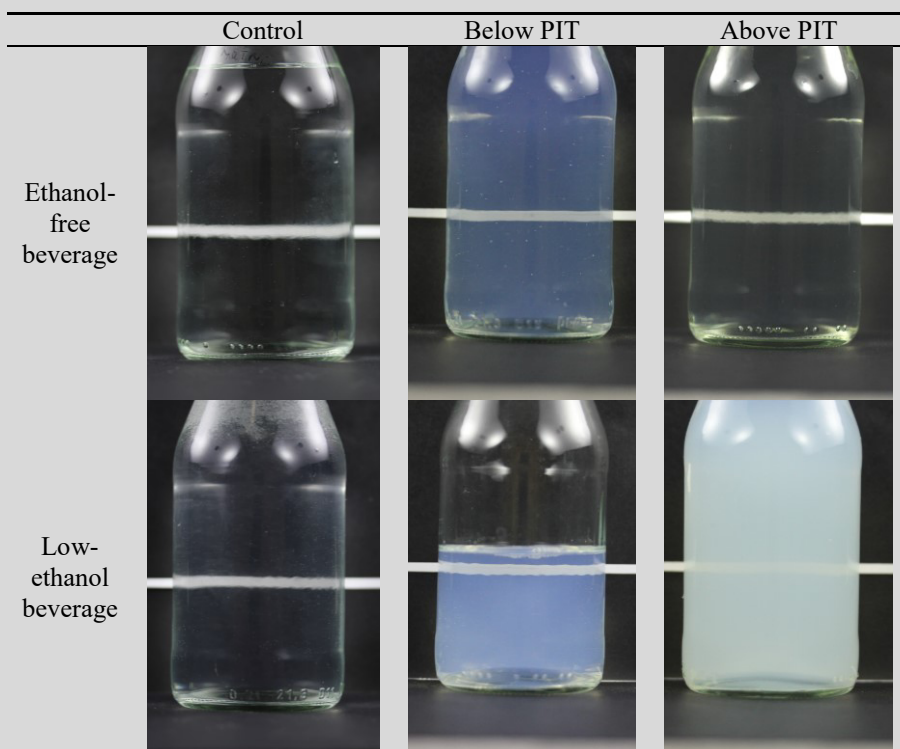


Figure II. Visual appearance of ethanol-free and low-ethanol beverages before (control) and after thermal treatment above and below microemulsion PIT.

Thermal treatments greatly affected the visual appearance of the beverages (Figure II). In particular, low-ethanol content beverage showed an increase of turbidity, increasing the intensity of the thermal treatment (data not shown). On the other hand, ethanol-free beverage had an increase in turbidity after treatments below the microemulsion PIT and surprisingly became optically transparent after treatment above microemulsion PIT. As well known and confirmed by HS-SPME-GC-MS, limonene was the most abundant volatile compound present in lemon oil, followed by α - and β -pinene, and γ -terpinene (data not shown). In order to understand the effect of thermal treatments on volatile compounds, limonene variations in beverage prototypes were analyzed by HS-SPME-GC.

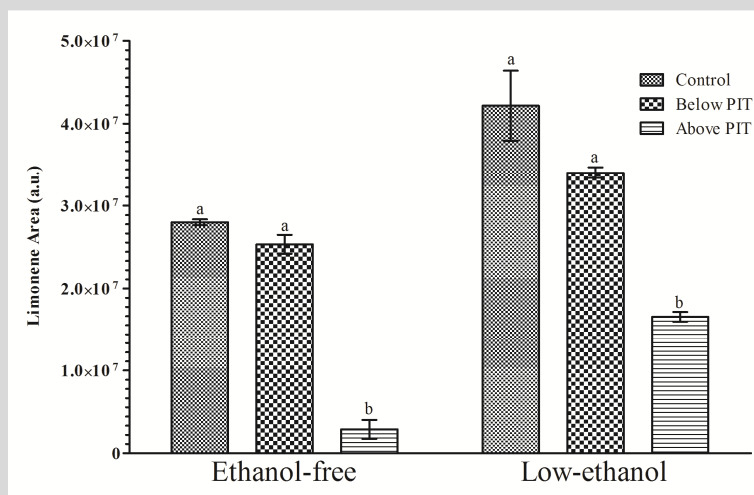


Figure III. Limonene area for ethanol-free and low-ethanol beverage prototypes before (control) and after thermal treatment above and below microemulsion PIT. Different letters within the same beverage prototype indicate statistically significant differences ($p < 0.05$).

Figure III shows limonene area variation for both ethanol-free and low-ethanol beverage prototypes before and after thermal treatments. It can be noted that thermal treatment below the PIT did not affect significantly limonene concentration for both beverage prototypes respect to controls. On the other hand thermal treatments above the PIT strongly reduced limonene concentration. It seems that microemulsions were not able to protect lemon oil against degradation (such as oxidation) at temperatures above microemulsions PIT. This can be due to changes in surfactant geometry induced by the temperature that destabilized micelles inside beverages, and led to an increase of the opalescence of the samples as well as a reduction of the limonene concentration. Thus, it seems that microemulsions can be used as effective lemon oil carrier in different environments (different pH and ethanol content) but because of Tween 80 susceptibility to temperature, only moderate thermal treatments can be applied in order to avoid microemulsion destabilization and lemon oil degradation in beverage prototypes. Finally, microemulsions added with curcumin were diluted in ethanol-free beverage prototype. The addition of curcumin did not affect the physical properties of microemulsion. Indeed, transparent systems with a mean particle diameter of about 20 nm were obtained (Figure IV).



Figure IV. Visual aspect of transparent microemulsion containing 20% (w/w) oil with 3:1 ratio (lemon:peanut oil) added with 0.06% (w/w) curcumin, and an aqueous phase of 30% (w/w) Tween 80 in 0.8 M NaCl.

Figure V shows the visual appearance of ethanol-free beverage prototypes added with transparent emulsion reported in Figure IV before and after thermal treatment below the PIT. An additional sample after thermal treatment was added with carbon dioxide.

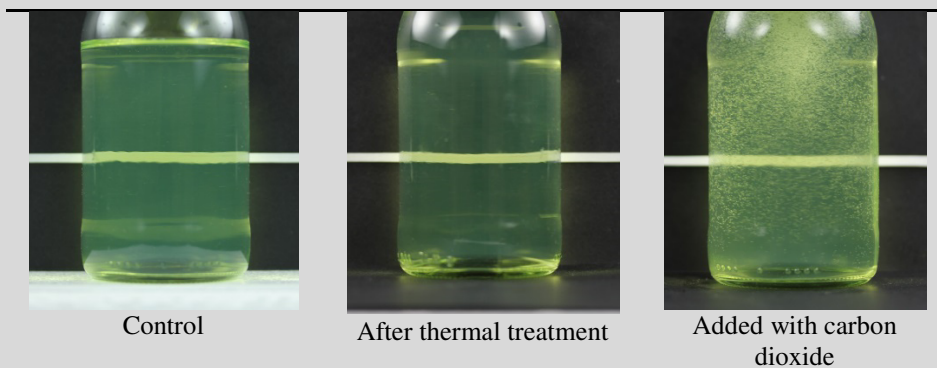


Figure V. Visual appearance of ethanol-free beverage prototypes added with transparent emulsion containing 20% (w/w) oil with 3:1 ratio (lemon:peanut oil) added with 0.06% (w/w) curcumin, and an aqueous phase of 30% (w/w) Tween 80 in 0.8 M NaCl, before and after thermal treatment below the PIT. An additional sample after thermal treatment added with carbon dioxide is also reported.

Both thermal and carbonation treatments did not affect the transparency of the final beverage prototype. However, a significant decrease in curcumin concentration during 20 days of storage at 20 °C in the dark of the beverages shown in Figure V was found (data not shown).

Conclusions

Selected transparent emulsion showed a feasible applicability in beverage prototypes with different chemical composition. Tested transparent emulsion showed a good delivery and protection ability on lemon oil aroma against moderate thermal treatments. However, as pointed out in the last part of this insight, this system has a reduced ability on curcumin protection against degradation. More research is needed in order to better understand the observed results as well as to design a better delivery system able to protect bioactive molecules against degradation.

General conclusions and future directions

In this Ph.D. thesis, the ability of selected self-assembly molecules to form structures in different environments was studied at different length scales (nano, micro, and macro). In particular, the attention was pointed on hydrophobic as well as a mixture of hydrophobic and hydrophilic media.

In particular, Part I was focused on the structuring ability of polar lipids such as fatty alcohols and monoglycerides. Selected resulting systems were then used as solid fat replacer and polyunsaturated fatty acids delivery systems in real foods. On the other hand, Part II was focused on delivery systems for lipophilic bioactive compounds where the physical state of the delivering systems was tuned and the stability of the guest molecule was studied.

Results acquired highlighted that in order to obtain the desired structured material, a careful control of the building blocks, environment, and processing conditions as well as the interaction among system components has to be performed. However, the design of a specific structure is not sufficient. Indeed, the performance of resulting materials in real food systems has to be taken into account. Food matrices are, in most cases, complex systems that can interact with the structured material in different ways giving rise to complex interplays extremely difficult to be fully predicted. Thus, food structure design has to consider not only the design and production of a certain structure but also its application and integration in foods, the effect of food processing and storage, as well as its consumption.

Systems studied within this Ph.D. thesis can be further developed and implemented. As an example, gelled emulsions can be incorporated with hydrophilic as well as hydrophobic bioactive compounds and the stability of both, system and guest molecules, can be studied. In *vitro* as well as in *vivo* bioaccessibility can be then assessed. Regarding nano and microemulsions, it would be interesting study the effect of different environmental stresses on long term systems stability. Moreover, an implementation of the insight proposed at the end of this manuscript can be done taking into account different factors and levels of prototype beverage ingredients as well as different dilution levels. Sensory and clinical trials can be then performed on the most promising systems.

References

- AACC (American Association of Cereal Chemists). (2000). Approved methods of the AACC (10th ed.). S. Paul (MN): The Association.
- Ahmadi, L., Wright, A. J., & Marangoni, A. G. (2008). Chemical and enzymatic interesterification of tristearin/triolein-rich blends: Chemical composition, solid fat content and thermal properties. *European Journal of Lipid Science and Technology*, *110*(11), 1014-1024.
- Ahmed, K., Li, Y., McClements, D. J., & Xiao, H. (2012). Nanoemulsion- and emulsion-based delivery systems for curcumin: Encapsulation and release properties. *Food Chemistry*, *132*(2), 799-807.
- Anese, M., Bortolomeazzi, R., Manzocco, L., Manzano, M., Giusto, C., & Nicoli, M. C. (2009). Effect of chemical and biological dipping on acrylamide formation and sensory properties in deep-fried potatoes. *Food Research International*, *42*(1), 142-147.
- Anese, M., Nicoli, M. C., Verardo, G., Munari, M., Mirolo, G., & Bortolomeazzi, R. (2014). Effect of vacuum roasting on acrylamide formation and reduction in coffee beans. *Food Chemistry*, *145*, 168-172.
- Anese, M., Quarta, B., Peloux, L., & Calligaris, S. (2011). Effect of formulation on the capacity of l-asparaginase to minimize acrylamide formation in short dough biscuits. *Food Research International*, *44*(9), 2837-2842.
- Anton, N., Benoit, J. P., & Saulnier, P. (2008). Design and production of nanoparticles formulated from nano-emulsion templates-a review. *Journal of Controlled Release*, *128*(3), 185-199.
- Anton, N., & Vandamme, T. F. (2009). The universality of low-energy nano-emulsification. *International Journal of Pharmaceutics*, *377*(1-2), 142-147.
- AOAC. (2000). Official methods of analysis. Washington, DC: Association of Official Analytical Chemists.
- Augustin, M. A., & Hemar, Y. (2009). Nano- and micro-structured assemblies for encapsulation of food ingredients. *Chemical Society Reviews*, *38*(4), 902-912.
- Azais-Braesco, V., Brighenti, F., Paoletti, R., Peracino, A., Scarborough, P., Visioli, F., & Vogege, C. (2009). Healthy food and healthy choices: A new European profile approach. *Atherosclerosis Supplements*, *10*(4), 11.
- Bain, L. E., Awah, P. K., Geraldine, N., Kindong, N. P., Sigal, Y., Bernard, N., & Tanjeko, A. T. (2013). Malnutrition in Sub-Saharan Africa: burden, causes and prospects. *The Pan African Medical Journal*, *15*, 120.
- Ball, C. O. (1923). Thermal process time for canned food. *Bulletin of the National Research Council*, *7*, 37.
- Batte, H. D., Wright, A. J., Rush, J. W., Idziak, S. H. J., & Marangoni, A. G. (2007a). Effect of processing conditions on the structure of monostearin-oil-water gels. *Food Research International*, *40*(8), 982-988.
- Batte, H. D., Wright, A. J., Rush, J. W., Idziak, S. H. J., & Marangoni, A. G. (2007b). Phase behavior, stability, and mesomorphism of monostearin-oil-water gels. *Food Biophysics*, *2*(1), 29-37.
- Beaucage, G. (1995). Approximations leading to a unified exponential power-law approach to small-angle scattering. *Journal of Applied Crystallography*, *28*(6), 717-728.
- Beaucage, G. (1996). Small-angle scattering from polymeric mass fractals of arbitrary mass-fractal dimension. *Journal of Applied Crystallography*, *29*(2), 134-146.
- Beaucage, G., & Schaefer, D. W. (1994). Structural studies of complex systems using small-angle scattering: a unified Guinier/power-law approach. *Journal of Non-Crystalline Solids*, *172-174*, 797-805.

- Bhushan, B. (2010). Introduction to Nanotechnology. In B. Bhushan (Ed.), *Springer Handbook of Nanotechnology* (pp. 1-13): Springer Berlin Heidelberg.
- Bianchi, F., Careri, M., Mangia, A., & Musci, M. (2006). Development and validation of a solid phase micro-extraction-gas chromatography-mass spectrometry method for the determination of furan in baby-food. *Journal of Chromatography A*, *1102*(1-2), 268-272.
- Blake, A. I., Co, E. D., & Marangoni, A. G. (2014). Structure and Physical Properties of Plant Wax Crystal Networks and Their Relationship to Oil Binding Capacity. *Journal of the American Oil Chemists' Society*, *91*(6), 885-903.
- Blake, A. I., & Marangoni, A. G. (2015a). The Effect of Shear on the Microstructure and Oil Binding Capacity of Wax Crystal Networks. *Food Biophysics*, 1-13.
- Blake, A. I., & Marangoni, A. G. (2015b). Factors affecting the rheological properties of a structured cellular solid used as a fat mimetic. *Food Research International*, *74*, 284-293.
- Blake, A. I., & Marangoni, A. G. (2015c). Plant wax crystals display platelet-like morphology. *Food Structure*, *3*, 30-34.
- Blake, A. I., & Marangoni, A. G. (2015d). The Use of Cooling Rate to Engineer the Microstructure and Oil Binding Capacity of Wax Crystal Networks. *Food Biophysics*, 1-10.
- Boots, J. W., Chupin, V., Killian, J. A., Demel, R. A., & de Kruijff, B. (1999). Interaction mode specific reorganization of gel phase monoglyceride bilayers by beta-lactoglobulin. *Biochimica et Biophysica Acta*, *1420*(1-2), 241-251.
- Borel, P., Grolier, P., Armand, M., Partier, A., Lafont, H., Lairon, D., & Azais-Braesco, V. (1996). Carotenoids in biological emulsions: solubility, surface-to-core distribution, and release from lipid droplets. *Journal of Lipid Research*, *37*(2), 250-261.
- Bot, A., & Agterof, W. G. M. (2006). Structuring of edible oils by mixtures of gamma-oryzanol with beta-sitosterol or related phytosterols. *Journal of the American Oil Chemists' Society*, *83*(6), 513-521.
- Bot, A., den Adel, R., Roijers, E. C., & Regkos, C. (2009). Effect of Sterol Type on Structure of Tubules in Sterol plus gamma-Oryzanol-Based Organogels. *Food Biophysics*, *4*(4), 266-272.
- Brathen, E., & Knutsen, S. H. (2005). Effect of temperature and time on the formation of acrylamide in starch-based and cereal model systems, flat breads and bread. *Food Chemistry*, *92*(4), 693-700.
- Brooker, B. E. (1996). The role of fat in the stabilisation of gas cells in bread dough. *Journal of Cereal Science*, *24*(3), 187-198.
- Calligaris, S., Arrighetti, G., Barba, L., & Nicoli, M. C. (2008). Phase transition of sunflower oil as affected by the oxidation level. *Journal of the American Oil Chemists' Society*, *85*(7), 591-598.
- Calligaris, S., Da Pieve, S., Arrighetti, G., & Barba, L. (2010). Effect of the structure of monoglyceride-oil-water gels on aroma partition. *Food Research International*, *43*(3), 671-677.
- Calligaris, S., Mirolo, G., Da Pieve, S., Arrighetti, G., & Nicoli, M. C. (2014). Effect of Oil Type on Formation, Structure and Thermal Properties of gamma-oryzanol and beta-sitosterol-Based Organogels. *Food Biophysics*, *9*(1), 69-75.
- Cencic, A., & Chingwaru, W. (2010). The role of functional foods, nutraceuticals, and food supplements in intestinal health. *Nutrients*, *2*(6), 611-625.
- Chanamai, R., & McClements, D. J. (2002). Comparison of Gum Arabic, Modified Starch, and Whey Protein Isolate as Emulsifiers: Influence of pH, CaCl₂ and Temperature. *Journal of Food Science*, *67*(1), 120-125.

- Chandler, D. (2005). Interfaces and the driving force of hydrophobic assembly. *Nature*, 437(7059), 640-647.
- Chen, C. H., & Terentjev, E. M. (2009). Aging and metastability of monoglycerides in hydrophobic solutions. *Langmuir*, 25(12), 6717-6724.
- Chen, C. H., & Terentjev, E. M. (2010). Effects of water on aggregation and stability of monoglycerides in hydrophobic solutions. *Langmuir*, 26(5), 3095-3105.
- Chen, L. Y., Remondetto, G. E., & Subirade, M. (2006). Food protein-based materials as nutraceutical delivery systems. *Trends in Food Science & Technology*, 17(5), 272-283.
- Chin, N. L., Rahman, R. A., Hashim, D. M., & Kowng, S. Y. (2010). Palm Oil Shortening Effects on Baking Performance of White Bread. *Journal of Food Process Engineering*, 33(3), 413-433.
- Chung, C., Degner, B., & McClements, D. J. (2014). Understanding multicomponent emulsion-based products: Influence of locust bean gum on fat droplet - Starch granule mixtures. *Food Hydrocolloids*, 35, 315-323.
- Claus, A., Carle, R., & Schieber, A. (2008). Acrylamide in cereal products: A review. *Journal of Cereal Science*, 47(2), 118-133.
- Clydesdale, F. M. (1978). Colorimetry-methodology and applications. *Critical Reviews in Food Science and Nutrition*, 10(3), 243-301.
- Co, E. D., & Marangoni, A. G. (2012). Organogels: An Alternative Edible Oil-Structuring Method. *Journal of the American Oil Chemists' Society*, 89(5), 749-780.
- Combrinck, J., Otto, A., & du Plessis, J. (2014). Whey protein/polysaccharide-stabilized emulsions: Effect of polymer type and pH on release and topical delivery of salicylic acid. *AAPS PharmSciTech*, 15(3), 588-600.
- Cornacchia, L., & Roos, Y. H. (2011). Stability of beta-carotene in protein-stabilized oil-in-water delivery systems. *Journal of Agricultural and Food Chemistry*, 59(13), 7013-7020.
- Da Pieve, S., Calligaris, S., Co, E., Nicoli, M. C., & Marangoni, A. G. (2010). Shear nanostructuring of monoglyceride organogels. *Food Biophysics*, 5(3), 211-217.
- Da Pieve, S., Calligaris, S., Panozzo, A., Arrighetti, G., & Nicoli, M. C. (2011). Effect of monoglyceride organogel structure on cod liver oil stability. *Food Research International*, 44(9), 2978-2983.
- Daniel, J., & Rajasekharan, R. (2003). Organogelation of plant oils and hydrocarbons by long-chain saturated FA, fatty alcohols, wax esters, and dicarboxylic acids. *Journal of the American Oil Chemists' Society*, 80(5), 417-421.
- Davidovich-Pinhas, M., Barbut, S., & Marangoni, A. G. (2015). The gelation of oil using ethyl cellulose. *Carbohydrate Polymers*, 117, 869-878.
- EFSA. (2013). Commission recommendation of 8 November 2013 on investigations into the levels of acrylamide in food sets new levels for acrylamide. *Official Journal of the European Union*, 301, 15.
- European Community. (1991). Regulation 2568/91, L 248, *O.J.E.C.*
- Euston, S. E., Singh, H., Munro, P. A., & Dalgleish, D. G. (1995). Competitive Adsorption between Sodium Caseinate and Oil-Soluble and Water-Soluble Surfactants in Oil-in-Water Emulsions. *Journal of Food Science*, 60(5), 1124-1131.
- Fernandez, P., Andre, V., Rieger, J., & Kuhnle, A. (2004). Nano-emulsion formation by emulsion phase inversion. *Colloids and Surfaces A-Physicochemical and Engineering Aspects*, 251(1-3), 53-58.
- Firoozmand, H., & Rousseau, D. (2013). Microstructure and elastic modulus of phase-separated gelatin-starch hydrogels containing dispersed oil droplets. *Food Hydrocolloids*, 30(1), 333-342.

- Floros, J. D., Newsome, R., Fisher, W., Barbosa-Canovas, G. V., Chen, H. D., Dunne, C. P., German, J. B., Hall, R. L., Heldman, D. R., Karwe, M. V., Knabel, S. J., Labuza, T. P., Lund, D. B., Newell-McGloughlin, M., Robinson, J. L., Sebranek, J. G., Shewfelt, R. L., Tracy, W. F., Weaver, C. M., & Ziegler, G. R. (2010). Feeding the World Today and Tomorrow: The Importance of Food Science and Technology An IFT Scientific Review. *Comprehensive Reviews in Food Science and Food Safety*, 9(5), 572-599.
- Food Drink Europe. (2013). Food Drink Europe Acrylamide Toolbox, Available from www.fooddrinkeurope.eu/publications/category/toolkits/.
- Gabriele, D., de Cindio, B., & D'Antona, P. (2001). A weak gel model for foods. *Rheologica Acta*, 40(2), 120-127.
- Gandolfo, F. G., Bot, A., & Flöter, E. (2004). Structuring of edible oils by long-chain FA, fatty alcohols, and their mixtures. *Journal of the American Oil Chemists' Society*, 81(1), 1-6.
- Gokmen, V., & Senyuva, H. Z. (2006). Study of colour and acrylamide formation in coffee, wheat flour and potato chips during heating. *Food Chemistry*, 99(2), 238-243.
- Goldstein, A., Marangoni, A. G., & Seetharaman, K. (2012). Monoglyceride Stabilized Oil in Water Emulsions: an Investigation of Structuring and Shear History on Phase Behaviour. *Food Biophysics*, 7(3), 227-235.
- Goldstein, A., & Seetharaman, K. (2011). Effect of a novel monoglyceride stabilized oil in water emulsion shortening on cookie properties. *Food Research International*, 44(5), 1476-1481.
- Gomez, M., del Real, S., Rosell, C. M., Ronda, F., Blanco, C. A., & Caballero, P. A. (2004). Functionality of different emulsifiers on the performance of breadmaking and wheat bread quality. *European Food Research and Technology*, 219(2), 145-150.
- Govindaraj, M. (2015). Is Fortification or Bio Fortification of Staple Food Crops will Offer a Simple Solution to Complex Nutritional Disorder in Developing Countries? *Journal of Nutrition & Food Sciences*, 5(2).
- Gravelle, A. J., Barbut, S., & Marangoni, A. G. (2012). Ethylcellulose oleogels: Manufacturing considerations and effects of oil oxidation. *Food Research International*, 48(2), 578-583.
- Gravelle, A. J., Barbut, S., Quinton, M., & Marangoni, A. G. (2014). Towards the development of a predictive model of the formulation-dependent mechanical behaviour of edible oil-based ethylcellulose oleogels. *Journal of Food Engineering*, 143, 114-122.
- Gravelle, A. J., Davidovich-Pinhas, M., Zetzel, A. K., Barbut, S., & Marangoni, A. G. (2016). Influence of solvent quality on the mechanical strength of ethylcellulose oleogels. *Carbohydrate Polymers*, 135, 169-179.
- Gutiérrez, F. J., Albillos, S. M., Casas-Sanz, E., Cruz, Z., García-Estrada, C., García-Guerra, A., García-Reverter, J., García-Suárez, M., Gatón, P., González-Ferrero, C., Olabarrieta, I., Olasagasti, M., Rainieri, S., Rivera-Patiño, D., Rojo, R., Romo-Hualde, A., Sáiz-Abajo, M. J., & Mussons, M. L. (2013). Methods for the nanoencapsulation of β -carotene in the food sector. *Trends in Food Science & Technology*, 32(2), 73-83.
- Hammersley, A. P., Svensson, S. O., Hanfland, M., Fitch, A. N., & Hausermann, D. (1996). Two-dimensional detector software: From real detector to idealised image or two-theta scan. *High Pressure Research*, 14(4-6), 235-248.
- Heertje, I., Roijers, E. C., & Hendrickx, H. A. C. M. (1998). Liquid crystalline phases in the structuring of food products. *Lebensmittel-Wissenschaft Und-Technologie-Food Science and Technology*, 31(4), 387-396.

- Helgason, T., Awad, T. S., Kristbergsson, K., Decker, E. A., McClements, D. J., & Weiss, J. (2009a). Impact of surfactant properties on oxidative stability of beta-carotene encapsulated within solid lipid nanoparticles. *Journal of Agricultural and Food Chemistry*, *57*(17), 8033-8040.
- Helgason, T., Awad, T. S., Kristbergsson, K., McClements, D. J., & Weiss, J. (2009b). Effect of surfactant surface coverage on formation of solid lipid nanoparticles (SLN). *Journal of Colloid and Interface Science*, *334*(1), 75-81.
- Himawan, C., MacNaughtan, W., Farhat, I. A., & Stapley, A. G. F. (2007). Polymorphic occurrence and crystallization rates of tristearin/tripalmitin mixtures under non-isothermal conditions. *European Journal of Lipid Science and Technology*, *109*(1), 49-60.
- Hughes, N. E., Marangoni, A. G., Wright, A. J., Rogers, M. A., & Rush, J. W. E. (2009). Potential food applications of edible oil organogels. *Trends in Food Science & Technology*, *20*(10), 470-480.
- Hyde, S., Andersson, S., Larsson, K., Blum, Z., Landh, T., Lidn, S., & Ninham, B. W. (Eds.). (1997). *The Language of Shape, the Role of Curvature in Condensed Matter: Physics, Chemistry and Biology* (1st ed.). Amsterdam: Elsevier Science B. V.
- Ilavsky, J., & Jemian, P. R. (2009). Irena: tool suite for modeling and analysis of small-angle scattering. *Journal of Applied Crystallography*, *42*(2), 347-353.
- Ilavsky, J., Zhang, F., Allen, A. J., Levine, L. E., Jemian, P. R., & Long, G. G. (2013). Ultra-Small-Angle X-ray Scattering Instrument at the Advanced Photon Source: History, Recent Development, and Current Status. *Metallurgical and Materials Transactions A-Physical Metallurgy and Materials Science*, *44A*(1), 68-76.
- Inoue, C., Hagura, Y., Ishikawa, M., & Suzuki, K. (2002). The dielectric property of soybean oil in deep-fat frying and the effect of frequency. *Journal of Food Science*, *67*(3), 1126-1129.
- Inoue, T., Hisatsugu, Y., Yamamoto, R., & Suzuki, M. (2004). Solid-liquid phase behavior of binary fatty acid mixtures. 1. Oleic acid/stearic acid and oleic acid/behenic acid mixtures. *Chemistry and Physics of Lipids*, *127*(2), 143-152.
- Joardder, M. U., Kumar, C., & Karim, M. A. (2015). Food Structure: Its Formation and Relationships with Other Properties. *Critical Reviews in Food Science and Nutrition*, *0*.
- Kentish, S., Wooster, T. J., Ashokkumar, A., Balachandran, S., Mawson, R., & Simons, L. (2008). The use of ultrasonics for nanoemulsion preparation. *Innovative Food Science & Emerging Technologies*, *9*(2), 170-175.
- Klaessig, F., Marrapese, M., & Abe, S. (2011). Current Perspectives in Nanotechnology Terminology and Nomenclature. In V. Murashov & J. Howard (Eds.), *Nanotechnology Standards* (pp. 21-52): Springer New York.
- Klucker, M. F., Dalencon, F., Probeck, P., & Haensler, J. (2012). AF03, an alternative squalene emulsion-based vaccine adjuvant prepared by a phase inversion temperature method. *Journal of Pharmaceutical Sciences*, *101*(12), 4490-4500.
- Kremer, F., Huwe, A., Schönhals, A., & Rozanski, S. A. (2003). Molecular dynamic in confining space. In F. Kremer & A. Schönhals (Eds.), *Broad Band Dielectric Spectroscopy* (pp. 171-224). Berlin: Springer.
- Kristensen, D., Orlie, V., Mortensen, G., Brockhoff, P., & Skibsted, L. H. (2000). Light-induced oxidation in sliced Havarti cheese packaged in modified atmosphere. *International Dairy Journal*, *10*(1-2), 95-103.
- Kumar, D., Singh, A., & Tarsikka, P. S. (2013). Interrelationship between viscosity and electrical properties for edible oils. *Journal of Food Science and Technology*, *50*(3), 549-554.

- Laredo, T., Barbut, S., & Marangoni, A. G. (2011). Molecular interactions of polymer oleogelation. *Soft Matter*, 7(6), 2734-2743.
- Larsson, K. (2009). Lyotropic liquid crystals and their dispersions relevant in foods. *Current Opinion in Colloid & Interface Science*, 14(1), 16-20.
- Laughlin, R. G., Bunke, G. M., Eads, C. D., Laidig, W. D., & Shelley, J. C. (2002). Preparation and physical characterization of pure beta-carotene. *Chemistry and Physics of Lipids*, 115(1-2), 63-76.
- Laugier, J., & Bochu, B. (2000). CHECKCELL. <http://www.CCP14.ac.uk/tutorial/lmgp/>.
- Leenhouts, J. M., Demel, R. A., deKruijff, B., & Boots, J. W. P. (1997). Charge-dependent insertion of beta-lactoglobulin into monoglyceride monolayers. *Biochimica Et Biophysica Acta-Biomembranes*, 1330(1), 61-70.
- Lehn, J. M. (2002). Toward complex matter: supramolecular chemistry and self-organization. *Proceedings of the National Academy of Sciences of the United States of America*, 99(8), 4763-4768.
- Li, Y., Le Maux, S., Xiao, H., & McClements, D. J. (2009). Emulsion-based delivery systems for tributyrin, a potential colon cancer preventative agent. *Journal of Agricultural and Food Chemistry*, 57(19), 9243-9249.
- Lizhi, H., Toyoda, K., & Ihara, I. (2008). Dielectric properties of edible oils and fatty acids as a function of frequency, temperature, moisture and composition. *Journal of Food Engineering*, 88(2), 151-158.
- Long, G. G., Jemian, P. R., Weertman, J. R., Black, D. R., Burdette, H. E., & Spal, R. (1991). High-Resolution Small-Angle X-Ray-Scattering Camera for Anomalous Scattering. *Journal of Applied Crystallography*, 24(1), 30-37.
- Lopez-Martinez, A., Charo-Alonso, M. A., Marangoni, A. G., & Toro-Vazquez, J. F. (2015). Monoglyceride organogels developed in vegetable oil with and without ethylcellulose. *Food Research International*, 72, 37-46.
- Lopez-Martinez, A., Morales-Rueda, J. A., Dibildox-Alvarado, E., Charo-Alonso, M. A., Marangoni, A. G., & Toro-Vazquez, J. F. (2014). Comparing the crystallization and rheological behavior of organogels developed by pure and commercial monoglycerides in vegetable oil. *Food Research International*, 64, 946-957.
- Lopez, C., Lavigne, F., Lesieur, P., Keller, G., & Ollivon, M. (2001). Thermal and structural behavior of anhydrous milk fat. 2. Crystalline forms obtained by slow cooling. *Journal of Dairy Science*, 84(11), 2402-2412.
- Lowe, M. R., & Butryn, M. L. (2007). Hedonic hunger: a new dimension of appetite? *Physiology & Behavior*, 91(4), 432-439.
- Maleky, F., & Marangoni, A. G. (2008). Process development for continuous crystallization of fat under laminar shear. *Journal of Food Engineering*, 89(4), 399-407.
- Manohar, R. S., & Rao, P. H. (1999). Effect of emulsifiers, fat level and type on the rheological characteristics of biscuit dough and quality of biscuits. *Journal of the Science of Food and Agriculture*, 79(10), 1223-1231.
- Manzocco, L., Anese, M., Calligaris, S., Quarta, B., & Nicoli, M. C. (2012a). Use of monoglyceride hydrogel for the production of low fat short dough pastry. *Food Chemistry*, 132(1), 175-180.
- Manzocco, L., Calligaris, S., Da Pieve, S., Marzona, S., & Nicoli, M. C. (2012b). Effect of monoglyceride-oil-water gels on white bread properties. *Food Research International*, 49(2), 778-782.
- Marangoni, A. G., Acevedo, N., Maleky, F., Co, E., Peyronel, F., Mazzanti, G., Quinn, B., & Pink, D. (2012). Structure and functionality of edible fats. *Soft Matter*, 8(5), 1275-1300.

- Mazzanti, G., Guthrie, S. E., Sirota, E. B., Marangoni, A. G., & Idziak, S. H. J. (2004). Novel shear-induced phases in cocoa butter. *Crystal Growth & Design*, 4(3), 409-411.
- McClements, D. J. (2012). Nanoemulsions versus microemulsions: terminology, differences, and similarities. *Soft Matter*, 8(6), 1719-1729.
- McClements, D. J. (2013). Edible lipid nanoparticles: digestion, absorption, and potential toxicity. *Progress in Lipid Research*, 52(4), 409-423.
- McClements, D. J. (Ed.). (2005). *Food Emulsions: Principles, Practices, and Techniques* (2nd ed.). Boca Raton: CRC Press.
- McClements, D. J., Decker, E. A., Park, Y., & Weiss, J. (2009). Structural design principles for delivery of bioactive components in nutraceuticals and functional foods. *Critical reviews in food science and nutrition*, 49(6), 577-606.
- McClements, D. J., & Rao, J. (2011). Food-grade nanoemulsions: formulation, fabrication, properties, performance, biological fate, and potential toxicity. *Critical Reviews in Food Science and Nutrition*, 51(4), 285-330.
- Mela, D. J. (2006). Eating for pleasure or just wanting to eat? Reconsidering sensory hedonic responses as a driver of obesity. *Appetite*, 47(1), 10-17.
- Mendes, A. C., Baran, E. T., Reis, R. L., & Azevedo, H. S. (2013). Self-assembly in nature: using the principles of nature to create complex nanobiomaterials. *Wiley Interdisciplinary Reviews. Nanomedicine and Nanobiotechnology*, 5(6), 582-612.
- Metivaud, V., Lefevre, A., Ventolà, L., Negrier, P., Moreno, E., Calvet, T., Mondieig, D., & Cuevas-Diarte, M. A. (2005). Hexadecane (C₁₆H₃₄)+1-hexadecanol (C₁₆H₃₃OH) binary system: Crystal structures of the components and experimental phase diagram. Application to thermal protection of liquids. *Chemistry of Materials*, 17(12), 3302-3310.
- Midmore, B. R., Hunter, R. J., & O'Brien, R. W. (1987). The Dielectric Response of Concentrated Lattices. *Journal of Colloid and Interface Science*, 120(1), 210-217.
- Nik, A. M., Langmaid, S., & Wright, A. J. (2012). Nonionic surfactant and interfacial structure impact crystallinity and stability of beta-carotene loaded lipid nanodispersions. *Journal of Agricultural and Food Chemistry*, 60(16), 4126-4135.
- Ollivon, M., Keller, G., Bourgaux, C., Kalnin, D., Villeneuve, P., & Lesieur, P. (2006). DSC and high resolution X-ray diffraction coupling. *Journal of Thermal Analysis and Calorimetry*, 85(1), 219-224.
- Ostertag, F., Weiss, J., & McClements, D. J. (2012). Low-energy formation of edible nanoemulsions: factors influencing droplet size produced by emulsion phase inversion. *Journal of Colloid and Interface Science*, 388(1), 95-102.
- Patel, A. R., Babaahmadi, M., Lesaffer, A., & Dewettinck, K. (2015). Rheological profiling of organogels prepared at critical gelling concentrations of natural waxes in a triacylglycerol solvent. *Journal of Agricultural and Food Chemistry*, 63(19), 4862-4869.
- Patel, A. R., Cludts, N., Bin Sintang, M. D., Lewille, B., Lesaffer, A., & Dewettinck, K. (2014a). Polysaccharide-Based Oleogels Prepared with an Emulsion-Templated Approach. *Chemphyschem*, 15(16), 3435-3439.
- Patel, A. R., & Dewettinck, K. (2015). Comparative evaluation of structured oil systems: Shellac oleogel, HPMC oleogel, and HIPE gel. *European Journal of Lipid Science and Technology*, n/a-n/a.
- Patel, A. R., Rajarethinem, P. S., Gredowska, A., Turhan, O., Lesaffer, A., De Vos, W. H., Van de Walle, D., & Dewettinck, K. (2014b). Edible applications of shellac oleogels: spreads, chocolate paste and cakes. *Food & Function*, 5(4), 645-652.

- Patel, A. R., Schatteman, D., Lesaffer, A., & Dewettinck, K. (2013). A foam-templated approach for fabricating organogels using a water-soluble polymer. *Rsc Advances*, 3(45), 22900-22903.
- Pelan, B. M. C., Watts, K. M., Campbell, I. J., & Lips, A. (1997). The stability of aerated milk protein emulsions in the presence of small molecule surfactants. *Journal of Dairy Science*, 80(10), 2631-2638.
- Pernetti, M., van Malssen, K., Kalnin, D., & Flöter, E. (2007). Structuring edible oil with lecithin and sorbitan tri-stearate. *Food Hydrocolloids*, 21(5-6), 855-861.
- Peyronel, F., Ilavsky, J., Mazzanti, G., Marangoni, A. G., & Pink, D. A. (2013). Edible oil structures at low and intermediate concentrations. II. Ultra-small angle X-ray scattering of in situ tristearin solids in triolein. *Journal of Applied Physics*, 114(23), 234902.
- Peyronel, F., Ilavsky, J., Pink, D. A., & Marangoni, A. G. (2014a). Quantification of the physical structure of fats in 20 minutes: Implications for formulation. *Lipid Technology*, 26(10), 223-226.
- Peyronel, F., Pink, D. A., & Marangoni, A. G. (2014b). Triglyceride nanocrystal aggregation into polycrystalline colloidal networks: Ultra-small angle X-ray scattering, models and computer simulation. *Current Opinion in Colloid & Interface Science*, 19(5), 459-470.
- Peyronel, F., Quinn, B., Marangoni, A. G., & Pink, D. A. (2014c). Ultra small angle x-ray scattering in complex mixtures of triacylglycerols. *Journal of Physics: Condensed Matter*, 26(46), 464110.
- Peyronel, F., Quinn, B., Marangoni, A. G., & Pink, D. A. (2015). Edible fat structures at high solid fat concentrations: Evidence for the existence of oil-filled nanospaces. *Applied Physics Letters*, 106(2), 023109.
- Pink, D. A., Quinn, B., Peyronel, F., & Marangoni, A. G. (2013). Edible oil structures at low and intermediate concentrations. I. Modeling, computer simulation, and predictions for X ray scattering. *Journal of Applied Physics*, 114(23), 234901.
- Prevc, T., Cigic, B., Vidrih, R., Poklar Ulrih, N., & Segatin, N. (2013). Correlation of basic oil quality indices and electrical properties of model vegetable oil systems. *Journal of Agricultural and Food Chemistry*, 61(47), 11355-11362.
- Purhagen, J. K., Sjöo, M. E., & Eliasson, A. C. (2011). Starch affecting anti-staling agents and their function in freestanding and pan-baked bread. *Food Hydrocolloids*, 25(7), 1656-1666.
- Qian, C., Decker, E. A., Xiao, H., & McClements, D. J. (2013). Impact of lipid nanoparticle physical state on particle aggregation and beta-carotene degradation: Potential limitations of solid lipid nanoparticles. *Food Research International*, 52(1), 342-349.
- Quinn, B., Peyronel, F., Gordon, T., Marangoni, A., Hanna, C. B., & Pink, D. A. (2014). Aggregation in complex triacylglycerol oils: coarse-grained models, nanophase separation, and predicted x-ray intensities. *Journal of Physics: Condensed Matter*, 26(46), 464108.
- Rao, J., & McClements, D. J. (2010). Stabilization of phase inversion temperature nanoemulsions by surfactant displacement. *Journal of Agricultural and Food Chemistry*, 58(11), 7059-7066.
- Rao, J., & McClements, D. J. (2011). Food-grade microemulsions, nanoemulsions and emulsions: Fabrication from sucrose monopalmitate & lemon oil. *Food Hydrocolloids*, 25(6), 1413-1423.
- Razul, M. S., MacDougall, C. J., Hanna, C. B., Marangoni, A. G., Peyronel, F., Papp-Szabo, E., & Pink, D. A. (2014). Oil binding capacities of triacylglycerol crystalline

- nanoplatelets: nanoscale models of tristearin solids in liquid triolein. *Food & Function*, 5(10), 2501-2508.
- Relkin, P., Jung, J. M., & Ollivon, M. (2009). Factors affecting vitamin degradation in oil-in-water nano-emulsions. *Journal of Thermal Analysis and Calorimetry*, 98(1), 13-18.
- Rogers, M. A. (2016). Naturally occurring nanoparticles in food. *Current Opinion in Food Science*, 7, 14-19.
- Rogers, M. A., Wright, A. J., & Marangoni, A. G. (2008a). Crystalline stability of self-assembled fibrillar networks of 12-hydroxystearic acid in edible oils. *Food Research International*, 41(10), 1026-1034.
- Rogers, M. A., Wright, A. J., & Marangoni, A. G. (2008b). Engineering the oil binding capacity and crystallinity of self-assembled fibrillar networks of 12-hydroxystearic acid in edible oils. *Soft Matter*, 4(7), 1483-1490.
- Rogers, M. A., Wright, A. J., & Marangoni, A. G. (2009a). Nanostructuring fiber morphology and solvent inclusions in 12-hydroxystearic acid / canola oil organogels. *Current Opinion in Colloid & Interface Science*, 14(1), 33-42.
- Rogers, M. A., Wright, A. J., & Marangoni, A. G. (2009b). Oil organogels: the fat of the future? *Soft Matter*, 5(8), 1594.
- Roisnel, T., & Rodríguez-Carvajal, J. (2000). *WinPLOTR: a Windows tool for powder diffraction patterns analysis*. Materials Science Forum, Proceedings of the Seventh European Powder Diffraction Conference (EPDIC 7), Eds. R. Delhez & E. J. Mittenmeijer, pp. 118-123.
- Romoscanu, A. I., & Mezzenga, R. (2006). Emulsion-templated fully reversible protein-in-oil gels. *Langmuir*, 22(18), 7812-7818.
- Rosmaninho, R., & Melo, L. F. (2006). The effect of citrate on calcium phosphate deposition from simulated milk ultrafiltrate (SMUF) solution. *Journal of Food Engineering*, 73(4), 379-387.
- Saberi, A. H., Fang, Y., & McClements, D. J. (2013). Fabrication of vitamin E-enriched nanoemulsions by spontaneous emulsification: Effect of propylene glycol and ethanol on formation, stability, and properties. *Food Research International*, 54(1), 812-820.
- Saberi, A. H., Fang, Y., & McClements, D. J. (2015). Formation of thermally reversible optically transparent emulsion-based delivery systems using spontaneous emulsification. *Soft Matter*.
- Sacchetti, G., Di Mattia, C., Pittia, P., & Mastrocola, D. (2009). Effect of roasting degree, equivalent thermal effect and coffee type on the radical scavenging activity of coffee brews and their phenolic fraction. *Journal of Food Engineering*, 90(1), 74-80.
- Sadeghpour Galooyak, S., & Dabir, B. (2015). Three-factor response surface optimization of nano-emulsion formation using a microfluidizer. *Journal of Food Science and Technology*, 52(5), 2558-2571.
- Sagalowicz, L., & Leser, M. E. (2010). Delivery systems for liquid food products. *Current Opinion in Colloid & Interface Science*, 15(1-2), 61-72.
- Sanphui, P., Goud, N. R., Khandavilli, U. B., Bhanoth, S., & Nangia, A. (2011). New polymorphs of curcumin. *Chemical Communications*, 47(17), 5013-5015.
- Sasson, A. (2012). Food security for Africa: an urgent global challenge. *Agriculture & Food Security*, 1(2), 1-16.
- Sato, K. (2001). Crystallization behaviour of fats and lipids - a review. *Chemical Engineering Science*, 56(7), 2255-2265.
- Sato, K., Bayes-Garcia, L., Calvet, T., Cuevas-Diarte, M. A., & Ueno, S. (2013). External factors affecting polymorphic crystallization of lipids. *European Journal of Lipid Science and Technology*, 115(11), 1224-1238.

- Sato, K., Ueno, S., & Yano, J. (1999). Molecular interactions and kinetic properties of fats. *Progress in Lipid Research*, 38(1), 91-116.
- Sawa, K., Inoue, S., Lysenko, E., Edwards, N. M., & Preston, K. R. (2009). Effects of purified monoglycerides on Canadian short process and sponge and dough mixing properties, bread quality and crumb firmness during storage. *Food Chemistry*, 115(3), 884-890.
- Sawalha, H., Margry, G., den Adel, R., Venema, P., Bot, A., Flöter, E., & van der Linden, E. (2013). The influence of the type of oil phase on the self-assembly process of gamma-oryzanol plus beta-sitosterol tubules in organogel systems. *European Journal of Lipid Science and Technology*, 115(3), 295-300.
- Sekhon, B. S. (2010). Food nanotechnology - an overview. *Nanotechnology, Science and Applications*, 3, 1-15.
- Shantha, N. C., & Decker, E. A. (1994). Rapid, sensitive, iron-based spectrophotometric methods for determination of peroxide values of food lipids. *Journal of AOAC International*, 77(2), 421-424.
- Shinoda, K., & Saito, H. (1968). The effect of temperature on the phase equilibria and the types of dispersions of the ternary system composed of water, cyclohexane, and nonionic surfactant. *Journal of Colloid and Interface Science*, 26(1), 70-74.
- Siro, I., Kapolna, E., Kapolna, B., & Lugasi, A. (2008). Functional food. Product development, marketing and consumer acceptance-a review. *Appetite*, 51(3), 456-467.
- Smith, K. W., Bhaggan, K., Talbot, G., & van Malssen, K. F. (2011). Crystallization of Fats: Influence of Minor Components and Additives. *Journal of the American Oil Chemists' Society*, 88(8), 1085-1101.
- Solans, C., & Solè, I. (2012). Nano-emulsions: Formation by low-energy methods. *Current Opinion in Colloid & Interface Science*, 17(5), 246-254.
- Sterling, C. (1964). Crystal-Structure Analysis of Beta-Carotene. *Acta Crystallographica*, 17(10), 1224-&.
- Stortz, T. A., & Marangoni, A. G. (2013). Ethylcellulose solvent substitution method of preparing heat resistant chocolate. *Food Research International*, 51(2), 797-803.
- Su, D., & Zhong, Q. (2015). Lemon Oil Nanoemulsions Fabricated with Sodium Caseinate and Tween 20 using Phase Inversion Temperature Method. *Journal of Food Engineering*.
- Toro-Vazquez, J. F., Morales-Rueda, J. A., Dibildox-Alvarado, E., Charo-Alonso, M., Alonzo-Macias, M., & Gonzalez-Chavez, M. M. (2007). Thermal and textural properties of organogels developed by candelilla wax in safflower oil. *Journal of the American Oil Chemists' Society*, 84(11), 989-1000.
- Ventolà, L., Calvet, T., Cuevas-Diarte, M. A., Oonk, H. A. J., & Mondieig, D. (2004). Solid-solid and solid-liquid equilibria in the n-alkanols family: C18H37OH-C20H41OH system. *Physical Chemistry Chemical Physics*, 6(13), 3726-3731.
- Ventolà, L., Calvet, T., Cuevas-Diarte, M. A., Ramirez, M., Oonk, H. A. J., Mondieig, D., & Negrier, P. (2004). Melting behaviour in the n-alkanol family. Enthalpy-entropy compensation. *Physical Chemistry Chemical Physics*, 6(8), 1786-1791.
- Ventolà, L., Ramírez, M., Calvet, T., Solans, X., Cuevas-Diarte, M. A., Negrier, P., Mondieig, D., van Miltenburg, J. C., & Oonk, H. A. J. (2002). Polymorphism of N-Alkanols: 1-Heptadecanol, 1-Octadecanol, 1-Nonadecanol, and 1-Eicosanol. *Chemistry of Materials*, 14(2), 508-517.
- Walker, R. M., Decker, E. A., & McClements, D. J. (2015). Physical and oxidative stability of fish oil nanoemulsions produced by spontaneous emulsification: Effect of surfactant concentration and particle size. *Journal of Food Engineering*, 164, 10-20.

- Weiss, J., Decker, E. A., McClements, D. J., Kristbergsson, K., Helgason, T., & Awad, T. (2008). Solid lipid nanoparticles as delivery systems for bioactive food components. *Food Biophysics*, 3(2), 146-154.
- Weiss, J., Takhistov, P., & McClements, D. J. (2006). Functional materials in food nanotechnology. *Journal of Food Science*, 71(9), R107-R116.
- Wooster, T. J., Golding, M., & Sanguansri, P. (2008). Impact of oil type on nanoemulsion formation and Ostwald ripening stability. *Langmuir*, 24(22), 12758-12765.
- Yamamoto, T., Nozaki, K., & Hara, T. (1990). X-ray and thermal studies on the rotator phases of normal higher alcohols C17H35OH, C18H37OH, and their mixtures. *The Journal of Chemical Physics*, 92(1), 631.
- Yang, Y., Marshall-Breton, C., Leser, M. E., Sher, A. A., & McClements, D. J. (2012). Fabrication of ultrafine edible emulsions: Comparison of high-energy and low-energy homogenization methods. *Food Hydrocolloids*, 29(2), 398-406.
- Yilmaz, E., & Ogutcu, M. (2014). Properties and Stability of Hazelnut Oil Organogels with Beeswax and Monoglyceride. *Journal of the American Oil Chemists' Society*, 91(6), 1007-1017.
- Yilmaz, E., & Ogutcu, M. (2015). The texture, sensory properties and stability of cookies prepared with wax oleogels. *Food & Function*, 6(4), 1194-1204.
- Yu, L., Li, C., Xu, J., Hao, J., & Sun, D. (2012). Highly stable concentrated nanoemulsions by the phase inversion composition method at elevated temperature. *Langmuir*, 28(41), 14547-14552.
- Zetzi, A. K., Marangoni, A. G., & Barbut, S. (2012). Mechanical properties of ethylcellulose oleogels and their potential for saturated fat reduction in frankfurters. *Food & Function*, 3(3), 327-337.
- Zhang, L., Hayes, D. G., Chen, G., & Zhong, Q. (2013). Transparent dispersions of milk-fat-based nanostructured lipid carriers for delivery of beta-carotene. *Journal of Agricultural and Food Chemistry*, 61(39), 9435-9443.
- Zulim Botega, D. C., Marangoni, A. G., Smith, A. K., & Goff, H. D. (2013). The potential application of rice bran wax oleogel to replace solid fat and enhance unsaturated fat content in ice cream. *Journal of Food Science*, 78(9), C1334-1339.

List of publications relevant to this Ph.D. research activity

- Anese, M., Valoppi, F., Calligaris, S., Lagazio, C., Suman, M., Manzocco, L., & Nicoli, M. C. (2015). Omega-3 enriched biscuits with low levels of heat-induced toxicants: effect of formulation and baking conditions. *Food and Bioprocess Technology*, 1-11.
- Calligaris, S., Manzocco, L., Valoppi, F., & Nicoli, M. C. (2013). Effect of palm oil replacement with monoglyceride organogel and hydrogel on sweet bread properties. *Food Research International*, 51(2), 596-602.
- Calligaris, S., Valoppi, F., Barba, L., Anese, M., & Nicoli, M. C. (2014). Mutual effect of fat and beta-carotene on fat crystal network structure and carotenoid bleaching. *Food Research International*, 66, 257-263.
- Valoppi, F., Calligaris, S., Barba, L., & Nicoli, M. C. (2015a). Compositional phase diagram, rheological and structural properties of systems containing UHT skim milk, sunflower oil, saturated monoglycerides and co-surfactants. *Food Biophysics*, 10(1), 94-102.
- Valoppi, F., Calligaris, S., Barba, L., & Nicoli, M. C. (2015b). Structural and viscoelastic characterization of ternary mixtures of sunflower oil, saturated monoglycerides and aqueous phases containing different bases. *Food Research International*, 74, 224-230.

List of additional publications

- Manzocco, L., Ignat, A., Anese, M., Bot, F., Calligaris, S., Valoppi, F., & Nicoli, M. C. (2015). Efficient management of the water resource in the fresh-cut industry: Current status and perspectives. *Trends in Food Science & Technology*, 46(2), 286-294.
- Manzocco, L., Ignat, A., Valoppi, F., Burrafato, K. R., Lippe, G., Spilimbergo, S., & Nicoli, M. C. (2016). Inactivation of mushroom polyphenoloxidase in model systems exposed to high-pressure carbon dioxide. *The Journal of Supercritical Fluids*, 107, 669-675.

List of submitted and in-progress manuscripts

- Manzocco, L., Calligaris, S., Valoppi, F., Lagazio, C., Anese, M., & Nicoli, M. C. (2015). Shelf life validation by monitoring food on the market: the case study of sliced white bread. *Journal of Food Quality*, under review.
- Valoppi, F., Calligaris, S., & Marangoni, A. G. (2016a). Phase transition and polymorphic behavior of binary systems containing fatty alcohols and peanut oil. *Crystal Growth and Design*, under review.
- Valoppi, F., Calligaris, S., & Marangoni, A. G. (2016b). Structure and physical properties of organogels containing peanut oil and even fatty alcohols from C₁₄OH to C₂₂OH. *Crystal Growth and Design*, under review.
- Valoppi, F., Calligaris, S., Šegatin, N., Poklar Ulrih, N., & Nicoli, M. C. (2015). Relationship between dielectric properties of (edible) oils and structure and physical properties of monoglyceride-based organogels. *European Journal of Lipid Science and Technology*, under review.
- Valoppi, F., Frisina, R., & Calligaris, S. (2015). Development of transparent microemulsions by phase inversion temperature (PIT) delivering lemon oil in beverage prototypes. *Food Chemistry*, under review.

Contributions to national and international conferences

- Anese, M., Calligaris, S., Valoppi, F., Barba, L., & Nicoli, M. C. Effect of fat crystal network structure on β -carotene bleaching. In *Proceedings of "13th Euro Fed Lipid Congress, Oils, Fats and Lipids: New Challenges in Technology, Quality Control and Health"*, p. 155, Florence (Italy), 27-30 September 2015.
- Calligaris, S., Valoppi, F., Anese, M., & Nicoli, M. C. Influence of fat crystal network structure on the oxidation rate of lipophilic bioactive molecules. In *Proceedings of "1st Congress On Food Structure Design, Innovation in Food Structure Properties – Relationships"*, Porto (Portugal), 15-17 October 2014.
- Calligaris, S., Valoppi, F., Anese, M., & Nicoli, M. C. β -carotene bleaching as affected by fat crystal lattice structure. In *Proceedings of "Food Structure and Functionality Forum Symposium, from Molecules to Functionality"*, Amsterdam (The Netherlands), 30 March-2 April 2014.
- Calligaris, S., Valoppi, F., Barba, L., Anese, M., & Nicoli, M. C. Effect of fat crystal network structure on β -carotene bleaching. In *Proceedings of "DOF 2015 – 6th International Symposium on Delivery of Functionality in Complex Food Systems Physically – Inspired Approaches from the Nanoscale to the Microscale"*, p.108, Maison de la Chimie – Paris (France), 14-17 July, 2015.
- Calligaris, S., Valoppi, F., Pizzale, L., Conte, L., & Nicoli, M. C. Curcumin-loaded microemulsions prepared by phase-inversion temperature (PIT) method: effect of formulation on curcumin degradation. In *Proceedings of "13th Euro Fed Lipid Congress, Oils, Fats and Lipids: New Challenges in Technology, Quality Control and Health"*, p. 34, Florence (Italy), 27-30 September 2015.
- Valoppi, F., Calligaris, S., Barba, L., & Nicoli, M. C. Development and characterization of milk-oil-monoglyceride gels. In *Proceedings of "3rd International ISEKI_Food Conference, Food Science and Technology Excellence for a Sustainable Bioeconomy"*, p. 63, Athens (Greece), 21-23 May 2014*.
- Valoppi, F., Calligaris, S., Barba, L., & Nicoli, M. C. Rheological and structural properties of monoglyceride hydrogels containing milk. In *Proceedings of "1st Congress On Food Structure Design, Innovation in Food Structure Properties – Relationships"*, Porto (Portugal), 15-17 October 2014*.
- Valoppi, F., Calligaris, S., Manzocco, L., & Nicoli, M. C. Saturated fat reduction in sweet bread by using monoglyceride nanostructuring properties. In *Proceedings of "First FVG PhD Symposium (Nanotechnology - Biomedicine – Bioinformatics)"*, p. 40, Grado (Italy), 7-9 October 2013.
- Valoppi, F., Calligaris, S., Nicoli, M. C., Šegatin, N., & Poklar, U. N. Effect of dielectric properties of lipid matrices on the structure of organogel made with saturated monoglycerides. In *Proceedings of "13th Euro Fed Lipid Congress, Oils, Fats and Lipids: New Challenges in Technology, Quality Control and Health"*, p. 376, Florence (Italy), 27-30 September 2015.
- Valoppi, F., Manzocco, L., Calligaris, S., & Nicoli, M. C. Saturated fat reduction in sweet bread by using monoglyceride organogel and hydrogel. In *Proceedings of "11th Euro Fed Lipid Congress, Oils, Fats and Lipids: New Strategies for a High Quality Future"*, p. 161, Antalya (Turkey), 27-30 October 2013*.
- Valoppi, F. Study on biopolymer structural hierarchies for the development of innovative structures in food formulation. In *Proceedings of "XVIII Workshop on the developments in the Italian PhD research on food science technology and biotechnology"*, pp. 389-390, Conegliano (Italy), 25-27 September 2013.
- Valoppi, F. Study on biopolymer structural hierarchies for the development of innovative structures in food formulation. Interactions between lipids and proteins: the case study of milk-oil monoglyceride systems. In *Proceedings of "XIX Workshop on the*

developments in the Italian PhD research on food science technology and biotechnology", pp. 219-220, Bari (Italy), 24-26 September 2014.

*: oral communication.

Ringraziamenti

Un giorno, prima di intraprendere il percorso di dottorato, un mio caro amico mi disse: "a volte ci dimentichiamo quello che abbiamo fatto, guardiamo solo a quello che dovremo fare perdendo di vista il percorso che ci ha resi quello che siamo. Ora fermati e guarda indietro. È bello vedere da dove si è partiti e renderci conto di quello che è stato fatto nel nostro passato". Questo è il momento di fermarsi e guardare indietro.

In tre anni di dottorato ho imparato tanto, cercando di assorbire il più possibile dalle persone che erano attorno a me, dagli ambienti in cui mi trovavo e sbattendo la testa più volte contro argomenti difficili e diversi. Imparare è faticoso, ma è sempre un piacere arrivare all'intima essenza di un concetto o di un'idea.

Questa tesi racchiude tutti gli insegnamenti, lo scambio di idee, la voglia di mettersi in discussione e di imparare, l'evoluzione del modo di pensare, e le esperienze vissute in tre anni. Tutto questo non sarebbe stato possibile senza l'aiuto e l'intervento di certe persone che desidero ringraziare. È comunque difficile in poche parole esprimere la giusta gratitudine e i giusti ringraziamenti alle persone che hanno contribuito a tutto questo, ma ci provo.

Vorrei ringraziare in modo più personale alcune persone che ho citato in precedenza negli acknowledgments ed altre persone che non sono state precedentemente menzionate.

La mia gratitudine più profonda va ai miei supervisors, la prof.ssa Maria Cristina Nicoli e la dott.ssa Sonia Calligaris. Senza il loro aiuto, supporto, dedizione, incoraggiamenti ed insegnamenti non sarei arrivato a questo importante traguardo.

Pertanto, ringrazio la prof.ssa Maria Cristina Nicoli che mi ha dato l'opportunità di svolgere questo dottorato, mi ha supportato scientificamente, finanziariamente ed umanamente, continuando a credere in me e nelle mie capacità.

Ringrazio la dott.ssa Sonia Calligaris che mi ha guidato ed aiutato in questi anni, insegnandomi molto e facendomi crescere continuamente, spronandomi o fermandomi nei momenti in cui ne avevo più bisogno.

Ringrazio la dott.ssa Luisa Barba che mi ha insegnato tutto quello che so sull'analisi XRD con luce di sincrotrone. Mi ha aiutato e pazientemente insegnato come analizzare i campioni ed elaborare i dati.

Ringrazio le prof.sse Monica Anese e Lara Manzocco per i loro aiuti, e scambio di idee. Contribuendo a rendere questi tre anni interessanti e stimolanti.

Ringrazio il prof. Corrado Lagazio per il suo aiuto e per avermi, con pazienza e dedizione, insegnato tutta la statistica che conosco, uno strumento fondamentale che purtroppo molto spesso viene sottovalutato.

Ringrazio la dott.ssa Marina Munari che mi ha supportato tecnicamente aiutandomi nelle analisi in laboratorio.

I would like to thank prof. Alejandro G. Marangoni that accepted me in his lab and entrusted me a really interesting project. I was very lucky to work in his lab. That team of scientists is one of the world leading groups in food materials research!

I would like to thank dr. Fernanda Peyronel that trained and helped me in the lab, and outside the lab during my stay in Canada. She introduced me to USAXS which, in my opinion, in the next future will become one of the most important techniques for the study of food structured materials.

I would like to thank prof. Nataša Poklar Ulrich and dr. Nataša Šegatin for their help with dielectric properties measurements and for the stimulating talks during my stay in Slovenia.

I would like to thank Dr. Sandy Smith for her technical assistance and guidance with SEM analysis, and for our "less scientific" talks.

Un grande ringraziamento va alla mia piccola e grande famiglia. In questi tre anni mi hanno aiutato, supportato, sopportato e regalato infinite gioie. Grazie a mia moglie Tania, mia figlia Maya, al nostro futuro pargoletto, a mia mamma Giacomina, mio padre Pierino, ai

miei nonni Ugo e Pierina, e a mia suocera Olga. Un grazie ed un particolare pensiero vanno alla nostra amica di famiglia Eva che purtroppo è scomparsa durante la mia permanenza in Canada.

Voglio ringraziare Giacomo, che considero il fratellino che non ho mai avuto, per la sua amicizia ed i suoi aiuti. Un grazie va anche a Linda e Giovanni, per la loro amicizia.

Come non ringraziare i colleghi che con me hanno condiviso parte di questa esperienza di dottorato: Agnese, Alexandra, Francesca, Jeancarlo, e Stella. Grazie ragazzi per aver reso così piacevole questo periodo!

Vorrei ringraziare tutte le persone che ho incontrato in Canada che mi hanno aiutato e che hanno contribuito a rendere quegli 8 mesi un periodo davvero piacevole: Andrew, Braulio, Carolin (grazie anche per le misure del melting profile con il p-NMR), Cendy, Chloe (grazie anche per aver letto e corretto la bozza di un articolo), Claudia e famiglia, famiglia Ball, famiglia Krug, famiglia Venditti, Lida, Lucy e famiglia, Nick, Pere, Rafael, e Veronica.

Ringrazio per tutti gli scambi di idee e per avermi insegnato qualcosa tutti gli studenti che ho seguito: Emanuele, Elisa, Enrico, Fabio, Federica, Francesca, Giulia, Maddalena, Niccolò, Rita, Rossella, Samuele, Serena, Sofia, e Veronica.

L'insegnamento più grande che ho appreso in questo periodo è che tutto va affrontato con gioia e serenità. Non perdetevi mai la speranza e la vostra curiosità, ma coltivatele sempre come un dono prezioso.